UNIVERSITY OF SOUTHAMPTON

FACULTY OF SOCIAL AND HUMAN SCIENCES

Geography and Environment

Geomorphology and Channel Network Patterns of the Mekong River in Cambodia

by

Liubov Vladimirovna Meshkova

Thesis for the degree of Doctor of Philosophy

May 2012

ABSTRACT

Published, well-described examples of multiple mixed bedrock-alluvial character systems largely pertain to small to medium systems. No descriptions exist for large river systems such as the Mekong River in Cambodia (South East Asia). The published literature concerning the 120km long and up to 5km wide multichannel study reach are outdated and do not provide sufficient levels of detail. Therefore the first part of the thesis offers an amplified portrait of the modern and palaeo-Mekong based upon limited published literature, updated by ground survey data and complemented by analyses of remote sensing data. The second part of the thesis is devoted to applying quantitative channel network characteristics in order to describe the Mekong River but importantly to separate mixed bedrock-alluvial from alluvial multichannel rivers. The key question in this respect is whether the planform characteristics of the river networks reflect whether they are within alluvial settings or are influenced by bedrock controls. The channel metrics comparison is accompanied by a specially designed methodology based upon standard GIS tools so that the results obtained in this study could be later incorporated into subsequent channel network metrics research using a larger dataset for these or other rivers.

Geomorphological findings reveal that the multichannel pattern of the Mekong is comprised by primary channels, secondary channels, cross-channels and blind channels, divided by two classes of islands: major and seasonally-inundated islands. The riverbed is represented by outcrops of Mesozoic bedrock and temporally and spatially fixed sand bars whereas the planview variations in the disposition of sand bodies versus bedrock define the extent of longitudinal geomorphological zones. Structurally and qualitatively diverse geological units are dissected by regional and local faults which partially control channel alignments. Topographic and dating control of river terraces and palaeochannel deposits show that the river incised during the Last Glacial Maximum but was essentially within the same course as seen today for at least last 70ka. Distinctive floristic associations emphasise an important role that vegetation plays in channel dynamics in this mixed bedrock-alluvial system.

Comparative study of channel network metrics shows that reach-scale standard planform indices (e.g., braiding intensity, channel sinuosity) are less effective than non-standard indices developed at scales less than the reach-scale (e.g., channel network bifurcation angles asymmetry, island convexity) in successfully separating channel patterns. In addition, DEM trend surfaces reveal variable topographic trends generic for the mixed bedrock-alluvial patterns only. Ultimately, it shows that the mixed bedrock-alluvial pattern classification might be more effectively based on channel cross-section properties, e.g. variations between bedrock/alluvium as a part of a channel continuum.

Contents

List of figures

List of tables

List of Equations

List of accompanying materials

Meshkova, L.V., & Carling, P.A., (2012), The geomorphological characteristics of the Mekong River in northern Cambodia: a mixed bedrock-alluvial multi-channel network, *Geomorphology*, vol. 147-148, pp. 2-17.

Meshkova, L.V., Carling, P.A., Buffin-Banger, T., (2012). Nomenclature, Complexity, Semi-Alluvial Channels and Sediment-Flux-Driven Bedrock Erosion. In: Church, M., Biron, P., Roy, A. (Eds.), *Gravel Bed Rivers: Processes, Tools, Environments*. John Wiley & Sons, Ltd., Chichester, UK. doi:10.1002/978119952497.ch31.

DECLARATION OF AUTHORSHIP

I, Liubov Vladimirovna Meshkova

declare that the thesis entitled

Geomorphology and Channel Network Patterns of the Mekong River in Cambodia

and the work presented in the thesis are both my own, and have been generated by me as the result of my own original research. I confirm that:

- this work was done wholly or mainly while in candidature for a research degree at this University;
- where any part of this thesis has previously been submitted for a degree or any other qualification at this University or any other institution, this has been clearly stated;
- where I have consulted the published work of others, this is always clearly attributed;
- where I have quoted from the work of others, the source is always given. With the exception of such quotations, this thesis is entirely my own work;
- I have acknowledged all main sources of help;
- where the thesis is based on work done by myself jointly with others, I have made clear exactly what was done by others and what I have contributed myself;
- parts of this work have been published as:
    - Meshkova, L.V., & Carling, P.A., (2012), The geomorphological characteristics of the Mekong River in northern Cambodia: a mixed bedrock-alluvial multi-channel network, Geomorphology, vol. 147-148, pp. 2-17.
    - Meshkova, L.V., Carling, P.A., Buffin-Banger, T., (2012). Nomenclature, Complexity, Semi-Alluvial Channels and Sediment-Flux-Driven Bedrock Erosion. In: Church, M., Biron, P., Roy, A. (Eds.), Gravel Bed Rivers: Processes, Tools, Environments. John Wiley & Sons, Ltd., Chichester, UK. doi:10.1002/978119952497.ch31.

Signed: ……

Date: 02/05/2012……

Acknowledgements

This thesis would not have been possible without the financial support of the Mekong River Commission (MRC) and the School of Geography, University of Southampton, UK. I am also grateful to the Funds for Women Graduates (FFWG) for the financial support during the final extension of my study. Acknowledgement goes to the Optimising Access to Spot Infrastructure for Science (OASIS) programme which provided remote sensing (SPOT) images. The British Society for Geomorphology (BSG) and the International Association of Sedimentologists (IAS) awarded me research grants for the cost of luminescence dating of sediment samples and Dr Ruth Robinson of St Andrews University provided the luminescence dates reported herein. Special recognition has to be given to Penroong Bamrungrach, Manithaphone Mahaxay, Jorma Koponen, and Matti Kummu for preparing the Mekong bathymetry data and Niladri Gupta who has provided digital dataset for the Ganga River.

The deepest gratitude is due to my scientific supervisor Prof. Paul Carling who has helped me grow as a scientist and has shown that '…there are no limits, only distant horizons'. Special thanks are due to Iwona Conlan, Pavel Vedenskiy and Tatjana Semina for helpful consultations contributing to this work. Sergei Krasnoshchekov, Hai Quang Trieu and Tri PD Van shared the tribulations and successes of preparing doctoral dissertations. Prof. Steve Darby provided additional support, especially in the field and made available unpublished material.

Finally, I am deeply obliged to my family and friends whose unconditional love and support have been the biggest motivations throughout the dissertation and beyond.

Abbreviations

3D	Three dimensional
3S Basin	Se Kong, Se San and Sre Pok drainage basin
ACF	Autocorrelation Function
AR	Auto Regression
ASTER	Advanced Spaceborne Thermal Emission and Reflection Radiometer
CASC	Cambodian Agronomic Soil Classification
CC	Cross-correlation
CEGIS	Center for Environment and Geographic Information Services
Danida	Danish International Development Assistance
DEM	Digital Elevation Model
DHRW	Department of Hydrology and River Works, Cambodia
FAM	Finite Age Modeling
FAO	Food and Agriculture Organization of the United Nations
GCP	Ground Control Point
GDCG	General Department of Cadastre and Geography
GDEM	Global Digital Elevation Model
GIS	Geographical Information Systems
GPS	Global Positioning System
HF	Hydrofluoric acid
JICA	Japanese International Cooperation Agency
LANDSAT	Land-Use Satellite
LGM	Last Glacial Maximum
LST	Lithium hetero- polytungstate
MBG	Minimum Bounding Geometry
METI	Ministry of Economy, Trade, and Industry (Japan)
MLMUPC	(Cambodian) Ministry of Land Management, Urban Planning and Construction
MRC	Mekong River Commission
MRC-RFMMC	Mekong River Commission Regional Flood Management and Mitigation Centre
NASA	National Aeronautics and Space Administration (United States of America)
NGA	National Geospatial Intelligence Agency (United States of America)
NGO	Nongovernmental Organization
OASIS	Optimising Access to Spot Infrastructure for Science
OSL	Optically Stimulated Luminescence

PAF	Partial Autocorrelation Function
RMS	Root Mean Square
SAR	Single Aliquot Regeneration
SPOT	Satellite Pour l'Observation de la Terre
TLM	Topographic Line Maps
TSS	Total Suspended Sediments
UN	United Nations
UNESCO	United Nations Education and Social Commission
UTM	Universal Transverse Mercator
WGS84	World Geodetic System ('84' stands for '1984' - the year of this coordinate system creation)

List of Notation

ΔA - subtracted area of change, square metres

Δt - length of interval, years

$\Delta \sigma$ - the differential subsidence rate over the lateral distance

A_L/A_R - left/right anabranch width, metres

BI_T - braiding intensity (total)

C - channel lateral rate of migration

H - water level, masl

K - sector area, square meters

L - bifurcation angle between two downstream channels, degrees

L_1 - bifurcation angle between upstream and right downstream channel, degrees

L_2 - bifurcation angle between upstream and left downstream channel, degrees

L_{CB} - channel link length of confluence/bifurcation

L_L - length of channel links (segments), meters

L_r - reach length, meters

L_y - lateral distance, meters

N_L - number of links (braids)

O - order of magnitude

P_T - sinuosity

Q - discharge, cumecs

Q_{bf} - bankfull discharge, cumecs

r - circle radius, meters

R - horizontal retreat of the water surface, meters

R_A - island aspect ratio

S_x - channel slope in the downstream direction

S_y - cross-channel slope

S_v - valley slope

T_c - channel time scale

T_t - time for channels to be steered by cross-channel tilting alone

W - channel width, meters

W_c - the total width of wetted channels (in the case of multichannel network)

W_{cor} - the width of river corridor

X_E/Y_E - X/Y - coordinates in metres of ending points of a polyline

X_m - maximum island width, metres

XS - cross-section

X_S - length of the side of the ΔA polygon (shortest)

X_S/Y_S - X/Y coordinates in metres of starting points of a polyline

α - confluence angle, degrees

α_S - segment angle, decimal degrees

θ - circle segment angle, radians

θ- bank slope, degree

1. Introduction

Rivers have always been vitally important for human livelihood, providing potable water and food needs, irrigation and water for domestic animals and transport routes, and they often become part of history and culture of a region. Large rivers have been exploited by riparian populations throughout generations since the time of ancient civilisations. Within recent years the interest in large rivers has significantly increased (Gupta, 2007; Latrubesse, 2008; Campbell, 2009; Latrubesse et al., 2009) due to the fact that complete understanding of generic river processes would enable correct predictions to be made in respect of river management and regulation in response to natural and human-induced interventions. Human activities can help prevent or alleviate environmental disasters, notably flooding, and can regulate the use of river water in a sustainable way.

In agreement with the definition of Latrubesse (2008) a large river is that with an annual discharge of more than 1000 cumecs. The Mekong River in South East Asia with a mean annual discharge 14900 cumecs is one such example (Figure 1.1). This thesis is focused on the multichannel section of the Mekong in north-east Cambodia (Figure 1.1B and Figure 1.2) where access is complicated due to remoteness, and the complex bedrock-alluvial multichannel character of the channel (Gupta & Liew, 2007) hinders navigation by vessels. The current known facts and detailed geomorphological descriptions of the area are not available in a great level of detail. Meanwhile, due to the political situation in Cambodia at the end of the last century, specific environmental data collection had been interrupted for nearly 20 years. Yet a channel belt up to 5 km wide and river islands from 100m to 40km long, together with complex topography, geology, tectonics and specific riverine vegetation and fauna, comprise unique environmental settings for the river and its floodway, and thus deserve special attention. In particular, detailed geomorphological descriptions of mixed bedrock-alluvial rivers are limited (van Niekerk et al., 1995; Heritage et al., 2004; Tooth and McCarthy, 2004) and there are no amplified reports on channels of this type for large rivers within South East Asia. The importance of documenting the system is even more urgent due to the rapidly declining Mekong population of internationally endangered river dolphins (Beasley et al., 2007) and proposals to impose a series of dams on the river (ICEM, 2010), which would result in an impoundment from the Lao PDR border to Kratie (Figure 1.3).

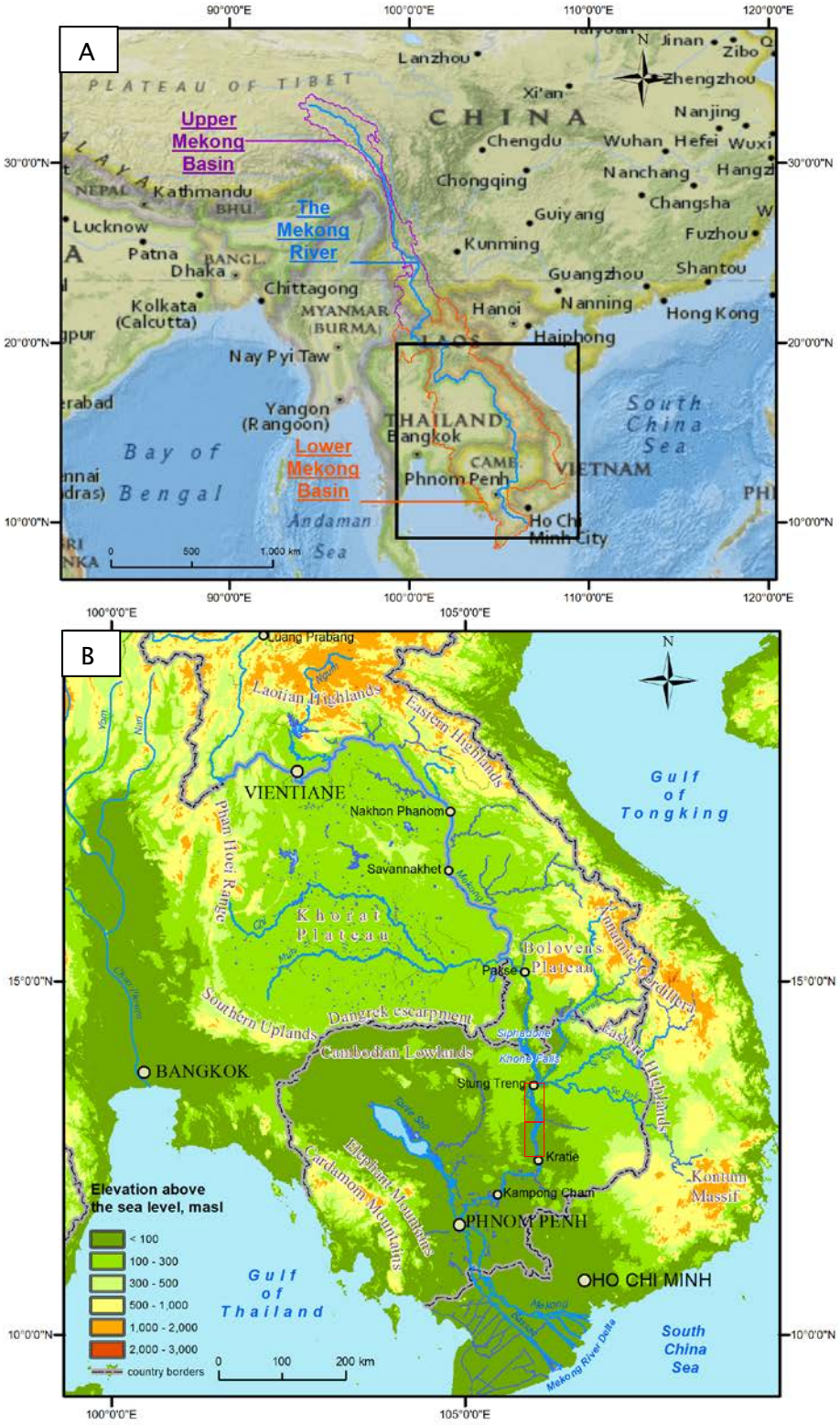

Figure 1.1. Location map: the Upper and Lower Mekong Basins (A) and enlarged Lower Mekong Basin with geomorphological features mentioned in the text (B).

Map A background is National Geographic et al, 2011 with added MRC Digital Dataset Data; map B – MRC digital dataset. Two red rectangles on map B represent the extent of the study area shown on Figure 1.2 A and B (top and bottom rectangles respectfully).

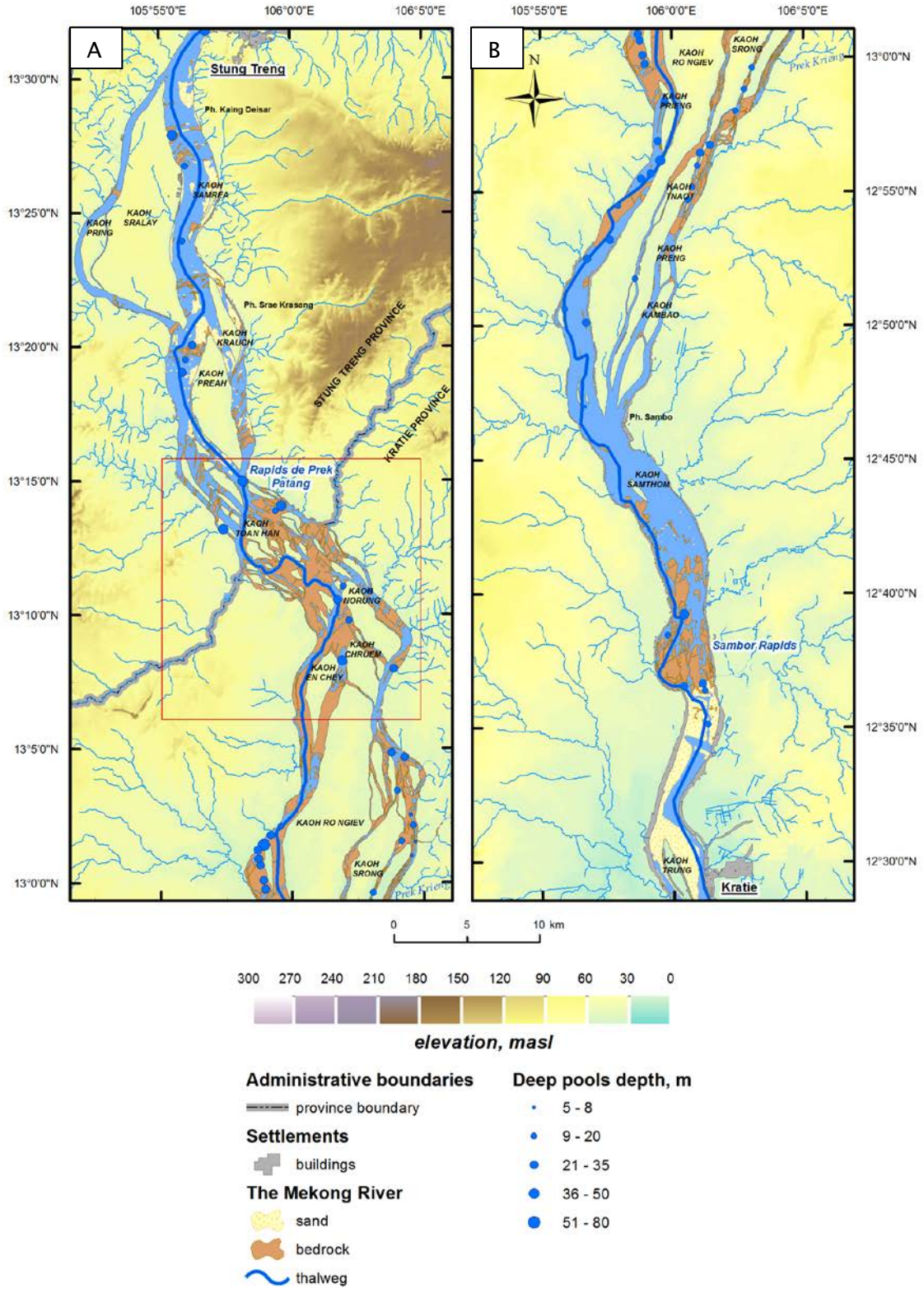

Figure 1.2. Location map: study area of the Mekong River from Stung Treng (A) to Kratie (B).

The extent of the study area is shown on Figure 1.1B. The red rectangle on map B shows the extent of the study sub-area. Both maps are composed using MRC digital dataset.

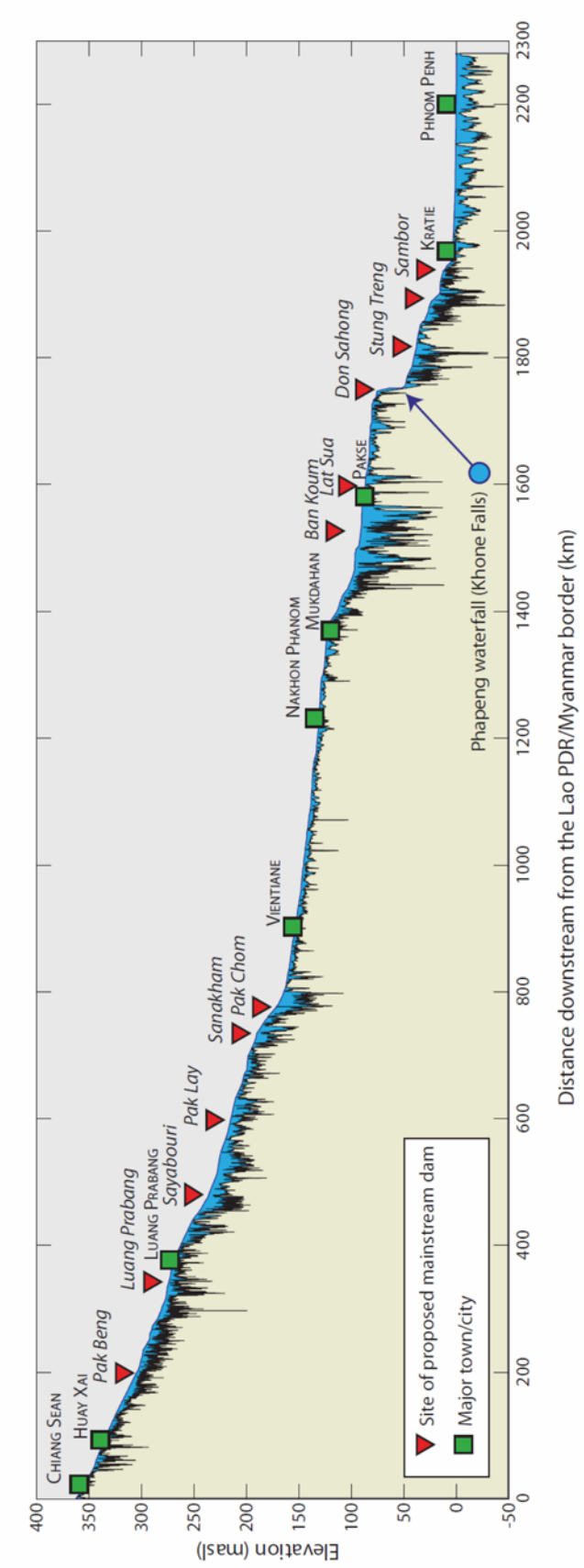

Figure 1.3. Longitudinal profile of the Mekong riverbed and dry season water surface from the China-Lao PDR border to Phnom Penh (Cambodia) and location of proposed hydropower dams (modified after Halls & Kshatriya, 2009).

Thus prior to any further examination of the multiple channels system, the first objective of this research is to provide a detailed description of the Mekong in north-east of Cambodia. This aim is to be achieved through: 1) gathering information from available literature sources; 2) on-ground verification of known facts obtained from the literature review, i.e. personal visits to the study area; and 3) analyses of remote sensing and digital topographic data. Physical exploration of the area will enable: 1) checking of the literature statements against field evidence; 2) observation and classification of geomorphological units comprising river landforms; 3) collection of samples of geological sub-divisions within the riverbanks, islands and multiple bedrock outcrops allowing an update and extension of geology; 4) contribution of information on historical river changes by investigating the Mekong terraces and its sediments; and 5) documentation of key vegetation types attributive to the river and its floodway for subsequent understanding of its role in the Mekong geosystem. Digital data available for the research are represented by aerial photographs (years 1959, 1992), satellite images (years 2003-2006) and set of topographic data (GIS vector layers and DEMs). Interpretation of aerial photographs will allow delineation of structural and fault elements and verify the degree of any structural control of channel pattern. Historical comparison of remote sensing images allows evaluation of system dynamics by assessing sand bars distribution and bank erosion/accretion locations whereas additional qualities of the Mekong channel pattern can be obtained from digital topographic dataset and a DEM. The accomplished 'preliminary' study would enable an outline geomorphological portrait of the Mekong and its environmental settings in northern-eastern Cambodia and provide the conceptual framework for the second objective of the research.

The visual assessment of a river planview pattern is one of the primary qualities used in every classification scheme to distinguish between single and multiple thread rivers (e.g. Leopold & Wolman, 1957; Miall, 1977). Furthermore, the human eye is able readily to detect the similarities or differences of one pattern from another. It is known that current channel pattern classifications offer subdivisions defined on a basis of hydro-physiographic and morphological conditions (e.g. Rosgen, 1994; Nanson & Knighton, 1996) whereas geometrical properties of channel networks are measured by only a few designated indexes such as, for instance, channel sinuosity or braided intensity (Egozi & Ashmore, 2008). The multichannel pattern of the mixed bedrock-alluvial study-reach of the Mekong is visually distinctive from alluvial anastomosed or braided river patterns but such differences have never been shown using quantitative planimetric characteristics of each network. Thus, this lack of characterisation justifies the second objective of the research which is to develop metrics that quantitatively describe and distinguish the mixed bedrock-alluvial networks from alluvial

multichannel networks. The geometry of channel networks for several 'classic' examples of planform types is going to be analysed using widely recognized indices (braiding intensity, channel sinuosity, channel width and slope variations) but with additional emphasis being given to less common metrics such as network bifurcation angles and island shape characteristics (e.g., aspect ratio, compactness, roundness, convexity). The data obtained on the Mekong channel metrics will allow a quantitative description of the multichannel network of the Mekong. In addition, a river of similar pattern, the Orange River, South Africa (Figure 1.4) can be compared and contrasted with the alluvial anastomosed Upper Columbia, Canada (Figure 1.5) and braided Ganga, India/Bangladesh (Figure 1.6) rivers. Complementary to examination of planview channel geometries, limited involvement of terrain characteristics derived from digital elevation models (DEMs) shall enable definition of sets of distinctive characteristics peculiar to each network. As within any other comparative study, the exact methodology based on standard functions within currently existing GIS software shall be provided. The expected outputs should help to understand the nature of the mixed bedrock-alluvial system and its place in channel pattern classifications.

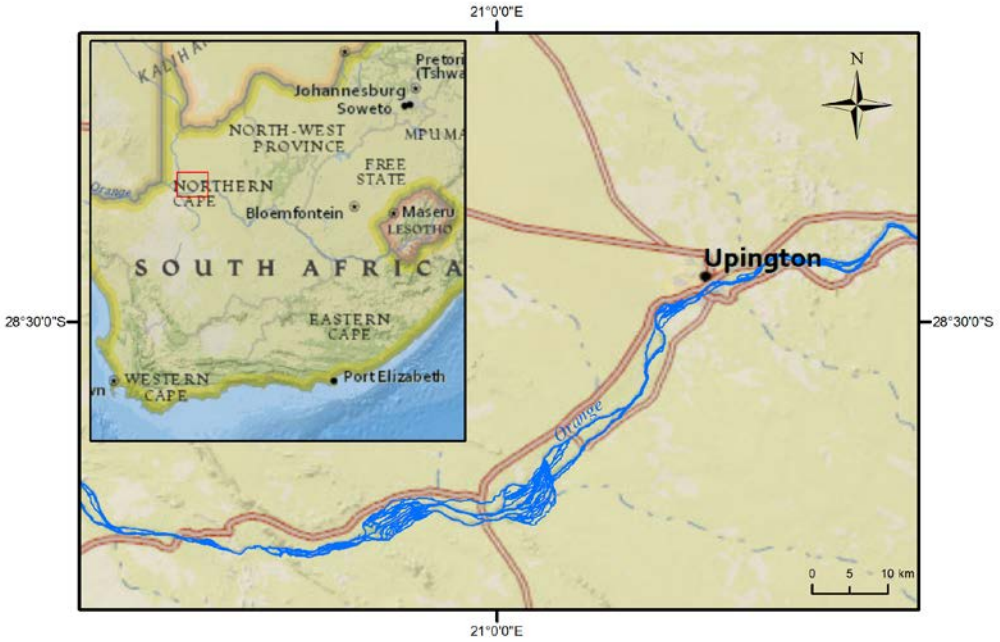

Figure 1.4. Studied reach of the River Orange.

Inset map (upper left corner) shows an extent of the studied reach (red rectangle) in a regional context. The map background is National Geographic et al., 2011.

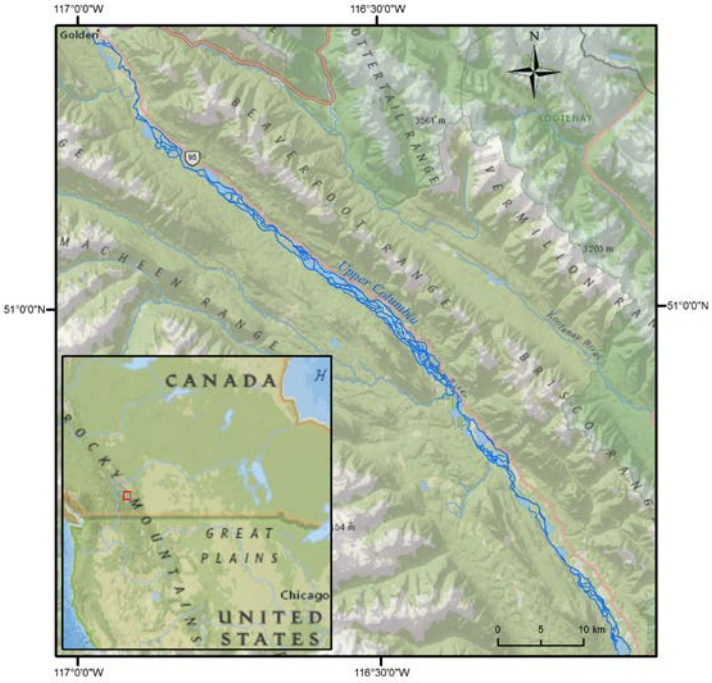

Figure 1.5. Studied reach of the Upper Columbia River.

Inset map (bottom left corner) shows an extent of the studied reach (red rectangle) in a regional context. The map background is National Geographic et al., 2011; contours of the Upper Columbia River are from Government of Canada et al., 2005.

Figure 1.6. Studied reach of the Ganga River.

Inset map (upper right corner) shows an extent of the studied reach (red rectangle) in a regional context. The map background is National Geographic et al., 2011, digital contours of the Ganga river are captured from the LANDSAT images (2000).

2 Literature Review

The first part of this Chapter describes available literature and briefly outlines the most prominent results of previous research on the Mekong River in Cambodia. The second part introduces the river patterns and describes key characteristics of alluvial (anastomosed and braided) and mixed bedrock-alluvial multichannel rivers. In the third part of the Chapter consideration is given to literature on channel network planview metrics, fluvial island shape measurements and examples of bank erosion in relation to the lateral stability of channel networks.

2.1 Existing Knowledge of the Mekong in NE Cambodia

The north-east region of Cambodia is one of the less densely populated areas in the country. Due to its remoteness and the complex character of the Mekong River with its multiple channels, navigation is obstructed by plentiful rapids, waterfalls and bedrock exposures. Consequently, the Mekong River geomorphology between Stung Treng and Kratie has never been studied in any level of detail. River islands from 100m to 40km long that are present within multichannel sections of the river, together with complex topography, geology, tectonics and a specific riverine vegetation, altogether comprise a unique environmental setting for the river and its floodway and thus deserve a devoted study. In order to understand why, at the beginning of 21th century, still not much is known about one of the most complex portions of this great river, an excursion into the history of the country and relevant scientific publications is indispensable.

The Khmer civilisation once embraced most of the vast lands of the Indochinese peninsula. Today, the worldwide famous international heritage temple complex at Angkor Wat, built in the 12th century, still stands as a reminder of its bygone might (Ooi, 2004). However, there are no records of ancient environmental studies which could have contributed towards the first systematic explorations of the Mekong initiated by French in the middle of 19th century. After the 15th century, at the time of the Khmer civilisation decay, occasional trips to this region were made by a few European travellers, which allowed the plotting of South East Asia on the historical 16th-17th century maps of a global scale (Suárez, 1999). Those maps depict the Mekong River in an indicative manner, showing its presence rather than its accurate spatial position and the exact configuration of the main channel(s) (Bellin, 1751;

Dankworth, 1832). Later, in 1866, did group of French explorers undertake the first journey along the Mekong aiming to identify its source (Osborne, 1996). Reported observations and sketches emanating from this expedition are considered to be first definitive description of the river from the Vietnamese delta up to Yunnan province in China or, in modern terminology, the Lower Mekong Basin. The expedition and its outputs also attracted public and scientific attention to a hardly known region.

In 1880, France took control of Cambodia and expanded its sway across the whole Indochinese region by the first decade of 20th century (Chandler, 2000). French colonisation marks a significant stage in the history of South East Asian explorations by virtue of diverse reports published by a number of highly ranked individual scientists and research institutions. Cambodia, as well as several other countries of Indochina, remained a French protectorate until 1953, but the French authorities continued to elaborate and influence the Cambodian research structures until the 1970s (Jumsai, 1996). Internal problems in the 1970s associated with the Khmer Rouge (Pol Pot) regime and the following two decades of civil war stopped all types of natural exploration in the country (Kiernan, 2002). Moreover, all research institutions and the majority of scientifically important documents stored in Cambodian libraries were destroyed; indeed the intelligentsia as a class of a society had disappeared. Political stability came at the beginning of 1990s when the civil war ended and a constitutional monarchy was established within the country. However, environmental investigations and outputs since then and up until now remain sparse, scattered and as a rule have been developed by foreign scientists, companies or international organisations, rather than Cambodian scientists.

Returning to the investigations of the Mekong in the area of interest, it ought to be noted that first realistic depictions of multichannel sections of the Mekong at Khone Falls and in the north-east of Cambodia appeared on the regional scale topographic maps of Indochina at the end of the nineteenth century (Migeon, 1880; Royal Geographical Society, 1893). Approximately at the same time, initial geological investigations allowed the composition of the first geological map of Indochina at a scale of 1:4 000 000, which was published in 1882 (UN, 1993). Later, in the 1920s, Ch. Jacob took the lead in instigating field work in Laos and Cambodia, aiming to produce a geological map of the area at a scale of 1:500 000. Those works involved many French specialists, and the most valuable contributions were made by E. Saurin and J. Gulber. Their report covering central/southern Vietnam and eastern/western parts of Cambodia was published in 1935. In parallel, J. Fromaget and colleagues made investigations of Cambodian geology, tectonics, stratigraphy and vegetation. The geological map of Indochina at a scale of 1:2 000 000 complied by J. Formaget was

published in 1937 and re-issued in 1952. Much of the work on tectonics, volcanism and mineral resources had been done by J. Blondel, who eventually had replaced Ch. Jacob as a director of Geological Services of Indochina. Due to the 2nd World War, all the sheets of the resulting 1:500 000 geological map of Indochina were only published by the South Vietnam Department of Geography in 1963 (DGM, 2000). Among the published geological maps and notes, two notable basic tractates by J. Fromaget and E. Saurin reflecting the current understanding of Indochina's tectonic and geology, were produced in 1941 and 1956.

The attainment of Cambodian sovereignty in 1953 stimulated the foundation of the national geological services. Nevertheless, all further works and surveys were conducted with the assistance of French specialists from the Bureau de Recherches Géologiques et Miniéres (1966-1970), Chinese geologists (1960-1962), and professionals from the United Nations agencies. The country mineral resources report was produced in 1973 in cooperation with French specialists and consisted of 14 geological map sheets at a scale of 1:200 000 (SNMGP, 1973). Geological investigations at this level of detail, based on 1:50 000 USA Army Service topography maps and the previous works of French geologists, remain the best regional syntheses. Unfortunately, the accompanying notes to these maps are not publicly accessible but, nonetheless, they are used as background materials in the current research. From time to time, large-scale geological surveys of small areas with respect to proposed dam construction or evaluation of mineral resources extraction have been carried out locally (Stapledon et al., 1961, 1962; Poduzeće za primijenjenu Geofizika, 1968).

Significant contributions towards the geological exploration of Cambodia were made by J.P. Contri, O. Dottin, P. Fleuriot de Lange, J.P. Carbonell, H. Fontaine and D.R. Workman in the 1960s. The works of the latter concerning the geology and mineral resources of Cambodia, Laos, Thailand and Vietnam were published in 1972 and 1978. Although published in 1989, the Phan Cu Tien edition 1:1 000 000 Geological Map of Kampuchea, Lao and Vietnam with accompanying notes (based on the investigations of Vietnamese geologists) remains the best map summary. The most recent complex works on regional tectonics and geology of South East Asia can be found in a book by Hutchinson (1989) and in the Encyclopedia of European and Asian Regional Geology (Fontaine & Workman, 1997).

A renaissance of geological studies started at the beginning of the 1990s by the National Department of Geology. Significant contributions to modern investigations are supported by large international organisations such as JICA (Japanese International Cooperation Agency), Danida (Danish International Development Assistance) and the

FAO (Food and Agriculture Organization of the UN). Currently, the Cambodia Reconnaissance Survey Data prepared by JICA in 2003 are used for official documentation. It consists of digital layers of updated topography, land use and geology/geomorphology information based on interpretation of recent satellite and air photo images (1990 – 2000), as well as 1950s topographical maps at a scale of 1:50 000. The basic advantage of this dataset is established by well-depicted boundaries of conspicuous features; nevertheless, ground verification of the content has not been applied.

Understanding of tectonics of the area was formerly performed in parallel with geological investigations made by leading French geologists where the major tectonic and sedimentological event of Triassic-Jurassic periods and the Indosinian Orogeny cycle was fully described (Dickins et al., 1997). However, the precise age of the main Indosinian sedimentological units, e.g. the sandstones, remains disputed (Hutchinson, 1989). The advent of the plate tectonics paradigm corrected views on the tectonic development of South East Asia and resulted in re-evaluation of tectonic and structural evolution of the region and new interpretations of key faults and rift basins (Lovatt Smith et al., 1996; Morley, 2002; Hall, 2002; Hanebuth et al., 2011).

The most complete works on Quaternary sediments in Cambodia date back to the 1960-70s (Takaya, 1967; Carbonnel, 1972). Recently, only a few studies have been published on the sediments of the Holocene, as conditioned by the South East Asian monsoonal climate (Maxwell, 2001; Maxwell & Liu, 2002; Wang, 2005a) and the Quaternary sediments on the Mekong floodplain around Phnom Penh (Kubo, 2008).

The most important investigations of the Cambodian flora were performed by Lecompte (1907-1942), Rollét (1962, 1972), Martin (1970-1978), Blasco (1971, 1996, 2000), Dy Phon (1970-1972, 1981-1984, 1999-2000) and Ashwell (1993, 1997, 2004) amongst others, including occasional FAO, MRC, Cambodian governmental organizations and environmental NGOs projects (CTSP/Danida, 2000; Ashwell et al., 2004). Among recent works, the report by Bezuijen et al. (2008) is the most relevant in terms of describing vegetation communities in the riverine environment.

The first fundamental pedological studies were undertaken by C.D. Crocker in the 1960s. Sixteen soil types were identified and placed into three major groups (zonal, intrazonal and azonal) according to the soil maturity and conditions of formation (Crocker, 1962). This work resulted in the publication of a 1:1 000 000 scale soil map with accompanying exploratory survey notes. The FAO Soil Map of the World released in 1988 represents Cambodia according to the FAO/UNESCO Soil Classification System.

The latest Cambodian Agronomic Soil Classification (CASC) was developed in 1995 by White et al. (1997) and aimed to identify the agricultural suitability of various soils. In the CASC, the distinguishing of soil groups is based on pedogenic and morphological criteria; each group has a local name. This latter work includes a manual for soil identification and management that is for practical application. It does not substitute previous classifications but complements them. However, no field surveys in the north-east region of Cambodia have been carried out since the 1960s; therefore modern soil maps in the area of interest are based on the soil units mapped by Crocker with the terminology of the FAO (FAO/UNESCO, 1988).

The archive and current hydrological database for the Mekong are a result of the establishment in 1995 of the international Mekong River Commission (www.mrcmekong.org). This organization manages various environmental programmes and issues annual flood reports on the Mekong containing information on river monitoring and related topics (MRC, 2007a; MRC, 2008) as well as single reports and technical papers on biodiversity, fisheries and sustainable river management, for example (MRC, 2005; MRC, 2007b). Apart from their own reports of their own activities, the MRC publishes the proceedings of the Annual Mekong Flood Forum which is conducted in order to exchange ideas and knowledge on the Mekong and its basin (CNMC, 2006; Heng, 2008; ICEM, 2010).

Complete environmental and social data at the national level has been recently gathered and published in the Atlas on Cambodia (SWC, 2006). Existing scientific publications related to the Mekong, its specific parts or features that have been published within the last decade come from manifold sources (Hori, 2000; FA/Danida/DED, 2003; ICEM, 2003; MWBCSUP, 2005; Try & Chambers, 2006; Beasley et al., 2007; Gupta, 2007; Gupta & Liew, 2007; Kummu & Varis, 2007; Buschmann et al., 2008; Conlan et al., 2008; Costa-Cabral et al., 2008; Kummu et al., 2008; Luu et al., 2009; Campbell, 2009). Thus, the problem with the Mekong in the area between Stung Treng and Kratie is that regional scale studies do not give enough detail on the area, while local investigations focused explicitly on the reach of interest have never been instigated.

With the advent of new GIS technologies, 1993 is a key date with the instigation of a national digital geospatial dataset infrastructure at the Ministry of Agriculture. Initially GIS in Cambodia was used to maintain land-use, land-registration and land-planning by the Land Use Mapping Office. At the governmental level, and according to a 1999 sub-decree, the General Department of Cadastre and Geography (GDCG) was authorized to administer all Cambodian base map generation, their updates and distribution. There

are two departments within GDCG: Geographic and Technical; the latter plays a significant role in national GIS data set development. These authorities are responsible for survey works, installation of geodetic networks, map administration and production. The Cambodian Ministry of Land Management, Urban Planning and Construction (MLMUPC) is engaged in spatial data generation such as topographic and cadastral maps, aerial photo capture and production, state land mapping and registration. The National GIS Task Force deals with Cambodian metadata standardization, datum study and geographical names for the national Gazetteer.

2.2 Multichannel river networks

2.2.1 Alluvial multichannel rivers

According to classic views of plan view morphology, rivers can be classified into single and multichannel forms (Figure 2.1), which may be split into four main river types: single, meandering, braided and anastomosing (Rust, 1978; Miall, 1981, 1996; Bridge, 2003).

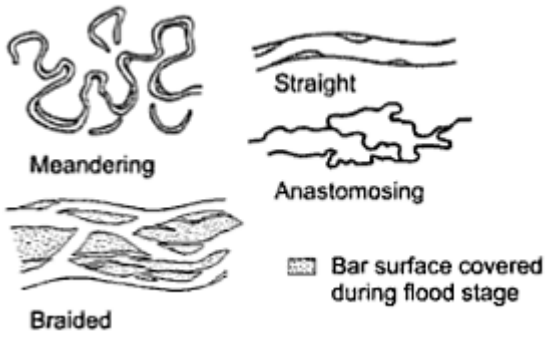

Figure 2.1. Main channel types accordingly to plan view morphology (Miall, 1977)

Anastomosing river systems, which some researchers term ‘anabranching’ river systems, initially were mentioned in the literature at the end of the 20th century (Nanson & Knighton, 1996). Perhaps the lack of accurate mapping techniques and difficulties in accessing multiple channels limited studies on such rivers before the occurrence of modern airborne and space remote sensing technologies. Thus, in the middle of last century generally only three different river patterns based on a planview morphology - straight, meandering and braided - were recognized widely and

discriminated in respect of valley slope and water discharge (Leopold & Wolman, 1957) and it took nearly two more decades to draw a conclusion that anastomosing rivers should be considered as a distinctive individual group (Schumm, 1968; Rust, 1978). The evolution of definition and classification suggested by various scientists (Brice, 1975; Mollard, 1973; Miall, 1977; Schumm, 1977; Brice, 1982; Schumm, 1985; Church, 1992; Rosgen, 1994) in attempts to describe and segregate multichannel rivers is covered in the seminal review by Nanson and Knighton (1996). They define a multichannel (anabranching) river as:

"… a system of multiple channels characterized by vegetated or otherwise stable alluvial islands that divide flows at discharges up to nearly bankfull" (Nanson & Knighton, 1996, p.218)

Within this classification, a specific anastomosed river type is determined as:

"cohesive sediment rivers with low width/depth ratio channels that exhibit little or no lateral migration" (Nanson & Knighton, 1996, p.217).

Nanson & Knighton's (1996) classification of multichannel rivers relies on the assessment of stream power and distinguishes subtypes accordingly to morphology, sediments and fluvial processes. However, due to the diverse nature and complexity of Indogangetic and South East Asian rivers and lack of published studies (Nanson & Knighton, 1996, p. 219) these latter rivers are excluded from the above mentioned classification. In addition, a classification of anastomosing rivers produced by Makaske (2001) separated a group of anastomosed rivers from anabranching rivers by taking the floodplain geomorphology into consideration and includes a definition of anastomosing rivers as those which are:

"… composed of two or more interconnected channels that enclose floodbasins" (Makaske, 2001, p. 149).

In other words, anastomosing rivers are composed of either single, meandering or braided channels within a channel belt (Makaske, 2001).

In either of these two classifications, flood dominated regime, cohesive river banks, bed aggradation of an active multiple channels and planform stability are the primary criteria for the river to be recognized as anastomosing. Makaske (2001) points out that his classification is designed for alluvial rivers due to the presumed different character of alluvial versus bedrock and mixed bedrock-alluvial rivers. Listed limitations in either

of Makaske's (2001) or Nanson & Knighton's (1996) classifications are partly conditioned by the fact that alluvial multichannel river systems have been investigated more than those systems which are bedrock controlled. Indeed, anastomosed alluvial rivers (or more accurately, anastomosing river reaches) as a part of a channel belt continuum have been found all over the world in various climatic and physiographic environments (Smith & Smith, 1980; Wende & Nanson, 1998; Knighton & Nanson, 2000; Gradziński et al., 2003; Adams et al., 2004; Tooth & Nanson, 2004; Wang et al., 2005b; Makaske et al., 2009).

Anastomosed rivers are distinguished from braided streams by a wide variety of characteristics, e.g. planview shape, fluvial morphological features, sediment load, river bank materials, channel width, depth and gradient, water discharge and velocities and so on. Interaction of those factors determines the particular nature of a given river.

In terms of morphology, there are a few key differences between braided and anastomosed rivers. Braided rivers have a network of channels that braid around depositional sand/gravel bars (braid bars) or islands which often are subject to vigorous lateral changes conditioned by easily erodible banks. In contrast, the islands in anastomosed rivers exhibit stability due to their cohesive banks, explaining the relatively long-lasting configuration of channels (Nanson & Croke, 1992). Inter-channel islands on anastomosed rivers are, in most cases, well-vegetated by trees and bushes unless climate conditions are adverse to a closed canopy, or primary vegetation is absent due to human interference. The lateral dimension of islands separating channels in alluvial anastomosed systems is relatively large compared with the widths of the intervening river branches (Knighton & Nanson, 2000) or the largest bars (Bridge, 2003). Each channel in an anastomosed alluvial river can be independent from one another, maintaining its own water level at a given river cross-section (Figure 2.2). Anastomosed rivers may have a main channel containing the largest portion of discharge (Makakse et al., 2009) whereas each of the subsidiary channels may be at a different stage of development; often, channels close to abandonment are significantly occupied by vegetation (Gradziński et al., 2002). In contrast, for braided stream the main stream tends to occupy the centre of the braidplain, while its margins are occupied by temporal depositional branches (Ashworth et al., 2007). The same conclusion comes from the results of experimental investigations of braided stream behaviour which shows 50 to 90 percent of total flow being allocated in a main channel (Egozi & Ashmore, 2009). However, water levels within braided river channels are not independent, especially as water levels rise and bars begin to become inundated.

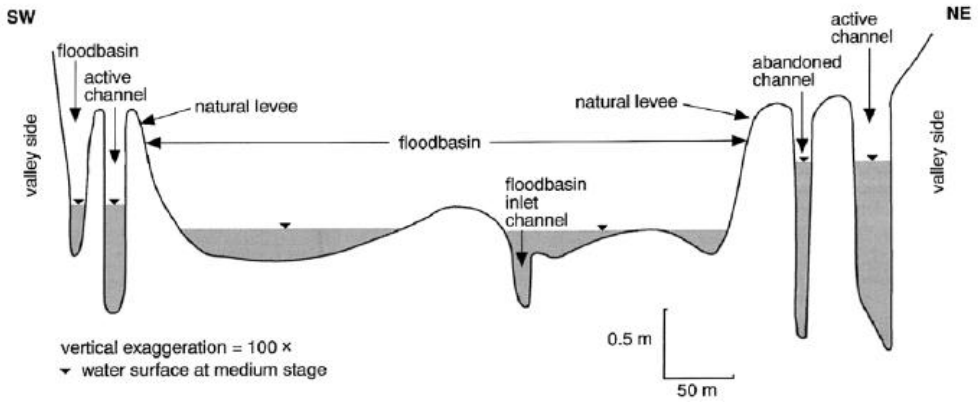

Figure 2.2. Cross-section of the anastomosed Alexandra River, Alberta, Canada (Smith & Smith, 1980).

Natural levées are common features of anastomosed alluvial river morphology occurring through sedimentation during high water stage (Nanson & Croke, 1992) meanwhile braided rivers do not form levées, primarily due to their low bank resistance. The presence of levées symbolises vertical accretion dynamics within low gradient floodplains and indicates water flux between the channel and floodplain (channel-floodplain connectivity). The height of levées in alluvial anastomosed rivers is usually up to a few metres, while their widths may reach up to a few kilometres away from the river (Brierley et al., 1997). Sedimentary units composing levées are established by sandy, silty and muddy splays where the fine fraction increases with distance away from a channel (Morozova & Smith, 2000). Case studies on the Columbia and Saskatchewan Rivers (Adams et al., 2004) have shown two underlying mechanisms of levée formation in regard to their planimetric and vertical dimensions. It is has been found that narrow and steep levées of the Columbia River, occurring in conditions of a high degree of channel-floodplain connectivity, are constructed by diffusive sedimentary processes in contrast to the wide gently sloping levées of Saskatchewan River, which are formed by advection of suspended sediments.

Studies on alluvial rivers sediments are closely related to channel gradient which partially defines the flow energy available for mobilizing suspended, mixed and bed load materials (Schumm, 1985; Church, 2006; Makaske et al., 2009). Typically, alluvial anastomosed rivers exhibit predominantly fine sediments which grade to coarse sand (Knighton & Nanson, 1993; Törnqvist, 1993; Wang et al., 2005b; Makaske et al., 2009) in combination with a low stream power available for their transportation (Figure 2.3). According to the work of Latrubesse (2008) summarizing data on large rivers, the median diameter of bed materials in alluvial anastomosed reaches of large rivers tends to be 0.1-0.5mm.

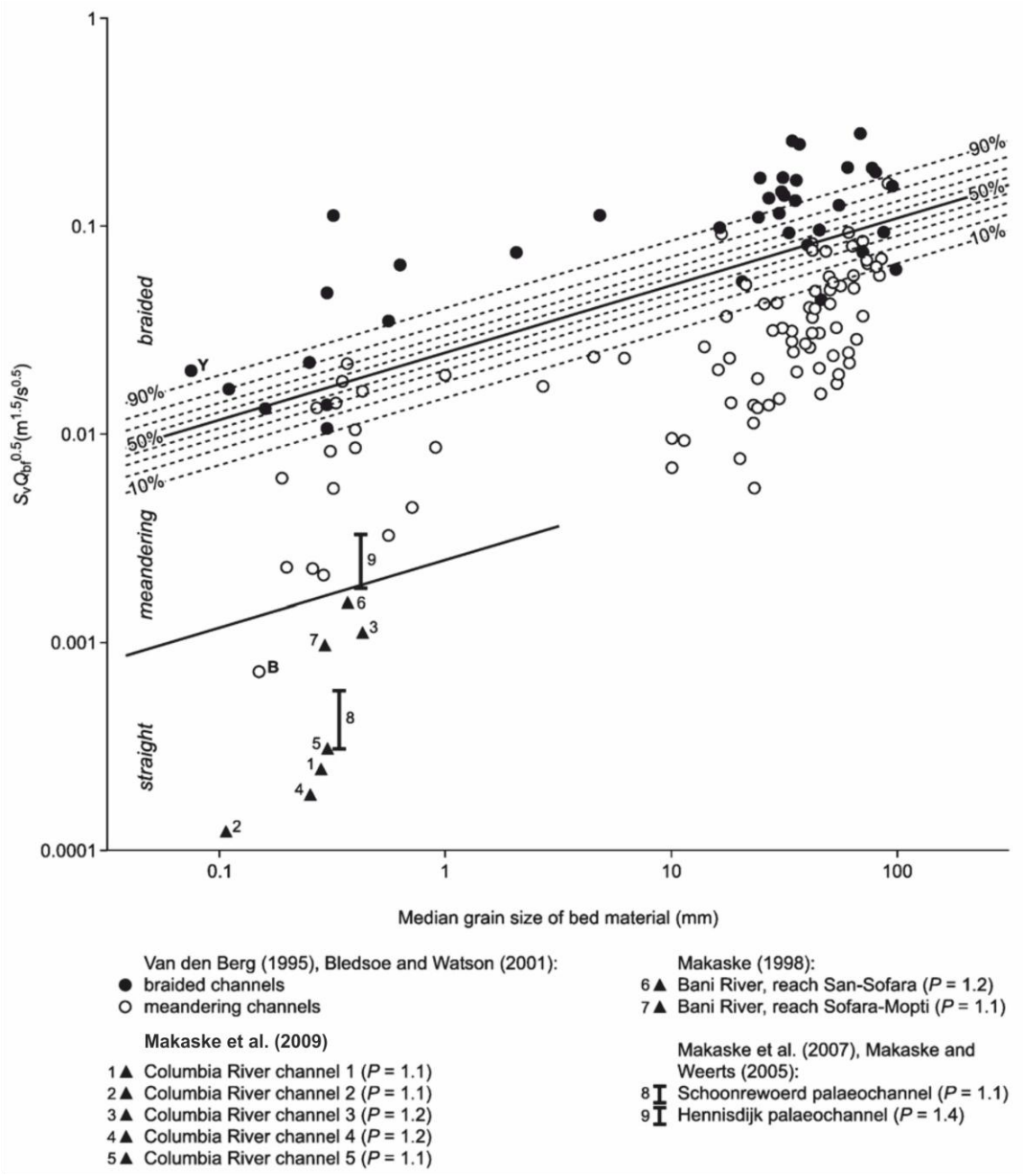

Figure 2.3. Channel type in respect of sediment grain size and the flow energy parameter $S_v\sqrt{Q_{bf}}$ where S_v is valley slope and Q_{bf} is bankfull discharge (from Makaske et al., 2009).

Points B and Y stand for Barlow and Yellow Rivers respectively. Columbia River data points and Makaske (1998), Makaske et al. (2007), Makaske & Weerts (2005) represent data for anastomosed rivers.

Channel continuum and development of the river pattern is closely related to the combination of several factors; an example of the interpretation of these relationships is shown in Figure 2.4 (Church, 2006) although most investigators would see anastomosed channels as stable (contrary to Church, 2006). Correlations between the quality and quantity of transported sediments in relation to channel slope examines

the stability of each fluvial channel type, in such analyses anastomosed rivers appear as very stable due to their indigenous low gradient and fine sediments.

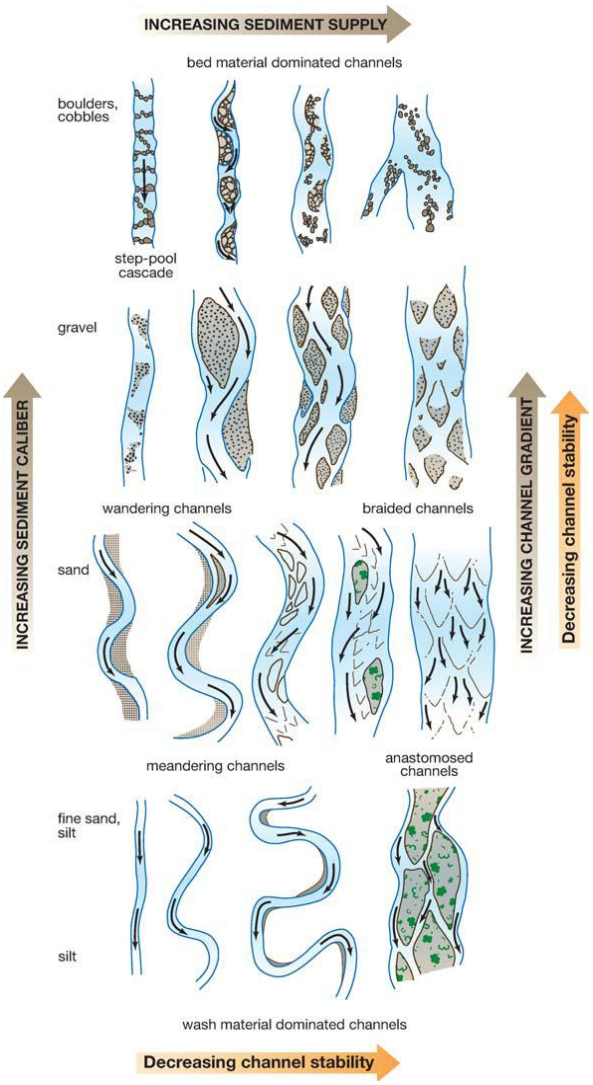

Figure 2.4. Channel types and the principal governing factors (Church, 2006).

It is believed that anastomosed alluvial river's evolution is organized through several processes, namely avulsion, widening and deepening of a new channel, lateral or vertical channel infilling, and channel abandonment (Makaske et al., 2002). Avulsion appears as a sudden change of a river course and formation of a new channel within a channel belt with subsequent abandonment of an existing channel. The newly formed channel is forced to join existing channels as often the sides of an anastomosed floodplain valley are confined (Makaske, 2001). Reoccupation of an abandoned channel due to a base level rise or aggradation processes within an active channel is also recognized as avulsion (Aslan & Blum, 1999). Typical trigger events include floods, any sort of physical waterway blockage (e.g. ice-jams, log-jams, debris dams) or relocation of downstream bars (Slingerland & Smith, 2004). According to Stouthamer & Berendsen

(2007), avulsion processes can be either allogenic (extrabasinal) or autogenic (intrabasinal). A case study on the Rhine–Meuse delta revealed that the interavulsion period, avulsion frequency and location are related to base-level, climate and tectonics (i.e. belong to an extrabasinal factors group), while the period of activity of the channel belt is conditioned by autogenic processes. Thus, understanding the processes governing avulsion and its mechanism gives a key to interpret fluvial processes going on within multichannel river belts.

The stability of anabranching channels at bifurcations is conditioned by equilibrium between the channel's capacity and the supplied sediment load, resulting in deposition when the amount of sediment supply is greater than capacity or erosion in the opposite case (Slingerland & Smith, 2004). However, the ability to bifurcate also depends on stream power, river bank cohesion and aggradation of the river bed; low stream power prevents bank erosion and causes an increase in stored sediment volume which eventually reduces channel capacity and sediment flux. This mechanism leads to occurrence of new lateral channels within a floodplain (Makaske, 2001). The channel gradient and topography of the floodplain accommodating a river channel can also regulate the formation of new channels. For alluvial rivers, the chances of avulsion increase with the ratio of the avulsion course and the existing channel slope because lowering of existing channel gradient does not allow water and sediment to be transported through an existing channel in quite the same volume (Heller & Paola, 1996; Jones & Schumm, 1999). Nevertheless, Stouthamer & Berendsen (2007) concluded that despite the avulsion slope ratio being responsible for avulsion in some cases, it does not necessarily always stimulate new episodes of avulsion. The composition of a riverbed and distribution of channels across the floodplain at some localities could be more important for avulsion then simply the slope ratio (Aslan et al., 2005). The primary importance of sediment regime in stimulation of avulsion is shown by Phillips (2009) in a Texas rivers case study, where avulsion is controlled by different stages of valley infill. Less frequently, avulsion is observed as a result of faulting, tectonic bank breaching or bank collapse (Smith et al., 1997; Peakall et al., 2000). In addition, an avulsion observed within anastomosed rivers is supported by incision of a newly formed channel into a floodplain in order to maintain channel boundaries and integrate into the existing channel network (Slingerland & Smith, 2004).

2.2.2 Mixed bedrock-alluvial multichannel rivers

As noted in the section above, the majority of published studies on multichannel fluvial systems consider rivers with an alluvial character and sandy sediments, rather than bedrock rivers or mixed rivers with gravel/sand/mixed sediment fills over bedrock (Howard et al., 1994). The appearance of the Mekong River in the north-east of Cambodia is defined as "anastomosed channel in rock and alluvium" (Gupta & Liew, 2007), which points out that numerous bedrock outcrops occur along the channel belt. Indeed, there is a gradation of natural streams in respect of their morphological composition from fully bedrock to fully alluvial (Meshkova et al, 2012).

Schumm (1981) suggested three major groups - bedrock, semi-controlled and alluvial - for natural streams on the basis of the underlying substratum such as bedrock or sediment composition through which rivers flow. Developing this idea, Kale (1990) conducted research on upland rivers in the Deccan Trap, India using the classification introduced by Schumm and specified a 40% threshold of bedrock exposures within cross-section channel perimeter (e.g. alluvial rivers showing no bedrock outcrops, semi-controlled with less than 40% bedrock outcrops and bedrock controlled if more than 40% of the cross-section perimeter comprises bedrock).

A similar sub-division was proposed by Chengkun (1985) who has divided river pattern into three types: alluvial, semi-alluvial and non-alluvial. Semi-alluvial rivers as a separate group were distinguished by Kellerhals & Church (1989). As noticed by Ashmore & Church (2001), semi-alluvial rivers are "… not strictly alluvial, but neither are they constrained in their adjustment to the same extent as bedrock streams". A revised continuum of channel types which includes mixed anastomosed channels is suggested by Heritage et al. (2001) according to available energy, sediment transport and channel pattern (Figure 2.5). Note that Heritage et al. (2001) use the term 'anastomosed' in the sense of multichannel without inferring a fine-grained alluvial system is present. In contrast, Tooth & McCarthy (2004) adopted the term 'anabranching' introduced by Nanson & Knighton (1996) in the description of the multichannel mixed bedrock-alluvial Orange River, although it must be noted that Nanson & Knighton (1996) excluded bedrock systems from their classification. To avoid confusion, this study adopts the term 'multichannel' to describe the network character of channels, generally with 'anastomosed' used to define fine-grained alluvial systems Section 2.2.1), unless otherwise qualified.

The margin between bedrock and mixed bedrock-alluvial channels also can be drawn with reference to Tinkler & Wohl's (1998) definition of bedrock channels as "those reaches along which a substantial proportion of the boundary (≥ 50%) is exposed bedrock, or is covered by an alluvial veneer which is largely mobilized during high flow such that underlying bedrock geometry strongly influences patterns of flow hydraulics and sediment movements". According to this definition, bedrock channels that have less than 50% of their area as bedrock could be termed 'mixed bedrock-alluvial' rather than pure bedrock. After all, the unavailability of a strict and widely accepted definition of mixed bedrock-alluvial multichannel rivers is confusing as some researchers might consider a river as being bedrock whereas, at a closer look it may appear that it belongs to a mixed type. For example, the Narmada River in India (Kale et al., 1996) has been included in a bedrock channels description (Wohl, 1999) and in a mixed bedrock-alluvial review by Tooth & McCarthy (2004). Note that classification based on sediment cover (e.g. 40% or 50%) is purely arbitrary and not based on any process understanding. Thus, there is more work to be done to clarify the mixed bedrock-alluvial multichannel rivers definition in order to distinguish them from either alluvial or bedrock multichannel rivers.

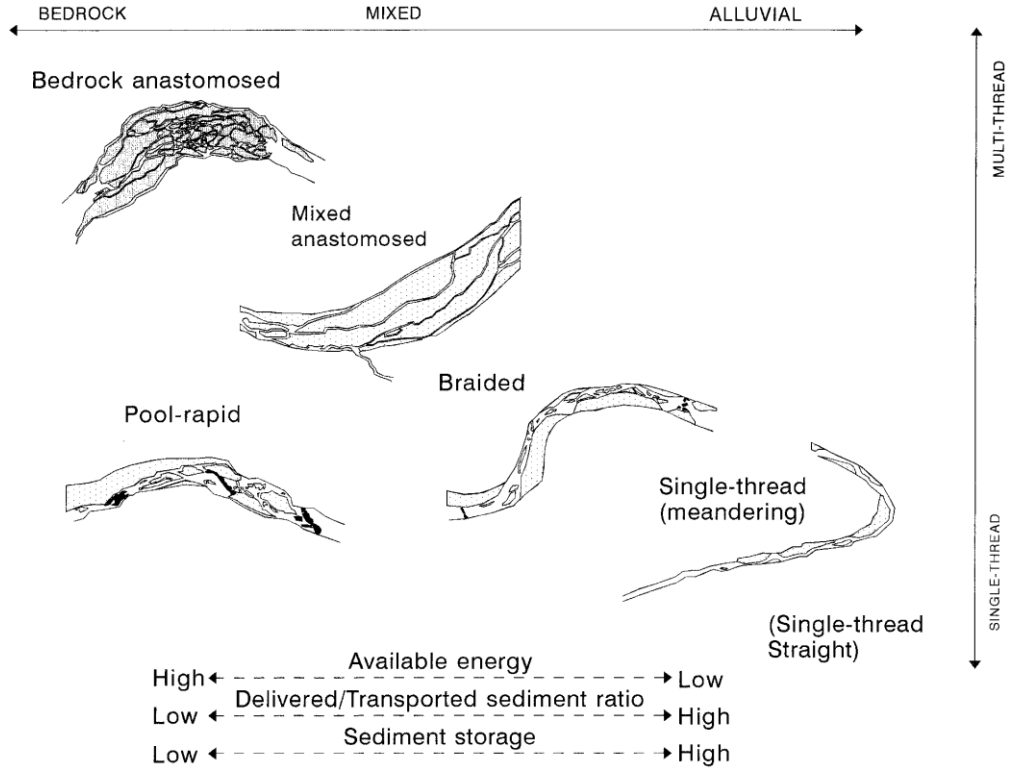

Figure 2.5. River channels continuum in respect to morphological composition (from Heritage et al., 2001).

Known localities of mixed bedrock-alluvial multichannel rivers are reported mainly from warm semi-arid, tropical humid and monsoonal climate zones in Africa, India and Amazon Basin (Tooth & McCarthy, 2004) however, recently they have been identified in harsh continental climatic and sub-arctic zones (Chalov & Chalov, 2009). River sections with mixed multichannel morphology develop widths of a few kilometres and may extend for tens of kilometres downstream. The bedrock riverbed largely defines the architecture of the river pattern and serves as a framework for deposition of fluxes of suspended and bedload sediments into the reaches as well as bedrock erosion materials sourced within the reaches (Figure 2.6).

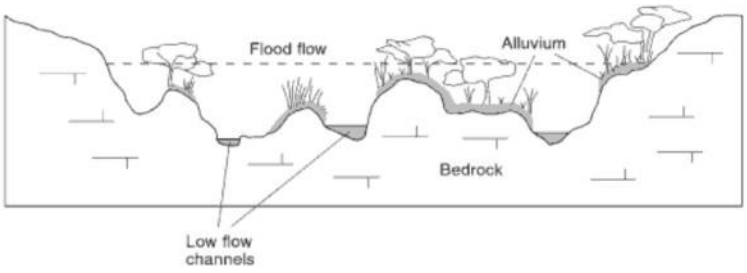

Figure 2.6. Mixed bedrock-alluvial river cross-profile (from Charlton, 2007).

As shown by van Niekerk et al., 1995 (Table 2.1) the main sedimentary morphological units in mixed bedrock-alluvial river are comprised of a variety of sand/gravel bars but in contrast to purely alluvial rivers, typically for bedrock channels series of rapids, waterfalls, riffles and deep pools are also present (Table 2.1). As a rule, the divided river branches of bedrock systems are rarely, if ever, conjoined as one flood-water sheet as flood waters do not rise above the levels of the intervening interfluves and bedrock-cored islands, indicating the often incised character of this river type (Garner, 1966; Heritage et al., 2004) but occasionally, floodplains and levées may be present (Tooth & McCarthy, 2004) as well as river terraces (van Niekerk et al., 1995).

As follows from Table 2.1, the configuration of mixed bedrock-alluvial channels is sensitive to water levels whereby the low flow channel network is only fully exposed during dry seasons. The terrain topography and the structural elements of underlying rocks are used by the flow to create water passes which eventually turn into sets of inner distributary (secondary) channels (Heritage et al., 2004). In a vertical cross-channel profile, secondary channel beds may be super-elevated in comparison with a main channel bottom. Lateral connectivity in secondary channel networks increases with a water level rise, but in the dry season some channels may become completely isolated from the rest of the network (Heritage et al., 1999). Similar to anastomosed alluvial rivers, the water surface elevations between channels in mixed bedrock-alluvial systems may vary across the river (Broadhurst & Heritage, 1998; Van et al., 2012).

Table 2.1. Morphological forms and their description of the Sabie River, South Africa (from van Niekerk et al., 1995).

Morphological unit	Description
Macrochannel bank	Banks of the incised river within which all fluvial deposits are contained.
Rapid	Steep bedrock sections, high-velocity concentrated flow.
Erosional bench	Subhorizontal terrace-like feature on bedrock representing a former active-channel surface.
Pool	Reach of channel below the level of the average channel gradient line. May be bedrock, upstream of a bedrock control; alluvial, upstream of an accumulation of sediment or mixed, a bedrock feature presently accumulating sediment.
Riffle	Accumulation of coarser sediment as a topographic high point as part of an alluvial pool-riffle sequence.
Isolated rock	Outcrop of bedrock or boulder that has no significant impact on the gradient of the water surface.
Braid bar	Accumulation of sediment in midchannel, causing the flow to diverge over a scale that approximates to the channel width.
Lateral bar	Accumulation of sediment attached to the side of the channel, may occur sequentially downstream as alternate bars.
Point bar	Accumulation of sediment on the inside of a meander bend.
Bedrock core bar	Accumulation of finer sediment on top of bedrock in bedrock anastomosing areas.
Lee bar	Accumulation of sediment in the lee of flow obstructions.
Backwater	Stationary or near-stationary bodies of water in bedrock or alluvium or a mixture of both, adjacent to the active channel.
Chute channel	High discharge distributary channel on the inside of point and lateral bars.
Boulder bed	Accumulation of locally derived material exceeding .25 m.
Armored area	Accumulation of coarser sediments due to winnowing of finer material.
Distributary	Individual bedrock, alluvial, or mixed active channel in an alluvial braided or anastomosing system.
Island	Large midchannel sediment accumulation that is rarely inundated.
Terrace	Relic floodplain or valley floor deposits above the present river level.

Bedrock channel morphology is determined by the resistance of bedrock in relation to the power of fluvial processes (Tinkler & Wohl, 1998). Non-uniformity of channel gradient is expressed through alternations of steep with low to moderate gradient zones creating steps in a long profile. Mainly the nature of the longitudinal gradient is due to the fact that such rivers cross diverse geological units along their courses (Figure 2.7). The reported compositions of underlying bedrocks are often those with a higher degree of resistance, e.g. crystalline basement rocks (granites, gneisses, gabbro, rhyolites) and quartzite dykes (Tooth & McCarthy, 2004) or other igneous and metamorphic rocks (Heritage et al., 2004). Channel gradient variations create a reference to a local base-level for the upstream reaches and ultimately regulate an adjustment of the whole anastomosed section relative to sea-level (Keen-Zebert & Curran, 2009).

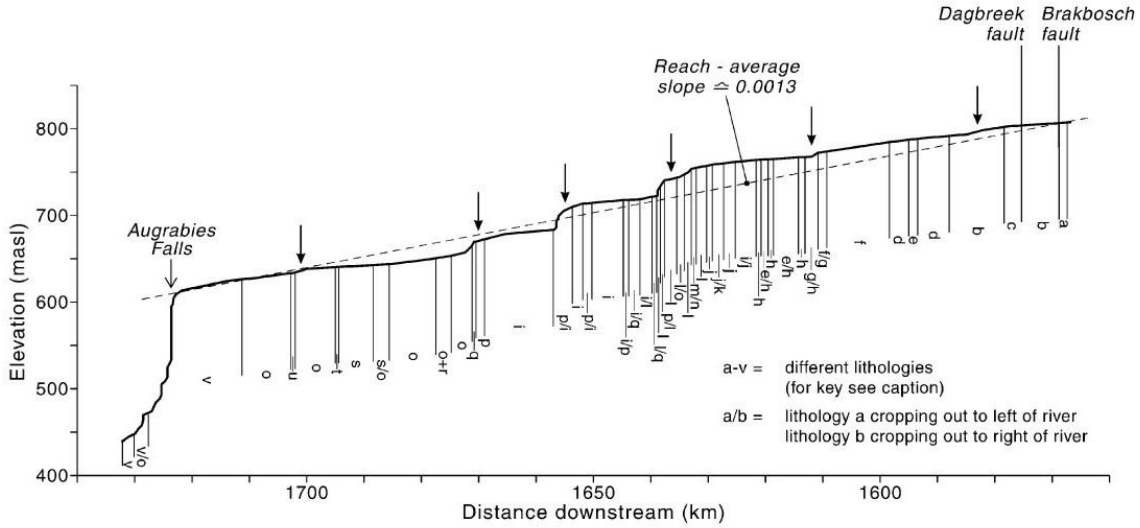

Figure 2.7. Long profile of the mixed bedrock alluvial anabranching Orange River showing alternation of geological units along the river course (from Tooth & McCarthy, 2004). Steeper reaches (bedrock or bedrock-alluvial) are indicated by arrows.

Key to geology: a = metabasalt, felsic lavas, greenschist, conglomerate, ferruginous chert; b = quartzite and schist grading into banded gneiss and migmatite; leucogneiss, amphibolite and serpentinite lenses; c = porphyroblastic biotite gneiss; d = weakly foliated biotite granite; e = migmatitic, biotite-rich and aluminous gneisses; f = amphibolite, amphibole gneiss, biotite gneiss, pelitic gneisses, lenses of calc-silicate rocks; g = unfoliated, granophyric granite porphyry; h = light-grey, moderately to well-foliated granite; i = charnockitic adamellite; j = medium-grained, moderately foliated, mesocratic or porphyritic granite; k = brown weathering, porphyroblastic to megacrystic gneiss; l = mesocratic, well-foliated, adamellitic granite gneiss; m= coarsely crystalline to megacrystic, quartz-feldspar gneiss; n = fine- to medium-grained, banded biotite gneiss, muscovite gneiss and sillimanite-bearing gneisses; o = pink weathering granite gneiss with a granular or augen texture; p = quartzite, sericitic and/or feldspathic in places; conglomerate lenses; q = quartz-rich and mafic calc-silicate rocks with wollastonite and marble lenses; staurolite schist; r = leucocratic quartz-microcline gneiss, amphibole gneiss, quartzite; s = migmatitic, porphyroblastic biotite gneiss with amphibolite lenses, leucogneiss; t = quartz-plagioclase-amphibole gneiss; u = quartz-topaz gneiss; v = grey to red-brown granite gneiss;

Variable channel gradient responsible for common rapids and waterfalls fosters swift currents and provides acceleration to the mainstream flow producing diverse sculpted bedrock erosion forms. Submergence of several erosional features, for instance potholes, leads to enlargement of distributary channels network through creation of new inner channels. Bedrock is also subject to chemical weathering processes but the rates of rock destruction vary with environmental conditions and each rock type (Wohl, 1999).

Multichannel mixed bedrock-alluvial rivers show high lateral stability of pattern over time due to bedrock confinement and (less commonly) cohesive bank materials (Tooth & McCarthy, 2004). Changes occurring within a main channel are manifested by a volume and/or location of mobile alluvial content and riverbed vertical incision (Moon

et al., 1997). The models of rates of incision suppose it to be dependent upon bed erodibility, flow characteristics, drainage area and channel gradient (Howard et al., 1994), all of which are conditioned by bed lithology and climate (Rosenbloom & Anderson, 1994; Jansen et al., 2010).

Differentiation of sediment flux in multichannel rivers of mixed bedrock-alluvial morphology is not described in the literature as a matter of specialized interest but, relying on depositional forms, it is reasonable to suggest that sediments cover a wide range of particle size from fine sand to large boulders, relevant to either bedrock or alluvial anastomosed channels (e.g., Jansen & Brierley, 2004).

Table 2.2. Example of vegetation from semi-arid climate associated with geomorphological features of the Sabie River, South Africa (from Moon et al., 1997).

Plant community	*Characteristic species*	*Morphological association*
1 Reed-shrub	*Phragmites mauritianus, Securinega virosa, Phyllanthus reticulatus*	Active channel bars
2 Bedrock riparian forest	*Breonadia salicina, Syzigium guineense, Kraussia floribunda*	Bedrock core bars, bedrock anastomosing channels
3 Alluvial riparian forest	*Combretum erythrophyllum, Lantana camara, Ficus sycomorus*	Islands, seasonal and macro-channel bars
4 Transition	*Diospyros mespiliformis, Acacia robusta, Euclea natalensis*	Macro-channel slopes, macro-channel islands
5 Savanna	*Spirostachys africana, Dicrostachys cinerea, Grewia bicolor*	Upper macro-channel slopes, older macro-channel islands

Tropical monsoonal climate rivers usually exhibit abundant riparian plant communities (e.g. Maxwell, 2001; Try & Chambers, 2006; Bezuijen et al., 2008). Moreover, it is documented that even in semi-arid climates, mixed bedrock-alluvial rivers exhibit riverine vegetation associated with each particular part of their morphology (Table 2.2). The presence of distinctive plant species is of primary importance in maintaining a natural balance in riparian ecosystems, and may influence such geomorphological factors as bank stability and bank profile. Plants distributed within channels are involved in the regime of sedimentation and may indicate channel evolution processes such as channel age, sediment and flood fluxes (Moon et al., 1997). Described within mixed bedrock-alluvial reaches, vegetation communities reflect the substrate character and help classification of each environment as a part of a channel pattern continuum (Van Coller et al., 1997). The association of a particular vegetation type with a river landscape may be useful in remote mapping of multichannel mixed bedrock-alluvial rivers using satellite images, granting the relationships are known in each given case (MacAlister & Mahaxay, 2009).

2.3 Planview channel metrics

2.3.1 Channel networks

The prevailing published studies on river networks mainly analyse “tree” or “dendritic” type (Figure 2.8) river networks extracted through calculations of DEM parameters or by processing vector or raster data representing a fluvial system (Turcotte et al., 2001; Mayorga et al., 2005; Colombo et al., 2007; Zang & Huang, 2009). Multichannel rivers by definition have got numerous channels which form a “looped” channel network (Figure 2.8). A distinguishable characteristic of a looped network is that, in contrast to a dendritic pattern, it has several possible flow passes from one point to another (Wu, 2007). Channel network morphologies are popularly described numerically through braiding intensity and sinuosity indices and calculations of the hydraulic characteristics of links within the network streams (Howard et al., 1970; Mosley, 1981; Nanson & Knighton, 1996; Chew & Ashmore, 2001; Egozy & Ashmore, 2008; Rhoads et al., 2009). Besides, channel networks can be extracted from historical materials where lateral channel shift is detected by comparing channel middle lines rather than contours of the entire network (Micheli & Kirchner, 2002). The latter approach is fully applicable to the Mekong within the study area because historical maps and aerial photography can be compared with more recent maps and images. Furthermore, the analyses of spatial overlays of channel/bedrock channel networks and GIS layers representing topography, geology, tectonics and land cover may reconcile correlation between channel pattern and environmental conditions of the river within an area of interest.

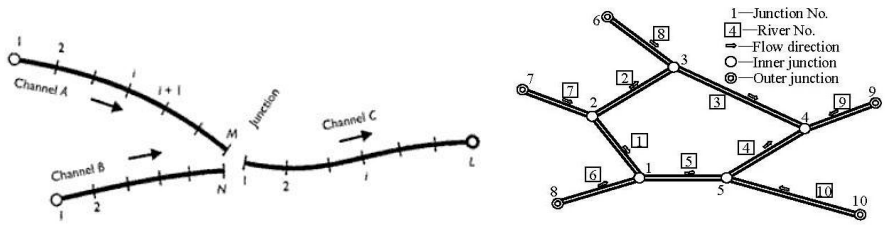

Figure 2.8. Dendritic (left; (Wu, 2007)) and looped (right; Sen & Garg, 2002) channel networks.

Each segment in a looped channel network is represented by a line along a channel which splits the area of a channel onto two equal parts, (i.e. the channel centre line). Numerically, the width of an irregular polygon can be obtained from calculation of the

minimum dimension rectangle with the same area and perimeter as a given polygon. In the case when a polygon approaches a circular shape, its width value equals the square root of its area (Buckingham & Whitney, 2007). Hence, a numerical value of each channel width is not sufficient for the network construction. Diverse spatial orientation of channels in a looped network makes an attempt to delineate and connect channels manually complicated, therefore a few studies suggest specially designed automated methods (Mayorga et al., 2005; Olivera et al., 2006; Pavelsky & Smith, 2008). Known techniques in use include raster data thinning algorithms and manual digitizing of the approximate location of mid-channel lines (Hasthorp & Mount, 2007).

Numerous works on river confluences have gradually led to an interest in the scientific society towards investigations of channel bifurcations resulting from avulsion processes. Geometrical parameters of braided streams at points of bifurcations as well as hydrological properties of partitioned flow in newly formed channels have been the subject of numerous flume experiments and case studies based on full scale rivers (Wang et al, 1995; Federici & Paola, 2003; Burge, 2006; Ashworth et al., 2007; Hundey & Ashmore, 2009). Channel networks planform assessment often employs a parameter of bifurcation angles observed either in a field or during flume simulations of braided streams (Frederici & Paola; 2003; Miori et al., 2006; Bertoldi & Turbino, 2007; Bertoldi et al., 2009; Egozi & Ashmore, 2009).

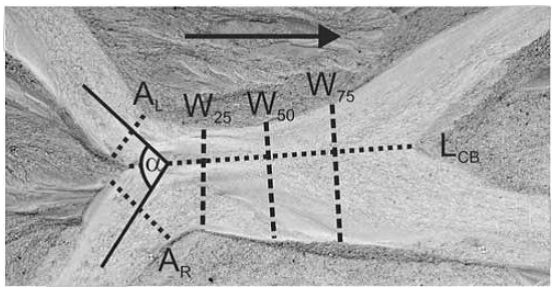

Figure 2.9. Definition diagram for measurement of channel length (L_{CB}), channel width (W_{25}, W_{50}, W_{75}), anabranch width (A_L/A_R stand for left and right branches respectively) and confluence angle (α) (from Hundey & Ashmore, 2009).

Laboratory research on braided streams under variable hydrological and sediment supply performed by Frederici & Paola (2003) distinguished two types of channel bifurcations such as “stable” when both channels remain open and “switch” if one or both channels experience processes leading to closure. They found that the stability at bifurcations is determined by uniformity of flow and high Shields stress. The same authors specified that braided streams bifurcation angle between 40-60 degrees is typical for those maintaining equilibrium. Comparison of this value with data on other

rivers allowed Burge (2006) to conclude that bifurcation angles are not related to Shields stress or vegetation cover and practically are similar for different braiding rivers. The latest work of Hundey & Asmore (2009) describing experiments on braided flume-streams and applying the same procedures on full-scale rivers revealed a linear relationship between channel link length (L_{CB}) (Figure 2.9) which is equal to 4-5 times of a main channel width; confluence/bifurcation length increases with higher discharge values. Experiments under conditions of constant discharge and sediment supply have shown that the number of braided stream bifurcations increases as a function of dimensionless water discharge (Bertoldi et al., 2009). These results resonate with data from Ashmore (2001) showing that bifurcation/confluence node density is close to the square root of the discharge. Flume experiments reproducing braiding streams are important as a theoretical basis for research into real world multichannel rivers. However, despite the advantages inherent in laboratory studies such as regulated input parameters, detailed documentation of water/sediments dynamics and precise output measurements, flume experiments cannot model, for instance, complex topographic settings of floodplain, bedrocks or palaeo-channels which nevertheless can play a significant role in bifurcation processes. Besides, laboratory stream behaviour cannot be linearly scaled up and directly applied to fluvial systems which are greater by at least one order of magnitude (Parsons et al., 2007).

Despite differences in the way to describe and classify multichannel rivers, various morphological indices and ratios are commonly applied to separate natural stream types. Basic planimetric measurements indicating the width and length of features such as channels at different stages of discharge, channel belt (including floodplain), inter-channel islands and bars, are often combined with channel depth and channel bed (or water slope) gradient measurements, with the aim of showing distinctions in fluvial system morphology and identifying a river system response to external controls (Brice, 1960, 1964; Howard et al., 1970; Rust, 1978; Hong & Davies, 1979; Mosley, 1981; Germanoski & Schumm,1993; Nanson & Knighton, 1996; Chew & Ashmore, 2001; Rhoads et al., 2009). Channel metrics are used to calculate widely recognized parameters of channel sinuosity (ratio of channel length to the length of meander belt axes (Brice, 1964)) and braiding intensity (number of channels per cross-section (Howard et al., 1970)). Despite the long history of use of these parameters, a systematic assessment of measuring methodology has only been undertaken recently. A flume constant-discharge experiment was conducted in order to identify two main morphological parameters such as channel count and total sinuosity (Egozi & Ashmore, 2008). Verification of a braided stream sampling procedure has revealed that cross-sections employed in channel counting should be spaced at an average wetted width

distance within an indicative 10 times average wetted width length of a stream in order to obtain a precision of 20% of the mean.

The importance of the study of channel network bifurcation angles is indicated by a continuing project on the Jamuna, Padma and Ganga Rivers using the CEGIS monitoring system (CEGIS, 2010) where the range of channel network bifurcation angles captured from satellite images is a parameter in erosion models and is recognized as an important component for the prediction of lateral channel migration (Gupta, 2007). Numeric modelling in deltaic environments shows the connection between the angular characteristics of channel bifurcations and sediment cohesiveness (Edmond & Singerland, 2010). The most recent studies involving measurements of channel bifurcation angles also show its relationship with the curvature of the upstream bend, which is also an element of planimetric channel network configuration (Kleinhans et al., 2008; Hardy et al., 2011).

2.3.2 Channel islands

Characteristics and ratios between parameters obtained from polygonal planview shapes in combination with remote sensing techniques are used to identify a range of ground features such as urban surface types, lakes, and icebergs (Vila & Machado, 2004; Silva & Bigg, 2004; Frohn et al., 2005).

The interest in planform island metrics arose in the 1970s and 1980s when a number of papers on streamlined islands and their minimum-drag forms were published (Baker, 1979; Baker & Kochel, 1979; Komar, 1983; Kehew & Lord, 1986). The shape of streamlined islands was set equal to the lemniscate loop where island length (L) is assumed to be the longest axis of the lemniscate and width (W) is the shortest (Figure 2.10).

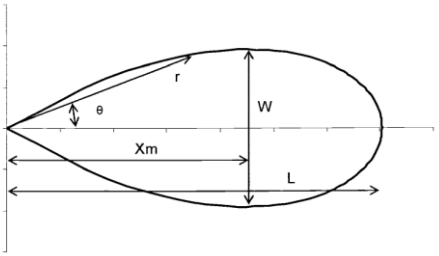

Figure 2.10. The lemniscate shape dimensions (from Wyrick, 2005); see text for more details.

The aspect ratio (L/W) is very common in describing island morphology in different types of fluvial systems. The parameters of fluvial streamlined island shape described by Komar (1983) has been specified so that the streamlined island aspect ratio lies between 3 and 4 (Baker, 1979) and the position of a maximum island width X_m (Figure 2.10) is 0.6-0.7 of its length (Wyrick, 2005). Furthermore, recent studies show a connection between morphological characteristics of river features and its hydrology (Zanoni et al., 2008). For instance, it is evident that the minimal stream energy loss occurs when the aspect ratio is around 3 (Wyrick, 2005) which agrees well with the conclusions of Baker (1978). In braided rivers, the aspect ratio of braid-bars has been related to channel-belt width and channel depth such that reach-scale predictions of morphology can be made in a reflexive fashion (Kelly, 2006).

2.3.3 Lateral channel stability assessment

Modern fluvial erosion studies offer a number of approaches based upon aerial photographs (Gurnell, 1997; Fuller, 2007), satellite images (Kummu et al, 2008; Peixoto et al., 2009), DEM or 3D data (Li et al., 2007), GPS surveys, vector thematic layers (Sarma & Phukan, 2004) and their combination (Lawler , 1993; Uribelarrea et al., 2003; Buckingham & Whitney, 2007; Lehotský et al., 2009). For example, it is possible to follow chronological modifications of landscape features using plan view images of the floodplain area and layers containing different time series of river bank positions (Li et al., 2007). Selection of a method to analyze river changes in historical context is based upon available datasets, software and qualification of people implementing it.

Technical implementation of bank erosion analyses is based on estimation of bank retreat/aggradation, ultimately represented as a polygonal feature obtained as a result of overlay of digital layers representing planview contours of a river. GIS assessment of irregular polygon width is possible via constructing bounding rectangles (see Section 4.1.3.3 for more details) where dimensions of a rectangle with the same area and perimeter as an original polygon are measured (Buckingham & Whitney, 2007). Another way of obtaining irregular polygon width is to draw a number of cross-sections normal to the base-line and then measure the length of each line (Rhoades et al., 2009). This method is known for coastal and river erosion studies represented by linear elongated polygons and also applied in the topologically constrained lines construction method (Moran, 2003; Liu & Sherman, 2008). Hence, it is not directly applicable in assessing the width of erosion/accretion polygons framing islands due to the base line required to be a polyline object; while islands are represented by circular form polygonal

objects. Often, the technical aspect or methodology which allows extraction of erosional measurements by analysing vector layers using ArcInfo/ArcView GIS is not precisely specified. Currently, a GIS tool especially designed for river bank erosion exercises is not supplied within any software package, hence assisting scripts and small software applications are available (Thieler et al., 2003; Moran, 2003; Clark et al., 2008; Liu & Sherman, 2008). Thus, development of the methodology allowing assessment of river bank erosion using a standard set of functions included in ArcGIS remains important due to additional software either being costly or not publicly available. At present, river bank erosion assessment requires time consuming preparation of the input data and learning the way software operates.

3 Study area

This chapter represents the description of the study area comprised from existing literature up to date (see Section 2.1). It summarizes known facts on geomorphology, geology, tectonics, hydrology, vegetation and soils in order to outline the area of interest and provide a background for further expansion and filling gaps in knowledge on the multichannel mixed bedrock-alluvial section of the Mekong River in north-east Cambodia.

3.1 General description

The selected study area in Cambodia represents a well-developed complex of multiple channels of the Mekong River between the left bank towns of Stung Treng and Kratie, in the north-east part of Cambodia. The study area does not embrace all the watershed area of the Mekong in north-east of Cambodia because this research focuses on an investigation of the multichannel section of the Mekong alone. The main study area is framed by a rectangle with coordinates of the left top corner and right bottom corner 105°51'42.05''E/13°31'7.40'' and 106°7'40.77''E/ 12°28'33.98'' respectively (Chapter 1, Figure 1.2A and 1.2B). The study area covers 3604 km^2 of terrain and a distance of 126 km along the main river length. Additional to the main study area, a study sub-area (Chapter 1, Figure 1.2A) lying within the limits of the frame mentioned above was chosen. The latter territory represents a good example of the multichannel section of the Mekong where the dynamics in channel morphology (lateral erosion/accretion) can be accessed via the comparison of the historical remote sensing images (see Section 4.1.2.2).

The Mekong flows from north to south and within the study area has no significant tributaries on either side of the river. The Sekong, Se San and Sre Pok Rivers are the only major left hand side tributaries (i.e. east bank) which join the Mekong just north of Stung Treng as one conjoined confluence (see Chapter 1, Figure 1.1B). Together these rivers make a significant contribution to the discharge of the Mekong equal to 25% of the mean annual flow volume in Cambodia. Until recently the only possibility to cross the Sekong River was by a single vehicle ferry which ensured problematic access to Stung Treng overland from the north of the country.

Stung Treng is a small town with a 15,514 population (SCW, 2006) and is situated in a rural environment. The town is the capital of the Stung Treng province that includes five districts, which are further subdivided into 34 communes (villages). The river discharge gauging station at Stung Treng operates since 1910 till present (CNMC, 2006) therefore it has a well calibrated long record of the local Mekong River hydraulic regime (see Section 3.4). The Mekong River at Stung Treng is represented by a single wide (from 1 to 2 km) and deep (up to 18m) channel with high banks (15m) that are locally sloping and these are often used for river gardens (Figure 3.1).

Figure 3.1. The Sekong River at the junction with the Mekong. River gardens at the foreground and Sekong Friendship Bridge at the background.

The macrochannel, defined as the total channel width between the macrochannel banks (Section 2.2.2, Table 2.1), remains single thread over the next 5 km downstream of Stung Treng, but becomes 1 km wider (i.e. total width < 3km) and is then split by Kaoh Sralay island into two channels (Chapter 1, Figure 1.2A). The distance between the right and left banks of the Mekong then increases up to 5 km. At this point significant channel bifurcations occur within this 5km wide channel corridor and the first bedrock outcrops can be seen as ridges of rocks often orientated obliquely across the river. South of Kaoh Sralay island a multichannel reach that consists of bedrock-constrained channels occurs (the study sub-area) which is called Rapids de Prek Patang (Chapter 1, Figure 1.2A).

At this point, the Mekong changes from a general north-south alignment and flows to the south-east, occupying a broad area characterised by numerous channels that

extend for 20 km through the rapids. The majority of the channels are not navigable by commercial small ships during the dry season due to outcrops of bedrock occurring transverse to the main flow direction (Figure 3.2) and are only passable by small canoes.

Figure 3.2. Prek Patang Rapids near east side of the Toan Han island (dry season). Flow right to left.

After passing the Rapids de Prek Patang, the river course changes again to the south-west and then back to south-east but the multichannel character still can be observed until it comes to the Sambor Rapids lying 35 km north of Kratie. The multichannel reach of the Mekong between the Rapids de Prek Patang and the Sambor areas is characterised by narrow and deep channels separated by elongated islands. In this latter section of the river, linearly extended bedrock exposures appear aligned in accordance with the direction of the flow (Figure 3.3). The greatest distance between the two main river banks (11 km) is observed at the Kaoh Ro Ngiev island area whereas downstream of Sambor Rapids the distance between the main banks reduces significantly, being 1.5-2 km on average close to Kratie.

Figure 3.3. Bedrock outcrops in the middle of the river channel.

In the 1960s, sites at Stung Treng and at Sambor were proposed for dam construction for the purpose of hydroelectricity, irrigation support, navigation and flood control. Potential dam sites were investigated in detail; however, the dams were not commissioned. Investigations of the surroundings of the Sambor Rapids revealed a single buried channel extending along the west riverbank from Sambor to Kratie (Stapledon et al., 1961). The buried channel is filled by alluvial sand and gravel deposits and is around 2 km wide and 13.7 m deep (maximum) within the same range of riverbed elevation values as the present main channel. At present there are several small perennial lakes which additionally indicate the evident limits of the abandoned channel (see Section 3.2, Figure 3.6).

The Sambor Rapids are represented within the main channel by numerous bedrock exposures and a few small islands, all vegetated by bushes (Figure 3.4). At Kratie the river is unimpeded by rapids and thus appears calm and is a meandering alluvial channel with high (20 m above the dry season water level) river banks.

Figure 3.4. The Sambor Rapids in Kratie province. View from the left bank of the Mekong, dry season. Flow right to left.

Field investigations of the study area and the sub-area are hindered by the low quality or absence of roads along the Mekong and the impenetrability of some of the minor channels by boat due to numerous bedrock outcrops, rapids and water turbulence. By land, it is only possible to travel along the left bank of the Mekong for 20 km downstream of Stung Treng up to Srae Krasang village and 30 km upstream from Kratie up to Ph. Sambo village. Therefore remote sensing data are highly useful to this study.

3.2 Topology and morphology of the study area

The study area is situated within the limits of the Cambodian northern plain, framed by the Dangrek Escarpment to the north (aligned with 14°30'N latitude and forms a natural border between the Khorat Plateau in Laos), the Cardamom (Kravanh) Mountains in the south west of Cambodia and the Eastern Highlands (Figure 1.1.B). The latter uplands are the source of the Sekong, Se San and Sre Pok rivers with 60% of the total catchment area lying in Vietnam and the rest in Cambodia. Hence, within the study area, low ridges that are terminations of ranges of the Eastern Highlands are the only features that provide the highest elevation marks (up to 130m) within the study area. A typical termination of an upland ridge can be seen in the area to the south-east of Stung Treng. Apart from that, no other significant regional-scale elevated landscape features can be identified, the study area being dominated by a low plain that is extensive to the west and more restricted east of the Mekong River (Figure 3.5).

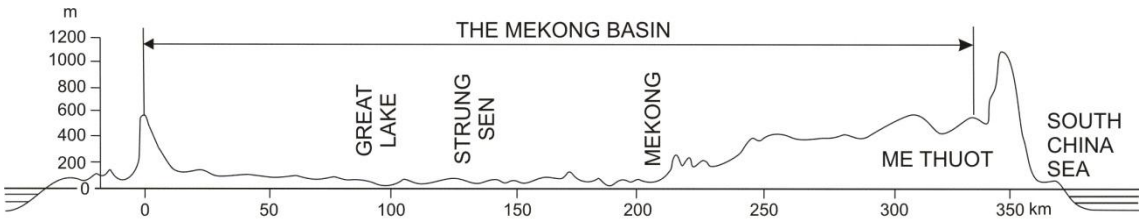

Figure 3.5. Latitudinal profile of the topography either side of the Mekong River at 12°40'N (nr. Kratie) (Hori, 2000).

In general, elevation reduces from the north to the south through the study area from 60 m above mean sea level at Stung Treng to 20 m at Kratie; the gradient is 0.32 m per kilometre on average. This parameter is surprisingly high as here the river crosses the broad Cambodian Lowlands, but the gradient is similar to the gradient of the Mekong River in northern Laos where the river runs through a mountainous region. In fact, downstream of Vientiane, rapid change of elevation along the course of the river can be observed only twice: at the Khone Falls (Chapter 1, Figure 1.3) and at the rapids area in the north-east Cambodia (i.e. the Rapids de Prek Patang and Sambor Rapids), which includes the present study area.

The plain either side of the river is slightly undulating, which mostly likely is due to Cenozoic epeirogenic folding (UN, 1993), with swells and lows orientated approximately west to east. The river is slightly incised throughout the study area and is closely confined by the plain to the east and to the west. The terrain surface gently elevates away from the river, reaching 80-160 masl within the limits of the study area. The axis of a major regional-scale syncline crosses the Mekong at the Rapids de Prek Patang (see Section 5.1.3, Figure 5.31) trending from the north-west to the south-east. It extends for 150 km and presumably guides the river course within the northern portion of the study sub-area to the south-east (UN, 1993). Thus, the Cenozoic folding of the older plain and the regional syncline, together with local fault alignment, provides an important control on the topographic complexity and channel alignment at the regional and local scales.

Natural levées appear on both riverbanks only in the south of the study area immediately downstream of the Sambor Rapids (JICA, 2003) and these are also well-developed further downstream on the Mekong south from Kratie (Figure 3.6). Their width varies from 200 to 600 metres; the height of levées may be up to 10-15 m above the floodplain (UN, 1968). It remains unclear whether the levées are ancient or recently active flood features but the current extent of annual flooding includes the area of their development. The surface of levées descends away from the riverbank with

gradients between 0.1 (prominent levées right bank downstream of Sambor) and 0.005-0.001 (gently elevated levées near and downstream of Kratie).

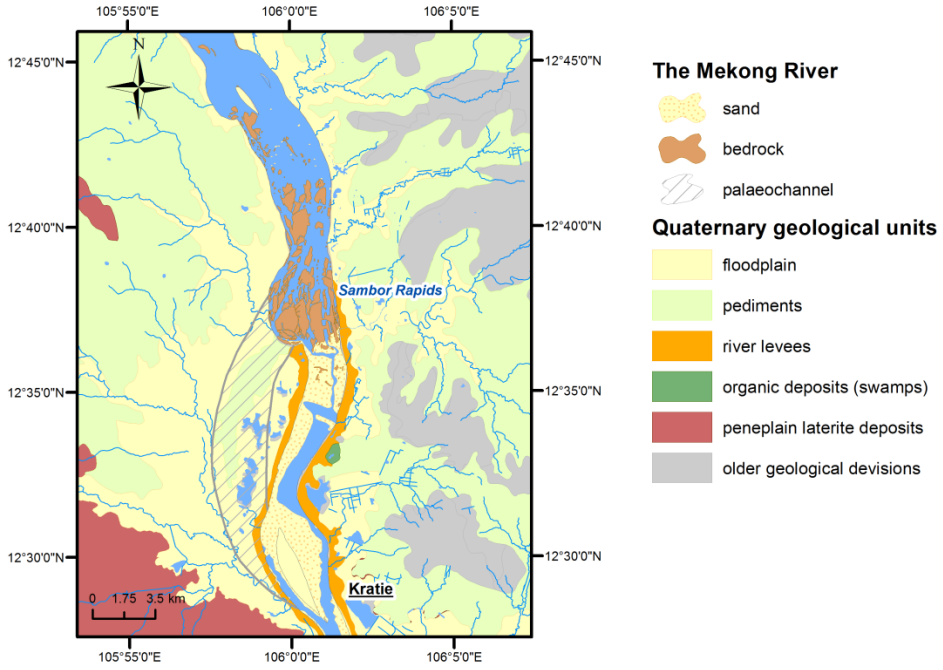

Figure 3.6. The development of natural levées in the south of the study area (produced using digital data from JICA, 2003).

A notable attribute of the studied reach of the Mekong River is the general absence of modern river terraces close to the river. Nevertheless, ancient terraces of the Mekong in Cambodia were reported by Takaya (1967) and Carbonnel (1972). The findings of these publications correspond broadly with the results of investigations of the ancient river terraces of the west bank of the Mekong in northeast Thailand, Nakhon Phanom province (Wongsomsak, 1992), located approximately 450 km upstream of Stung Treng. As reported by Takaya (1967), there are six Quaternary formations across Cambodia (Figure 3.7) whereas river alluvium is confidently identified at altitudes not exceeding 30 masl; exposed at the higher altitudes is a Thick Laterites Formation, represented by heavily weathered deposits which could have fluvial origins (i.e. composed of alluvium). It ought to be noted that the profile established by Takaya (1967) is based on data collected in areas of the Mekong from Sandan (25 km upstream of Kratie) to as far downstream as the Tonlé Sap, therefore outcrops of Quaternary age in north-east Cambodia located at the higher altitudes were not explored and included in the profile. Nonetheless, Takaya (1967) shows a correlation

of the described Mekong terrace formations with those found in Thailand and defines their age as Pleistocene and Holocene.

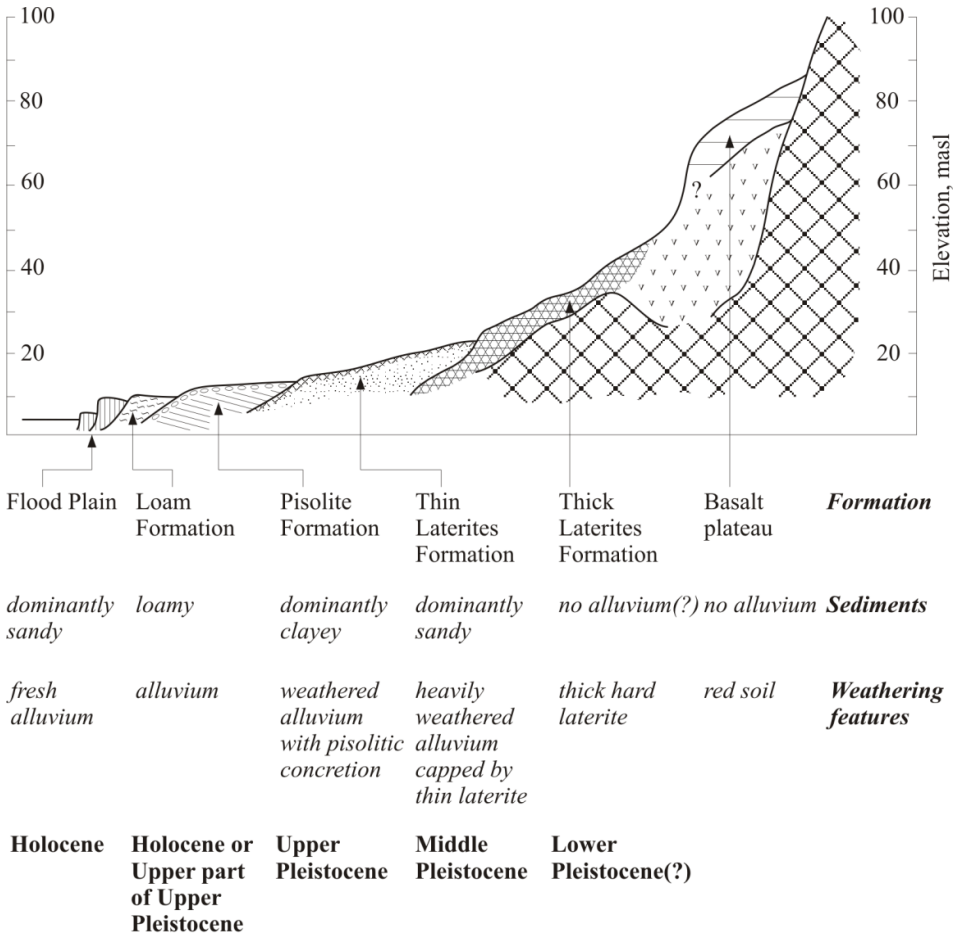

Figure 3.7. Cross-section of the Quaternary geological units in Cambodia (redrawn from Takaya, 1967).

Soon after the publication by Takaya (1967), Carbonell (1972) investigated the east bank of the river within the area of interest. There are several surfaces that he refers to as terraces; the significant altitudes being a 100, 40 and at 20masl level. The highest, the 100m terrace, located outside of the study area, is degraded severely and tectonically warped and in places covered by basalt flows; the age of the latter is Neogene-Quaternary (Ragin et al., 1995). This 100m level was dated in the 1960s as c. 650,000 years BP (Middle Pleistocene) using fission track dating of the basalts with a similar age ascribed to tektites found on the terrace gravels (Carbonnel, 1972). Carbonnel (1972) also reported possible terrace fragments between 15m and 2m above the low flow level of the river.

Reporting and interpretation of the average depth of the river in this area would have no physical meaning because the Mekong has plentiful rapids, local shallows and

minor pools as well as so-called 'deep pools' within all channels. The deep pools are defined as elongated bathymetric lows in accordance with the direction of the main stream flow which are significantly deeper than the surrounding riverbed. These deep pools retain water throughout the dry season (Chan et al., 2003). Among 65 pools identified in the study area by interviewing local fishermen, the majority are 25-30m deep during the dry season whereas the deepest ones reach up to 80 m; areas may vary from 10 ha to 200 ha as a maximum (Chan et al., 2003). Deep pools provide an important habitat for fish, dolphins and other aquatic biota. Currently, the number of fish species in this reach of the Mekong is up to 200 (Beasley et al., 2007). Hence, the area from the Laos-Cambodian border as far south as Kratie is very famous for Irrawaddy (*Orcaella brevirostris*) dolphins, as it is known that river dolphins choose deep fresh water habitats in tropical and subtropical climate where fish are abundant.

From the results of the latest studies of the Lower Mekong Basin deep pools morphology (Conlan et al., 2008), there are six pool types which are conditioned by morphology of channels and river network in total (Figure 3.8). Conlan et al. (2008) report that the main characteristics of deep pools such as width, length, depth and spacing correlate with channel type and channel width, water surface gradient, bedrock resistance and ultimately can indicate the age of the river channel which points out that deep pools investigation is important in context of understanding the morphology of the entire fluvial system.

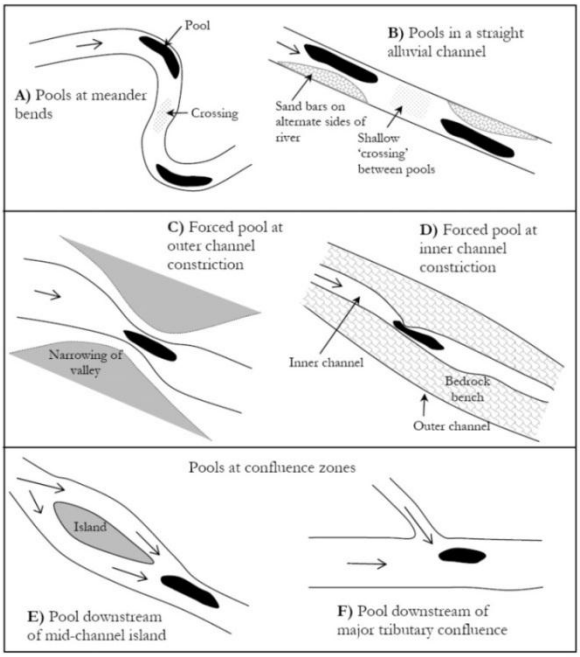

Figure 3.8. Major pool types found on the Lower-Mekong River (from Conlan et al., 2008).

The number and position of observed pools (Chapter 1, Figure 1.2A and B) contributes towards the idea that locally there is intensive vertical erosion rather than lateral erosion. Narrow channels, frequently obstructed by coherent rocky outcrops, are often occupied by a constellation of closely-spaced, shorter, deep pools in contrast to alluvial reaches where pools are fewer but more extensive and relatively shallow. Due to the topographic and structural complexity of the study area, which is expressed throughout in the form of synclinal and anticlinal zone alternations frequently dissected by faults (e.g., the Sambor Rapids or the channel between Kaoh Ro Ngiev island and the right riverbank), the spacing and depth of the majority of pools might be constrained by local tectonic structures. Because there only have been limited geological surveys of this area (UN, 1993), it is impossible to associate the location of most deep pools or the alignment of islands and channels with specific mapped geological structures. Rather, taking Kaoh Ro Ngiev as an example, it is possible to suggest tentatively that alignments are in accord with the trend of known and probable faults seen in air photographs either side of the river course.

3.3 Geology and tectonics

3.3.1 Geology of the study area

As was noted in Section 3.2, the area of interest lies between two significant terrain features: the Eastern Highlands and the Cambodian Plain. In terms of regional geology, the study area is situated in the Mesozoic Truong Son Fold Belt (Eastern Highlands) which may be subdivided into three provinces within Cambodia. The river section between Stung Treng and Kratie belongs to the minor latitudinal strike provinces of the Belt, namely the gently folded Terrains Rouge Plateau and the moderately to strongly-folded strata of the South-East (Dalat) Fold Belt occupying the northern and southern halves of the study area respectively (Figure 3.9). In the recent publication of Dickins et al. (1997), Permian-Triassic rocks in the north east of Cambodia are included into the Dalat Stungtreng Fold Belt elongated in a north-west/south-east direction (see Section 3.3.2, Figure 3.14).

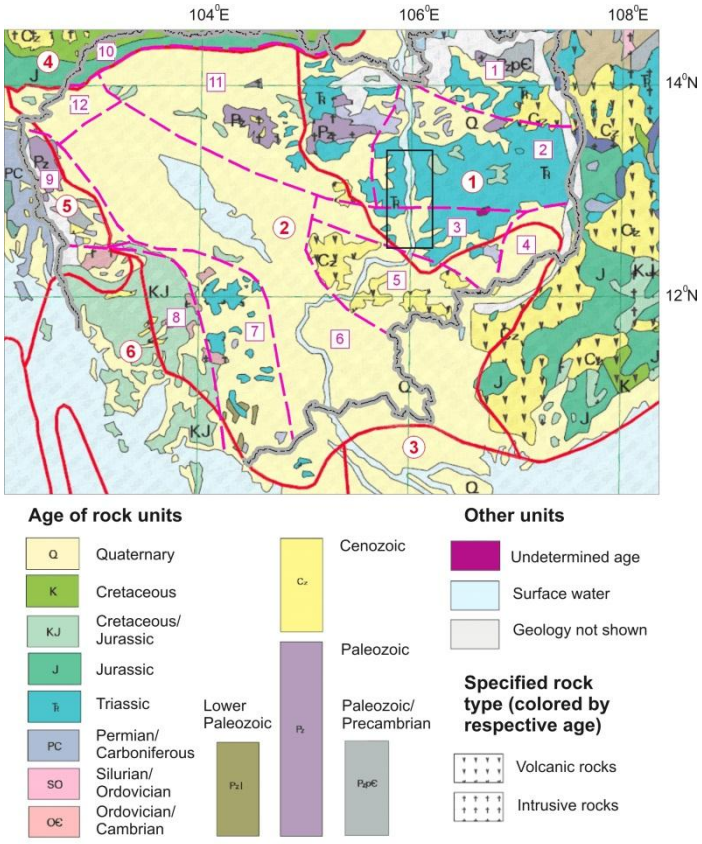

Figure 3.9. Geological provinces in Cambodia (based on UN, 1993 and Steinshouer et al., 1997). Extent of the study area is framed by black rectangle.

Solid red lines outline the regional provinces in Southeast Asia. Numbers in circles are: 1 – Truong Son Fold Belt, 2 – Tonle Sap – Phnom Penh Basin, 3 – Mekong/Cuulong Nung Tau Basin, 4 – Khorat Platform, 5 – Thailand Mesozoic Basin Belt, 6 – Panjang/Cardomomes Basin (Steinshouer, 1997).
Dash red lines are boundaries of provinces in Cambodia. Numbers in squares are: 1 – Ratana Kiri Highlands, 2 – Terrains Rouges Plateau, 3 – South-East (Dalat) Fold Belt, 4 – Chhlong Plateau Volcanics, 5 – Southeast Volcanic Belt, 6 – Tonle sap Mekong Plains, 7 – Pursat Kampot Fold Belt, 8 – Cardamom Highland, 9 – Pailin Meta & Fold Belt, 10 – Khorat Plateau, 11 – Siem Reap – Stung Treng Volcano – Sedimentary Fold Belt, 12 – Battambang Plain.

The study area is situated in the north of the country which has no major industrially-attractive natural resources. Due to this fact, geological knowledge, particular at a scale better than 1:200 000, remains insufficient. Geological maps covering the area of interest are available (SNMGP, 1973) at a scale of 1:200 000 and from JICA (2003) at a scale of 1:500 000 (Figure 3.10, Map A and Map B respectively). Some minor geological studies are available for small areas immediately to the north and south of the study area and describe potential dam sites near Stung Treng (Poduzeće za primijenjenu Geofizika, 1968) and the Sambor Rapids (Stapledone et al., 1961, 1962). The latter reports provide data on tectonic structures, traced lineaments and bedding planes located at the Sambor Rapids and surrounding areas which are shown on Figure 3.10A.

Although contours of geological features on both maps may coincide, the age and composition of geological units often is controversial, therefore neither of them is reliable. Another weak quality of these maps is that the geology of numerous bedrock outcrops within the Mekong macrochannel (see Chapter 1, Figure 1.2) is either only partly recognized or often not shown, which can lead to misinterpretation of the geomorphological composition of the entire multichannel section. Besides, the most recent sediments (e.g. ancient, recent and present alluvium - Figure 3.10A) or pediments, floodplains, terrace alluvial deposits (Figure 3.10B) do not correlate with knowledge of the Mekong terraces provided by Carbonnel (1972); the extent, composition and age of these sediments also need further clarification. Some faults and structural elements shown in the north of the study area and abundantly occurring in the south do not however present in the middle of the area of interest; another observation is that structural elements and faults are marked predominantly on the west river bank, whereas higher altitudes and the main parts of the *Dalat StungTreng Foldbelt* occur on the east riverbank. This fact can be questioned according to the regional settings of the territory which is described as a marginal part of the *Dalat Fold Belt* (Dickins et al., 1997). Thus, both the geology and tectonics of the Mekong in north-east Cambodia requires revision based upon published information, field observations and information obtained from the remote sensing materials.

The main sedimentary rocks observed within the study area are Triassic-Jurassic series. There is no evidence of any exposures of older rocks apart from the Lower Paleozoic slates and phtanites (white quartz schists) found in the bed of the Mekong River at the confluence with the Sekong River (Poduzeće za primijenjenu Geofizika, 1968) which, due to the limited data available, can be interpreted either as an exposure of the metamorphic basement or as products of local metamorphism of rocks composing the territory.

Triassic-Jurassic sediments, namely the *Terrain Rouge* and the *Grés Supérieures* deposits, cover large areas in the north-east of the country. Together they comprise the Lower and Upper "*Indosinias*" respectively (Hutchinson, 1989). Those facies had been formed during the Triassic-Jurassic periods within a 'shallow sea' (Hutchinson, 1989). Due to the vast extent and impressive thickness (up to 2000 m) the precise chronological identification differs from upper Triassic to middle Jurassic, depending on location. This succession generally grades upwards from marine through lagoonal to continental sedimentary units of sandstones, sandy shales, marls and their intercalations formed over the mentioned time period. As for the whole formation, it includes rhyolites, dacites and equivalent tuffs (UNESCO, 1972) which are observed abundantly within the Rapids de Prek Patang (study sub-area).

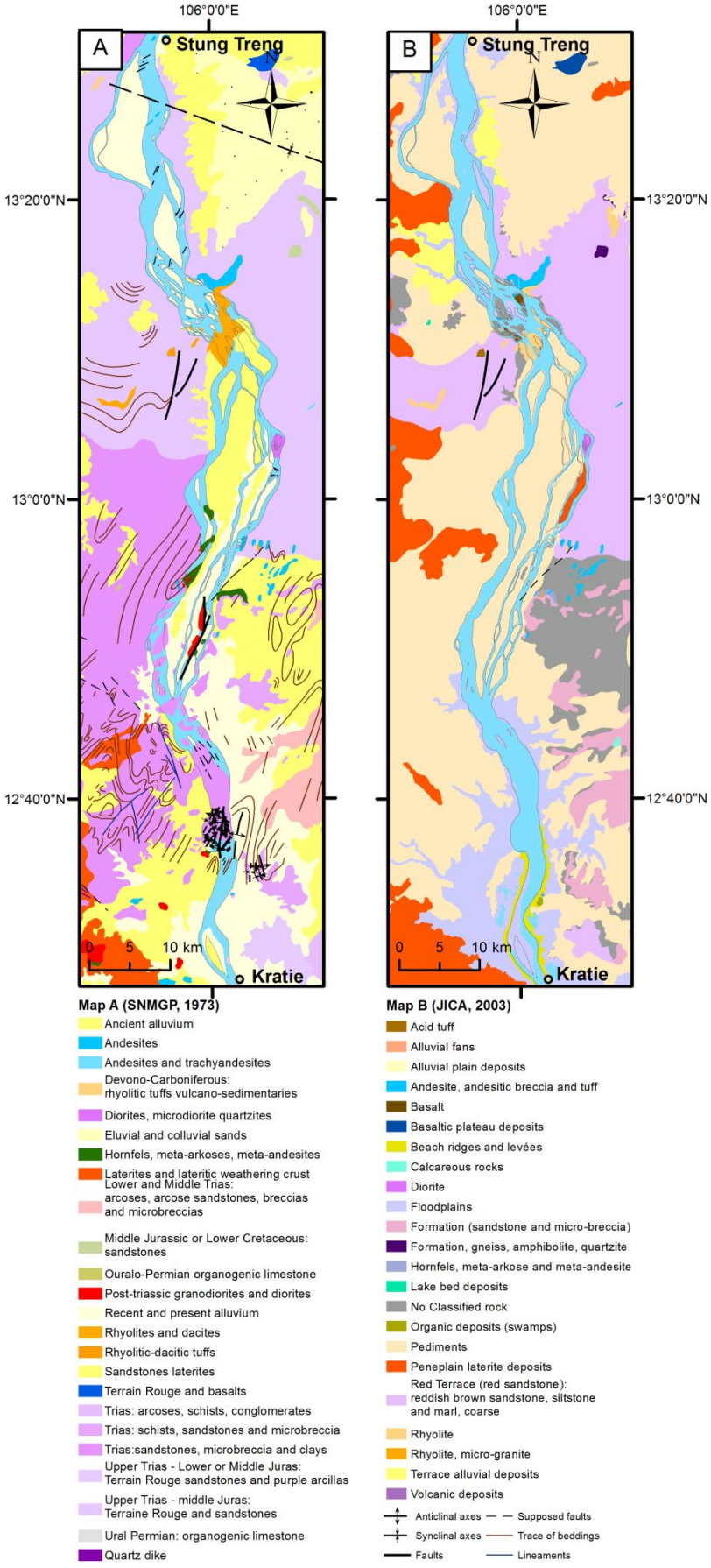

Figure 3.10. Geological maps of the study area (see text for more details).

The Terrain Rouge Plateau is mainly comprised of the *Terrain Rouge* (red terrain) sedimentary facies which extends 20 km to the west from the right bank of the Mekong 30 km downstream of Stung Treng and to the east from the left riverbank to the Vietnamese border. The name of this unit is due to the dominating continental red beds comprised of conglomerates, sandstones (Figure 3.11) and siltstones.

Figure 3.11. Outcrops of weathered Terrain Rouge sandstones at the left riverbank near Stung Treng, Ph. Kaing Deisar village (13°28.240'N/105°56.398'E). Thickness of layers vary from very thin (2 mm) to thick (up to 1 m), bedding planes are (near) horizontal. Man is pointing to the place of field sample collection which is a sandstone with ash component (up to 20%) and has been termed a 'tuffaceous sandstone'.

Within the study area, lower-middle Jurassic *Terrain Rouge* reddish-brown sandstone, siltstones, marls and shales outcrop along both riverbanks of the Mekong. The appearance of these rocks varies from massive to thin, fine to coarse graded, hard to weakly cemented (UN, 1968).In the vicinity of Stung Treng, layers of the sediments are described as slightly curved, but mainly sub-horizontal continental and lagoonal facies with readily-recognizable joints and bedding planes (Poduzeće za primijenjenu Geofizika, 1968) occur at both riverbanks and within the riverbed (SNMGP, 1973).

"*Grés Supérieures*" (upper sandstones) is the upper/middle Jurassic sub-division of Indosinias are dominant in the South-East (Dalat) Fold Belt (Figure 3.9) (UN, 1993). The units of *Grés Supérieures* extend both to the east and to the west of the Mekong in the southern part of the study area and form the Cato Formation. It occurs on a base of *Terrain Rouge* sediments and can be distinguished from the latter by lithological constitution or superimposition. Generally, *Grés Supérieures* sandstones, conglomerates (Figure 3.12), marls and shales are similar to Triassic bottomset beds

(Hutchinson, 1989). Light-colour, coarse-grained quartz sandstones may be cemented by argillaceous material, but frequently they are not. Intercalations or nodules of chert are likely to be found.

Figure 3.12. Robust conglomerates (*Grés Supérieures* (?)) at an inundated island (12°54'42.8''/106°00'27.3''); 20 cm length chisel on the inset picture at the right bottom corner provides scale.

The products of volcanic activity associated with the *Terrain Rouge* deposits are found at the Rapids de Prek Patang (Figure 3.10) and include rhyolites, dacites, andesites, diorites and associated tuffs. These rocks appear in the form of lava flows, dykes and sills (UNESCO, 1972). However, granitic and granodioritic intrusions belonging to the *Diorite-Granodiorite Suite (Dinhquan Complex)* occur (UN, 1993) and can be seen in southern parts of the study area. Rocks of this intrusive complex form stocks, plugs and batholiths sparsely through the region, being mainly exposed in the Dalat region of Vietnam (UNESCO, 1972). Radiometric dates of the granites range from 64 to 172 My (UN, 1993). The thickness of volcanic rocks of the *Dalat Stungtreng Foldbelt* at some locations may vary from 300-400m up to 1000m (Dickins et al., 1997).

Neogene-Quaternary sediments consist of silts, sands, gravels and claystones, composing the "Older Alluvium" (ancient alluvium in Figure 3.10) and date back to 650000 years BP (UN, 1993). Deposits of more recent Quaternary and Holocene alluvium extensively cover areas of older sediments and are characterised by gravels, sands, silts, clays and mixtures of those constituents. Due to the hot and humid tropical climate, soil forming processes cause these surface sediments to form laterites

either in blocks or crust with estimated thicknesses around 10 to 20 metres (Poduzeće za primijenjenu Geofizika, 1968).

Mineral resource extraction in Stung Treng and Kratie provinces currently is undertaken mainly for iron and copper ore at the right bank of the Mekong, close to the confluence with the Sekong River (Try & Chambers, 2006). Mining and quarrying occurs for dolomite, marble, zircon and coal (Stung Treng province) and gravel, granite and lignite (Kratie province) (TWG-F&E, 2008). Alluvial gold formerly was exploited locally at some islands upstream of Sambor Rapids (author's personal communication with local people) but was small scale. Additional information about the economic potential of mineral resources within the study area is unavailable.

3.3.2 Tectonic history of the study area

The territory of Cambodia is situated within the Indochina terrane, sometimes known as Annamia, which also includes the southwestern part of China, the western part of Thailand, Laos and Vietnam (Lepvrier et al., 2004).

During Palaeozoic time, the two independent Precambrian continental terrains of Sibumasu and Indochina were separated from one another by branches of the Palaeotethys Ocean. The collision between them has resulted in consolidation of two geoblocks throughout the full (Indosinian) orogenic cycle. Those relocations have formed the suture zones while extend across the region from north to the south (see Figure 3.13).

The two major strata of the *Terraine Rouge* and the *Grés Supérieures*, which are widespread in the north-east of the country, were formed during the Indosinian Orogeny mainly in the Triassic and Jurassic and were also deformed and faulted during the orogeny. There are several pronounced stages of the orogeny to be distinguished (Dickins et al., 1997). The first phase of undulating folding of the terrain started at the end of Carboniferous (Moscovian) and continued up to the end of Permian period. The second folding phase followed in the Middle Triassic – Carnian and then, at the conditions of continental collision, two phases of maximal orogeny compressed folds in geosynclinal zones during the Middle-Late Triassic.

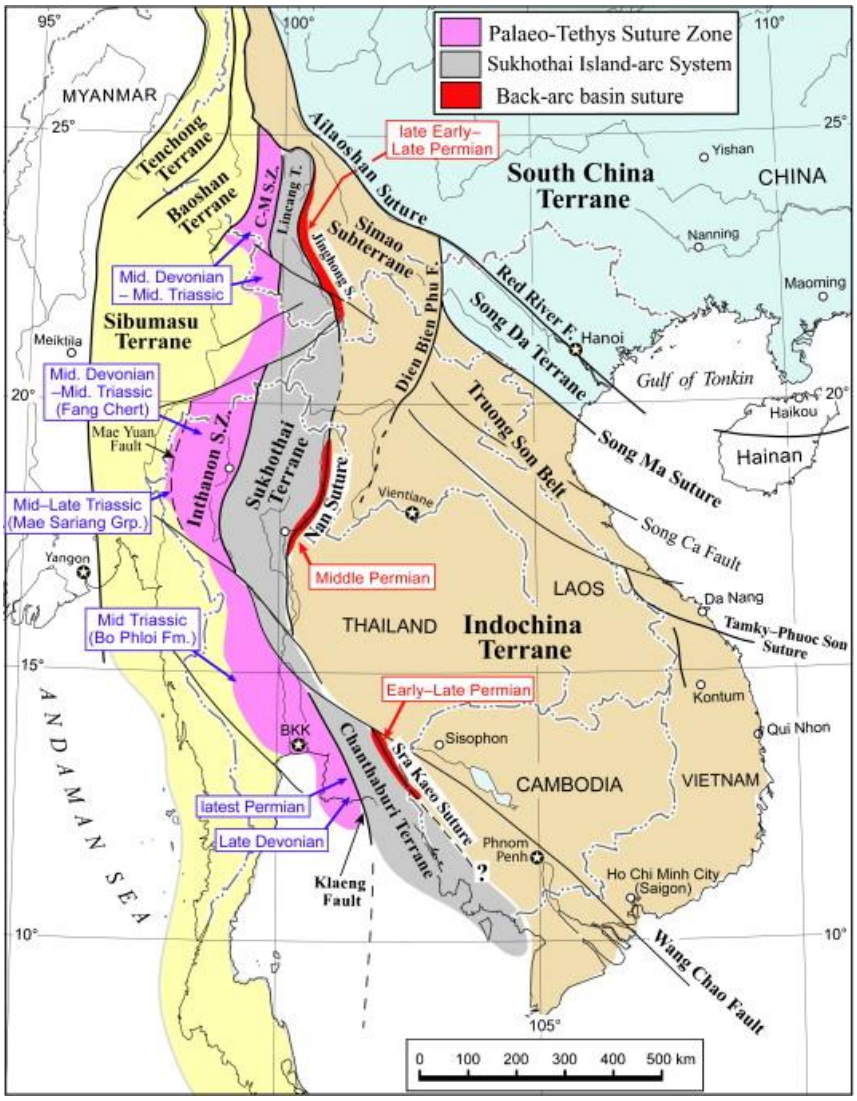

Figure 3.13. Tectonic subdivision of South East Asia, showing the Palaeo-Tethys Suture Zone and back-arc sutures.

The occurrence of deep-sea sediments in each local suture is indicated (for the Palaeo-Tethys Suture Zone in blue and for the back-arc basin in red). C-M S.Z = Changning–Menglian Suture Zone (from Lepvrier et al., 2004).

Phases of dynamic movements were accompanied by volcanic and sedimentary-volcanic products of eruptions as well as marine-lagoon-continental sedimentation alternation. By the end of the Triassic period, Indochina had become a consolidated terrane (Figure 3.13).

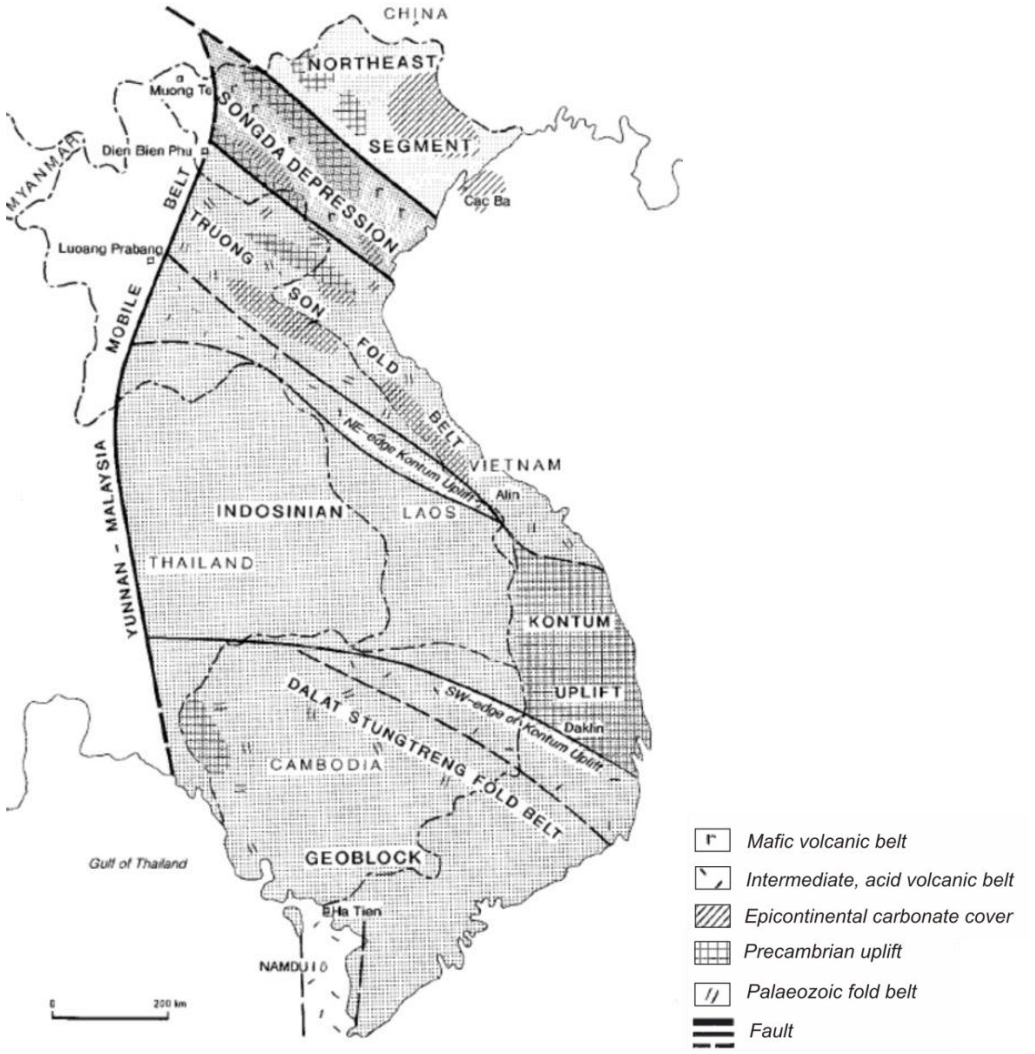

Figure 3.14. Late Palaeozoic structures and palaeogeography of Indochina (Dickins et al., 1997).

Post-Indosinian tectonic adjustments to the Cambodian territory are characterised by uplifting and erosion events during the Cretaceous and Palaeogene Periods. Rocks of these periods are not represented in the study area presumably owing to a lack of sedimentation and volcanic activity within the study area at that time or later erosion. Thus, structural development of the river section between Stung Treng and Kratie had ceased by the late Mesozoic Era. Neogene and Quaternary deposits were formed in continental conditions under the influence of weathering and fluvial processes and are not deformed by tectonism. However, volcanic activity of Indochina has resulted in occurrence of Neogene-Quaternary- basalts (Rangin et al., 1995) located outside of the study area boundaries (Figure 3.9). The latest publication considering the palaeo-course of the Mekong suggests that basalt bodies, e.g. those at the Bolovens Plateau (Chapter 1, Figure 1.1A) affected a former course of the river (Carling, 2009).

3.4 Climate and hydrology

Climate in the South East Asia region, including Cambodia, is controlled by the monsoon. Two main seasons alternate with short transition periods in April-May and October (Figure 3.15). The north-east monsoon brings continental air from China which causes a dry (<40 mm monthly rainfall) and cool (20-28°C) season from November to February (King et al., 2009). The transition period in March to May is the hottest time of the year (30-35°C), meanwhile the amount of precipitation gradually rises until it crosses the threshold of 200mm monthly precipitation, marking the beginning of the wet season. The second transition period at the end of September-October is usually shorter, cooler (temperature range is 25-30° C) and less rainy due to the retreat of the south-west monsoon. Around 80% of annual precipitation arrives during the monsoonal season from May to October (22-30°C), with the heaviest rainfalls in August-September. Wet season precipitation can be inconsistent and uncertain and this results in intra-seasonal variations of heavy rain (more than 5 mm daily (MRC, 2005)), average rainfall and even short dry periods. The seasonal pattern outlined above is applicable to all Cambodian regions, although the length and intensiveness of each season depends upon the exact location within the country (Figure 3.15).

Annual rainfall varies considerably across the country from 800 to 3500mm (Figure 3.16). The study area falls within the 1400-2400 mm category, with more precipitation in the Stung Treng area and less in Kratie. This is because a precipitation distribution gradient occurs from south-east/north-west due to orographic effects as Cambodia is framed by mountains towards the south-west and north-east borders. Thus, the driest areas lie in the centre of the Cambodian Lowlands, whereas coastal areas are the moistest. Annual evaporation in Cambodia indicates variations between 1500mm and 1700mm but there is little information on the regional values.

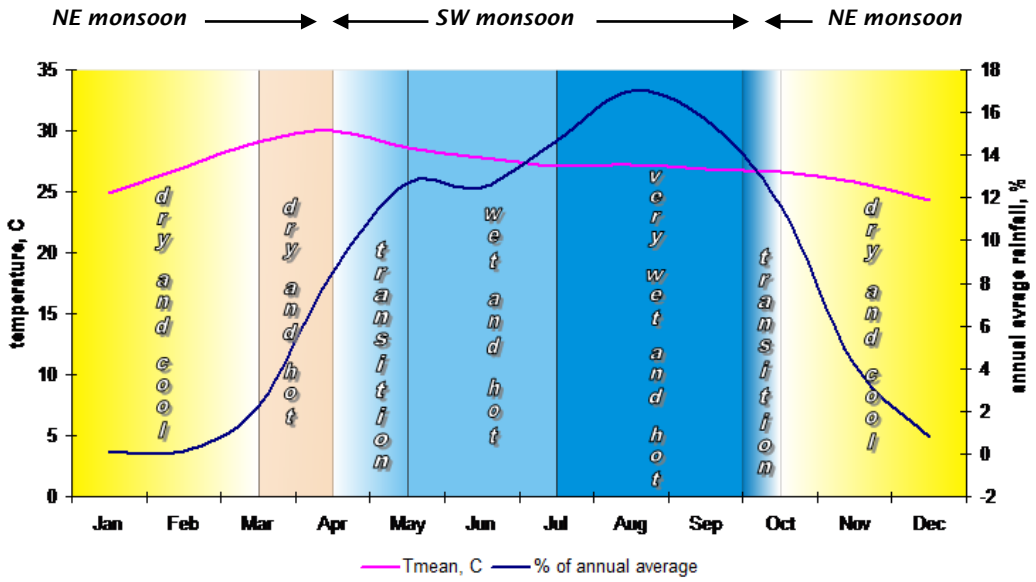

Figure 3.15. Seasonal variations of temperature and rainfall in Stung Treng (compiled temperature and rainfall values from FA/Danida/DED (2003) and Try and Chambers (2006), respectively).

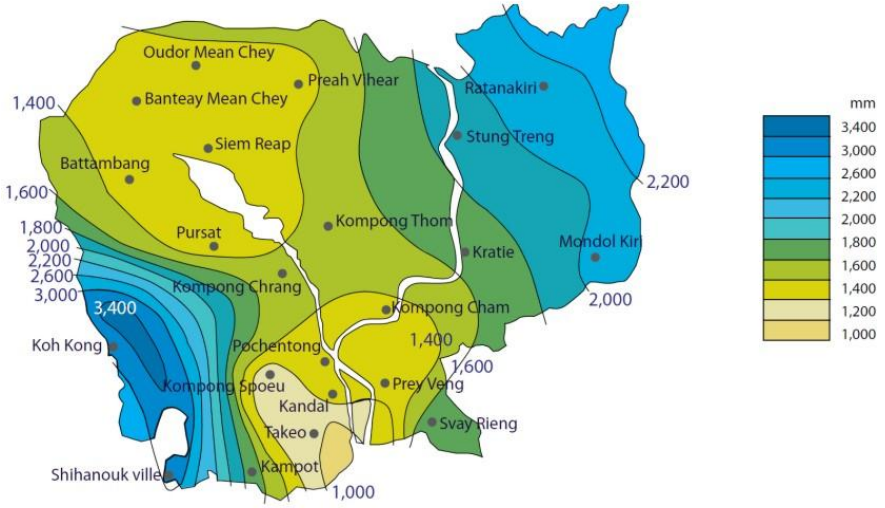

Figure 3.16. Mean rainfall in Cambodia (1984-1998) (King et al, 2009).

Based on 68 and 47 years of data collection, average annual rainfall values at Stung Treng and Kratie are respectively 1913 and 1743mm (FA/Danida/DED, 2003). The wet season in Kratie starts/finishes approximately two to three weeks later/earlier respectively compared with Stung Treng (Figure 3.17). Consequently, the duration of the dry season in the south of the study area is three months and four months in the north. The differences are due to the precipitation gradient noted above, with Stung

Treng being under the influence of the Eastern Highlands precipitation pattern whereas Kratie's rainfall is conditioned by rainfall patterns in the Cambodian Lowlands.

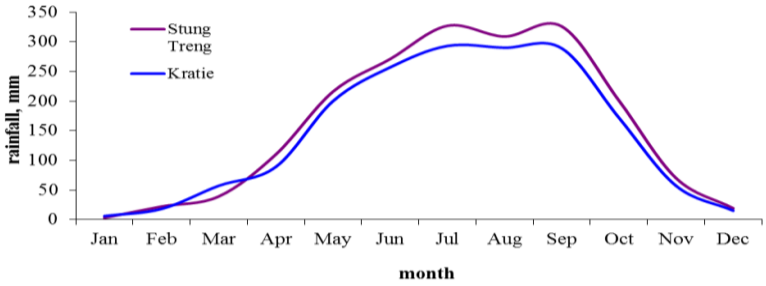

Figure 3.17. Monthly average rainfall in Stung Treng and Kratie (68 and 47 years of observations respectively). Based on data from (FA/Danida/DED 2003).

There is little spatial variation in air temperatures across the study area with a mean annual temperature of 26.9°C in Kratie and 26.6°C in Stung Treng (SCW, 2006). Usually, in the peak of the dry season (January) the lowest temperatures are +20°C. Maximum temperatures of +30-35°C are recorded in the hot and dry transition period between April and May. Relative humidity is around 80% throughout the year with a minimal value of 75% recorded during the dry winter season and a maximum 85% in the period August to October.

The dominant single peak in the annual distribution of rainfall coincides with a dominant single peak in the distribution of water discharge of the Mekong River, as is typical for rivers in the South East Asia region (Dudgeon, 1999; Gupta, 2007). Regular regional and local falls of rain, as well as more widespread precipitation brought by typhoons and storms occur mostly at the end of the wet season and are identified as short-lived peaks in discharge superimposed on the steady trend of the monsoon hydrograph. The major portion of the annual flooding water in the study area comes from the Mekong (i.e. from Laos), but local water supply from the Mekong tributaries (notably the Sekong) affect the study area and backflooding of the Tonlé Sap River affects areas immediately downstream of the study area and may cause local flooding events especially in the vicinity of tributary junctions. The inflow of Mekong River water at Stung Treng is from the upstream catchment area of 635 000 km^2, and this comprises 90% of total annual flow at this gauging station (MRC, 2005). The "Yunnan component" from China is not as readily detectable over the monsoon flood season in this part of the basin as it is in Laos, due to the distance from the Mekong headwaters. Nevertheless, during the dry season, it provides an average of 30% of the total flow with a maximum value of 40% in April (MRC, 2005). The Tonlé Sap backwater effect may entail short term but damaging flood events in the southern part of the study area in Kratie and upstream up as far as Sambor. Natural river bank levées (Figure 3.6) are

present in this area. At Stung Treng a similar, although lesser, backwater effect occurs in the area around the junction of the Mekong and the Sekong rivers when, during peak monsoon discharge, the high water level in the Mekong causes Mekong water to backflood the Sekong river and spill over the banks. In return, local and short term rises in the Mekong River water level at Stung Treng may be related to high discharges from the Sekong River caused by intensive rainfalls within the Se San, Se Kong and Sre Pok basins (Sok, 2008). Other Mekong tributaries within the study area have catchment areas less than 1000 km^2, except for the left-hand Prek Krieng tributary with a 3200 km^2 watershed (MRC, 2008). In total, all three minor tributaries contribute around 1% to the mean annual Mekong flow (MRC, 2005) but do not affect the annual flooding scheme.

There are two gauging stations within the study area which provide discharge measurements. The oldest one, at Stung Treng, records flow of the Mekong since 1910 until present. The data recorded are free from the influence of the seasonal reversed Tonlé Sap flow. Water discharge contributions of the Sekong, Se San and Se Pok tributaries are accounted for because the station is situated immediately downstream of the confluences of these tributaries (CNMC, 2006). The first records of the second hydrological station at Kratie date from 1924. This gauging station measures flow from a 646 000 km^2 watershed area but unlike the data from the upstream Stung Treng station, the records are not continuous due to gaps at the time of civil wars. Gauging stations on tributaries such as Se San and Sre Pok are located within the upper reaches of these rivers and thus are not able to provide complete runoff information. In contrast, the station on the Sekong is at a downstream section immediately upstream of the confluence with Se San and Sre Pok (MRC, 2008). The Stung Treng and Kratie stations update mainstream water level information daily (www.mrcmekong.org) whilst archive records are stored by the MRC and statistical summaries for these stations are published in MRC annual reports. Variations in the annual water levels of the Mekong River at Stung Treng and Kratie correspond with each other (Figure 3.18), reflecting the short reach between the two gauging stations and the lack of tributaries affecting the annual hydrograph within the study reach. The records demonstrate that the flow of the Mekong River mainstream determines the hydrological regime of the study reach despite the occasional Tonlé Sap backwater effects downstream and the local backwater flow effects at the Sekong confluence upstream of the study area.

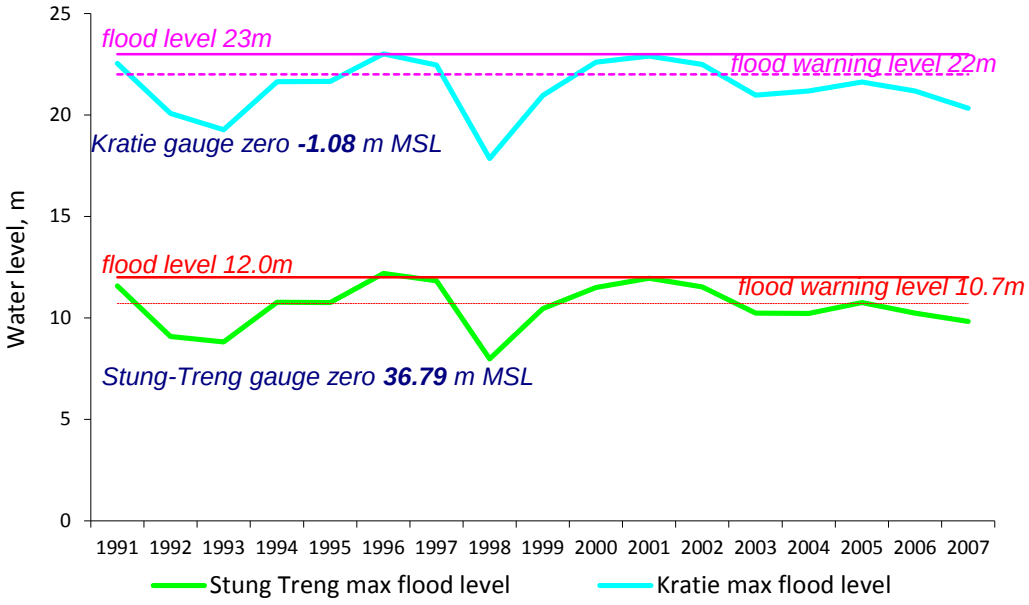

Figure 3.18. Water level for Stung Treng and Kratie during 1991-2007 years (based on data from Sok, 2008).

The distribution of the water level values throughout the year reflects the monsoon rainfall temporal pattern, as the Mekong is largely rain-fed, albeit with a seasonal glacier and snow melt component from the Himalaya. A limited variation of only one to two metres between the minimal and maximal levels of the normal dry season low flow level reflects the regional climatic control on the Mekong River flow whilst, during the monsoonal wet season the water level may rise and fall within a 5-6 meters interval or, in other words, 2-3 meters higher or lower than the mean (). Average annual water levels are 47.35 msl and 22.2 msl for Stung Treng and Kratie respectively (CNMC, 2006).

According to the MRC (2007a), rating equations for the Mekong at Stung Treng and Kratie are as follows:

Stung Treng $H = \left(\frac{Q}{1839}\right) * \left(\frac{1}{1.49}\right) + 0.94$ $Q = 1839 * (H - 0.94) * 1.49$

Kratie: rising stage $H = \left(\frac{Q*\left(\frac{1}{1.21}\right)+10.16}{8.16}\right)$ $Q = (8.16 * H - 10.16) * 1.21$

falling stage $H = \left(\frac{Q*\left(\frac{1}{2.5}\right)-1.26}{3.3}\right)$ $Q = (3.3 * H + 1.26) * 2.5,$

where *H* is water level, m and *Q* is discharge, cumecs.

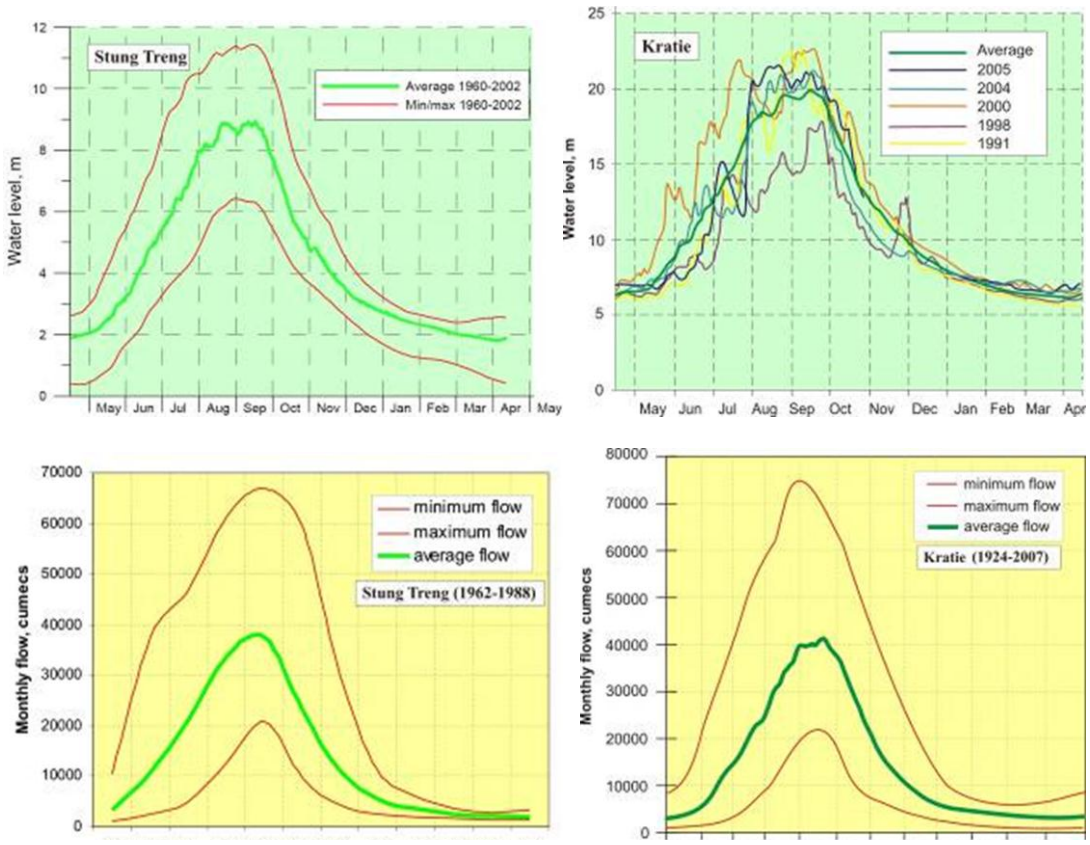

Figure 3.19. Water level and monthly flow at Stung Treng and Kratie.

Water level at Stung-Treng based on MRC-RFMMC&MRC (2007) and at Kratie: DHRW (2008). Monthly flow at Stung Treng based on data from Try & Chambers (2006) and for Kratie based on MRC (2008).

The rated section at Stung Treng is more stable than that at Kratie such that the rating curve for the former station is more reliable than that at the latter station. These differences also mean that there can be anomalous differences in the recorded discharges when comparing the stations, which need to be carefully accounted for.

Nevertheless, the overall trends in the recorded discharges and water levels at Stung Treng and Kratie both illustrate well the annual variations in the hydrograph behaviour throughout the dry and flooding seasons year by year. As seen from the historical range (Figure 3.21), the Mekong River at Kratie records more significant floods and droughts than at Stung Treng. The intensity of floods or droughts in this diagram is based on a mean annual flood volume of 320 km^3 at Stung Treng and 333.7 km^3 at Kratie.

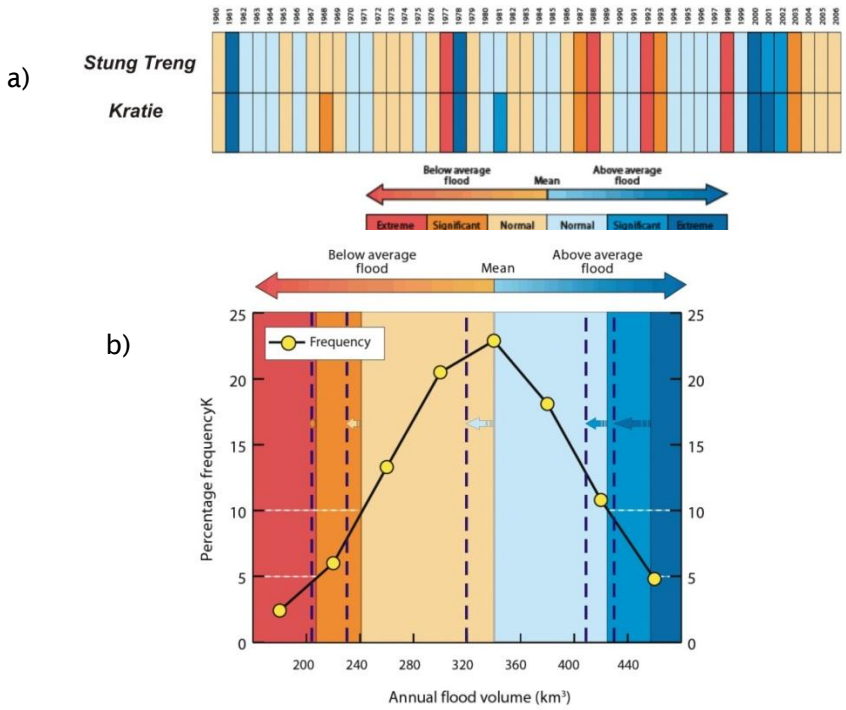

Figure 3.20. Annual flood volume variability at Stung Treng and Kratie (a) and historical histogram of flood volume frequency distribution at Kratie (b) (MRC, 2007a). Deep blue dash lines on diagram (b) mark margins of each hydrological event at Stung Treng.

Flood events are serious problems for many people living in local small villages along the river, not merely by virtue of their impact and the high vulnerability of low-income rural inhabitants, but also because many villages are not protected against flooding. Furthermore, flood refuges are not easily accessible and are often equipped poorly. Despite relatively recent human loss and damage to homes and infrastructure, and in view of the fact that both Stung Treng and Kratie are regional capitals of their eponymous provinces they also do not have any protection against flooding. As a rule, floods and droughts are assessed by balance of two main hydrological parameters: flow peak and flow volume (Figure 3.21). The panels A and B in Figure 3.21, however, come from different sources and may show mismatching values. The highest flood volumes within the study area are due to the rise of the upstream Mekong water level in 1939, 2000 and 2001. The largest flood in terms of peak flow volume (77 000 cumecs) in Kratie was documented in 1978 and was caused by tropical Typhoon Joe. In the years 1988 and 1998, flood volume and stages were the lowest in the history of observations at Stung Treng, meanwhile at Kratie the corresponding record years are 1992 and 1955. The most destructive flood occurred in September 1996 (CNMC, 2006).

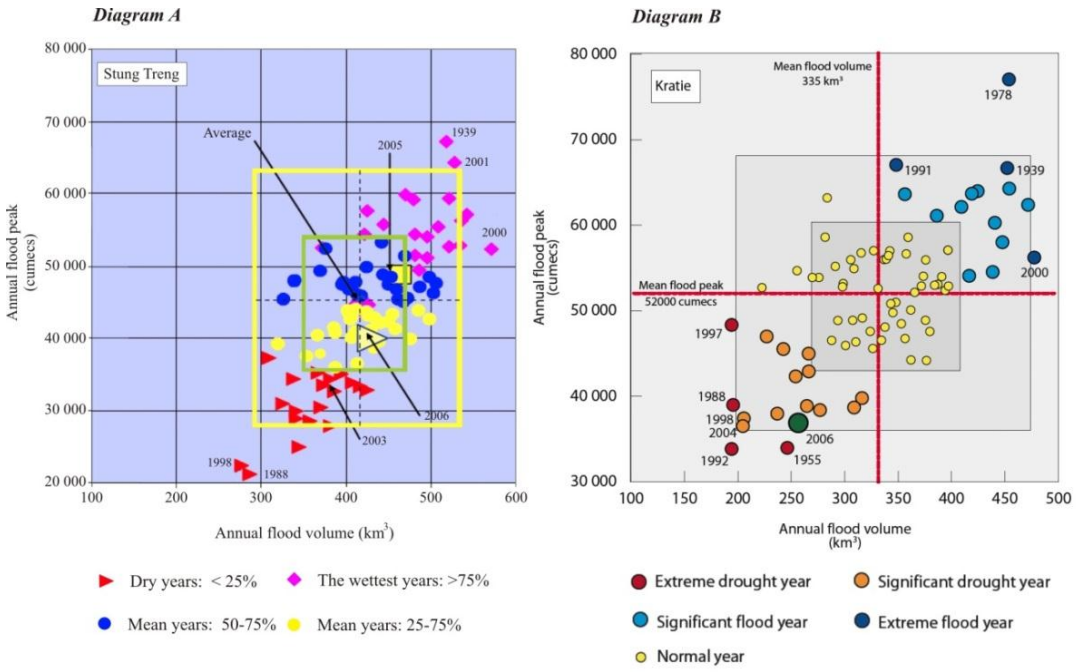

Figure 3.21. Annual flood peak vs flood volume of the Mekong at Stung Treng (1910-2006, Diagram A) and Kratie (1924- 2006, Diagram B) (Adapted from Saravuth (2008) and MRC (2007a)).

Green box (Diagram A) and dark grey box (Diagram B) outline one standard deviation (1ð); yellow box (Diagram A) and light grey box (Diagram B) indicate two standard deviations (2ð) for each variable above and below their respective means. Points outside of boxes labeled with a year of occurrence belong to extreme droughts/floods.

Historical data related to the duration of water levels exceeding flood warning levels for Stung Treng and Kratie are not available; personal communication with local people living in a village 15 kilometres downstream from Stung Treng, for example, indicate that the severe 1978 flood inundated the village for one month. The duration of the flooding period (Figure 3.22) is distinguished by mainstream flow parameters. The lowest discharge during the dry season usually is observed at the end of March or beginning of April. It is a reference point for identification of the hydrological seasonality. A doubling of this value marks the beginning of a spring transitional period. Next, the wet season starts at the time when flow discharge reaches and then exceeds the mean annual discharge value. The flood period finishes at the end of September or beginning of October when the flow volume is lower than the average. The second transitional period lasts until further discharge reduction returns the river to the base flow level. Maximal and minimal flooding season durations do not always coincide with outstanding floods and droughts.

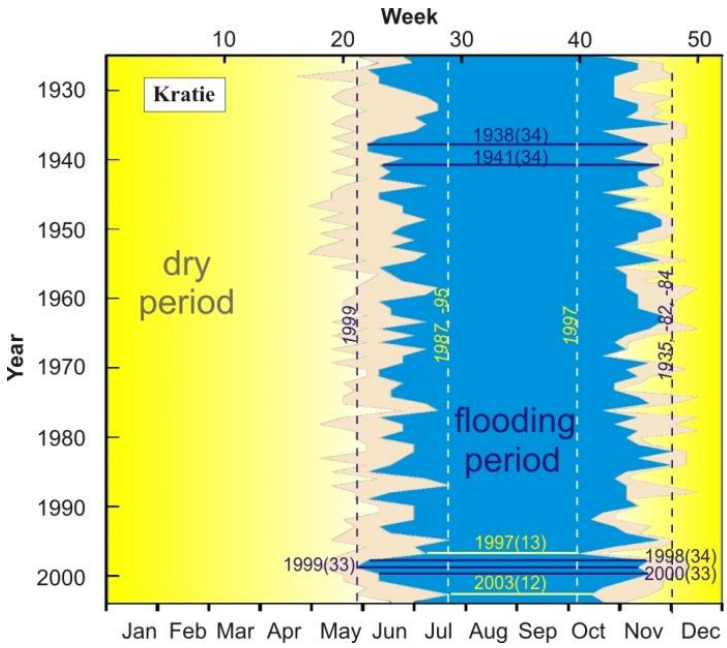

Figure 3.22. Historical onset and duration of the four flow seasons at Kratie (1924-2005) (MRC, 2007a).

Years with the longest flooding period are marked by deep blue labels of year and number of weeks in parentheses; the same in yellow colour shows the shortest flooding periods.

The groundwater resources in northwest Cambodia are able to satisfy only small domestic needs, such as drinking water supply in villages and local small-scale irrigation. The most productive horizons for the ground water extraction are the alluvium which yields up to 16m^3/h (Peng & Pin, 2003). The quality of water generally is good and suitable for drinking, but in some southern areas of Cambodia, including Kratie, a higher content of arsenic (As) has been reported (Luu et al, 2008; Buschmann et al, 2008).

Until recently, suspended sediment data for the Cambodian part of the Mekong remained largely unavailable except for a few data obtained in the 1960s (Hården & Sundborg, 1992). Kummu & Varis (2007) performed an evaluation of those relevant parameters for the Lower Mekong Basin based on data for the Mekong from the Chinese border to Pakse (Laos). In 1992, total suspended sediment concentration (TSS) data collection was started at Kratie with reported values for 2003 of 122 mg/l in comparison with 215 mg/l recorded for Pakse (Try & Chambers, 2006).

3.5 Vegetation

The tropical monsoon climate and the consequent annual flooding regime of the Mekong River support substantial natural vegetation cover and biodiversity. Currently, for non-botanical studies, it is common to consider vegetation as a component of 'land cover'. The interpretation of remote sensing images plays a key role in quick and reliable land cover classification and assessment. Assuming that vegetation within the river channels is a vital component of the river ecosystem, land cover data can be used in flooding extent/duration determination (Hess et al., 1995, 2003; Martinez & Toan, 2007), evaluation of bank erosion prone areas (Marston et al., 1995; Micheli & Kirchner, 2002), or calculations of the scale of sediment yield (De Rose et al., 2005).

Despite the natural floristic diversity there are only few main natural vegetation land cover types in the study area:

- Evergreen broad-leaved moist forest
- Dry deciduous forest
- Mixed forest of evergreen and deciduous species
- Bamboo and secondary forest
- Riparian (riverine/gallery) forest
- (Seasonally) flooded forest/shrubs

The east bank terrestrial forest is predominantly deciduous except for a patchy area just south of Stung Treng which is occupied by evergreen forest; on the west bank, the forest cover gradually changes through mixed evergreen and deciduous to the evergreen broad-leaved forest (Figure 3.23). In north-east Cambodia, the Mekong essentially provides the dividing line between those two dominating land cover types. Evergreen broad-leafed moist forest is dense and multi-storied with individual trees up to 45 metres in height. Its lowland bioclimatic type (less than 1000 metres altitude) is established by a variety of species from the *Dipterocarpus, Shorea, Parashorea, Hopea* and *Anisoptera* families (Stibig & Beuchle, 2003). The extent of this forest type, which is mapped on modern satellite-based land cover maps, may not coincide with strict floristic definition of evergreen forest.

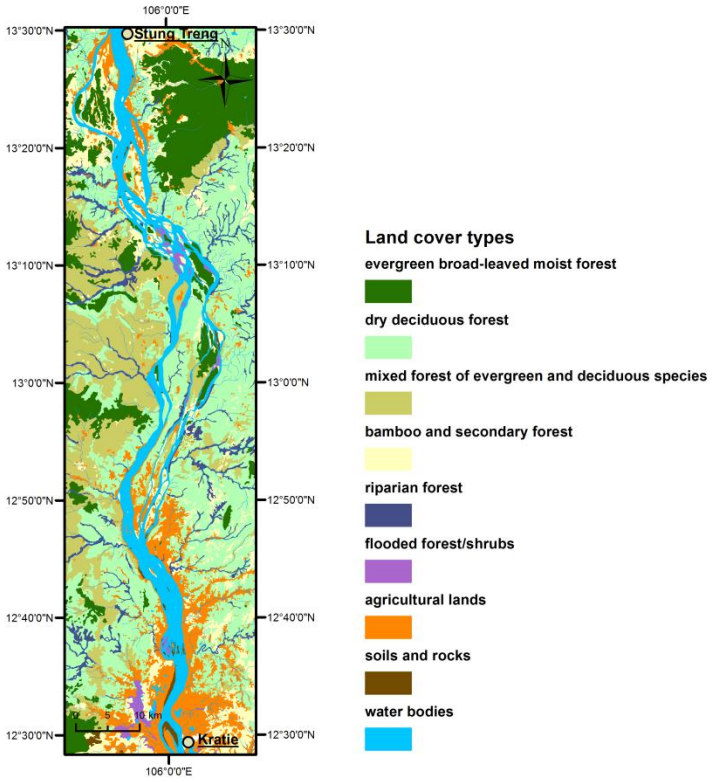

Figure 3.23. Land cover types within the study area (based on JICA, 2003).

Dry deciduous forest cover has a closed canopy (50-70%) and usually consists of three layers: grasses and herbs, 5-12 metres tall trees, and scattered 'emergents' (up to 20-25 m height) which project above the 12 metres canopy. This forest is also called "dipterocarp deciduous forest" following the name of the dominant *Dipterocarpaceae* tree species (Try & Chambers, 2006). Dipterocarps lose nearly all leaves during the dry season and flush and blossom during the rainy season, particularly in September-October. The majority of deciduous tree species in Cambodia are characterised as fire resistant which allows the deciduous forest to survive and regenerate subsequent to natural fires or fire clearance initiated by humans.

Mixed forest of evergreen and deciduous species represents the transition zone between the two types described above and is a further *primary forest* type with prevailing deciduous plants. Vast mainland areas on the west bank are occupied by this forest type along the entire length of the river within the study area.

Expansive agriculture, logging and fires lead to the *primary forest* depletion and subsequent occurrence of bamboo and secondary forest cover (Mittelman, 2001). Degraded tree cover (density lower than 20%) is interspersed with 4 metres high, quickly growing, bamboo thicket and such invasive tree species as *Diospyros*, *Lagerstroemia* and *Cratoxylon* (ITTO, 2006); however, none of the species can be

recognized as dominant. In the study area, this type of vegetation occurs on some of the Mekong islands, especially immediately downstream of Stung Treng where large islands are populated or are close to local settlements.

Riverine vegetation or gallery forest is found along the banks of numerous small tributaries or on the larger islands rather than along the Mekong main channel banks. This natural absence may be explained by the fact that main channel river banks are steep and high; more gently sloping banks, however, are likely to be occupied by village gardens and if riverine forest occurred here naturally these banks have been cleared of natural vegetation for agriculture or by over-grazing, chiefly by water buffalo (*Bubalus bubalis*). Often these kinds of trees have deep primary roots, which may offer mechanical support against high flow velocities (e.g. Wittman & Parolin, 2005) and so prevent or retard bank recession. Nevertheless, some 'riverbed' vegetation (trees and bushes) which are tolerant of immersion and high velocity flow are also included in this community. It can be seen as a sparse cover on numerous small sand and rocky bars within the macrochannel. These plants are rheophytic and amphibious by their nature, therefore they are well-adapted to seasonal fresh water flooding, swift currents and scour by mobile sediment. Tree species belong either to the *Acacia-Anogeissus* group (Maxwell, 2001) or to the semi-evergreen dipterocarps. The most populous species are *Homonoia riparia*, *Anogeissus rivularis* and *Acacia harmandiana.* The latter two occur as pioneer bushy vegetation on the seasonally submerged riverbed features. Riverine bushes, often in thick profusion, are characteristic of the rock outcrops across the river in many places; especially *Phyllanthus, Telectadium and Homonoia*. These bushes are always in the water during low flows and, except *Homonoia* which is a sand-loving plant, cling to the rocky substrate (Timmins, 2006). Shrubs help trap sediment downstream of the 'shrub forest' in the form of the small sand bars, however they never seems to get buried by sediment and thus probably does not lead to new island development. Riparian trees and bushes often bend over below the water surface under the influence of strong currents flowing through them during the flooding period (Figure 3.24). Altogether, the riverine group of species is kindred with wet evergreen forest of the mountainous area in the south-west of Cambodia (Try & Chambers, 2006).

Figure 3.24. Riverine vegetation of the Mekong riverbed exposure 25 km downstream of Stung Treng, January 2008. Flow right to left.

The gallery forest vegetation merges at lower elevations with the seasonally flooded forest/shrubs. This forest ecosystem is classified as a separate type because distinctive, highly-specialized flora and fauna take advantage of certain strict ecological conditions and, as explained below, makes it the unique forest type of the Mekong. Within the study area, flooded forest can be observed within the Rapids de Prek Patang and Sambor Rapids.

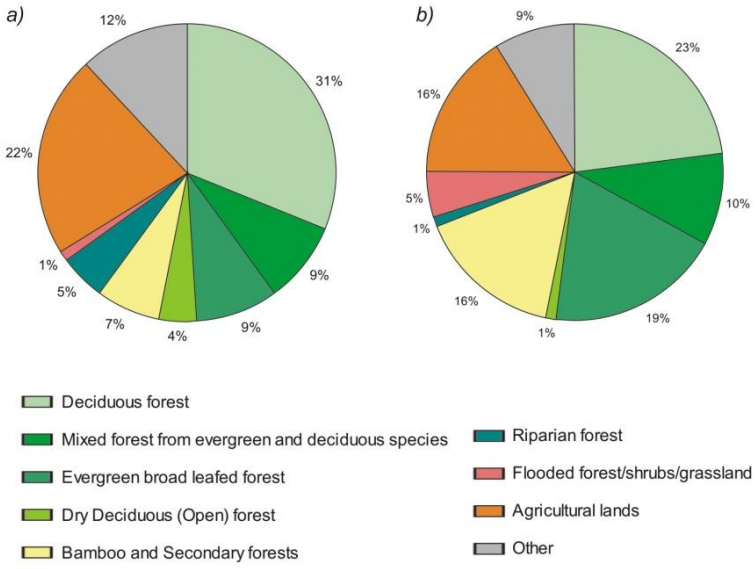

Figure 3.25. Distribution of main land cover types within the a) study area b) study area islands (the data derived from the digital dataset JICA, 2003).

As seen in Figure 3.25, it is more widely distributed among the river islands where it comprises up to 5% of their total area. In 1999 a similar wetland ecosystem in a section of the Mekong from the Cambodian border with Laos south to the junction with Se Kong at Stung Treng was recognized internationally as a 'Ramsar' site (ICEM, 2003). In Cambodia, the best known seasonally flooded forest is specialist forest in the riparian

zone of the Tonlé Sap lake and the surrounding wetland areas. However, the differences in the climatic and hydrological conditions of the Tonlé Sap compared with the Mekong River in the study area stipulate important differences between the two ecosystems. An analogue of the Mekong flooded forest called “várzea” exists on the Amazon River in Brazil (Wittman & Parolin, 2005).

In contrast to the gallery forest, flooded forest tree species experience total or partial submergence for up to six months a year, perhaps from the moment when water level begins to increase from base flow conditions (i.e. dry season low flow; Baird & Phylavanh, 1999). Typically the substrate of these low islands is comprised of bedrock, boulders and pebbles with fluvial sand dunes in spaces between trees and outcrops which indicate slackwater areas and spatial variation in the flow speed across the islands during flooding. Tree species such as *Barringtonia (Lecythidaceae)*, *Eugenia (Myrtaceae)*, *Acacia (Fabaceae-Mimosoideae), Ficus (Moraceae)* and *Anogeissus rivularis (Combretacaeae)* develop aerial roots (which absorb nutrients and oxygen) and, in some cases, buttress roots that may be important in supporting a tree from falling (MWBP, 2004). Besides, multi-stemmed tree forms with spongy-bark anchoring roots are common (Figure 3.26). Flooded shrubs forming the under-storey of the flooded forest are established by *Morindopsis (Rubiaceae)*. High water velocities sweep branches, aerial roots and any other exposed roots horizontally in the direction of the river flow. Flooded forest trees shed their narrow leaves during the high water period; blossoming is associated with the middle of the dry season.

Figure 3.26. Flooded forest on the Kaoh Toan Han island (13°12.009’/105°57.966).

Thus, within the macrochannel of the Mekong River the vegetation consists of grasses and herbs, shrubs and trees which are able to withstand regular flooding. Land cover of the Mekong islands as a rule repeats those of the mainland unless it is modified by agricultural and grazing activities. In a hydrological context as well as being a good protection against riverbank erosion, forest may also play a role in channel migration processes by directly blocking flow during high flood events and providing the woody debris that forms wood jams that may block minor channels over the flood periods. Exact determination of the floristic composition assists in identification of local hydrological parameters, basic substrate nature or submergence duration and in some cases the depth of submergence. For instance, spatially-banded species of *Anogeissus rivularis* found in the riverbed community indicate a short time exposure time of the rocky or pebbly substrate and strong currents during flooding; meanwhile the *Acacia* plants grow at the longer exposed places within the flood season where gentler currents are expressed through an abundance of sandy deposits (Timmins, 2006). In a flooded forest, more aerial roots are produced by the species growing in conditions of high and prolonged submergence whereas buttress trunks are related to the conditions of low, short floods and low sediment rates (Wittman & Parolin, 2005). It is probable that sedimentation and soil texture and soil maturity are linked to both the species composition of the flooded forest as well as the period of flood inundation and distance from the main river channels, with a possibility that sediment deposition decreases within increased elevation. Sediment texture (especially clay content) might also be expected to reflect species composition and elevation (Wittman et al., 2004). In the Amazon, late successional flood forest is a good indication of distance to the river with early successional stages being proximal to the river. Similar relationships probably occur in the Mekong forest but are unrecorded in any detail. It might be expected that the establishment of early successional stages would induce deposition of sands and gravels as the vegetation would impede flow. In the Mekong this is evident on some low-lying areas of islands where islands appear to be extending by pioneer vegetation inducing sedimentation and binding the deposited sediments, including sands transported by aeolian action. Some species of ground-hugging shrubs, with dense stem masses, appear to be unusually tolerant of mechanical damage caused by bedload scouring of bark and accrete fine gravels. However the establishment of larger trees subsequently often causes flood flows to be concentrated in distinctive corridors across the flood islands, leading to zones of intensive flood scour to bedrock and pool development, separated by zones of deep deposition of sands and gravels.

3.6 Soils

Soil diversity in the area of interest is based upon the unique geological, physiographic, climate and vegetation settings of the territory. The initial reason for pedological studies in Cambodia was for agronomic applications because the agricultural sector was always predominant in the economy of the country where available lands are widely used for cropping, gardening and forest growth. The main evaluated soil parameters used in Cambodia include fertility, water retention capacity, depth and susceptibility to erosion (Mund, 2003). Currently, there are three classification systems for Cambodian soils. The first fundamental investigations of soils in Cambodia were made by C.D. Crocker in the 1960s. Sixteen soil types were identified and placed into three major groups (zonal, intrazonal and azonal) accordingly to their pedological maturity and conditions of formation (Crocker, 1962). This work resulted in the publication of a 1:1,000,000 soil map with accompanying exploratory survey notes. The FAO Soil Map of the World released in 1988 establishes Cambodia according to the FAO/UNESCO Soil Classification System. The latest, Cambodian Agronomic Soil Classification (CASC) was developed in 1995 by White et al. (1997) and aimed to identify the agricultural suitability of various soils. In the CASC, the distinguishing of soil groups is based on pedogenic and morphological criteria; each group has a local name. This latter work includes a manual for soil identification and management that makes for practical application. It does not substitute previous classifications but compliments them. However, no field surveys in the north east regions of Cambodia have been carried out since the 1960s; therefore modern soil maps of the area of interest are based on the soil units mapped by Crocker (Figure 3.27) with the terminology of the FAO (FAO/UNESCO, 1988). There are about six soil types (Crocker, 1962) identified within the study area (Figure 3.27 and Table 3.1).

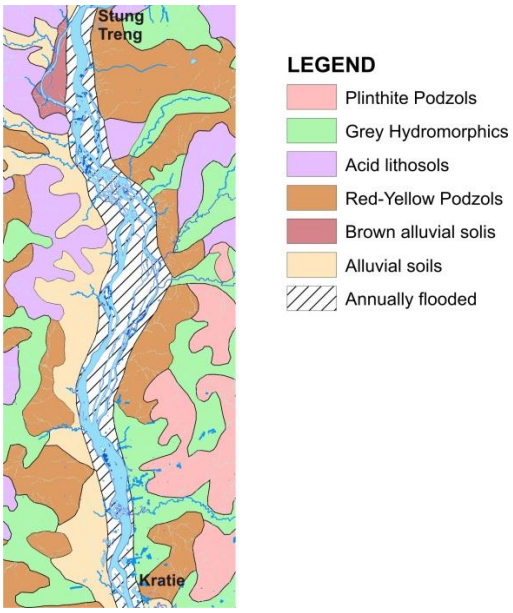

Figure 3.27. Soil maps of the study area (redrawn after Crocker, 1962 and MRC, 2002). Scale 1:2,000,000.

Table 3.1. Correlation between existing classifications of soils within the study area (Crocker (1962), FAO (1988) and White et al. (1997)).

Crocker, 1962	*Soil Type*	Red-Yellow Podzols	Plinthite Podzols	Grey Hydromorphics	Acid Lithosoils	Alluvial Soils	Brown Alluvial Soils
FAO, 1988	*Major Soil*	Cambisols	Acrisols			Gleysols	Fluvisols
	Soil unit	Ferralic	Ferric	Gleyic	Haplic	Eutric	Eutric
	Soil name	Ferralic Cambisols/ Ferric Acrisols	Ferric Acrisols/ Plinthic Acrisols	Gleyic Acrisols/ Dystric Planosols	Haplic Acrisols/ Dystric Leptosols	Eutric Gleysols	Eutric Fluvisols/ Eutric Gleysols
White et al., 1997	*Soil Group*	Plateah Lang Soil, Prey Khmer, Prateah Lang Soil	Prateah Lang Soil	Toul Samroung Soil	Absent due to low fertility for the rice growth	Krakor Soils, Kbal Po Soils, Kein Svay Soil	Kein Svay Soil

(1) Brown alluvial soils (pH 5.0-6.8) are characterized by a brown colour topsoil horizon and coarse texture. They originate from either active floodplain deposits or recent alluvium on river levées and associated backslopes and, being fertile, are

important for agricultural. Try & Chambers (2006) mentioned that this soil type often occurs on the Mekong islands. In the study area, a patch of brown alluvial soil is mapped by Crocker only on Kaoh Sralay island immediately downstream of Stung Treng, but according to the classification of White et al. (1997), the soil type is present in Stung Treng and Kratie provinces more generally. Surface and subsoil horizons of brown alluvial soils have a brown colour, loamy or clayey texture, friable or blocky structure. Occasionally pale red or yellow mottles may be found in the subsoil layer. Brown alluvium is resistant to submergence for substantial periods of time (e.g. more than three months a year) but would not be immersed as frequently and for so long as '**alluvial soils**'. This brown alluvium should be present widely on those islands which are not seasonally inundated. Sometimes, areas where river channels formerly were present may have an undulated landscape comprised of ancient levées covered by brown alluvial soils.

(2) Alluvial soils (pH 4.5-6.5) are similar to brown alluvial soils, but are supposed to be younger and so are not so mature texturally. They accumulate due to deposition of the annually-supplied alluvial suspended sediments derived from the local river bedrock as well as suspended sediment transported from upstream, and may be replenished each year. According to the map (Figure 3.27), they can be observed mainly on the right bank of the Mekong and along right bank tributaries. Alluvial soils have light-grey colour, fine texture with no significant differentiation; structure is blocky or crumbs (White et al., 1997). Those soils are resistant to flooding and water-logging and, due to seasonal upgrading of organic material, are favourable for cultivation. There is a good probability that this soil type occurs on the seasonally inundated islands with an additional sandy component. The thickness of soils of fluvial origin within the study area is not more than 3 m (Ohnuki et al., 2008).

(3) Red-Yellow Podzols (pH 4.2 – 6.8) are mature soils with poor structure and low nutrient content. The upper leached horizon is above a lower accumulative horizon of red, yellow or grey colour which contains iron and aluminium. In the study area, the red-yellow podzols are based on sandstones and volcanic rocks which widely outcrop on both river banks. Those soils are damaged by flooding and, due to the low productivity, are likely to be occupied by natural vegetation (Gregorio, 2005).

(4) Plinthite Podzols (pH 4.2-5.8) represent the mature stage of the **Red-Yellow Podzols**. A high accumulation of iron-bauxitic components in a mixture with silica and clay (plinthite) form a hard top surface. The poor nutrient content puts these soils into the agricultural low productivity group.

(5) Grey Hydromorphics are characterized by a shallow, grey coloured, top horizon overlying a loamy or clayey subsoil containing red, orange or black mottles (White et al., 1997). This soil can occur in localized depressions on a base of ancient alluvial deposits. High groundwater levels in association with high organic contents allow them to be classified as highly fertile land.

(6) Acid Lithosols are predominant in Cambodia. They occur on acid source materials; either volcanic (andesite, rhyloites and their tuffs) or sedimentary (acidic sandstones). Acid lithosols do not have well developed profiles due to their azonal character (Crocker, 1962). Within the study area they are occupied by natural vegetation such as deciduous, evergreen and mixed forest.

Taken together, the distribution of the brown earth alluvial soils and the alluvial soils helps map the extent of flooding of the modern Mekong with the brown earth alluvial soils generally occurring at higher elevations, often on the higher parts of the larger islands, for example, which are rarely flooded. Careful mapping of brown earth soils on islands might help constrain maximum historical flood elevations in any palaeoflood reconstructions. The alluvial soils are developed more prominently along the western flank of the river corridor, which may indicate that the river is migrating eastwards or that right-bank tributaries have contributed more recent alluvium to the river corridor than left-bank tributaries. The distribution of the other soil types indicates regions where the Mekong does not flood and, in some cases, helps define the rocktypes present. The distribution of soil type 5, lying above ancient alluvium, in some cases seems to define low-lying portions of tributary river courses but elsewhere there is no clear association. The significance, if any, of the distribution of this soil type on deciphering the incision history of the Mekong River requires further investigation.

4 Research Methods

The aim of this chapter is to describe the GIS methods (Section 4.1) and the geochronological and grain size analysis techniques (Section 4.2) applied in order to: 1) obtain quantitative and chronological characteristics of the Mekong and its floodplain; and 2) to compare channel pattern parameters extracted from the Mekong datasets with those of other anabranching river networks. As this chapter is essential part of the thesis wherein the chosen methods primarily relate to the available data, it is organized according to data types rather than research aims: cartographic materials are subject to GIS analyses whilst laboratory research techniques are applied to sediment and rock samples collected during field trips to the study area.

4.1 GIS methods for analysing channel patterns

4.1.1 Data and GIS

Geographical Information Systems (GIS) were invented in the early 1960s with the aim of managing geospatial information and using data to solve spatial problems (Lo & Yeung, 2007). One of the main GIS concepts obliges geospatial information being organized in a layer by layer manner where every individual layer contains data liable to a certain class of objects. Layers overlay one on top of another is constructing a schematic picture (map) reflecting the real world. By integrating data, technical and human resources, GIS offers numerical and cartographic outputs.

The first detailed topographic maps of Cambodia (including the study area) were produced by the American and Russian Military Services at a scale of 1:50 000 – 1:250 000 and appeared in the middle of the last century (1960s). In 1977-1978, another set of 1:50 000 Topographic Line Maps (TLM) was published by National Geospatial Intelligence Agency (NGA); these maps are based on a survey conducted in 1963-1967 and are available for research. The latest topographic maps obtained in 1990-2008 (e.g., MRC 1:50 000 digital data set created during 2001-2005 and JICA 1:100 000 paper maps from 1996-2003) are based on previously made American and Russian topographic maps, updated with modern aerial photographs or satellite images which nonetheless do not increase map resolution but renew information relative to on-ground objects. However, personal field observations have revealed one common

problem for all existing medium scale (1:50 000 to 1:200 000) topographic maps of Cambodia, i.e. an incorrect geodetic reference which most likely is inherited from older maps. Specifically, the longitude and latitude values recorded by GPS vary from those shown on topographic maps by 10s and sometimes 100s of metres, showing a systematic error throughout the study area. Therefore it ought to be concluded that: 1) there are no known cartographic outputs to trace planform changes of the Mekong beyond more than 50 years ago; 2) available historical topographic maps covering the study area are not of scale larger than 1:50 000; and 3) in historical change analyses, particular attention should be paid to georeferencing.

The MRC possesses a white-black aerial photography set made in 1959/1960 by the MRC Canada project at a scale of 1:40 000 which appear as the oldest reliable data in the context of historical change research. The next known aerial photography release belongs to the 1992-1994 survey at a scale of 1:25 000, covering the whole country which was conducted by the National Mekong Committee and FINNMAP. It offers the largest resolution aerial photography of the multichannel sections of the Mekong that were ever taken over the study area.

Satellite image production started in the 1970s, and coverage and quality for Cambodia during recent decades is particularly valuable because it covers a gap in cartographic production that occurred during the civil war (see Section 2.1). However, satellite images are usually expensive and do not always show the territory in full extent due to cloud cover. Nevertheless, it was possible to obtain recent SPOT images at 20 and 2.5 m resolution by competing in the OASIS (Optimising Access to Spot Infrastructure for Science) program (http://mediasfrance.org/oasis/).

The Advanced Spaceborne Thermal Emission and Reflection Radiometer Global Digital Elevation Model (ASTER - GDEM) at 30 m resolution and produced by the Ministry of Economy, Trade, and Industry (METI) of Japan and the United States National Aeronautics and Space Administration (NASA) were downloaded from the internet (http://www.gdem.aster.ersdac.or.jp/index.jsp) in order to perform trend surface analyses The Mekong 50 m resolution DEM was kindly provided by the MRC within a digital layers dataset.

The rest of data for the GIS analyses conducted in this research came from manifold sources both public and commercial. The Rivers Ganga, Orange and Upper Columbia were selected for planform metrics comparison with the Mekong in the study area (Chapter 1, Figures 1.4 - 1.6). The reasons for these selections are as follows. The Upper Columbia is a classic example of an anastomosed alluvial river as noted in the

Literature review. The Ganga is a classic example of a braided river and the Orange is a well-documented example of a multichannel, mixed bedrock-alluvial river. Other rivers were considered as potentially useful for comparison but there are quality comparable digital data sets available for the rivers selected, as is explained below.

The Orange River was digitized by the author from 1:50 000 topographic maps produced by Chief Directorate Surveys and Mapping (CDSM, 1998); the digital contours of the Ganga River were originally captured by N.Gupta from LANDSAT images (year 2000) and the Upper Columbia data at a scale of 1:50 000 (Government of Canada et al., 2005) were downloaded from the Natural Resources Canada web-site (www.nrcan.gc.ca).

In total, the coverage of gathered data according to the structure of this chapter is as follows:

1) 1959 aerial photographs (1:40 000) and 2003-2006 (20 m resolution) SPOT images of the Mekong (study area) were interpreted in order to obtain vector layers of retrospective and modern contours of sand bodies in order to recognize changes;
2) 1992 aerial photographs (1:25 000) and 2006 (2.5 m resolution) SPOT images of the Mekong (study sub-area) were used to define river/island bank contours and perform erosion/accretion analyses;
3) The Mekong, Ganga, Upper Columbia and Orange channel network vector layers were subject to planview metric analyses; island metrics were derived from the same dataset;
4) ASTER-GDEMs (Ganga, Upper Columbia and Orange River) and 50m DEM of the Mekong were used in the trend surface analyses.

All methods described in this chapter are designed for ArcGIS – ArcINFO (ESRI) software package version 9.2 and higher, including the latest version ArcGIS 10.

4.1.2 Historical changes of the Mekong

4.1.2.1 Sand bars

A fundamental issue when comparing historical material is to ensure that the comparison relates “like to like” features. Input data in this research were represented by black-and-white aerial photographs at a scale of 1:40 000 taken at the end of December 1959, SPOT-2 satellite images (dates of capture: 06/01/2003 and 20/10/2006) and SPOT-4 images (date of capture: 16/12/2006) with 20m resolution.

Unification of these data can be achieved by capturing information into vector layers in order to create an object-based data model (Lo & Yeung, 2007), and the performing a comparison using overlay techniques (Leys & Werritty, 1999). In an object-based data model, every object has certain or identifiable boundaries, for instance shorelines obstructed by vegetation and described by one or more characteristics assigned as its attributes. Figure 4.1 shows the major processing steps in the analyses of sand bar change starting from the raw data and finishing with the production of cartographic and table outputs.

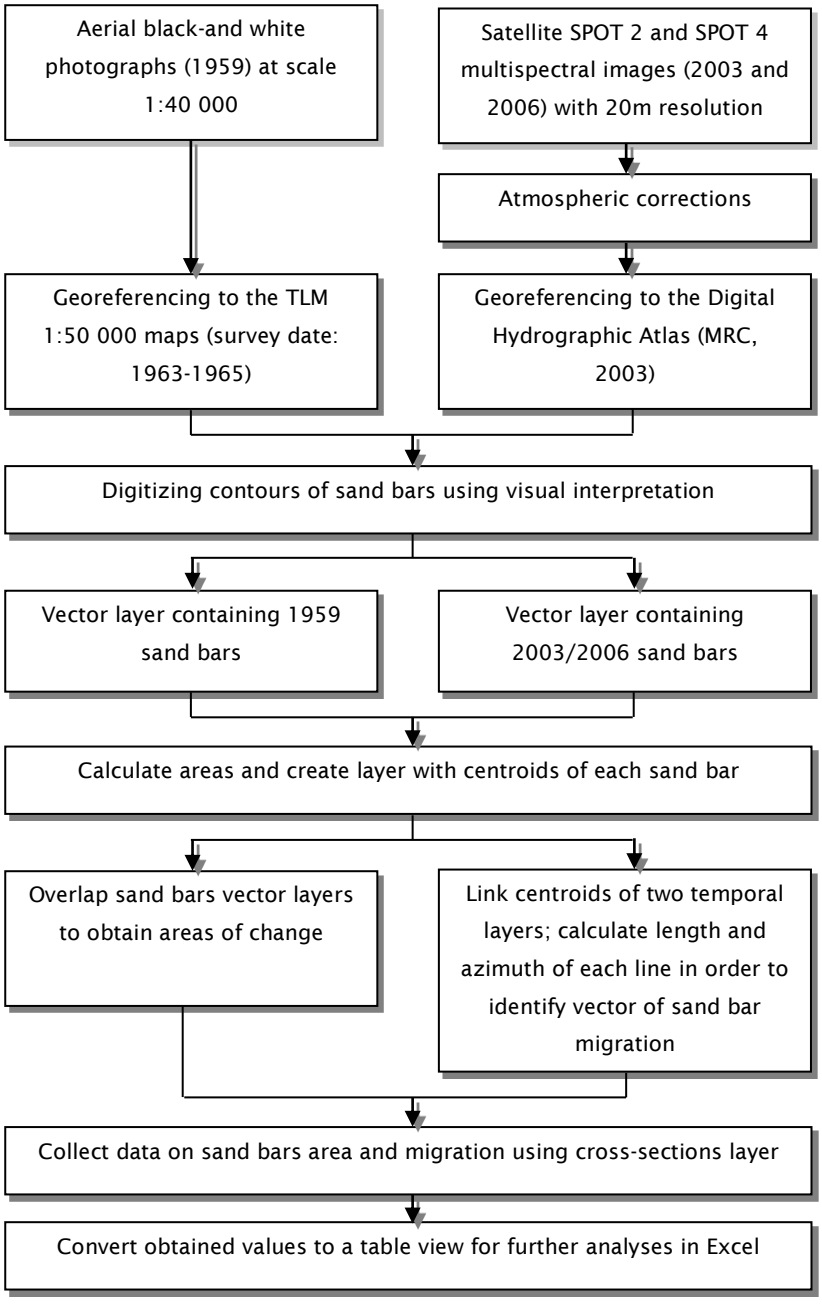

Figure 4.1. Methodology of sand bars historical change analyses.

Only big sand bars - longitudinal, lateral and diagonal (Section 5.1.1.1) - were chosen to map for the purpose of comparison while smaller medial sand bars were not considered. Detailed description of vegetation given in Section 3.5 shows that sand bars of the first three types are either sparsely vegetated by seasonal herbs or remain bare throughout the year; medial bars as a rule are occupied by riverine trees and bushes. From this observation it may be inferred that medial bars are rather fixed, perhaps due to their attachment to bedrock cores, whereas lateral, diagonal and longitudinal bars are more dynamic over time. The lack of vegetation on the latter types of sand bars means that visual identification and interpretation from aerial photographs and satellite images is readily achievable.

Thus, sand bars were recognized from images according to the following criteria: 1) consistent 'white' colour on SPOT images which contrast to the hue of the water or surrounding vegetated land masses and rock outcrops; 2) distinctive streamlined planview shapes and "serrated" edges (due to wet dune troughs and dry dune crests) in contrast to the angular shapes and straight edges of bedrock outcrops and 3) lack of vegetation and a uniform light grey colour on aerial photographs which, also, contrasts with the water and other terrain.

The biggest challenge of working with both sets of airborne images arises due to a lack of ground control points (GCPs) for the study area and missing camera parameters for the aerial photographs which are usually required for tilt and distortion corrections. To overcome such problems, georeferencing has focused on the river channels rather than the entire image and has been performed using the "image-to-map" technique (Gomarasca, 2009). Prominent features clearly identifiable on images such as bedrock exposures, tributary junctions, settlements and sometimes unchanged contours of main islands were applied as reference points in each individual case. A selection of these reference points were subsequently visited in the field to verify that their nature on the ground was the same as presupposed when viewing the images. First-order transformation during image rectification produced total root mean square (RMS) error values ranging between 12-16 m, values that are slightly higher than recommended (ESRI, 1994). ESRI (1994) recommend a target RMS of half a cell size, e.g. 10m given the resolution of the available imagery. However, the RMS errors were acceptable given the scale of the Mekong River sand bodies, as any morphologically-significant changes in sand body geometry and location would need to be of the order of a few tens to hundreds of metres.

Another important potential error is that related to the water level fluctuations between image dates (Table 4.1).

Table 4.1. Acquired images and corresponding water levels.
Water level data supplied by the MRC

Image and extent	Date of capture	Water level in Stung Treng, m	Water level in Kratie, m
SPOT 2 (Zones I&II)	2003-01-06	2.9	6.2
SPOT 4 (Zones II&III)	2005-12-16	3.4	5.7
SPOT 2 (Zones IV&V)	2006-10-20	7.4	17.56
Aerial photographs (study area)	Mid-end of December 1959	2.7	4.5
SPOT 5 (study sub-area)	2006-12-24	2.86	Not relevant
Aerial photographs FINNMAP (study sub-area)	End of November 1992	3.28 (average for the last 10 days of the month)	Not relevant

Sand bars usually have low surface gradients and are positioned low in any cross-sectional river profile. Consequently therefore increases or decreases of water level may significantly affect their planview geometry (Gurnell, 1997). This error is estimated using the Bruun (1988) formula detailed below (Equation 4.1) using water level records for Stung-Treng and Kratie provided by the MRC. The formula describes the relationship between horizontal retreat of the water surface/river bank interface (i.e. the shoreline; *R*, m) with the vertical rise of the water level (*H*, m) for a given river bank slope (θ, degrees):

$$R = \frac{1}{tan\theta} \times H \qquad \text{Equation 4.1}$$

Two out of three satellite images, as well as the 1959 aerial photographs, were taken in the middle of the dry season (December-January) when water levels are the lowest and only vary within a meter between different years. However, the SPOT2 image, covering the area around Kratie, captured at the end of October 2006 shows a 13.06 m higher water level with respect to the 1959 dry season level (4.5m) for Kratie. The slope of the riverbank at Kratie is equal to 80 degrees (ffw.mrcmekong.org), therefore lateral change in the strandline position due to water level differences between 2006 and 1959 is 2.3 m. Thus, the maximum possible cumulative error throughout the images is suggested to be ±18.3 m.

After all preparations and error assessments had been done, two vector layers representing the study area sand bars in 1959 and 2003-2006 were generated in WGS84 UTM, zone 48N projection via of on-screen digitizing. The area fields for each

layer were calculated and the centroid of each sand bar was extracted into a separate layer.

A cross section layer normal to the river centreline running from north to the south with 500m intervals was created (see Section 4.1.3.2 for more details) in order to plot sand bar changes with respect to the location of the river course. The spatial join option between two layers is applied to assign sand bars and their spatial characteristics (areas, centroids and movement vectors) to each cross-section line. This procedure has allowed the design of a set of diagrams with variable parameters based on one resulting GIS table containing distance along the river, areas of change, centroid movement distances and azimuths.

4.1.2.2 Erosion/accretion analyses (study sub area)

The absence of significant visible changes in channel configuration over the last 50 years stimulated a choice of high resolution images covering a smaller study sub-area in order to register bank erosion/accretion locations. The input data are represented by black-and-white aerial photographs at a scale of 1:25 000 taken at the end of November 1992 (FINNMAP) and a SPOT 5 multispectral 2.5m resolution image dated 24 December 2006 (OASIS program). Images were fully pre-processed (geometric and atmospheric corrections, orthorectification, georeferencing) by the suppliers.

Image content compatibility was achieved throughout by digitizing the visible contours of the channel network. In terms of the geomorphology (see Chapter 3 for full details), the study sub-area is comprised of numerous bedrock outcrops occupied by bushy vegetation, main islands with deciduous and evergreen forest cover, and seasonally inundated islands covered by flooded forest. A sand bar component in this area is insignificant and mainly occurs along bank shores forming a relatively narrow “beach” or “strand” zone (see Section 5.1.1.4, Figure 5.20). Bedrock exposures depict no noticeable lateral change over the short period of time (14 years); however, the planview extent of seasonally inundated islands is changing due to an abundance of bushy riverine vegetation along the lowest position in the river profile. Therefore the task was simplified in terms of digitizing only the contours of the main islands and riverbanks with the attached bare sand-bodies. The distinctive qualities used in sand bar recognition are listed in the previous section (p.76) whereas all other shores were easy to interpret with respect to visible trees rather than bushy cover (aerial photographs) and alteration between water (blue) and vegetation (red) pixels (SPOT

image). Bedrock exposures are covered by bushy vegetation during the dry season, therefore they were recognized as bushy patches (aerial photographs) and darker tone vegetated areas (SPOT image), but their contours were not included into output digital layers.

The fact that riverbanks are vegetated has introduced some uncertainty due to the presence of fringing trees and large tree crowns obscuring the channel boundary line (Figure 4.2). At such places, the most likely position of the shore was estimated by drawning "above" the vegetation cover (Rhoades et al., 2009). As a result of examining typical shoreline tree crowns from aerial photographs, the maximum uncertainty related to this issue is assumed to be ±2m, e.g. half of the biggest crown diameter. Variations in water level records for the appointed years (Table 4.1) do not bring significant errors into the analyses as levels remain similar one to another (2.86 m in 2006 versus 3.28 m in 1992).

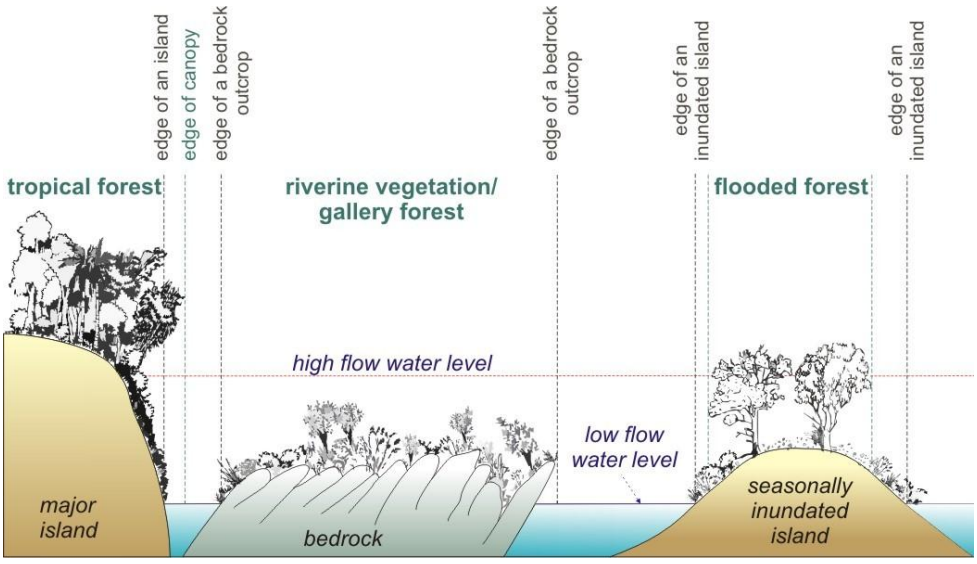

Figure 4.2. Schematic cross-section of geomorphological features across the study sub-area.

The method of erosion/accretion assessment demands the creation of two vector layers representing the riverbank/islands contours for given years, e.g. 1992 and 2006. The annual rates of the river bank erosion/accretion are calculated using the following formulae (Urban & Rhoads, 2004):

$$Areal\ rate\ of\ change\ = \Delta A/\Delta t \qquad \text{Equation 4.2}$$

where ΔA is subtracted area of change (m^2), and Δt is length of interval in years (ys).

$$Liner\ rate\ of\ change = \frac{\Delta A/\Delta t}{X_S} \qquad \text{Equation 4.3}$$

where X_s is the length of the shortest side of the ΔA polygon (m).

Any basic GIS software calculates an area of an object therefore an areal rate can be obtained as soon as erosion/accretion polygons are available. Linear rate estimation is more problematic because Equation 4.3 includes the shortest length parameter, e.g. width of each erosion/accretion polygon which cannot be detected automatically or easily obtained using dedicated GIS tool. Irregular polygon widths, however, can be obtained using the NEAR function (*ArcToolbox -> Analysis Tools -> Proximity Toolset)* which determines the shortest distance from each point in the input layer to the nearest polygon or polyline feature (Figure 4.3). The line representing a distance between an Input and a Near Feature is normal to a possible tangent at the Near Feature location and virtually equal to a perpendicular cross-section drawn from the Input Feature to the Near Feature.

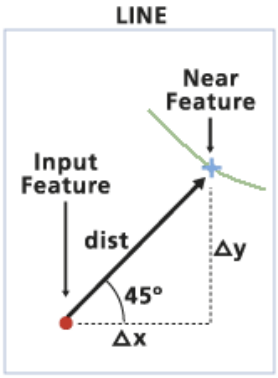

Figure 4.3. Illustration of the NEAR function principle showing measurements from point to polyline (ESRI, 2008).

This principle can be applied to determine the width of an elongated irregular polygon. One edge of a polygon should be converted into a set of regularly spaced points and then a distance from each point to the line representing the other side of the same polygon can be measured and treated as a polygon width. Figure 4.4 shows the structure of the proposed method using an example of two input islands; grey boxes are equivalent to ArcGIS Tool Box functions (ArcGIS 10) applied to the original dataset. The output linear erosion/accretion rates are presented in numerical view without mapping the position of a channel boundary for each intermediate year.

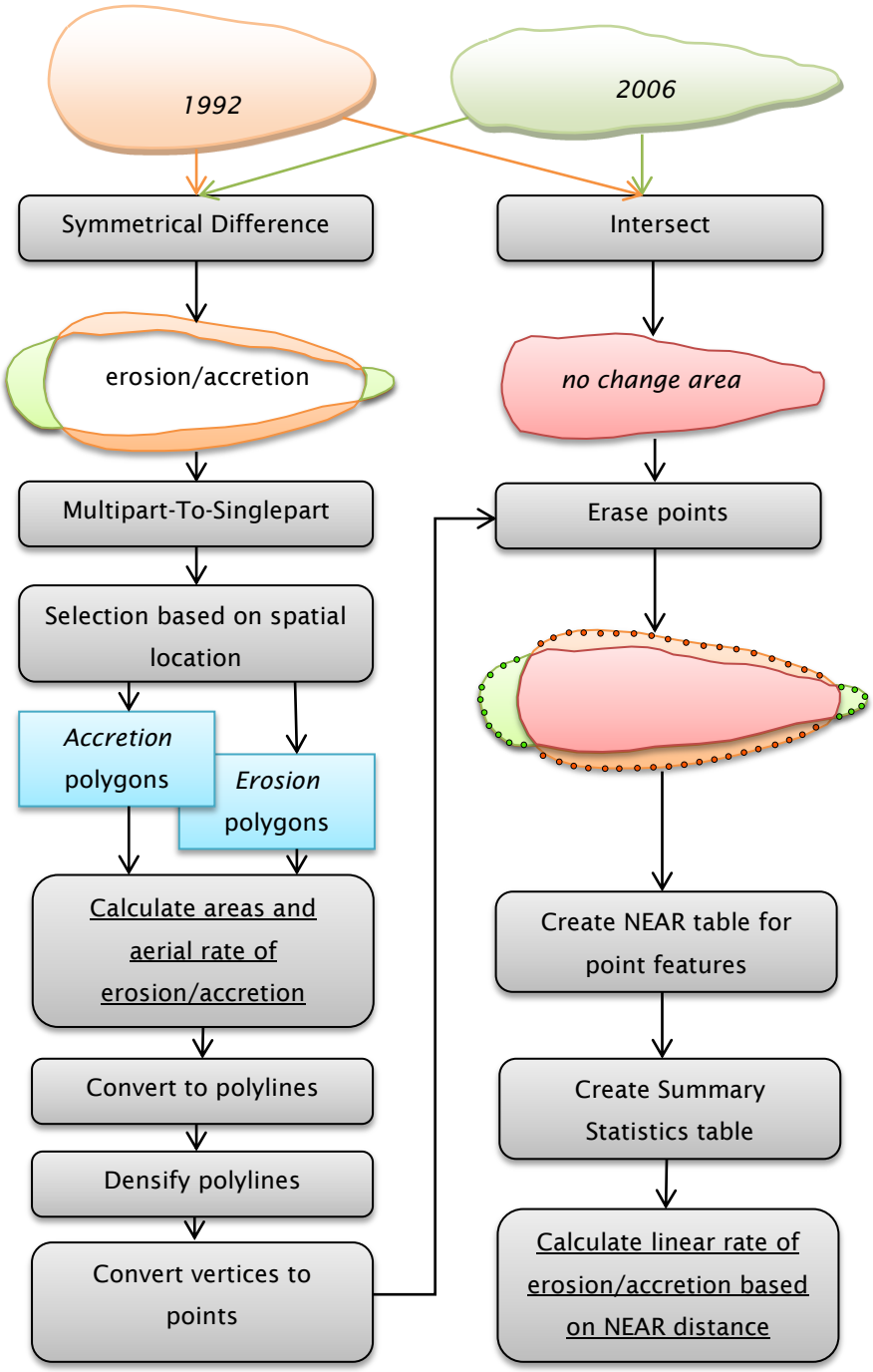

Figure 4.4. Bank erosion/accretion assessment using GIS

As the method was designed for bank erosion/accretion detection, it does not cover channel change identification and its measurements, e.g. newly formed sand bars or new channels which need be analyzed separately. Another limitation of the method occurs if the distance from the point of measurement to the other mainland or island

bank is less than the distance to the eroded/accreted bank. The solution is to relocate such polygons into a separate layer, apply the above method and join the data to the original data set in a final stage of analyses.

4.1.3 Quantitative description of channel networks

4.1.3.1 Constructing river centreline and channel networks

Anastomosed channel patterns are comprised of a variety of planview shapes leading to irregular distributions of channel widths and channel directions. When constructing the means to derive channel network metrics, the challenge of determining an irregular polygon middle line is assumed to be the equivalent of finding the half width of a polygon. ArcGIS contains two relevant functions that enable the building of a looped network and subsequently allows the extraction of river channel centrelines based on raster and vector data accordingly.

The first function is the *Thiessen* (also known as Voronoi) *proximal polygons* tool (ArcGIS 9.2). As shown in a Figure 4.5, the function processes a point layer and creates as output a polygonal layer where "…each polygon contains only one point, and any location within a polygon is closer to its associated point than to the point of any other polygon" (ESRI, 2007).

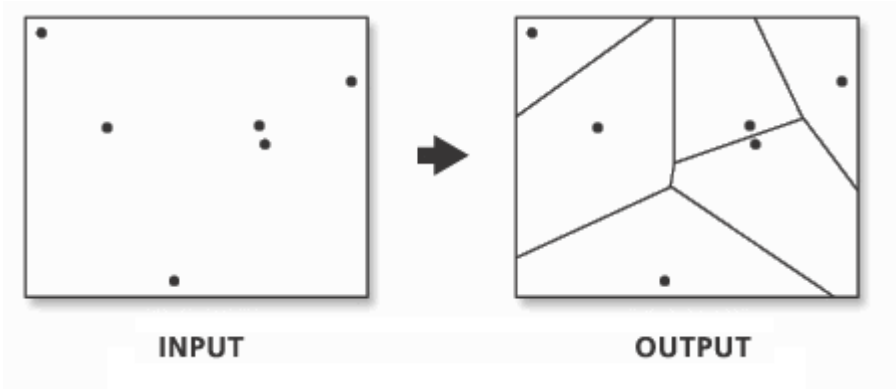

Figure 4.5. Illustration of the Thiessen Polygons function (ESRI, 2007).

This Thiessen function is applied herein to derive the centrelines of the macro-channel (Figure 4.6). For this purpose, contours of the left and right riverbanks are converted into points and used as input data for the *Create Thiessen* Polygon function. Later, the

segments comprising a middle line are copied into a separate polyline layer and processed with the *Smooth* operator in order to smooth sharp turns.

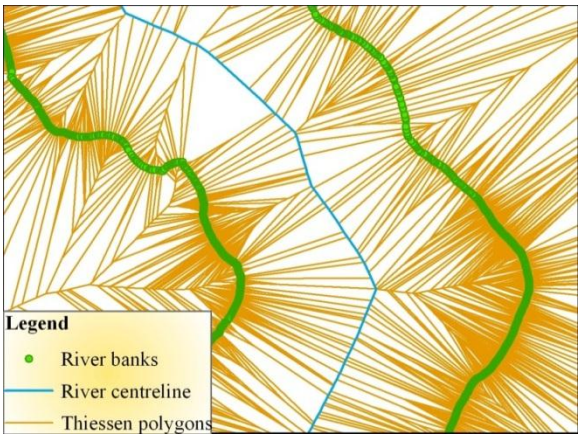

Figure 4.6. The Mekong macrochannel centreline (before applying *Smooth* function) and the supporting Thiessen polygons.

The Thiessen polygons method is appropriate to obtain one centreline but it is less desirable for channel network construction due to the time required to define the large number of lines needed to extract both polygon and polyline layers representing channels as input data. Instead, the *Euclidean Allocation* function working with raster data is employed. It produces a raster dataset where "…for each cell, the nearest source based on Euclidean distance is calculated" (ESRI, 2007) as shown in Figure 4.7.

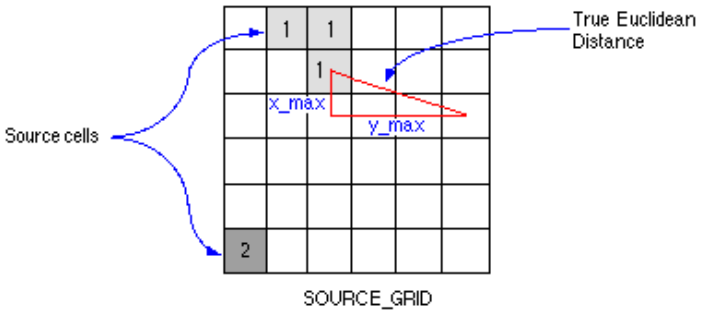

Figure 4.7. Illustration of the principles of the Euclidian distance function (ESRI, 2007).

In advance of implementing the *Euclidean Allocation* tool, the original vector layers have to be converted into a raster. Figure 4.8 shows a) the input dataset containing river network contours; b) the raster partitioned according to the Euclidian distance principle; and c) the looped channel network (green colour lines) obtained by converting the raster obtained from the previous stage into a vector layer. Smoothing and topological corrections of the resulting network have been done in order to get rid

of sharp un-natural corners and provide correct relations between objects (lines, polygons and nodes) participating in the network.

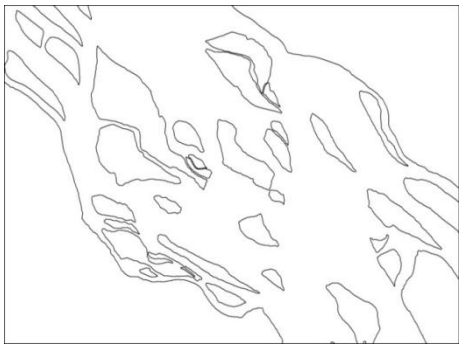
(a)

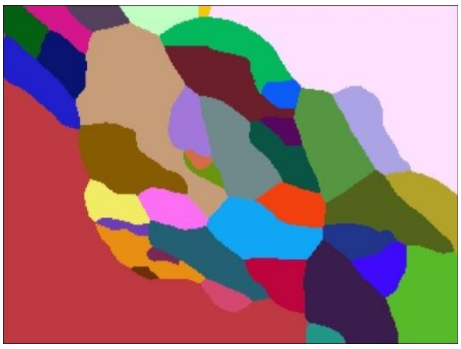
(b)

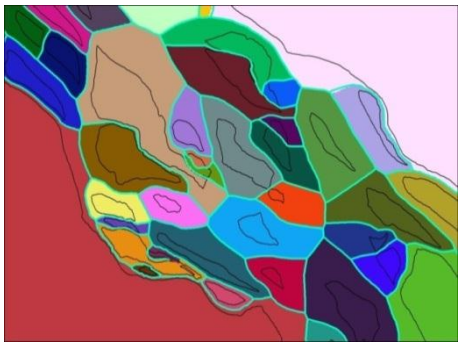
(c)

Figure 4.8. Looped channel network (portion of the Mekong study sub-area) using Euclidian Allocation function (ArcGIS 9.2, Spatial Analyst Extension; see text for details).

4.1.3.2 Obtaining channel network parameters: 'braiding' intensity, channel sinuosity and bifurcation angles

Further consideration of the generated looped networks enables the estimation of various planform parameters such as the number of channels per cross-section ('braiding' intensity), channel length between two consecutive bifurcation points

relative to the straight line distance between the two points (channel sinuosity), and channel network bifurcation angles. An additional layer depicting the location of cross-sections was required to assist in examining the channel network and referencing the above listed network parameters to distance along the macro-channel centreline. This layer was created with ET GEOWizard script (by ET SpatialTechniques, http://www.ian-ko.com) designed for ArcGIS. This latter script automatically builds a cross-sectional vector layer ("station lines") optionally on both sides of the river from the input polyline with predefined uniform length (distance from the input centreline to the end of cross-section) and step (spacing between cross-sections) expressed in map units, e.g. metres (Figure 4.9). Both length and step are chosen with reference to the river/network planimetric scale: length should not be less than the maximum width of the macrochannel, whereas step has to assure that the majority of channel lines are intersected by cross-sections whilst no intersections between cross-sections are allowed at river bends. Thus, as a result of practical exercises, cross-sections are spaced every 500 m along the Mekong, Orange and Columbia, and every 1000m along the Ganga. The length of sections selected to represent multiple channel patterns is around 100-120 kilometres for the Mekong, Orange and Upper Columbia and 220 kilometers for the Ganga River. Datasets for the Orange, Upper Columbia and the Mekong rivers are at a scale of 1:50 000, which enable comparison of their planview metrics without introducing scale errors into the results. The Ganga dataset at a scale of 1:100 000, but, considering the lateral dimensions (e.g. macrochannel width is up to 18km and islands length is up to 23 km) the Ganga is at least twice as large as the Mekong and so these data can be compared without additional corrections. Cross-section layer contains two numerical fields showing the line ID and the distance from the starting point of the polyline, i.e. the most upstream point of the macro-channel centreline. The intersection between the cross-sections layer and polygons representing riverbanks and islands results in evenly spaced channel width measurements. The same technique is applied in order to get the macro-channel width data using macrochannel boundary polygons.

'Braiding' intensity (total) (BI_T) or channel count (Figure 4.9) is estimated using the formula:

$$BI_T =< N_L > per\ XS \qquad \text{Equation 4.4}$$

where N_L is number of links (braids) and *XS* is the given cross-section (Egozy & Ashmore, 2008).

To obtain numerical values of braiding intensity, two layers (channel network and cross-sections) are spatially joined and the output layer, marking locations of intersections between them, is defined as "points". The resulting layer is subject to the *Frequency* function which produces a table based on a specified field, e.g. the cross-section number or distance along the river. The final table therefore shows the number of channel links intersected by each cross-section or, in other words, the braiding intensity (Figure 4.9).

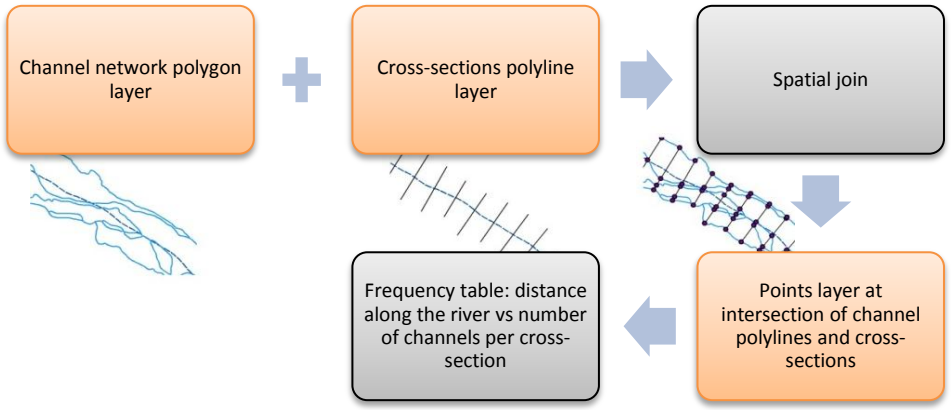

Figure 4.9. Estimating braiding intensity in GIS.
Grey boxes correspond to ArcGIS 9.3 functions, orange blocks symbolize digital layers with portions of the river channel network, river centreline cross-sections layer and output points layer.

The sinuosity index (Figure 4.10) is defined as channel length between two consecutive bifurcation points relative to the straight line distance between the two points:

$$P_T = \sum L_L / L_r \qquad \text{Equation 4.5}$$

where L_L is the length of links (segments, m) and L_r is reach length (m) (Hong & Davies, 1979).

The link length sum is an explicit parameter whereas the reach length may be ambiguous, particularly when the river course is changeable. Hence, for each individual channel, this attribute can be defined as the length of a segment connecting endpoints of a channel link (Figure 4.10).

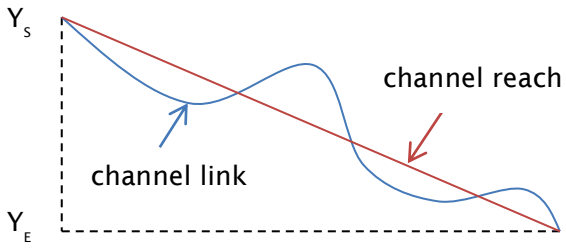

Figure 4.10. Channel link and channel reach length definition (planview).

Therefore, computation of the sinuosity index using GIS requires actual polyline length values (channel link lengths) and XY coordinates of the start and end points. Both values can be obtained by using the *'Calculate Geometry'* function when working with tabulated data in ArcGIS. Once known XY coordinates are determined, further channel reach length calculations proceed in accordance with the hypotenuse equation from the Pythagorean Theorem as follows:

$$L_r = \sqrt{(X_S - X_E)^2 + (Y_S - Y_E)^2}(\mathrm{m}) \qquad \text{Equation 4.6}$$

where X_S/Y_S and X_E/Y_E are *X/Y* coordinates (m) of the starting ($_S$) and ending ($_E$) points of a polyline.

The same method as applied to individual links also is applied to find the sinuosity of the entire multichannel reach based on the centreline geometry of the river section.

The next step in the planimetric analyses is to compute network bifurcation angles. At the preparation stage it has to be assured that the direction of each line in the channel network polyline layer coincides with the direction of the local flow. Apart from that, two new layers of polygons and points at each junction are required. These layers are complementary during the bifurcation angles calculation. Polygons are obtained from polylines conversion and a point layer can be formed using the *Build Network* function.

The whole procedure of extracting bifurcation angles, where each angle is marked in respect to a spatial position, can be divided into three major steps:

1) Distinguish the points of bifurcations for all junction points;
2) Calculate the angles between bifurcating channels;
3) Mark each angle according to the nature of the bifurcation adjustment as 'downstream', 'right' and 'left' (Figure 4.11).

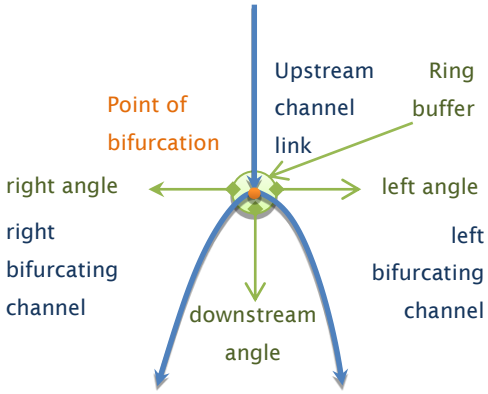

Figure 4.11. Definition of channel bifurcation components

Looped network bifurcations are described by one input and two output channel links connected to the input link, where the XY coordinates of each point are equal to the start and endpoint coordinates of these links accordingly. This definition is the core of the method which has been used to extract bifurcation points from the 'channel junctions' layer (Figure 4.12). The occasional situations when the main channel splits into three subsidiary channels has been excluded deliberately from datasets as they are rare and cannot contribute to the dataset for subsequent comparison.

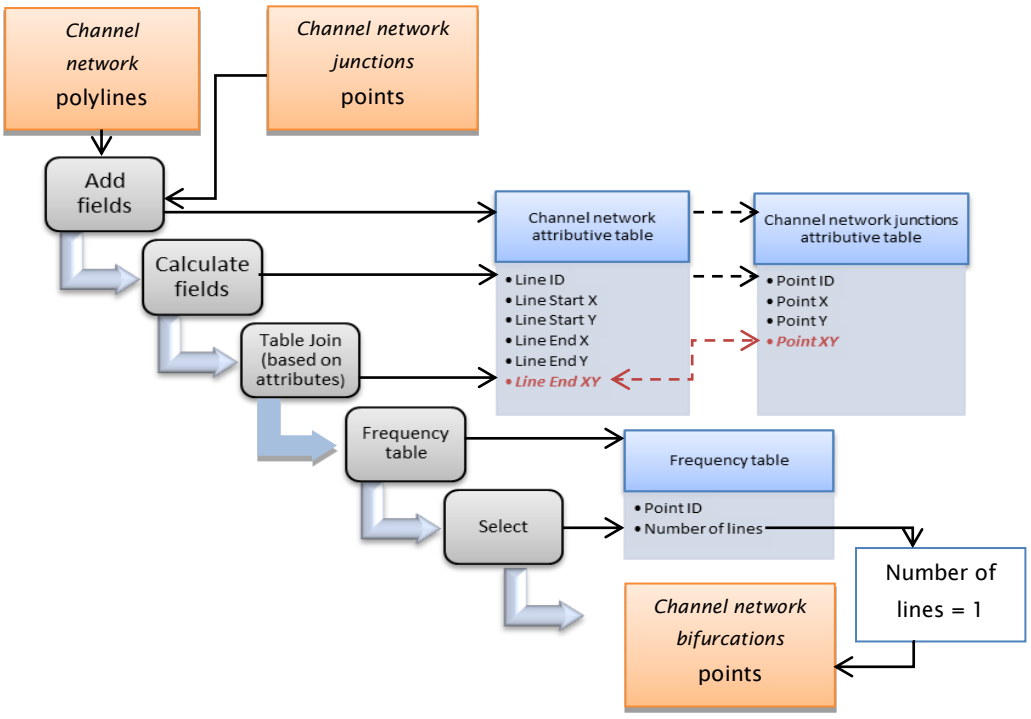

Figure 4.12 Extracting points of bifurcations.

Orange blocks symbolize vector layers, grey – GIS functions, attribute tables are in blue. Red color text corresponds to fields participating in join tables function.

When bifurcation points have been identified, another layer representing the channel network as polygons is involved. The angle between two bifurcating channels has to be measured in close vicinity to the junction because it is a matter of a few metres over which channel lines may be considered to be straight. As soon as a channel begins to curve it becomes more intricate to identify the uniform linear distance from the junction at which end points defining angles are located along the channel line, which leads to the dilemma that the angle between two curved lines based on their endpoints or points located on curved segments would significantly differ from the actual angle measured close to the point of bifurcation. Therefore, it is more convenient in terms of uniform methodology to specify a ring buffer around each point (Figure 4.11) with a consistent radius estimated in agreement with the value of a half of the shortest channel link length adjacent to the bifurcation. For all the data processed with this method the buffer distance does not exceed 10m.

The chosen distance of 10m allows the construction of ring buffers around each bifurcation point which have to be saved as a separate polygonal layer. Polygons representing the channel network are intersected with these buffers to obtain a polygonal layer of circles where each circle has a known radius (buffer distance) and is divided into three parts by lines coincident with channels connected to the bifurcation. Thus, angle measurements are carried out for circle segments using Equation 4.7 and transferred to decimal degrees according to Equation 4.8 (see below).

$$\theta = \frac{2K}{r^2} \qquad \text{Equation 4.7}$$

where θ is a circle segment angle (radians); K is a sector area (m^2) and r is a circle radius (m).

$$\alpha_S = \theta * 180/\pi \qquad \text{Equation 4.8}$$

where α_s is a segment angle (decimal degrees).

In practice, two new fields: ‘segment area’ and ‘angle’ should be added to the polygonal circle segments attribute table. Area field values are derived via the *‘Calculate Geometry’* table operator and the ‘angle’ field is updated using the formulae above.

Finally, when each areal buffer segment has designated angle values it should be marked in accordance with its position within the bifurcation. An assisting layer at this stage is created by clipping channel network polylines with ring buffers where each line has to have recalculated XY coordinates of its first and last points. This ‘clipped

channel links' layer is necessary because the line identified as the 'upstream link' can be also a 'downstream' link at its other end and vice versa. In order to store description of a line position, a new field 'position' should be added to the clipped channel links layer table. Once this is accomplished, the attributive table of this layer has to be joined to the bifurcation point layer on the basis of XY coordinates equality between the end points of the upstream link and the bifurcation point. A frequency table in this case is not required as the join type is one-to-one (e.g. only one upstream channel link is connected to each bifurcation). Thus, finally, selected records should have an 'upstream link' attribute in a 'position field'.

All remaining operations are performed using different types of selection based on the properties of the objects spatial locations. For example, once every upstream channel link has an adequate record in the attribute table, the circle segments which need to be marked as 'angle downstream of bifurcation' can be selected using spatial selection options (Figure 4.13).

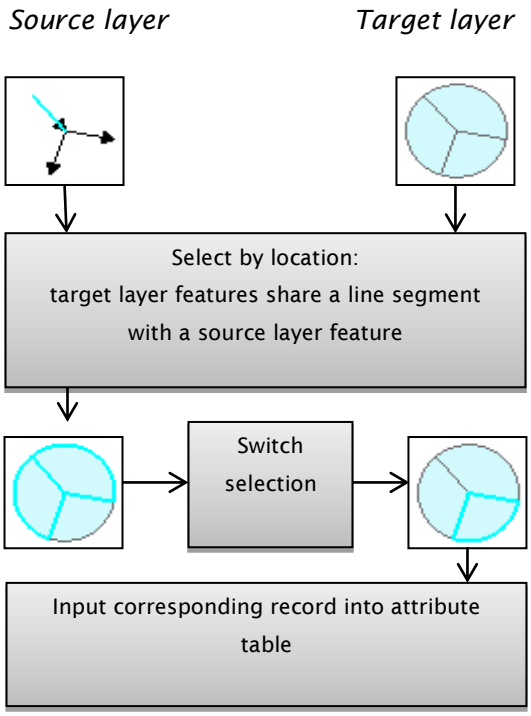

Figure 4.13 Selection of a circle segment to be mark as an 'angle downstream of bifurcation'.

The spatial position of segments containing angles between right or left bifurcating channel and upstream channel link is found by copying the upstream channel links with an insignificant offset distance, e.g. 1-2 metres to the left or right side and then spatially selecting underlying segments.

Obtained angular values between channels at bifurcations are used to calculate the bifurcation angles asymmetry ratio (*ΔL*) by the formula:

$$\Delta L = \frac{((180 - L_1) - (180 - L_2))}{L} \qquad \text{Equation 4.9}$$

where L, L_1 and L_2 are the downstream, right and left angles at the bifurcation respectfully, (in degrees).

After all the required data are extracted and recorded, they were exported from ArcGIS to Excel tables where more statistical analyses are available.

4.1.3.3 Islands metrics

Visual assessment of islands, which along with the associated channels comprise the bedrock-alluvial study system, shows that in most cases their silhouettes are far from the classic streamlined or lemniscate shapes. Instead, island shapes can rather be described as 'irregular', which has implications for the identification of basic parameters such as island length and width. Traditional length/width ratio formulae are designed to extract the maximum width of an island where the length is defined as a line connecting the most upstream and the most downstream island endpoints (Komar, 1983). However, the length of a crescent shape island measured using the method above, connecting end points, would return a result that is much smaller than the length of the curved centreline of the crescentic island. The representative width of an irregular-shaped island is rather ambiguous to define, e.g. there can be several width maxima within one island or width alongshore can decrease dramatically from its maximum value in contrast to the smooth changes in the width associated with a streamlined island. In terms of a GIS, the width of an object cannot be found using in-house functions; therefore personal judgement is involved when determining an actual location from where a width measurement can be taken. These various definition and measurement problems are not desirable when different channel network datasets need to be compared systematically. Therefore, apart from first defining the width/length ratio, the method described here offers estimation procedures to define other parameters which are better for the description of irregular shapes, including irregular islands.

In order to understand whether a difference between two types of island length measurements is crucial, the lengths and width of Mekong islands have been tested using two distinctive techniques.

The first method employs Minimum Bounding Geometry (MBG) ArcGIS toolbox operator (ArcGIS 10). It allows construction of the bounding features enclosing input polygons with respect of specified minimum bounding geometry type. Bounding feature measurements (length, width and rectangle orientation in decimal degrees clockwise from the north) can optionally be included into an attribute table as separate fields. MBG rectangles are available in two types in accordance with the initial principle of its construction, e.g. representing the smallest area and the smallest width enclosing the input feature (Figure 4.14). The best identity of the MBG rectangle length/width parameters to these original polygons (i.e. islands) is provided by the smallest width rectangle option.

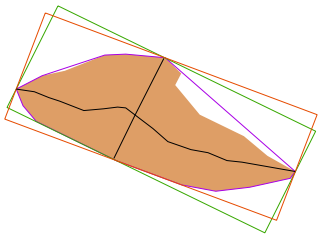

Figure 4.14. Minimum Bounding Geometry (MBG) Rectangles and Convex Hull polygon.

Brown polygon is an island; MBG rectangles: green - of the smallest area, orange – of the smallest width, purple – Convex Hull polygon. Black lines show width and length constructed with centrelines method.

The second method used to obtain island length values is to create and measure the centreline of each island using Thiessen polygons (see Section 4.1.3.1). The width is then equal to the length of a line drawn across the centreline at the widest place of an island (Figure 4.14). Finally, all captured width and length measurements were tabulated in Excel.

As follows from the figure above, width and length values can be rather different depending to the way they were obtained. The advantages of the MBG smallest width rectangle method are that values can be obtained in an automated way that does not require any personal justification. On the other hand, the length and width positions derived using centrelines seem more precise. However, not that many islands have particularly irregular shapes that require an individual approach. Therefore, the comparison between two datasets containing length/width value extracted using both techniques is essential to make a final decision on the most appropriate method to

use. If the range of output length/width ratios between them has not got much of a distinction, the MBG smallest width rectangle method is the one more preferable due to the easier and quicker implementation.

The same ArcGIS tool (MBG) enables the construction of *Convex Hull* polygons (Figure 4.14), i.e. polygons which contour the original object at the most prominent points where a line drawn between any two points contained by the original polygon would always fall inside of the convex polygon boundary. In other words, it bounds the original polygon in the same way a rubber string would. The perimeter of a convex polygon is one of the input components for formulae assessing shape *compactness*, *roundness* and *convexity* (Equation 4.10, Equation 4.11 and Equation 4.12). In fact, there are additional terms which might be used to describe irregular shapes (e.g., Pourghahramani & Forssberg, 2005), but these three terms had been specifically chosen as the most appropriate for describing anastomosed river islands.

Once each island is contoured using a convex polygon, the convex perimeter, island area and island perimeter can be derived using the '*Calculate Geometry*' function when working with the attribute table field. Compactness, roundness and convexity are calculated by the formulae below (Glasbey and Horgan, 1995):

$$Compactness = 4\pi \frac{area}{perimeter^2} \qquad \text{Equation 4.10}$$

$$Roundness = 4\pi \frac{area}{convex\_perimeter^2} \qquad \text{Equation 4.11}$$

$$Convexity = \frac{convex\_perimeter}{perimeter} \qquad \text{Equation 4.12}$$

All the above listed ratios are dimensionless and do not depend on scale or orientation of the input shape therefore they are highly appropriate for the purposes of comparison between different datasets. Table 4.2 shows calculated values of compactness, roundness and convexity for different shaped objects.

Table 4.2. Shape descriptors calculated for pieces of fruit and streamlined island shapes.
Modified after Van der Werff & Van der Meer, 2008.

Parameter / Shape	Apple	Pear	Carrot	Banana	Streamlined island (lemniscate)
Compactness	0.758	0.584	0.313	0.362	0.711
Roundness	0.758	0.603	0.315	0.369	0.711
Convexity	1	0.983	0.997	0.991	1

Convexity indicates the number and size of concaves in parental shape therefore such shapes as apple (circle) or streamlined island (lemniscate) would have it equal to 1 because their convex hull polygons are the same shape as the shape it was built upon. In such cases two other descriptors will be equal to one another. Thus, tabulated values enable identification of fluvial island shapes in terms of their boundary look-like and comparison with streamlined objects.

4.1.3.4 Trend surface and slice surface analyses

Channel gradient is one parameter which is often used to assist in channel pattern classification (Knighton & Nanson, 1993). Tooth and McCarthy (2004) had noted an association of switches between bedrock or mixed bedrock-alluvial anabranching reaches of the Orange River with steps in the long profile. However, the long profile of a river does not reflect the regional topographic settings of the entire terrain and, despite showing any gradient steps the long profile does not explain their nature. Tendencies in topography, and the adjustment of the river course to these trends at either local or regional scales, are better seen from trend surfaces interpolated from ground altitude values. By definition, a trend surface can be compared to 'a piece of paper' fitted between raised points (ESRI, 2007). The order at which the surface is constructed corresponds to a number of bends, e.g. the first order results in a straight surface tilted in one direction, the second order surface will be tilted in two directions, and so on. Surface order is specified by the user with respect to input data which can be either a digital point layer with altitude values at each point, or a DEM. General and local trend surfaces in this research have been obtained from point layers converted from input DEMs (see Section 4.1.1) using the Spatial Analyst extension in ArcGIS 10.

Previous research in the area of interest indicated significant altitudes marking surfaces referred to as ancient terraces (Section 3.2). Visualization of these surfaces

using modern techniques can be achieved with the assistance of DEM slice analyses (ArcGIS 10, Spatial Analyst). The output of this analysis (e.g. a raster image) shows the distribution of surface elevation values across the area in a distinctive way, where the DEM is classified into several zones according to the natural groupings of elevation values. Each zone boundary represents the 'natural breaks' option in DEM elevations. The obtained extent of each zone can be verified later by ground observations performed during field trips in the study area.

4.1.3.5 Spatial time series analyses

Time series analysis techniques (Chatfield, 1996; Hamilton, 1994) have been applied to spatial data series for all the studied rivers in order to determine whether a degree of spatial dependence exists between channel slope and river corridor width. For all rivers in the data set a single channel slope value for a given cross-section was determined by measuring the slope of individual channels within the cross-section using a DEM. These values were averaged and referenced to the respective cross-section and corresponding width value. Autocorrelation (ACF), Partial Autocorrelation (PACF) and Cross-correlation (CC) functions for data series have been derived using the MiniTab 16 (MiniTab Inc.) software. Autocorrelation analysis in this application describes the correlation of a spatial series to its own upstream or downstream values such that the ACF provides some indication of 'memory' in the data series along the channel. The PACF is difficult to define in simple language (Gottman, 1981, p.141) but importantly it truncates at the lag value that defines the autoregression (AR) process and thus it is useful to determine more precisely the significant lag value beyond which there is no statistical persistence (i.e. no memory).

4.2 Field samples processing methods

In order to characterize the sediments and depositional setting of the Mekong River, a number of field samples and sedimentary section descriptions have been collected during field trips as a part of this study (Figure 4.15 and Appendix I). These have included:

1) Rock samples of channel bedrock and bedrock outcrops along the riverbanks;

The structure, texture and mineral composition of collected hard rocks have been investigated to identify rock types because the geology of the study area, especially within the limits of the macrochannel, required more detailed description or verification (see Section 3.3. and Figure 3.12). The dips and strikes of outcrops have been carefully documented during sample collection and taken into account when updating existing geological maps. In parallel, photographs of a variety of bedrock erosion features established within a macro-channel have been taken.

2) Gravel, sand, silt, mud and soil samples from different localities along the river and its islands;

Samples of bedload gravel and sand, as well as samples of sand comprising depositional sand bars, were collected from river channels in order to obtain information about grain size distribution using the dry sieving technique. Silt, mud and soil samples containing some organic matter were obtained from the Mekong islands and riverbanks and processed further through dry sieving and by ashing to determine the organic component.

3) Palaeochannel borehole sediments sequences

The location of the single palaeochannel in the study area was identified from consideration of the report by Stapledon et al. (1961), which also contains palaeo-channel sediment grainsize distribution records and generalised engineering borehole logs gathered from three cores set within the limits of the former course of the river in this area (Figure 4.15). The above mentioned report does not provide any information concerning the age of these deposits, therefore a new borehole was made in order to collect material to describe the palaeochannel fill and to obtain luminescence dates (See Appendix I, Table A2). Dating was required to determine the time limits during which the palaeochannel was functioning and the time of abandonment, and thus contribute towards the knowledge of the river incision history. Due to coring equipment limitations (percussion hammer Cobra TT) the maximum depth achieved in the borehole (5.65m) is smaller than the nearest known depth of the basal sandstones (10 m). It means that the sediments related to the stage of initial river channel sedimentation were not extracted; nevertheless, the dates obtained from the higher sediment sequences have allowed an interpolated minimum age of the buried channel based on sedimentation rates calculated from the distance between dated horizons and the observed thickness of sedimentary facies. Finally, the most recent dates allow an estimation of the time of final channel abandonment.

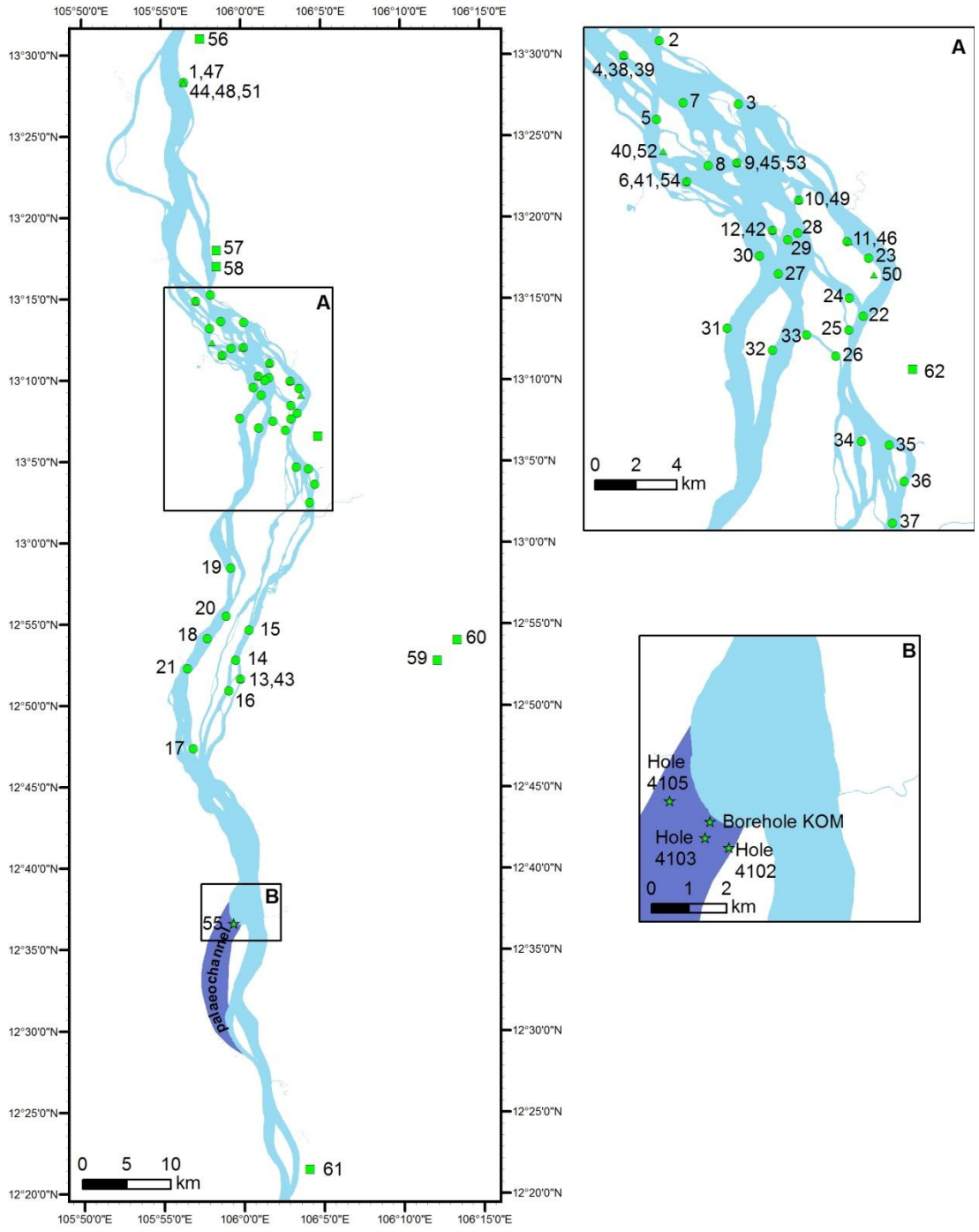

Figure 4.15. Field samples location maps.

Sample numbers (map on a left) are listed next to each location; see Appendix I for the inset map A (top right) - Tables A1, A3, A4 and Tables A2, A5 for the inset map B (bottom right). Symbols on the map: circle – rock sample, triangle – gravel, sand, silt or soil sample, square – palaeo-terrace section, star – borehole.

Five extracted core sections were photographed and sediments described according to their appearance, e.g. structure, texture, colour and depth relative to the ground surface. Nine sediment samples were selected to identify grain size using wet sieving techniques (Section 4.2.1) and another four were taken for the luminescence dating (see Section 4.2.2). Finally, the borehole log was correlated with those obtained in the 1960s.

4) Terraces

During the 2010 field trip to the study area, several locations revealing sections of the alluvial terraces of the Mekong were discovered (Figure 4.15; Table A1, "Terraces" section in Appendix I). Every site was fully documented and a number of sediment samples were taken to provide a summary description of the terraces. Five samples were taken for luminescence dating (Tables A3 and A4 in Appendix AI) and 150 grammes of wood from the basal blue clay layer of the 20 m terrace (location 61 on Figure 4.15; Table A1 in Appendix AI) were collected for radiocarbon dating.

4.2.1 Grain size analyses

Quantitative information on gravel, sand and silt particle distribution was obtained using dry and wet sieving techniques. This work was carried out within a research laboratory at the University of Southampton using a set of sieves (British Standards) with decreasing order of aperture size from 1024 mm to 63 microns, electronic scales, a mechanical sieve shaker and a drying oven. The data on grain sizes received in millimetres were transferred into φ (phi) units to conform with the Udden-Wentworth grain-size classification scheme (Wentworth, 1922).

Dry sieving was applied to dry samples of loose gravel, sand and silt varying in quantity from 100 to 400 grams. First, each sample was weighed and then put into the top sieve in a nested column of sieves arranged in decreasing mesh order (from the largest aperture size sieve on a top to the smallest one at the bottom of a column). After that, the sieve column was placed on the shaker and operated for 10 minutes of continuous sieving (shaking). When finished, the portion of material left in each sieve was weighed and the results of measurement tabulated.

Consolidated sediment samples of gravel, sand, silt and clay (e.g. the palaeo-channel borehole samples) were processed using a wet sieving technique. Sample preparation

included an overnight soaking of the sample in calgon (sodium hexametaphosphate) in order to disintegrate sedimentary aggregates. Then each sample was manually sieved using a sequence of decreasing mesh size sieves under the jet of a running tap until the water becomes clear. The portion of material drained out through the sieves was left to settle overnight and later the surplus water decanted. The remaining sediment fraction settled overnight was placed into an over at 40^{0}C for 24 hours in order to dry completely. Finally, the dry sediments were weighed and the results tabulated.

Samples containing organics were processed with wet or dry sieving methods in order to distinguish two fractions: the one coarser and the second one smaller than 63 microns using corresponding aperture size sieve. As a result, the organic component was isolated together with the finest inorganic part. Then this fraction was weighted and transferred into metal cups. The cups were placed into an oven at 450^{0}C for 2 hours so that the organic matter was incinerated while mineral grains remained the same. When removed from an oven, the weight of the ashed samples was documented and the difference between two measured weights calculated.

4.2.2 Luminescence dating of sediment samples

The optically stimulated luminescence (OSL) method was chosen to date sediment samples from the palaeochannel borehole and terrace sections. The samples were collected during a field trip by the author and the OSL analyses performed in the University of St Andrews Luminescence Laboratory by a third party.

Samples from the borehole are from vertical intervals because the borehole was made at 90° to the ground surface and samples were taking from along the percussion gouge. Terrace samples were collected horizontally from the freshly made clean sections that exposed sediment layers. In both cases, sediments were sampled using 4cm diameter and 15cm length aluminium or steel tubes with one capped end; each tube was pushed into the sediment layer until it was entirely filled, then extracted and fixed with a cap at the other end. Particular care was taken not to expose the contents of tubes to daylight as lack of light exposure is required for the OSL dating technique. Up/Bottom (for vertical samples) or In/Out (for horizontal) ends of a tube were marked and appropriate characteristics (sample depth, type of sediments) documented.

Collected samples were sent to the Luminescence Laboratory (see Appendix II) for details on method and the age determination.

4.2.3 Radiocarbon dating

A freshly excavated section of a 20m terrace situated within the limits of the Mekong active floodplain ~15km south of Kratie (see Figure 4.15 and Table A1, “Terraces” section in Appendix A1) had been described and palaeo wood pieces collected from the basal clay layer positioned at approximately 6 meters down from the modern ground surface. 150 grammes of wood were sent to the Beta Analytic Radiocarbon Dating Laboratory in order to determine an age of the accommodating horizon (see Appendix AIII).

5 Results

This chapter is subdivided onto two sections. The first part provides geomorphological description of the Mekong River within the study area based on author's research and findings whereas the second part is devoted to planimetric analysis and comparison of multichannel networks and island shapes using GIS techniques.

5.1 Qualitative, quantitative and chronological characteristics of the Mekong

5.1.1 Geomorphological features of the Mekong

5.1.1.1 Sand Bars and deep pools

In terms of appearance, there are four sand bar types in the Mekong River: longitudinal, lateral, diagonal and medial (in accordance with the classification of Church and Jones, 1982). Longitudinal bars of considerable dimensions (100s of metres in length) are situated at the upstream end of main islands (Figure 5.1) and at localities where channels broaden significantly, lateral sand bars (point and counter-point) can be observed against the river/island banks and elongated up to 2 000 metres. Diagonal sand bar deposits are formed where the water slows down after passing over bedrock outcrops (Figure 5.2); the length of those bars can be up to 800 m.

Figure 5.1 The upstream end of the Kaoh Samrea island – example of longitudinal bar. Figure for scale 1.6 m (flow direction: right to left).

Figure 5.2. Diagonal-channel sand bar between Kaoh Preah island and the left river bank.

Height of the section on the left is c. 1.5m, main flow direction during higher river stage was from background to the foreground. Local flow direction at the time of photograph was left to right.

The smallest (length scale 10s of metres) but perhaps the more numerous medial bars occur all around submerged rocky exposures and can be easily seen at the time of the dry season (Figure 5.3). The latter widespread type is not mapped in this thesis due to the seasonal character of their appearance and the scale of the cartographic materials used.

Figure 5.3. Example of small medial sand bar at a vegetated rocky outcrop.

Height of deposit is c. 1.5m, flow direction is from right to left.

Downstream of Stung Treng, where diagonal bars neighbour bedrock exposures, the thickness of the former can reach up to several metres. Usually these and other bars have a layered structure as a relict of previous flow events (Figure 5.4 and Figure 5.5). At the upstream end of islands, longitudinal bars typically have fluvial dunes exposed on their surfaces during dry season flows (Figure 5.1), but locally aeolian dunes may also be present during the dry season. At the river section downstream of the Sambor Rapids, lateral sand bars are the only features comprising the single meandering channel, and are large (up to 1.5 km in width).

Figure 5.4. Planar horizontally bedded sands (at base, c.0.5m thick) are conformably overlain by planar to slightly concave upwards cross-beds formed at the slip face of a diagonal bar, c. 1.5m thick.
Primary channel flow direction is from background to the foreground with a strong cross-channel component of flow from left to right of the view.

Figure 5.5. Point sand bar layered structure at the small scale exhibits ripple cross-bedding and small scale erosion and fill structures.
Flow direction is bottom left to the top right; cigarette lighter (8cm in length) provides scale.

Thus, deposition processes within the Mekong are clearly marked by the occurrence of sand bars throughout channels within the study area. Another plentiful, but less visible, geomorphological feature are deep pools indicating erosion (incision) events within the multichannel sections of the river which have been classified by Conlan et al. (2008). All types of pools as distinguished in the above mentioned report (see Section 3.2, Figure 3.9), can be found within the study area, but, the majority of them belong to the '*forced pools*' category associated with outer/inner channel constriction (Figure

5.6, box A and C). Pools at zones of confluences (Figure 5.6, box B) frequently are accompanied by erosion processes and can be especially deep (up to 80 m).
At some locations the spatial alignment of deep pools correlates with the trend of known and probable faults (Figure 5.6, Box C). Overall, the number and type of observed pools contributes towards the idea that locally vertical erosion predominates over lateral channel movements. Narrow channels, frequently obstructed by rock outcrops, are often occupied by a constellation of closely-spaced, short pools (Figure 5.6, box C) in contrast to alluvial reaches where pools are fewer, more extensive and relatively shallow.

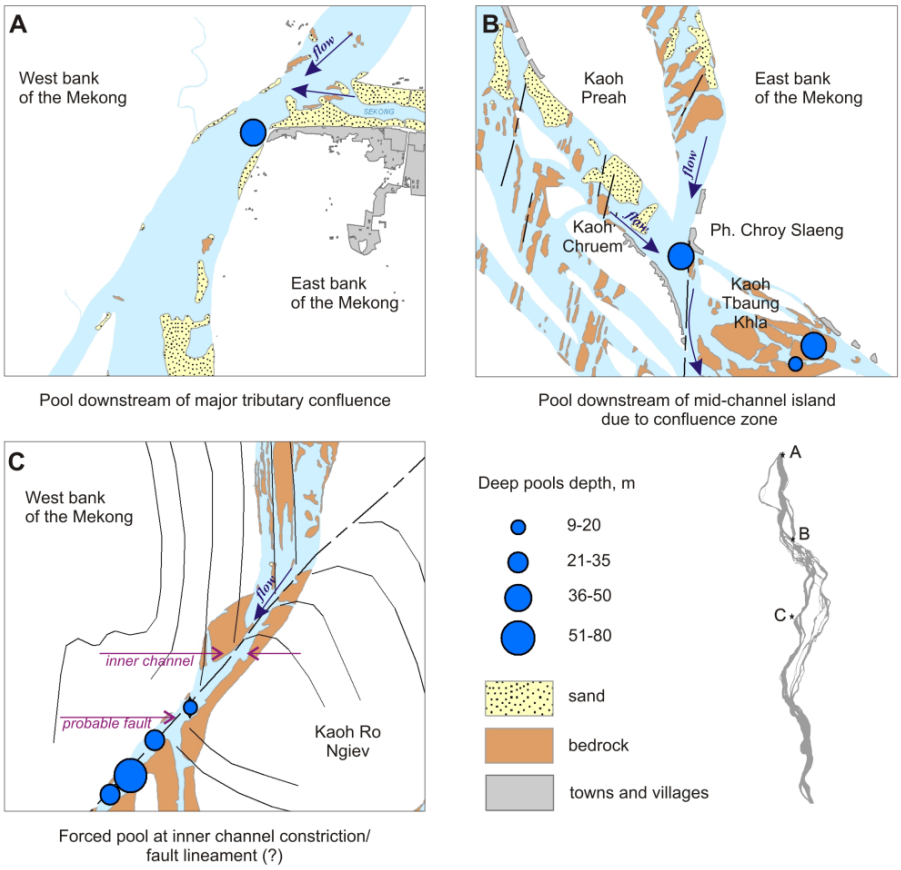

Figure 5.6. Explanatory diagram indicating key concepts with respect to location of deep pools, bedrock outcrops and sand bars (deep pool locations from Chan et al., 2003).

5.1.1.2 River channels

The multichannel pattern defines the character of the Mekong River within the study area. However, when defining channel types the complex as a whole cannot simply be

termed an anastomosed complex; i.e. a 'channel type'. Rather plan views of the complete channel networks allow distinction of four main channel types (Figure 5.7) that collectively compose the Mekong River system in the study area: (i) primary channels (sensu Knighton & Nanson, 1993; Figure 5.7B and C) are the major waterways which are permanently wet and define the major element of the plan view of the macrochannel. These channels are influenced by regional tectonics and macro-scale geological structure; (ii) secondary channels (sensu Knighton & Nanson, 1993; Figure 5.7D), are smaller than primary channels. Their courses are influenced strongly by local sand bars and bedrock outcrops and may be dry or isolated at times of low water; (iii) cross-channels (Figure 5.7B), as specifically defined here, are usually of similar scale to primary channels and may be seasonally dry but importantly they dissect large islands, the surface of the latter rising well above maximum flood levels; and (iv) blind channels (Figure 5.7C) are connected to any of the above mentioned channel types only at one end with the other end of the channel ending at an island or rock outcrop. The primary and cross-channel network remains visible in planview during high flows, operating as a single integrated network. In contrast, the majority of the secondary channels network is only visible when the water level is low. Blind channels can be found in either primary or secondary channel networks (Figure 5.7C and D). Thus, the complexity of the channel network is strongly stage dependant.

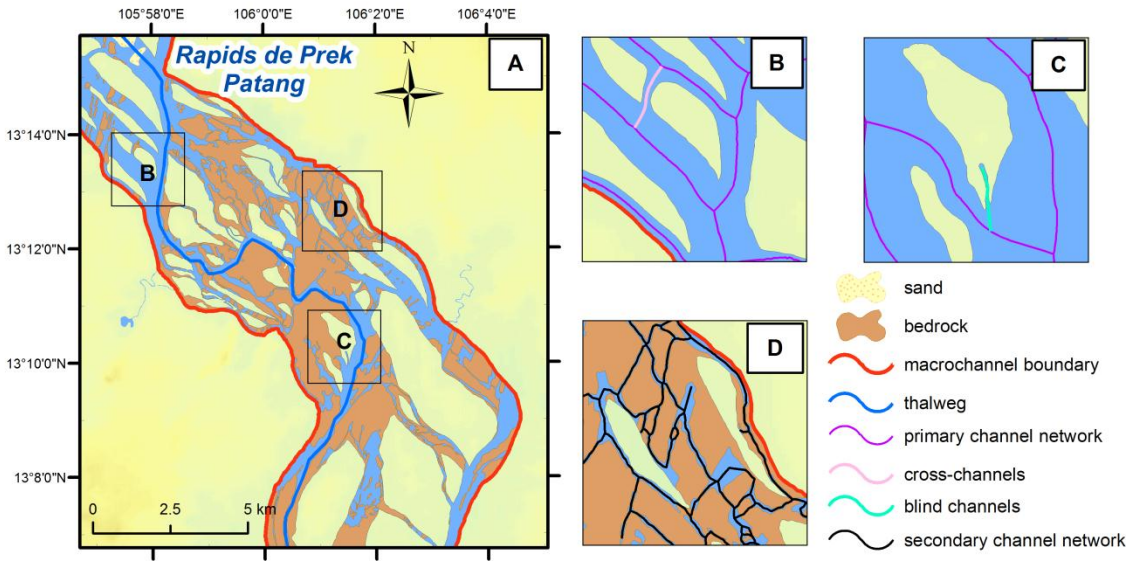

Figure 5.7. Planview channel network definitions. A) section of the Mekong River with macrochannel boundaries; B) primary channel network and cross-channels; C) primary channel network and blind channels; D) secondary channel network.

i) Primary Channels

The width of primary channels ranges from around thirty metres up to 2500 m within multichannel sections, and reaching up to 4500 metres at places where the primary channel is defined by the macrochannel boundaries, e.g. single channel reaches. Such channels are elongated in the regional flow direction, account for a significant proportion of the river conveyance during all flow stages and are often suitable for navigation. Depth varies from branch to branch and during the low flow period comprises 5m on average (CNMC, 2006). These primary channels are separated by large well-vegetated islands that rise about 5 - 10 m above the average low water level. The character of all the four channel types can vary along the study region from north to south. However, the basic character of the primary channels is determined by the relative contribution of sand and bedrock to the channel boundaries that is visible during low, dry season flows, and the streamwise classification that derives from the variation in sand and bedrock is presented in Section 5.1.1.4. This information, together with the variation in the total width of multiple channels and the frequency of such widths, allows distinctive streamwise geomorphological 'zones' to be defined, as is also detailed below (see Section 5.1.1.4).

ii) Secondary Channels

Given the geological and structural control, the areal distributional of outcrops defines the appearance of a network of secondary channel*s* that may be dry during low flows. These channels are usually less than 30 m wide and may be deep, narrow channels between rocky islands, or shallow channels, that are slots formed along zones of near parallel vertical joints or slightly opened joints and bedding planes. Importantly, because of the local structural control, the alignment of the secondary channels may be acute or obtuse to that of the primary channels, including junctions at 90° or more. Although these channels convey water during high monsoon stage, at that time they are completely inundated and their effect on the bulk flow structure is unknown. Sometimes, apart from water, opened joints are filled by sand, pebbles and vegetation roots. This channel type can also be observed at the Sambor Rapids with similar proportion of bedrock and open water spaces in combination. A cartoon of a cross-section across a portion of the macro-channel including secondary and primary channels is reproduced as Figure 5.8.

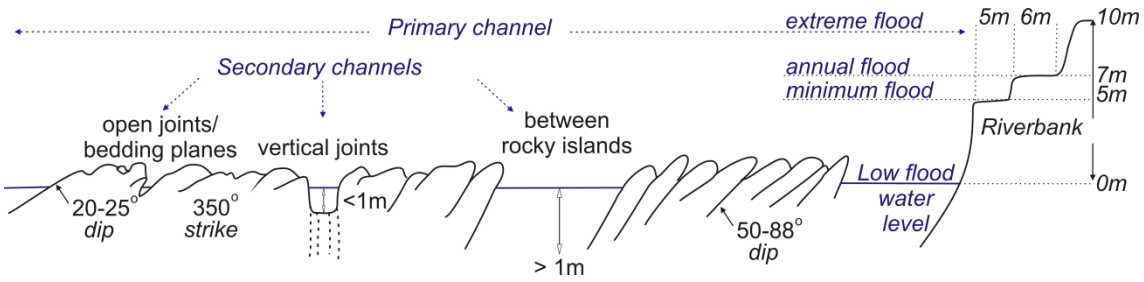

Figure 5.8. Looking along the strike of beds at the Rapids de Prek Patang (modified from sketches by Stapledon et al., 1962). Main flow out of image.

iii) Cross-Channels

This kind of channel is defined as a comparatively narrow alluvial river channel that connects two primary channels by flowing across a large island at an angle that is acute to the flow direction of the neighbouring primary channels. Often the cross-channels appear to have divided a previously undivided island into two or more separate parts (Figure 5.9). By this definition the spatial position of cross-channels are transverse or nearly transverse to the primary channel direction. The fact that previously intact islands have been cut by cross-channels is circumstantially proved by correlating elevation marks on the high level plain to similar variation in elevations on the islands either side of the zone of interest, and by the elevations of the channels in planview. Often the cross-channels occupy low areas on the islands that are also flanked by similar low areas on the plain. During the dry season, when water levels reach a minimum, a cross-channel may remain wet, but usually they are partly dry (due often to alluviation of one end of the channel) or completely dry. Such channels are vegetated by trees and bushes along the periphery (Figure 5.10) and often have pioneer vegetation that is tolerant of inundation established within the higher areas of the cross-channel. The beds are predominately sand often, with a small admixture of fine gravel, and may be characterised by fluvial dunes and ripples with seasonal development of aeolian dunes and ripples. However, a number of cross-channels have considerable depth and contain water throughout the year. The development stage of the cross-channels is unknown, but some examples of large cross-channels can be found which seem totally alluviated, revegetated by mature forest and appear to be relict whilst others are partially alluviated. It is not known if these channels are reactivated on occasion.

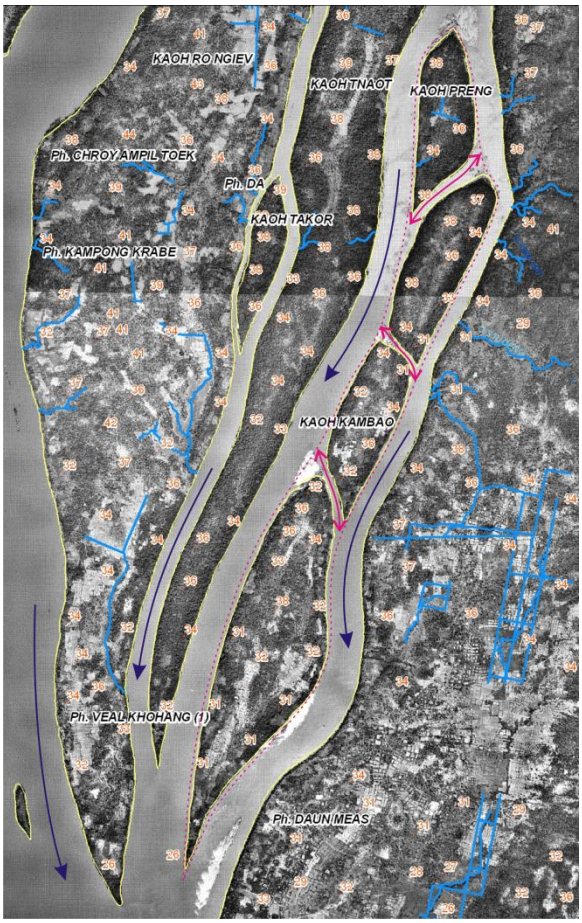

Figure 5.9. River cross-channels upstream of Sambor Rapids.

Purple arrows show primary channels flow direction; red dashed line depicts contour of the initial island; red arrows indicate cross-channels and flow direction. Map is based on modern river contours (yellow lines) with 1959 aerial photographs as a background (all courtesy of MRC).

Figure 5.10. Cross-channel between Kaoh Preng and the next downstream island (see Figure 5.9), view from east side towards west (dry season, January, 2008).

Primary channels flow direction is from right to left, figure for scale 1.6 m, cross-stream flow into the picture.

In order to trace the development of the cross-channels, at this point a brief comparison of historical data has been made (Figure 5.9). It shows the full coincidence of the modern riverbank lines (MRC, 2003) with the 1959 aerial photographs and displays a cross-channels in existence now and then, e.g. the cross-channel was relatively 'long lived' (i.e. present for at least 44 years).

iv) Blind Channels

Blind channels are connected to the channel network at one end only. In the study area, they can be observed within the major and/or seasonally-inundated islands (see Section 5.1.1.3), but even more often this type of channel can be found in the areas of outcropping bedrock.

Blind channels may merely store water with little conveyance until the bank tops are overtopped and, at low flows, they may provide lagoonal environments rather than be freely-flowing. Within fluvial multichannel systems smaller than the Mekong the possible reason for the development of blind channels is localised rapid bank scour by highly turbulent reverse flow created by vegetation root masses (Harwood & Brown, 1993), or by splay channel development due to overbank flow (Tooth & Nanson, 1999). Hence, the role of vegetation is important for the Mekong channel pattern, although it is subordinant in affecting the direction of the primary flow in contrast to bedrock outcrops. Secondary flow circulation created when the flow passes bedrock exposures may create an effect similar to that of vegetation root masses and stimulate bank erosion that targets the riverbank. The absence of levées or natural vegetation on some riverbanks as well as the presence of natural local topographic lows on river/island surfaces, facilitate overbank flow, and further scour development. Thus, blind channels participate in a linear dissection of the terrain (Tooth & Nanson, 1999) and act as slots of standing (low) or flood (high) water; this point will be returned to in a discussion (Chapter 6, Section 6.1). Alternatively, linear sand bars developed against river banks may be detached in a downstream direction (like coastal spits) such that blind channels develop between the bar and the river bank. Often the sand bars become maturely vegetated and appear to be part of the riparian terrain.

The secondary channel network has a significant number of blind channels occurring along joints and bedding planes as can be seen from the straight or linear blind channel configuration in planviews of the channel network. Often, the orientation of these blind channels does not correspond to the primary channels direction but corresponds to the strike/dip of the underlying bedrock.

5.1.1.3 River Islands

River islands can be classified according to their elevation and consequent differences in morphology. The first category is comprised of *major islands* in term of overall large plan area that have their highest elevations few meters above mean annual flood level. There are about 100 such islands within the study area boundaries. In terms of length, the biggest one, Kaoh Ro Ngiev is nearly 40km long (Chapter 1, Figure 1.2); the few others that are significantly elongated are from 10 to 17 km in length. The maximum width of the islands can be up to 5.6 km but more typically is 2-3 km. The subaerial vegetated surfaces of the islands are similar to these of the mainland, often mimicking the swells and lows of the high plain surface (see Section 5.1.1.4) and sometimes can be slightly higher. As such, the surface of these islands must be of similar age to the Cenozoic plain either side of the river. Usually, the major island surfaces lie 7-10 metres above the average low water level, have steep bank lines (Figure 5.11) and only flood very occasionally. These major islands often seem to have a significant alluvial component to their mass that has formed around bedrock cores, with well-developed soils over large parts of the higher surfaces and unweathered alluvium in those areas that flood occasionally. These islands tend to sustain large and small permanent villages in the areas that do not flood (or that flood only infrequently) and the presence of such villages on maps helps in mapping the location of major islands and flood limits.

Figure 5.11. East bank of the Kaoh Ro Ngiev island.
Banks are eroded and usually lack well developed natural vegetation due to livestock grazing. Flow direction is from right to left; low water conditions.

However, if the elevation of the island is less than 7 metres above the average low flow water level, it falls into a category of seasonally inundated islands which can be observed commonly throughout the multichannel sections of the Mekong from the Rapids de Prek Patang to the Sambor Rapids. These islands usually are smaller in plan area than the major islands. The banks of seasonally inundated islands are often low angle and smoothly sloping towards the water surface in contrast to the high, steep and abrupt cut-banks of the major islands (Figure 5.11). Seasonally inundated islands are abundantly vegetated by specific trees and bushes (Section 3.5) which comprise an important ecotone of the fluvial environment. The riparian vegetation often colonises sandy dunes formed by the river during the flooding period and, during the dry season, some water still remains in shallow ephemeral scour pools and channels that crossing the islands in parallel to the primary flow (Chapter 3.5, Figure 3.27). As a rule, these seasonally inundated islands have a minor alluvial component to their mass and little or no soil development except on the highest prominences and may be predominately bedrock complexes. This class of island has none of the characteristic swells and lows of the high plain surface. Thus the island surfaces are younger than the major islands. There are two possibilities to explain the occurrence of seasonally inundated islands. One is that the rock outcrops on which they are developed trapped sufficient sediment to allow the growth of specialised tree species which further retard flow velocities and promote additional alluviation. The alternative is that they are dissected and eroded plinths (i.e. remnants of large islands). Currently it is not possible to choose between these possibilities.

The seasonally inundated islands cannot be marked on a map of the study area with any confidence due to the absence of suitable images of the territory for periods of flooding. However, 1D flood level modelling in association with field elevation data and the distribution of human habitation and the inundation ecotypes would allow mapping more adequately than has been possible during this study. However, currently available materials has been used to establish preliminary inundation maps showing exposures of bedrock within the study sub-area (Figure 5.12).

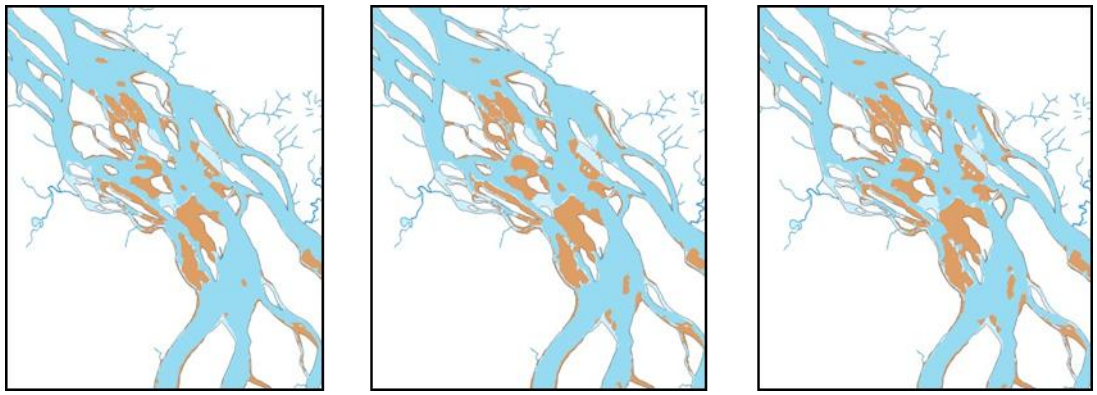

Figure 5.12. Inundation maps of the study sub-area (Rapids de Prek Patang) for August, September and October (from left to the right), year 2000.

Compiled based on RADARSAT ScanSAR Narrow B Mode Imageries of 50m resolution by the MRC. Blue areas are the seasonally low-flow wetted sections (all channel types) and brown areas are major areas of seasonally inundated bedrock outcrops and islands.

5.1.1.4 Geomorphological zonation

A previous regional zonation of the area has been performed considering only the terrestrial ecology (FA/Danida/DED, 2003) and more recently the floristic composition of the in-channel vegetation has been assayed (Bezuijen et al., 2008). Gupta & Liew (2007) and Carling (2009) assessed the Mekong within its basin at the regional scale where the reach between Stung Treng and Kratie was classified as “anastomosed channel in rock and alluvium” or “mixed bedrock-alluvial” river, respectively.

Thus, reviewing the known geomorphologic characteristics of the Mekong and existing knowledge, this research offers a further and refined geomorphological zonation of the studied reach. Several different and easily recognizable streamwise *longitudinal* geomorphological zones (Figure 5.13) initially can be distinguished with respect to (i) planview variations of sand/bedrock composition throughout the channel belt (Figure 5.14) and (ii) changes in river profile (Figure 5.15).

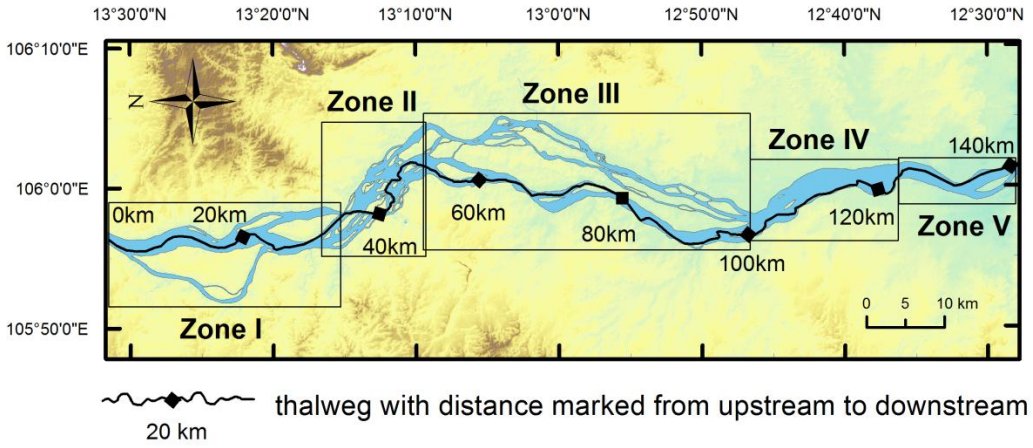

Figure 5.13. Extent of geomorphological zones (black boxes) from the north (left) to the south (right) of the study area and river thalweg with distance marked from upstream to downstream (based on digital data set MRC, 2003).

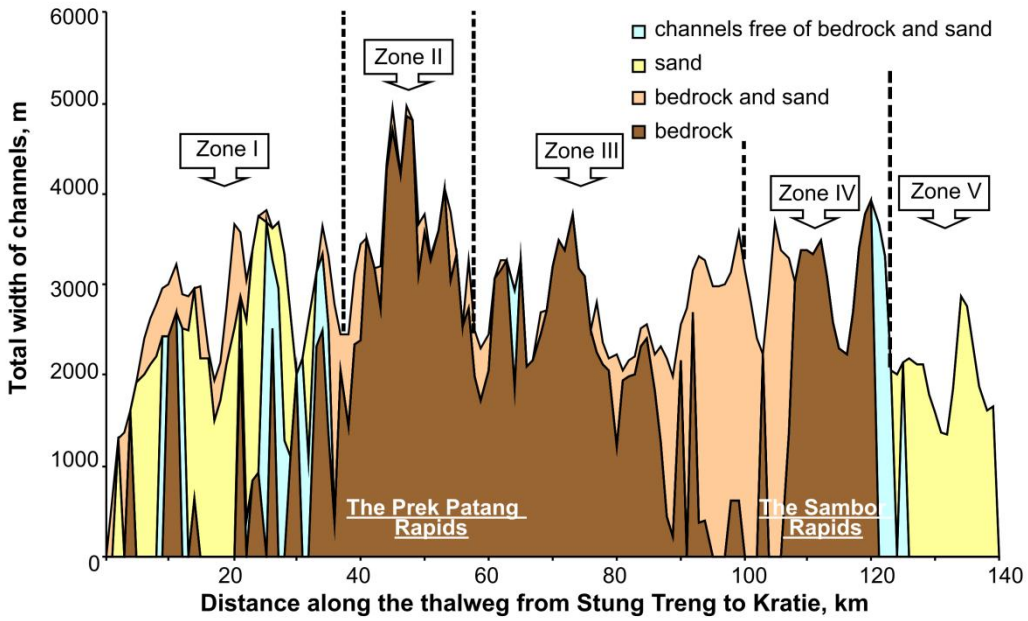

Figure 5.14. Planview composition of the macrochannel based upon 1km spaced cross-sections and the total width of the macro-channel of the Mekong within the study area from Stung Treng to Kratie. Based on the digital data set (MRC, 2003).

Please note that sand features of zones II and III are not indicated due to their insignificant extent (see noted for Figure 5.15).

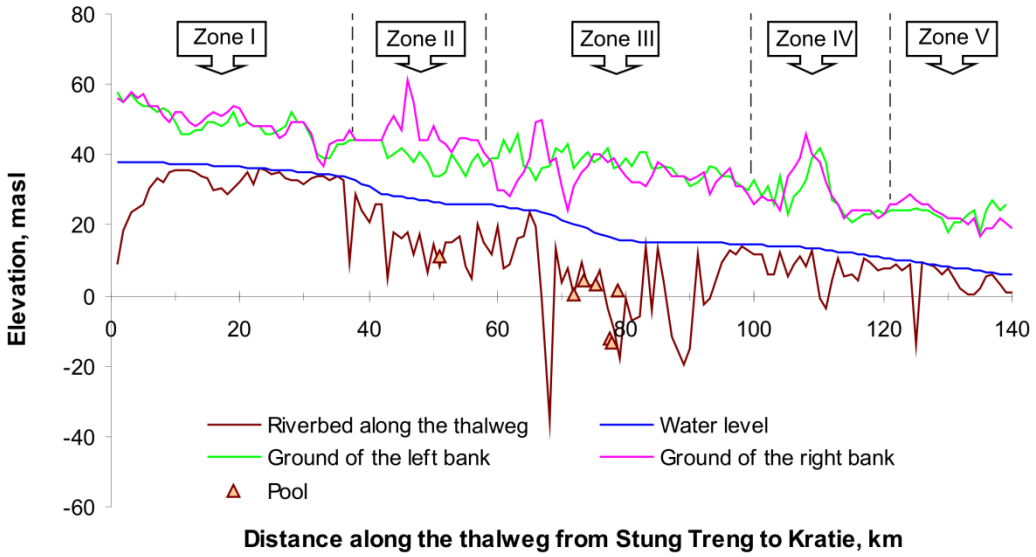

Figure 5.15. The elevation of the riverbed, dry season water level, main-channel deep pools and the ground elevation of both riverbanks.

Notes: here and in Figure 5.14 elevation data were obtained using cross-sections at every kilometre along the thalweg; for more information about the extent of each 'Zone', please see Figure 5.13 (Note: Bathymetric data for the riverbed profile are based on soundings performed in October 2003 by MRC for the Hydrographic Atlas of the Mekong River; Water level profile is based on the Mekong River Project data (Hunting Survey Corporation Limited) obtained in April, 1960 with horizontal scale 1:1 000 000 and vertical scale 1:1 000; Ground elevations of the river banks are obtained using the GIS database digital layers of the Hydrographic Atlas of the Mekong River, MRC, 2003; Deep pool locations from Chan et al., 2003).

The data comprising Figure 5.14 were obtained using an overlap between a digital layer containing channel composition (contours of primary channels with marked bedrock and sand bodies) and another layer with cross-sections spaced 1 kilometre apart, covering the investigated reach from north to south. When a cross-section overlapped bedrock within an individual channel, the channel was marked as "bedrock"; the same idea was applied to distinguish channels with sand, combination of sand/bedrocks, and channels free of either sand or bedrocks. Channels in Zone I are characterised by a complex of sand/bedrock primary channels, whereas in Zone II and III the multiple primary channels are largely bedrock only. Zones II and III are differentiated in terms of total channel width upstream and downstream of km 58. At the end of the bedrock dominated Zone IV the short area of mixed sand/bedrock channel composition belongs to the Sambor Rapids. Further downstream within Zone V the Mekong is represented by a single meandering channel with large sand bars.

The same zones are presented on Figure 5.15 showing vertical profiles of the riverbanks, riverbed and water surface. In general, elevation of the land surface reduces from the north to the south through the study area from 60 m above mean sea

level at Stung Treng to 20 m at Kratie showing the gradient to be ~0.3 m per kilometre on average. Yet the steepest gradients can be observed within Zone II, at the Rapids de Prek Patang (~1 m per km), Zone IV (~0.5 m per km in average where the Sambor Rapids gradient is ~0.8 m per km) and Zone III (~0.25 m per km); Zones I and V have lower gradient values of 0.3 and 0.2 m per km respectively. Cross-sectional vertical profiles indicate that the plain either side of the river is slightly undulating, which mostly likely is due to Cenozoic epeirogenic folding (UN, 1993), with swells and lows orientated approximately west to east, e.g. oblique to the river course. Often elevations correlate on either side of the river, which indicates that the river has incised predominately vertically into an ancient terrain with only local lateral movements of the river channel.

The overall incision into ancient alluvium is consistent throughout the study area and assessed to be around 15-20 meters (the difference between the average riparian plain elevation and riverbed elevation values). There are three distinctive peaks of higher elevations of the terrain (low hills) observed at the right riverbank (Zone II and III) and both riverbanks in the middle of Zone IV. The elevated surfaces of Zones II and III restrict modern lateral channel migration to the west whereas the left bank surface profile seems to be lacking significant elevation peaks.

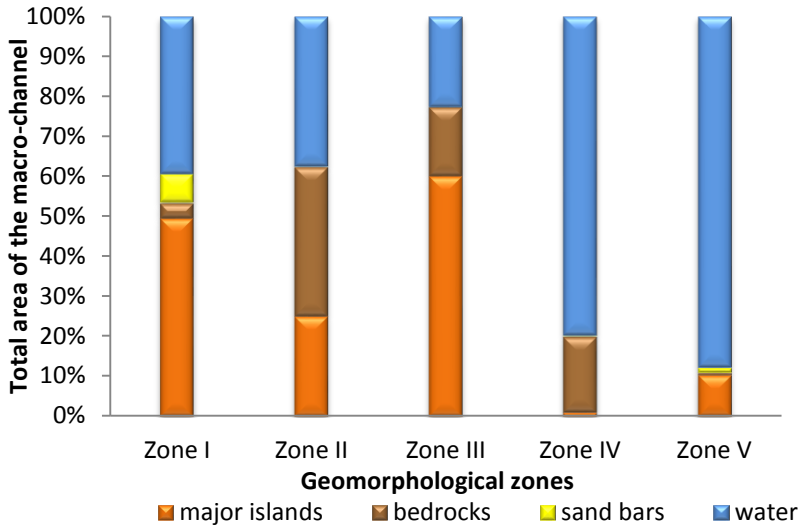

Figure 5.16. Major islands, bedrocks, sand bars and open water areas in proportion to the total area of the Mekong macro-channel in each geomorphological zone.

Zones I, II and III are characterized by a larger number of major alluvial islands in comparison to the downstream macrochannel represented mainly by a single primary channel in Zones IV and V (Figure 5.16). It has to be noted that Zone IV includes the Sambor Rapids where a secondary channel network of bedrocks and vegetated small

sand bars occurs within a macrochannel composed by single primary channel. Among the three first Zones described as anastomosed, Zone II (the Rapids de Prek Patang) has the smallest area of major islands and the proportion of bedrock exposed during a dry season is the largest (Figure 5.16). Thus, this is the most dissected (eroded) section of the river, with a gradient slightly higher than that of the Sambor Rapids (p. 115). Indeed, some islands mapped as major islands in this zone may actually be seasonally-inundated and therefore mis-recorded such that the real number of major islands in this area can be even smaller than as recorded in this current study.

The character of bedrock outcrops in each geomorphological zone varies according to the rock types recorded in the study area. Within the channels from Stung Treng to the Rapids de Prek Patang, in Zone I outcrops form narrow extensive parallel ridges oblique to the flow direction (Figure 5.17). These outcrops appear to be structurally related to the bedding planes. They form natural barriers to the dry season flow, acting like low artificial weirs, and during the low water season appear as shallow waterfalls and rapids lying obliquely across the river. Although they do not occupy the full channel width entirely, and allow water to spill over them and through small gaps, major gaps are few and often are restricted to one or two major gaps located at the lateral margin close to a river bank.

Figure 5.17. The channel between the Kaoh Sralay island and the left riverbank during dry season low flow, near Kangdeisar village (5km downstream from Stung Treng). Flow can over-top the barrier and pass through in narrow gaps, but the majority of flow is forced towards the right riverbank where a major gap allows flow to pass (see text for details).

Farther downstream, within the area comprising Zone II, the character of the rock changes as metamorphic rocks are replaced by broad fields of volcanic and sedimentary (pyroclastic) volcanic rocks (Figure 5.18). Weathered rhyolites, andesites, dacites and their tuffs intercalate with quartzites and quartzy albitophires. As these rocks are submerged during the high water period, frequently the visible rock surfaces

are watersmoothed and characterized by erosion marks (see more details in Section 5.1.3).

Figure 5.18. Typical rock exposures at the Rapids de Prek Patang (13°13.425'N/106°00.387E).

Primary flood flow direction is from foreground to the background; figure for scale 1.7m. Channel in middle of image is flowing transverse to the direction of the primary flow.

The composition of the basement rocks becomes more diverse downstream of the Rapids de Prek Patang. Here, in Zone III, prevailing sedimentary units of old conglomerates (Figure 5.19) and shales are interstratified with metamorphic hornfels and gneisses. Volcanic rocks are represented by granites, andesites, diorites and quartzite dykes. Within this zone overall, the proportion of outcrop within the channels is decreasing north to south until there is a complete absence, whilst at the same time the channel alignments are increasingly adjusted to the bedrock strike and series of faults.

Figure 5.19. Conglomerate outcrops in the primary channel at the beginning of ZoneIII, N 12°55.500'/E 105°58.934.
Strike 195°, dip of bedding plane 68°. Figure for scale 1.6m is pointing to the dipping bedding plane behind and downstream of him. The primary flow direction is into the image.

The last location bedrock is exposed extensively is in Zone IV (the Sambor Rapids). Vegetated multiple outcrops of sandstones, shales and conglomerates are densely placed in the primary single channel. Farther downstream (Zone V) in the vicinity of Kratie, bedrock outcrops are not visually evident within the Mekong channels. The transition at this point to an alluvial channel is in accordance with this location marking the northerly extent of the alluviated Cambodian plain.

Finally, a trend surface analyses of the terrain elevations either side of the river contributed towards the ultimate delineation of the extent of each zone and an explanation for the large-scale planview channel alignment. The general 1st-order altitudinal NE-SW trend of the area is shown as the background to the channel pattern map within Figure 5.20. At the regional scale, the river tends to follow this trend but nevertheless, being incised, overall shows a propensity to flow directly to the south. The NE-SW trend of the channels is often structurally influenced, with long, parallel primary channels being fault-aligned. Readjustments in channel alignment may occur abruptly with realignment to the SE. The best example is within Zone II (inset trend surface on Figure 5.20) where the local gradient is to the SE. Hence, the combination of

two trend surfaces (one regional and one local) explains the alteration of the river course at the Rapids de Prek Patang and may explain the broad extent of the channel network here as the south-easterly gradient is weak allowing high flows to deviate towards the SW.

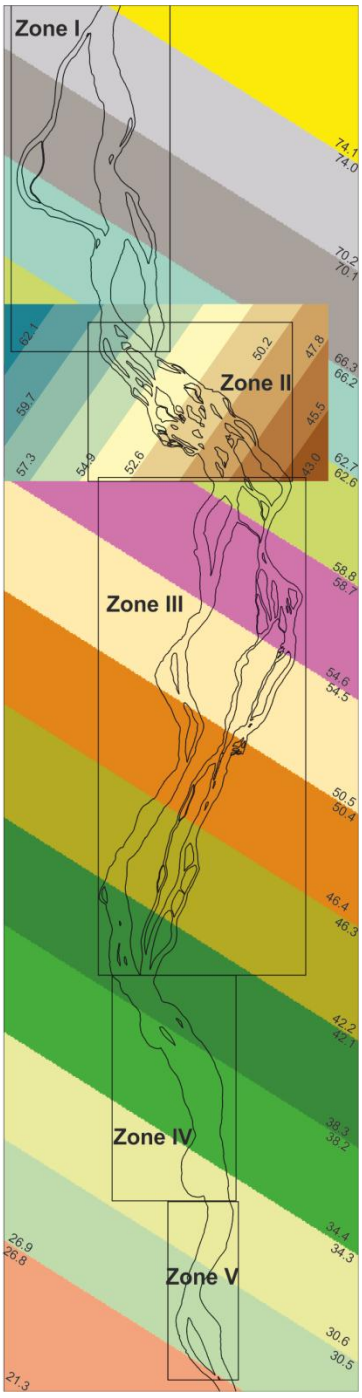

Figure 5.20. Geomorphological zones of the study area on a background surfaces indicating regional and local (Zone II) topography trends.
The figure is produced on a basis of 50m DEM (DEM courtesy of MRC, 2006).

Apart from the longitudinal zonation of the studied reach, a typical cross-section of the mixed bedrock-alluvial multichannel river has been composed (Figure 5.21) based on the published classification of riverine Mekong vegetation (Bezuijen et al., 2008) and geomorphological field observations made during the current study. Six zones have been distinguished according to the floristic components and specific environmental conditions (substrate, flow regime, sediments) comprising the habitat and every zone has been interpreted in a geomorphological context. The zones are laterally distributed across and away from the primary channels and, for a given elevation, correspond to a range of river stages, and hence annual duration of submergence, associated with the annual discharge regime. The longitudinal distribution of these zones varies according to the bedrock/alluvium content comprising the river.

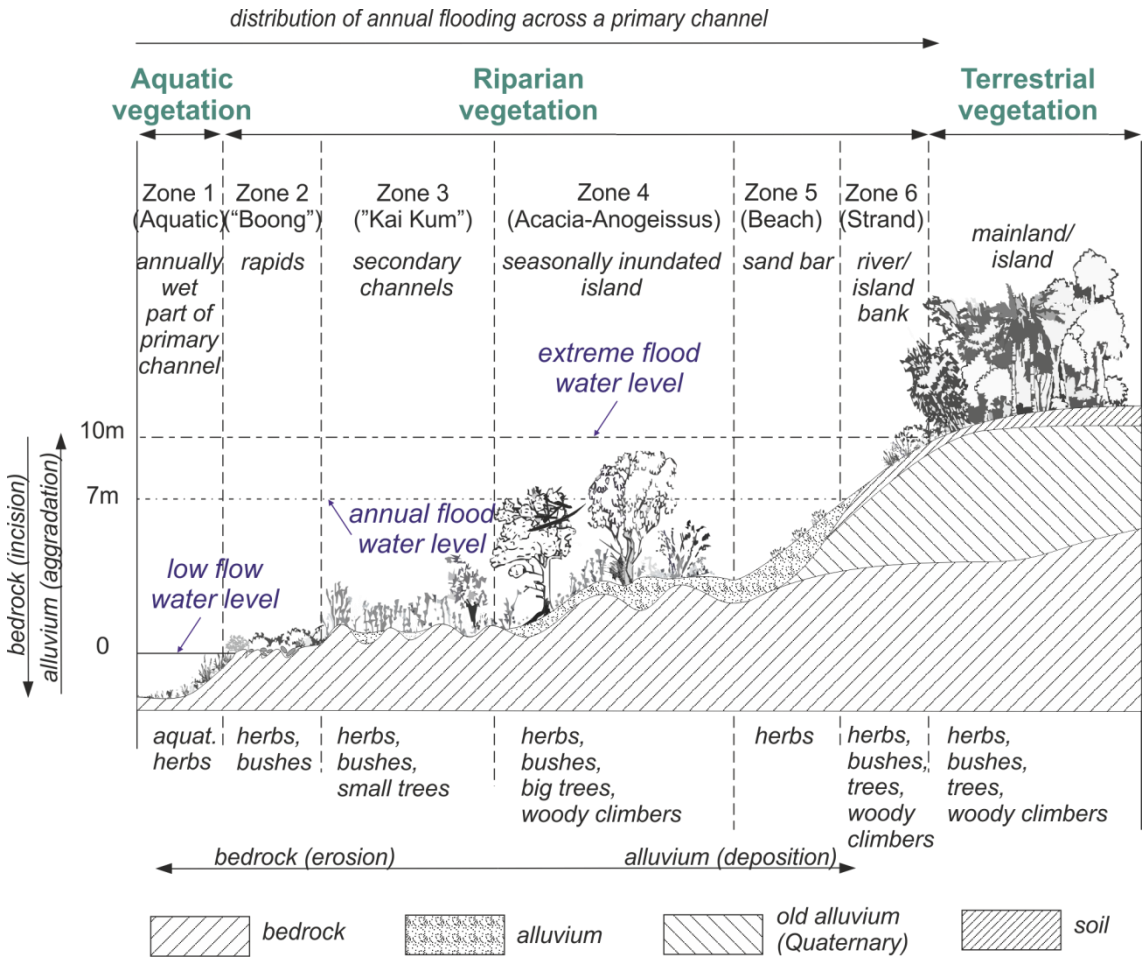

Figure 5.21. Stylised cross-section profile of vegetation types and related fluvial processes observed at the mixed-bedrock alluvial sections of the Mekong in Cambodia (modified from Bezuijen et al., 2008).
The core of the mainland/island may be also represented by bedrock.

The zones of riverine vegetation are sensitive to the presence of bare rock and the accumulation of sand-splays and large sand bars that constitute the fluctuating annual storage of sediment moving through the system. Consequently, it can be assumed that the sensitive balance between the two processes of sediment deposition and entrainment within the river across the channel belt is essential to maintain the ecotones.

5.1.2 The Mekong terraces and the Mekong palaeo-channel

There is a general absence of obvious terraces to the river, although Carbonnel (1972) reported several terraces in northern Cambodia. Fieldwork in the study area was undertaken in order to collect sediment samples and vertical profiles from the 100, 40 and 20 m terrace levels (Figure 5.22) indicated in published literature (see Section 3.2).

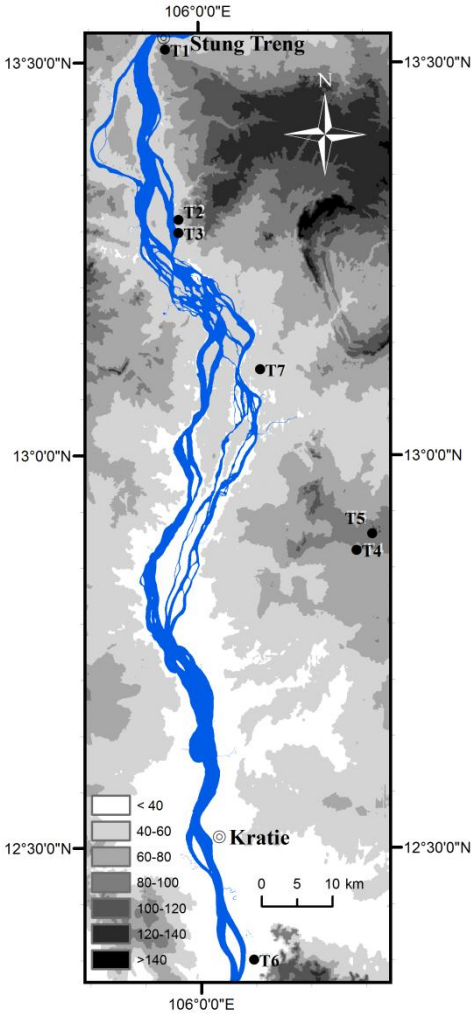

Figure 5.22. Elevation ranges and sampled terraces locations (see text for more details).

Terraces location details are given in Table A1, Appendix I.

Reclassification of the 50 m resolution ASTER DEM using *"Slice"* function (see Section 4.1.3.4 for more details on the method) allowed visualization of the elevation ranges in which the three main terraces might be sampled (Figure 5.22). Note that the elevation ranges do not accord precisely with the planview extent of individual terraces and include other landforms at these elevations. Variation in elevations across the study area reveals several zones which partly correspond to the 100, 40 and 20 masl significant terrace altitudes reported by Carbonnel (1972). As follows from Figure 5.22, the expected down-system reduction in terrace altitudes means that Carbonnel's notional 40masl terrace can include altitudes less than 40m, especially in the south and up to around 60m towards the east. Carbonnel's notional 100m terrace is found at altitudes between 80m and 100m, which accord with his reports of extensive dissection of the 100m level. Field visits to many locations on these various levels confirmed that these altitudinal ranges included evident terrace surfaces. However the terraces edges have not been mapped.

The Lower Quaternary (?) 100m terrace was sampled at the terrace section T5 (Figure 5.22) exposed at an altitude of 84 masl, 25 km to the east from the left riverbank. It is composed of well-rounded pebbles and cobbles varying in size approximately from 1 to 30 cm in a coarse-sand matrix overlying older bedrock (Figure 5.23, A). The gravel is distributed sparsely in the matrix; conglomerate bedrock underlying and protruding through the terrace gravel and found near this section, (Figure 5.23, B) may be a possible source of the gravel component observed in these terrace deposits but the provenance of the terrace gravels has not been explored

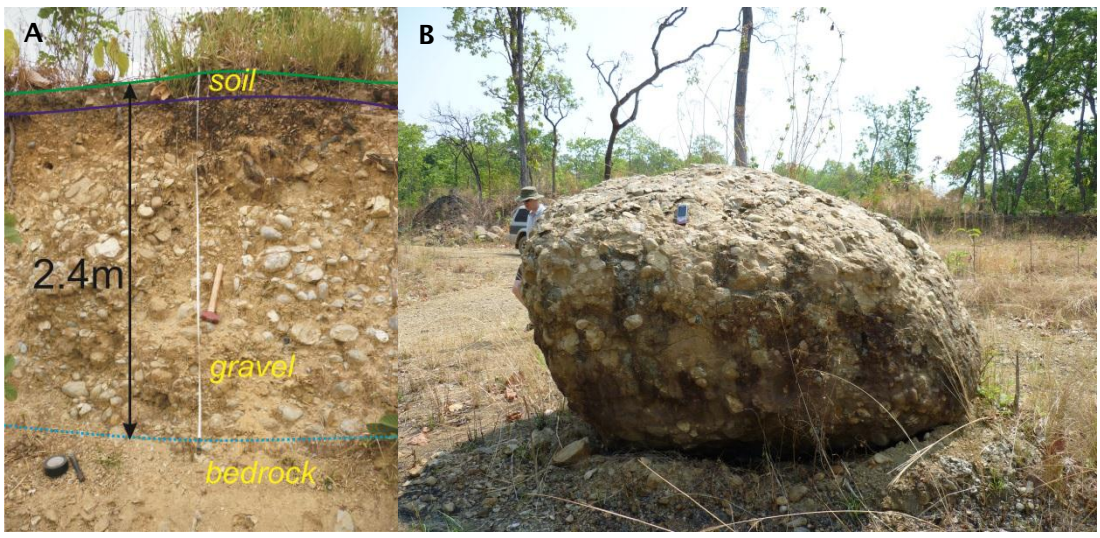

Figure 5.23. (A) Section of the 84masl elevation terrace (T5) deposits and (B) old conglomerate fragment found at the same location where there were additional conglomerate exposures.
Hammer for scale (A) is 30cm and figure for scale (B) is 1.8m.

The '40m terrace' level in the terrace sequence was also sampled at ~60masl. There are two sites for this altitude (T1 and T4, Figure 5.22) which have been explored within the study area. The first terrace section of this level (T1) is in the vicinity of Stung Treng, e.g. ~2km to the NE from the junction of the Mekong and the Sekong Rivers. It is composed of two different lithologic gravel facies; each has a thickness of 1.5-2m and together they are accumulated on a top of a massive dense clay horizon; sometimes, laterite up to 0.5 m in thickness is present at the top of a section (Figure 5.24A). The uppermost gravel layer seems to be more densely packed than the lower one, however, gravel in both facies is of a similar size (~ 1-5 cm) and roundness.

Another important finding at this site is petrified (silicified) wood, in the form of small logs and broken chunks, which is collected by local people from the gravel excavated at this location for construction purposes (Figure 5.24B). It is not known from which of the two gravel layers it comes, but there is evidence in the literature of this type of silicified wood being reworked in sediments of the Mekong terraces in Laos and Thailand as well as in Cambodia (Philippe et al., 2004). The wood appears to have been transported by fluvial action to be incorporated within the terrace gravels. Petrified wood of this type is widely found across the region (Thailand, Laos, Cambodia) within the continental rocks of the Khorat Group, whereas in Cambodia units containing petrified wood belong to the Middle Jurassic (Phillipe et al., 2004).

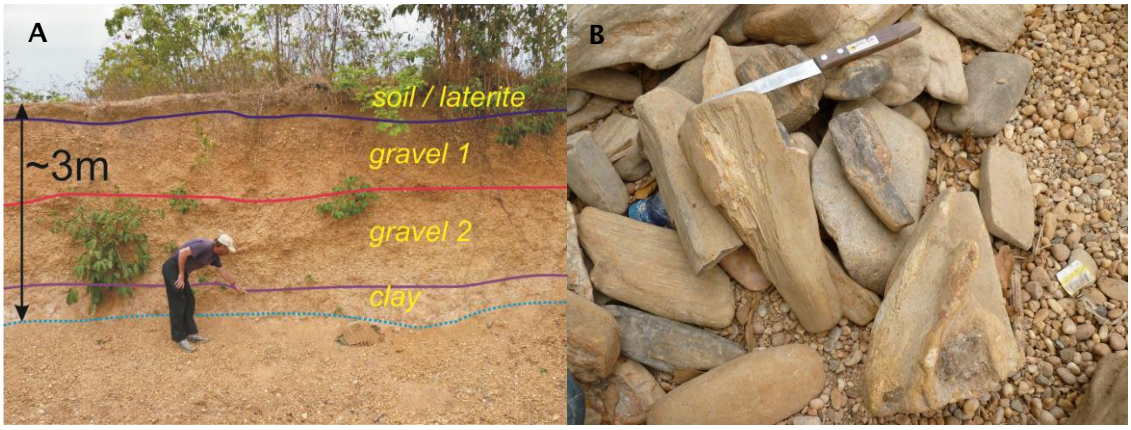

Figure 5.24. (A) Section of the 60 masl elevation (T1) of '40m terrace' in the vicinity of Stung Treng (see text for details).
The man in the picture is pointing to bottom of the gravel 2 layer. (B) Fragments of petrified wood; knife (15 cm long) is for scale.

The second examined 60m terrace elevation (T4 on Figure 5.22) is centrally placed in the study area but nearly 20km to the east of the present day river channels. In fact, the 80masl elevation sample site (T5) is located just a few kilometres further to the northeast above a steep terrace margin, therefore, it can be suggested that this second

60m site marks the local eastern border of the '40m terrace' in this area. The section is ~1.2m thickness in total where a ~0.5m layer represented by a mixture of gravel and pisoids (e.g. more than 2mm chemogenic grains of concentric or radial internal structure formally known as pisoliths (Bridge and Demicco, 2008)) and a 0.5-0.8m sand layer are deposited on a top of a clay horizon; the latter with a dense, massive structure (Figure 5.25, A). In the weakly cemented pisoids and gravel layer (Figure 5.25, B) gravel pieces are mainly rounded but sometimes exhibit a slightly angular shape reaching up to 2-3cm in size. Generally, all layers observed at this site are heavily weathered. According to the stratigraphic description of this terrace section by Demeter et al. (2010), the gravel layer contains petrified (silicified) wood pieces.

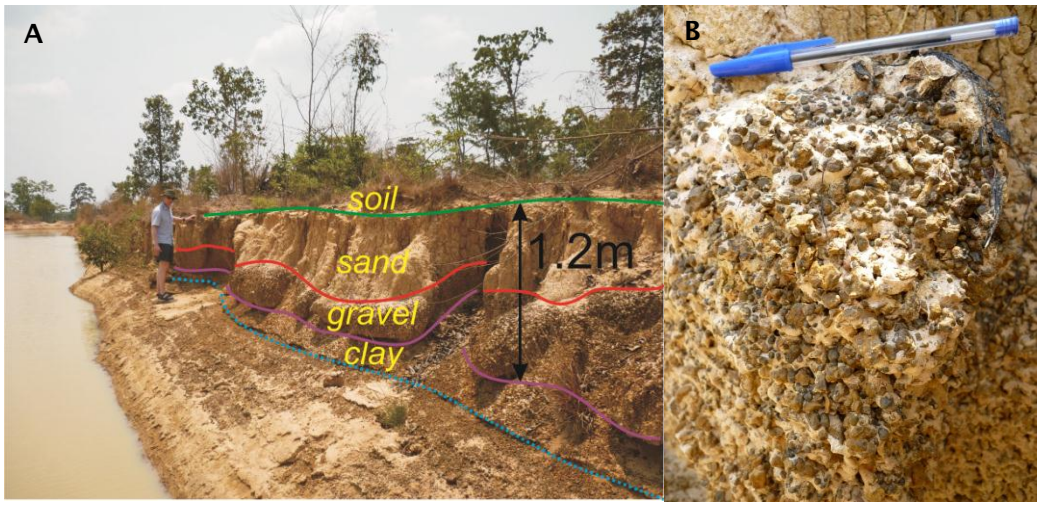

Figure 5.25. (A) The 60m elevation (T4) section exposure located near to the Sre Sbov village and (B) pisoids and gravel layer.
Figure for scale (A) is 1.8m; pen for scale (B) is 15 cm.

The additional 40masl level terrace (T2, T3 and T7 on Figure 5.22) locations are on the accessible east riverbank within a distance not more than 2 km from the current riverbank. These three sections can be described together on the basis of the similar composition and character of the gravel layer. This gravel layer is composed of well-rounded, up to 15cm size, pebbles and has a ~0.3-0.5m thickness in each of these three locations wherein it is deposited at a ~0.2-0.7m depth from the present day ground surface. In all three sections, sand or fine sand deposits overlie a gravel layer (see Figure 5.26A as an example); the gravel itself can be observed either on top of a massive structureless fine sand/clay horizon (section T2, Figure 5.26A) or directly on (weathered) bedrock (sections T3 and T7; see Figure 5.26B as an example). At the site T2 where terrace strata could be seen in a few metre-long sections, the gravel layer can be described as undulating with variable thickness along the sections. Intercolations of small clay lenses (up to a metre long and half a metre thick) can be seen between the gravel and an upper sand layer.

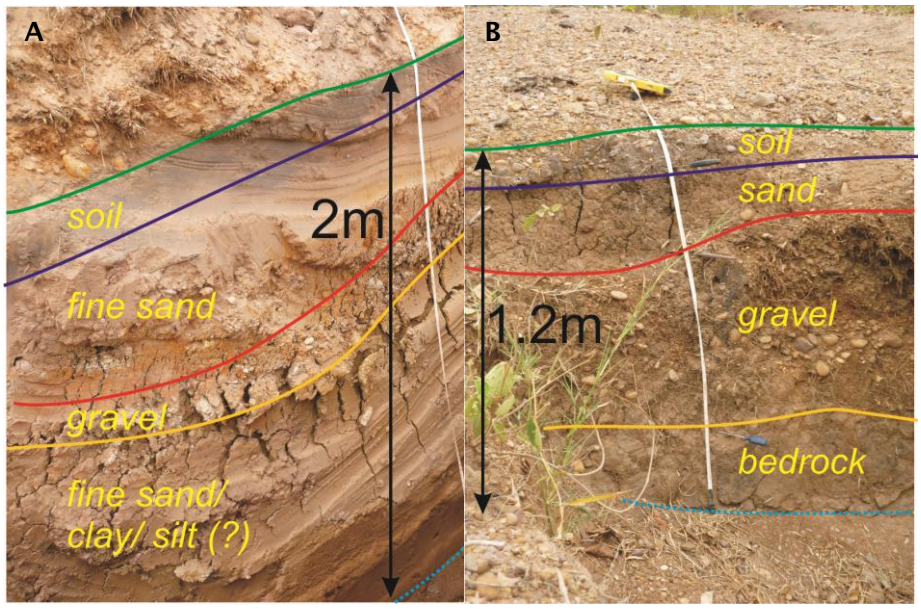

Figure 5.26. A) The 40masl terrace sections show undulating gravel layer on top of sandy deposits (see T2 on Figure 5.22 for the location). (B) 40masl terrace sediments deposited on a top of underlying bedrock (see T3 on Figure 5.22 for the location).

The 20masl elevation terrace (T6 on Figure 5.22), reported by Carbonnel (1972) was noted in the field in the south of the study area, located to the south of Kratie and 1 km to the east from the left riverbank, but could not be traced further north despite the elevation range including 20m levels much further north (Figure 5.22). Only one good exposure was located on the 20m surface but very close to the modern river. The Mekong at the T6 location floods the surrounding areas annually, therefore the section is within the limits of the active, modern, floodplain and it may actually be modern deposits abutting the 20m terrace rather than the ancient 20m terrace deposits themselves. The character of deposits observed at this site is completely different from the above described terraces. The extensive clean sections show 5-6 metres of sandy layers with a blue-clay layer at the bottom (Figure 5.27); the latter contains well-preserved remains of fossil (but not silicified) wood. Three (or sometimes only two) sandy layers are readily distinguishable from one another by a change of colour. The highest sand layer of approximately 0.5m thickness has a light-yellow colour ('weathered horizon' on Figure 5.27), the next layer down (similar thickness) is brown-yellow and the lowest, but thickest (up to 4m) layer is a beige-yellow, fine sand.

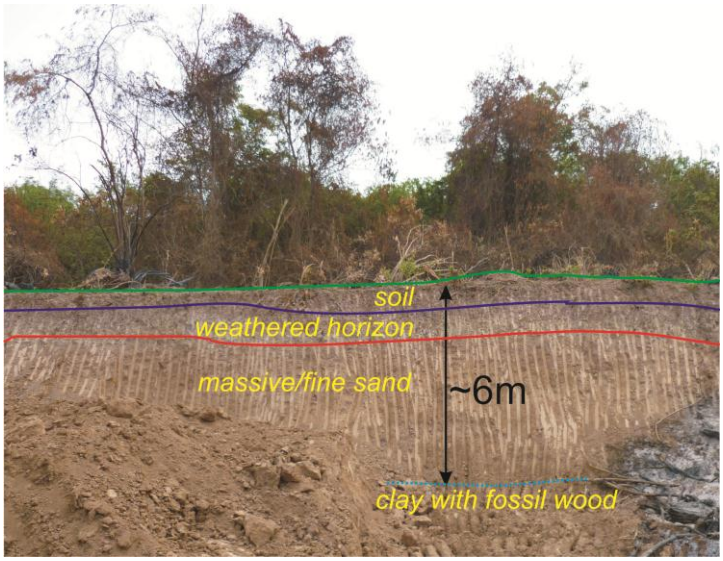

Figure 5.27. The 20masl elevation terrace (T6) section.
Note: the second layer of sand described as a 'brown yellow' in the text is not present in this illustrated section but was noted in other sections at the same general location.

Although the author did not find petrified (silicified) wood at the 40m terrace sections, Takaya (1967) mentions it being found at the 40m elevation within the east riverbank alluvial gravel deposits 7km north-east from Sandan (25km upstream of Kratie). Fossil (but not silicified) wood of the Mekong 40m and 20m terraces (according to Carbonnel, 1972) was previously examined throughout Cambodia (Vazenin-Serra & Privé-Gill, 1991 a, b). The latter cited work was conducted along east bank of the Mekong from Ban Na Pha (~10km upstream from Stung Treng) to Snoul (~40km south-east of Kratie) and confirms the continuity of these terraces. Hardwood (but not silicified) collected form 40m and 20m terrace elevations belongs to riverine species of the lower altitude deciduous forest, dated as pre-late Acheulean and post-Acheulean, respectively (Vozenin-Serra & Privé-Gill, 1991b). Transformation of the obtained age to the geological time scale means that according to the fossil (but not silicified) wood, the 40m terrace was formed in the Middle Holocene whereas the younger 20m terrace is Late Holocene.

Five samples from the terraces were taken for luminescence dating which was performed by Dr Ruth Robinson at the St Andrews University Luminescence Laboratory, Scotland. OSL dating of the 40m terrace deposits (T2 on Figure 5.22) indicates that the sand layer at 1.85m below the ground is 70.65 ± 5.13 ka (Sample MEKT-21 in Table A7, Appendix II), the base of the gravel layer (~0.8m below the ground) is 38.66 ± 2.40 ka (Sample MEKT 22 in Table A7, Appendix II) and the base of the upper sand layer (~0.5m below the ground) is 14.72 ± 0.95 ka (Sample MEKT 23 in Table A7, Appendix II). Sample MEK6 (Appendix II, Table A7) taken right below the gravel layer (1.10m below the ground) at the 64masl site (location T4 on Figure 5.22) is 21.30 ± 1.80 ka

whereas Sample MEK25 (Appendix II, Table A7) from the 84 masl elevation (location T5 on Figure 5.22) sand matrix taken at 1.95 m below the ground indicates an age of 16.20 ± 1.60ka. Incision from sample 1.8m below the '40m terrace level to the lowest point on the modern river bed (28m – MRC digital hydrographic data set) has occurred in about 70ka. Thus an estimate of the most recent incision rate from the 40m terrace level to the modern river bed level is 0.15m/ka.

The last date is given here to indicate that the sample was analysed, however, it strongly disagrees with the date given in the above cited literature (~650 ka BP). Indeed this location has the highest position in the investigated terraces vertical profile and the furthest distance away from the river, therefore the obtained luminescence analyses result cannot be accepted as correct with respect to the age of the terrace. Such a young age can be explained by bioturbation processes or by sediment disturbance by tree roots growing on the ground at the top of this 84masl section. Additionally the sampled material may represent some other palaeo drainage system and not the Mekong, However the age is too young to represent such a system. More likely the young age represents deposition of a local Holocene stream or is due to contamination as noted above. Only more extensive dating of additional samples can resolve this age issue.

From the results of the radiocarbon dating of the wood pieces found in a clay horizon (Figure 5.27) of the 20m terrace, the age is 450±50 years (see Appendix III). Such a result gives high sedimentation rates of ~ 0.01m per year (~5 m of sand deposited on a top of the clay layer containing fossil wood accumulated during ~500 years) assuming persistent deposition and no erosional events.

In addition to the terraces, the buried channel located at the west riverbank near the Sambor Rapids had been explored (Section 4.2.1, Figure 4.15). Stapledon et al. (1961) provide a delineation of the palaeo-channel extent and general, qualitative grain-size descriptions of sediments obtained from a set of engineering boreholes that reached a depth of 15m. From the maps of Stapledon et al. (1961), the fill of the former channel has elevations lower than the bounding terrace terrain, whereas its planview boundaries can be visualized in accordance with a string of oxbow-lakes observed on the west riverbank downstream of Sambor (Section 3.1, Figure 3.8). The overall dimensions of the palaeochannel are estimated as ~15 km long and ~3km wide with a maximum depth of 13.7m (Stapledon et al, 1961). The width, depth and slope parameters of this palaeochannel correspond to that of the modern single channel in this area which leading to the conclusion that, if the discharge remained unchanged, the palaeo-channel could have been the only major channel of the palaeo-Mekong in

this part of the course. The core logs (Stapledon et al., 1961) report fluvial sequences only as 'sandy sludge', sand, gravel and shale fragments deposited above either weathered or fresh bedrock (Figure 5.28). Deposits extracted from a shallow borehole made by the author correlate in a general sense with the boreholes made in the 1960s (Borehole KOM on Figure 5.28) but more precise correlation is not possible due to the lack of any detail in the core logs recorded by Staledon et al., 1961. Due to technical reasons the depth of the borehole made by the author was not sufficient to reach bedrock, but the core log shows at this location all the sediment facies of the palaeo-channel as noted by Stapledon et al., (1961) but more detailed grain-size results are reported for KOM. The composition of the Borehole KOM shows a layer of gravel at the bottom overlain by silt and sand deposits but instead of bedrock the bottom of the core is established by hardpan, clay and silt. These KOM sediments were analysed for grain-size distribution and, more importantly, their age was determined using luminescence techniques (Appendix II, Table A6 and Figure 5.28; Appendix IV, Table A8).

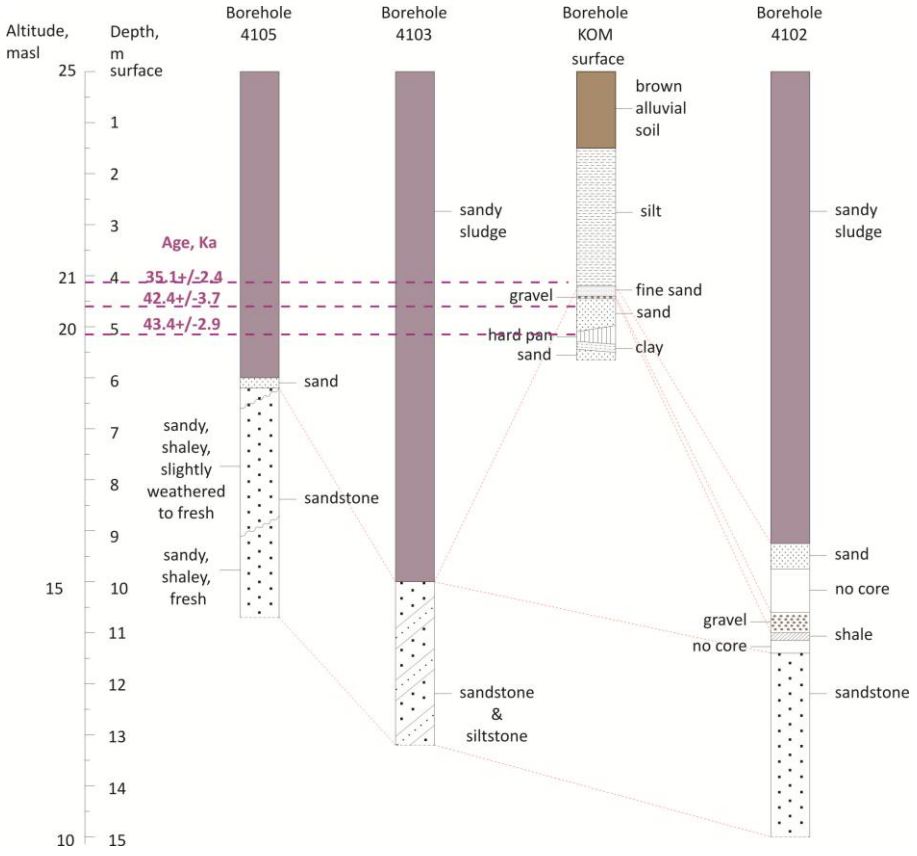

Figure 5.28. Correlation of the palaeo-channel borehole data obtained during the present research (Borehole KOM) with coring data from Stapledon et al. (1961). OSL samples positions are marked by red dashed lines with the age of each sample shown above the line. For the location map see Figure 4.15 in Chapter 4.2.1. Coordinates of borehole KOM are given in Table A1, Appendix I; location of Boreholes 4102, 4103 and 4105 can be found in Table A5, Appendix I. Detailed description of the borehole core is provided in Table A2, Appendix I.

Four samples from borehole KOM were analyzed for OSL age determination (Appendix II, Table A6) and nine samples were processed by wet sieving for the grain size distribution (Appendix IV, Table A8), with two also tested for their organic content (Appendix IV, Table A9). Mekong-2, -3, and -4 are 35.05 ± 2.42 ka, 42.42 ± 3.79 ka and 43.44 ± 2.91 ka, respectively, whereas Mekong-5 is only 31.57±3.68 ka yet sits stratigraphically below Mekong-4. Mekong 5 is recorded here for future reference but given the stratigraphic context with three other samples above all having assigned older dates the accuracy of Mekong 5 has to be questioned at this time (Appendix II, Table A6) and is not used in further interpretation.

Correlation of core data shows differences in lateral as well as vertical sedimentation profiles of the suggested palaeo-channel. The gravel layer explored by the author is 5cm thick whereas the thickness of a gravel layer in borehole 4102 (Stapledon et al., 1961) is ten times greater. Two other boreholes from the report cited above totally lack a gravel layer but are located within the limits of the proposed channel; at least one of them (borehole 4103) is sitting in the middle of the proposed palaeochannel and in close vicinity to the borehole KOM (see Figure 4.15B in Section 4.1). At the same time, as shown on Figure 5.28, the deposits in boreholes KOM and 4102 correlate well apart from the depositional depth. The variability in the thickness of the gravel layer might represent uneven deposition within the channel or later erosion and removal of gravel or no deposition of gravel at that location.

On the other hand, the age of a sample taken below the thin (~ 5cm) gravel layer found in the borehole KOM core appears to be nearly the same as that at the bottom of a gravel layer (Sample MEKT 22) on the 40m terrace (42.42 ± 3.79 ka versus 38.66 ± 2.40 ka). This fact stimulates the possibility that the gravel layers are coeval in both the borehole and the 40m terrace section, i.e. Upper (Late) Pleistocene. Such a conclusion might also be supported by the similarity in the vertical arrangement of the palaeochannel sediments where a gravel layer up to 0.5m thickness is underlain and overlain by sandy deposits similar to some 40m terrace deposits. This simple correlation might be coincidental, but nevertheless the similar ages for the palaeochannel and the 40m terrace suggest that the channel was being abandoned and silting-up at the same time as the 40m-terrace surface was finally deposited. Additional dated samples strategically located would be required to resolve this initial interpretation. This issue is to be further considered in the Discussion.

Summarizing the observations on the terraces and the palaeochannel data, there are several issues concerning the recent development of the Mekong:

1. The terrace in the vicinity of Stung Treng (T1) likely is a combined depositional surface related to the palaeo-junction of the Mekong and Sekong rivers due to the impressive gravel layers (that can be traced into the Sekong indicating that they emanate from the Sekong) that are present at this location, in sharp contrast to the thin gravel layers present in other terraces location sections further downstream.
2. The Khorat Plateau (Thailand) seems to be the major source of Mesozoic petrified (silicified) wood in the region, however, the same series of sandstones in the 3S Basin (basin of the Se San, Se Kong and Sre Pok rivers) also contain silicified wood (pers. comm. Tim Burnhill). The genera of the wood at the different locations varies (Phillipe et al., 2004) providing an opportunity to differentiate the source of the siliceous wood in the terrace near Stung Treng. Therefore, further investigation is required to identify the proportions of siliceous wood at stratigraphic locations in the Mekong terraces from these two sources. Such a study would provide additional information on the palaeo-development of the Mekong in this region.
3. The maximum lateral extent of the palaeo-course of the Mekong can be marked as lying 20km to the east of the present day river banks in accordance with the location of the 60 masl (T4) and 80 masl (T5) terraces limits. The extent of the Mekong ancient terraces on the west riverbank remains unknown.
4. The gravel facies vary and their relationships need working out. Gravel layer(s) thin(s) down system from Stung Treng towards Kratie and seem to reflect a distinctive input from the 3-S basin. In contrast, the Modern Mekong sediments are represented predominantly by sand. Therefore the noticeable changes in the character of sedimentation (gravel v. sand) shall be a matter of future investigations of the river to elucidate the influence of the Sekong on the Mekong in this region.
5. Although the number of sedimentary sections examined is not large the sedimentary styles are not dissimilar when comparing widely dispersed locations. Given the considerable lateral extent of the palaeo-Mekong, the thinness of the gravel layers in each 40m-terrace section, and the lack of obvious major cut-and-fill structures then the sedimentary style might indicate that the Mekong was formerly a sand-bedded (braided?) river or at least a sand-bedded river that carried a substantial gravel component that has been concentrated as lag layers, especially in the 40m terrace sediments. If major cut-and-fill structures were present then a meandering palaeo-river might be indicated but the absence of well-defined incised palaeochannels

(other than the single example noted above) on both riverbank terrace surfaces would contribute towards this hypothesis. The changes in the river style, from braided-alluvial to multichannel mixed bedrock-alluvial are likely to be related to regional processes stimulating incision.

6. The basal clay found at the bottom of each terrace section appears to be regional rather than local and may indicate extensive forest floodplain/braidplain wetlands existed (Vazenin-Serra & Privé-Gill, 1991 a, b) before the palaeo-Mekong deposited channel sediments across the area.

5.1.3 Updated geology and tectonic settings

Sampling of bedrock outcrop from the Mekong macrochannel and riverbanks has allowed geological maps of the study area to be updated. Despite some important findings, namely that some rock types were incorrectly mapped in the past and new rock types can be identified, the density of sampling did not permit either redrawing of boundaries of major outcropping bodies, or the accurate mapping of minor units. Such tasks require more systematic geological investigations of the area and fall outside of the present research aims and objectives. However, the descriptions of the rock samples (see Figure 4.15 in Section 4.2.1; Appendix I, Table A1 and Appendix V, Table A10) can offer a good basis for future in-depth geological investigations of the territory. More immediately, the descriptions allow identification of the composition of outcrops within the macro-channel and riverbanks. An overview of the sample diversity shows that non-sedimentary products are associated with Mesozoic andesite-diorite island arc volcanism (Rangin et al., 1995), with granite and granodiorite series in the south of the study area.

The majority of outcrop examined within the macro-channel are established to be red sandstones, widely spread in the upper/middle parts of the study area (geomorphological Zones I, II and beginning of Zone III, Figure 5.13) and belonging to the *Terraine Rouge* series. These sedimentary units are of regional importance (Section 3.3.1), therefore extensions of outcrops of sandstones in the channel can be traced outside of the channel to the broader river corridor (e.g. with the use of remote sensing images), as is shown at the end of this Section. Samples of red sandstones sometimes contain a tuffaceous component that often evidence for active volcanism associated with the deposition of red beds, or can be identified as meta-sandstones. The internal structure of the latter suggests that the sandstones have been subject to low-grade metamorphism without full recrystallization of the original rock resulting in

easily-visible packing of the groundmass and dissolution, or washing out, of some minerals. The resultant voids are often infilled with newly grown ferruginous minerals during the following period of stabilisation. The discovery of gneisses in channel outcrops transverse to the river course (Zone I) does not correlate either with the content of published geological maps, which show no metamorphic rocks in this location, or with the nomenclature of sedimentary series comprising the north of Cambodia. Therefore their occurrence can be explained by the high-grade regional metamorphism of the primary Triassic-Jurassic sedimentary rocks along the possible faults delineated in this area.

Volcanic bodies found in association with the red sandstones are established to be andesites, diorites and their tuffs, extending up to several kilometres across (Zone II) or tens of kilometres along (Zone III) the Mekong channels. On the east riverbank, diorites are found in the form of circular features (ring dykes), a few kilometres in diameter, which determine the contours of the river course at those locations (see). Numerous quartzite dykes pierce major volcanic structures, but, according to the field observations, their size is only from a few to tens of metres and so are much smaller than the accommodating volcanic bodies (e.g. andesites/diorites etc). Thus, more careful mapping would be required to determine the number and extent of quartzites in the area.

While red sandstones occupy the upstream parts of the studied reach, the presence of the *Grés Supérieures* sandstones (Section 3.3.1) is limited by Zone III. Outcrops of the *Grés Supérieures* conglomerates are seen close to the west riverbank and on some islands within Zone III (see Section 3.3.1, Figure 3.13 and Section 5.1.1.4, Figure 5.19). At the downstream locations of Zone III, the character of volcanic units switches to local exposures of granites. Their position corresponds with the “post-Triassic granodiorites and diorites” shown on Figure 3.13, Map A, Section 3.3.1 which proves that marginal parts of the Dinhquan Complex of southern parts of Vietnam can be found as far as the Mekong in Cambodia.

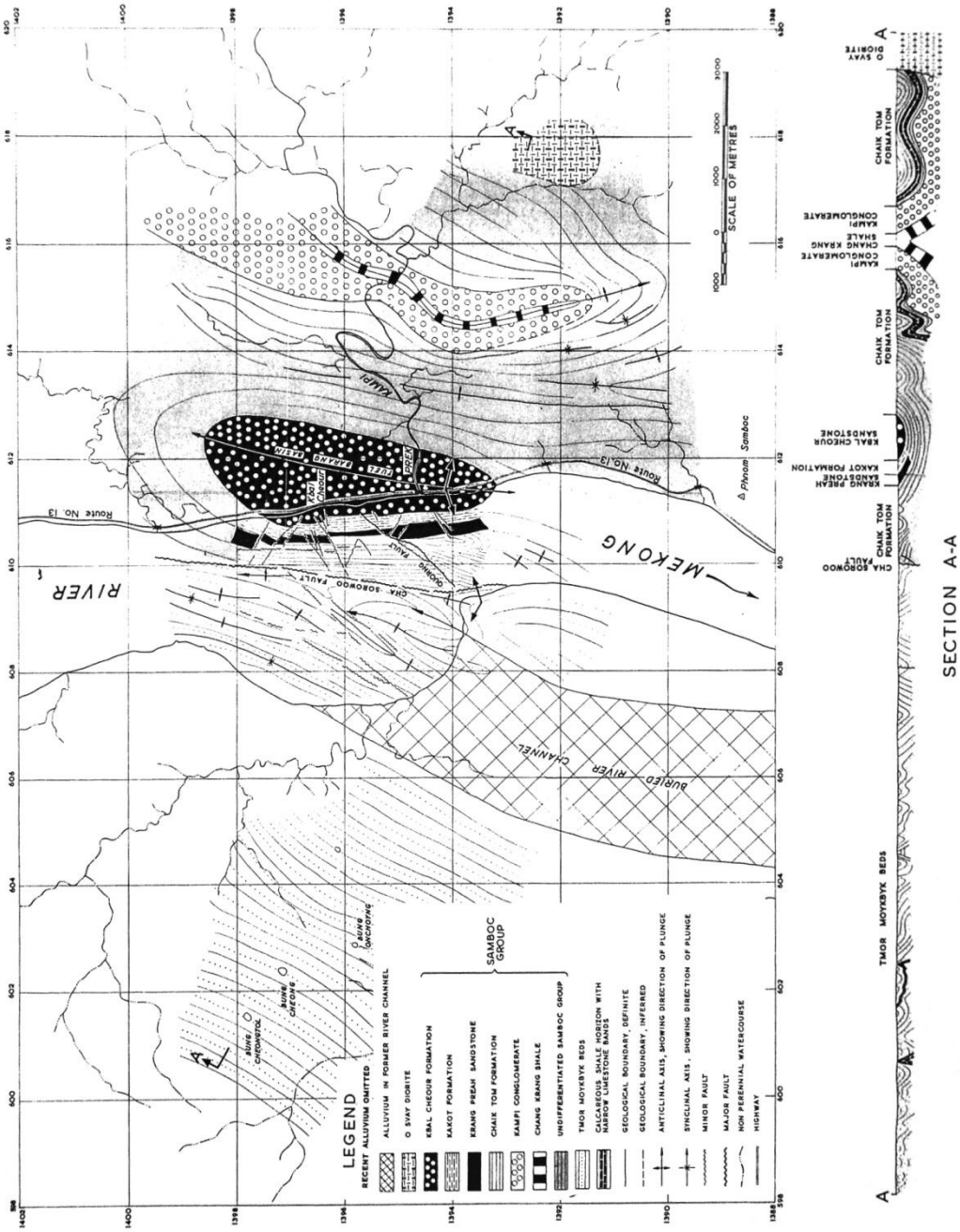

Figure 5.29. Sketched geology and cross-section of the Sambor Rapids (Stapledon et al., 1961).

Where volcanic rocks often are submerged intermittently in the river channel, they may be considerably weathered by sub-aerial processes and sometimes are also characterized by the development of hydraulically-controlled erosion features. Evident weathering is largely due to the abundance of iron minerals, which in a hot and humid monsoonal climate, can be modified easily to limonite and its variations (Figure 5.30). Such weathering affects not only the surface of exposed rocks, but penetrates inside and spreads along the joints and fault lines; but there are no data to identify and measure the thickness of limonitized zones within bedrock in the study sub-area. The variety of hydraulically-induced erosional bedforms noted on the rock outcrops and found on the seasonally inundated islands and other in-channel exposures includes potholes, furrows, polished surfaces, scallops, obstacle marks and surface sculpting, reflecting divergent patterns of flow direction (Richardson & Carling, 2005). Some examples are shown in Appendix V, Figures A1-A9.

Figure 5.30. Meta-sandstone has penetrating limonite veins (collected at the Rapids de Prek Patang). Cigarette lighter (8 cm length) provides scale

The diversity of sculpted forms is conditioned by the characteristics of the river flow and the nature of sediment transport. High-power stream flow may abrade a wide spectrum of simple and complex potholes and furrows in the rocks situated within the macrochannel boundaries. The larger examples may form chains of linked depressions which can contain stagnant or flowing water through the dry season and so collectively may comprise an example of secondary channels. Divergent local flow pattern and resulting erosion forms have also been observed on outcrops within primary channels while polished surfaces were mainly observed along the upstream flanks of seasonally

inundated islands. The appearance of polished surfaces primarily infers high velocity flow and suspended sediments acting together as an abrasion mechanism. The sculpted forms noted above can only be observed and studied during periods of low water. The lack of evidence of signs of chemical weathering and biological growth at these lower elevations supports a supposition of dominance of active hydraulic erosion (Wohl, 1999). Sculpted bedforms are less evident at the higher elevations within the channels that are inundated by the annual monsoonal flow. This observation might indicate that the monsoon high flow is not powerful enough or not sustained for long enough to sculpt the bedrock at these higher elevations. In addition the seasonal exposure of the higher elevations of the channels to sub-aerial processes might cause weathering features to dominate at these locations.

Weathering acting at the macro-scale is evident most visually in the case of volcanic rocks separating into distinct blocks along joints and other fractures, the edges of which are then subject to a degree of fluvial rounding. As shown in Figure 5.31, the conformability of the alignment and dip of the 'fitted' boulders testifies to the original presence of a massive but jointed rock body, the joints of which have been subject to weathering.

Figure 5.31. Weathered granite outcrops at an island (12°54'42.8''N/106°00'27.3''E) typically inundated by wet season flows. The bent tree indicates flow direction from right to left and the flood level (note the woody debris in the tree top) is at approximately 5 metres above the ground.

Information summarizing geological settings of the study area and the stratigraphy of the Mekong in north-east Cambodia can be represented as follows (Table 5.1).

Table 5.1. Stratigraphy, sediments and processes of the study area.

Era	Period	Epoch	Sediments and volcanics (**numbers of geomorphic zone are a bold in brackets**)		Formation/ Series/ Faces	Deposition environment		Tectonic episodes
Cenozoic	**Quaternary**	Holocene	Floodplain terrace	Sand (all zones, but limited in **I, II, III)**	Modern Mekong terraces	Fluvial		Not known
		Pleistocene	20m terrace	Sands (?) (**IV, V**)				Active uplift and basalt volcanism
			40m terrace	Sands, silts clays and gravel	Gravel bed braided (?) ancient Mekong terraces			
			60m terrace					
			100m terrace		Peneplenization/ weathering(?)	Fluvial/ Continental		Stable Cambodian Plain
	Neogene							
	Palaeogene		Granits and granodiorites(**III**)		the Dalat Stungtreng Foldbelt, Dinhquan Complex (mainly located in Vietnam)	Continental		Opening of the South China Sea
Mesozoic	**Cretaceous**							
	Jurassic	Upper		Sandstones, conglomerates, marls and shales **(III, IV)**		Grés Supérieures	Mainly continental	Indosinian Orogeny
		Middle	Sandstones, sandy shales, marls **(I,II,III)** Andesites, diorites, quartzites, rhyolitic-dacitic tuffs **(I, II)**	Andesits/dacites and their tuffs, granites **(III, IV)**	Terraine Rouge		Marine, lagoonal, continental	
		Lower						
	Triassic	Upper						
Palaeozoic	**Cambrian**	Lower	Metamorphic basement rocks: slates and phtanites, quartz gneisses (?)		Dalat Series	Old craton		Old craton

A compilation of available cartographic materials may be presented as a tectonic and a geological structure map (Figure 5.32) with a sample area for which the geological content was redrawn by the author.

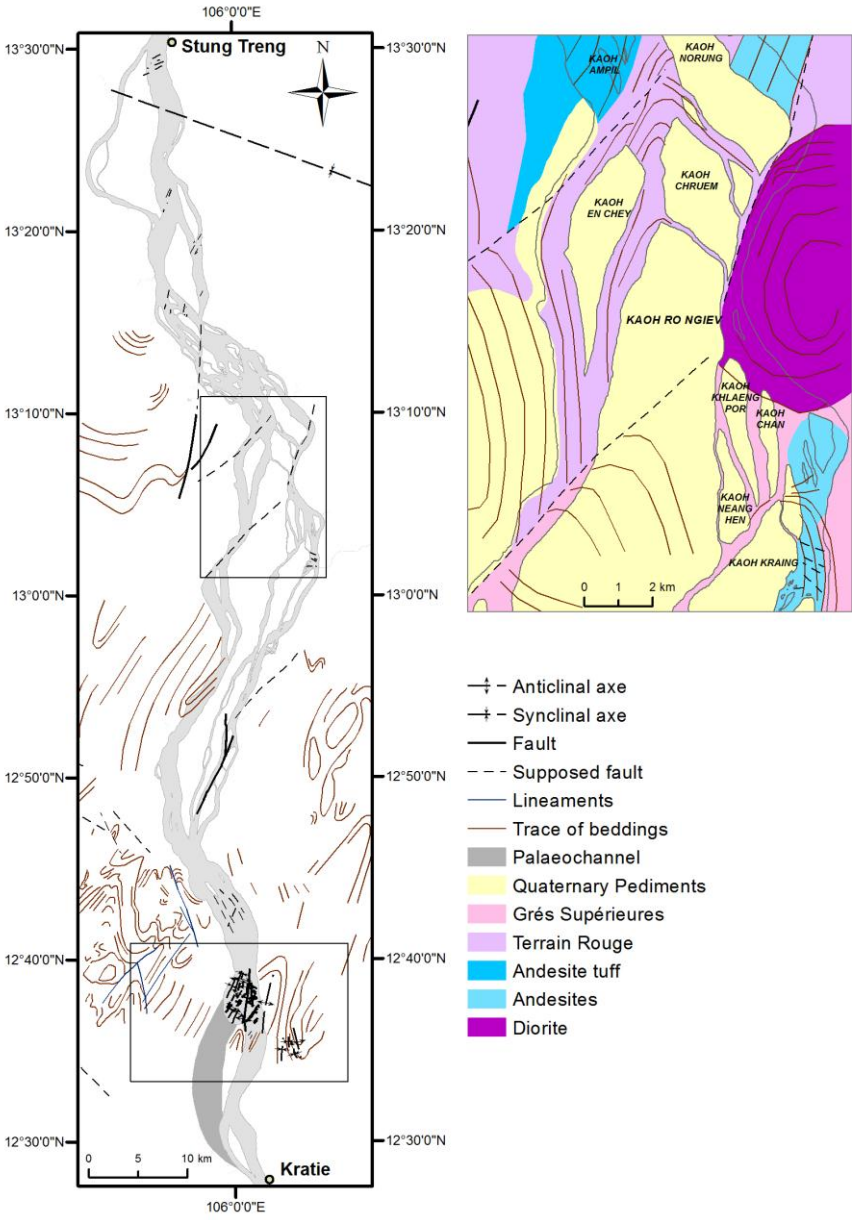

Figure 5.32. Tectonic and structural elements of the study area (left) and updated geological units of the sample sub-area (right).

Based on Stapledon et al., 1961, 1962; SNMGP, 1973; JICA, 2003; MRC, 2003; interpretation of aerial photography (Committee for Coordination of Investigations of the Lower Mekong Basin, 1959) and rock samples collected by the author.

The NW-SE alignment of the main channel of the Mekong within Zone II can be explained on the basis of the local topographic trend (Figure 5.20). The shift in the alignment of the Mekong bank to a more NE-SW trending tract within Zone III becomes readily interpretable after delineation of the three major NE-SW faults and well defined contorted beds. Triassic-Jurassic structures can be observed crossing both channels and island surfaces and continuing as surface features on the mainland on either side of the river. However, as was observed in the field, the eastern bank of the Mekong is occupied by terrace deposits, the thicknesses of which can be as little as 2 metres in total. The main trends of the structures of the older rocks at the surface can be seen from the remote sensing images where thin and incomplete alluvial cover occurs close to the river as well as across the riverine corridor, with deposition reaching up to 20-25 km away (see Section 5.1.2). Fault bearings are around normal in relation to the NW-SE direction of major tectonic movements in the region and may be referred to shear stress forces. Structural elements such as faults and well defined geology structures often confine distribution of the channels within the anastomosed reach, especially in Zones III and IV.

According to Ragin et al., 1995, the system of S-N faults in this part of Indochina occurred during the extrusion of Neogene-Quaternary basalts. Dates obtained by the author from the palaeochannel sediments suggest that the channel was in place at around 30-40 ka from present and abandoned, e.g. Upper Pleistocene, which coincides with the timing of neotectonics and basalts extrusions observed in Cambodia. The Sambor Rapids area in Zone IV shows a network of S-N faults and synclinal/anticlinal axes (Figure 5.29). The Cha Sorowoo Fault is the biggest fault within the rapids and today the river crosses the fault from NW to SE and the eastern bank is constrained by Kbal Cheour sandstones of the Tuel Barang Basin. However, the fault also demarcates the bifurcation of the modern river course from the palaeochannel course (Figure 5.32). The alignment of the palaeochannel is in accord with the strike of the Tmor Moykbyk beds whilst the modern river breaches the strike of the Samboc Group. The bulge in the west bank of the channel at the Sambor Rapids seems to demonstrate a propensity for the river to attempt to flow to the SW via the palaeochannel but it is possible that movement of the Cha Sorowoo Fault instigated the channel switch to the south-east. Without further geological investigation, nothing more can be deduced in respect of fault control as Stapledon et al., 1961, 1962 do not record the fault movement directions. Thus, although it is clear that many channels are fault-aligned there appears to be some evidence for fault movement influencing the locus of the main river course through avulsion at one location alone. However, as a rider it must be noted that channel realignment can be a complex process conditioned by fault and structural alignment as well as by local topography, rock type and regional gradient, in

addition to a propensity for incision with continuing falling sea levels after a high-stand around 110 ka (see Section 6.1).

5.1.4 Modern erosion and deposition

5.1.4.1 Sand bar dynamics

Analyses of sand bar areas and their migration according to positions of individual sand bar centroids over the 1959/2003-2006 period were performed in order to evaluate changes in the character and distribution of deposition within the study area.

Results of sand bar centroids migration analyses are presented on Figure 5.33 where data on bearings reflect the direction of sand bar migration and radial axes indicate distances of relocation. Dashed coloured arrows show an average direction of the main flow particular to each geomorphological zone, however, it should be noted that there are fluctuations (up to ~30° or, in case of cross-channels, ~80°) in individual channel bearings relative to the main flow direction. Zone II data are excluded from the diagram due to there being only a non-indicative single value available to plot as well as few stable sand bars data revealing movements not exceeding an accepted error value of 30m. The initial position of sand bars back to 1959 is used as a benchmark to measure distance and bearing of centriods relocation. Sand bar centroids showing upstream or downstream movements are established by circular and triangle symbols accordingly.

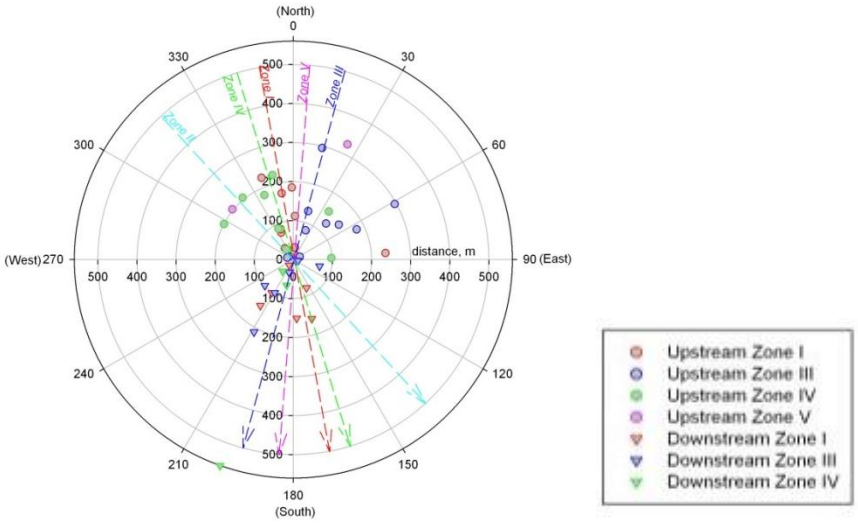

Figure 5.33. Distribution of sand bars migration across the study area (1959/2003-2006). See text for more details.

It is noted that the overall sand bars migration is upstream and in the south of study area, Zone V, migration is upstream only. Hence, the two largest in the study area sand bars are located within Zone V and represent on-going sand accumulation within the alluvial channel. The variety of sand bar migration bearings is more diverse for the upstream movements whereas downstream relocations are taking place mainly in parallel with the main flow direction. Average relocation distances increase from north to south of the study area (except Zone II where the sand component is virtually absent) with the same magnitude either up- or downstream as seen on the diagram ("average distance") starting from ~ 100m and reaching more than 250 meters at Zone V, near Kratie.

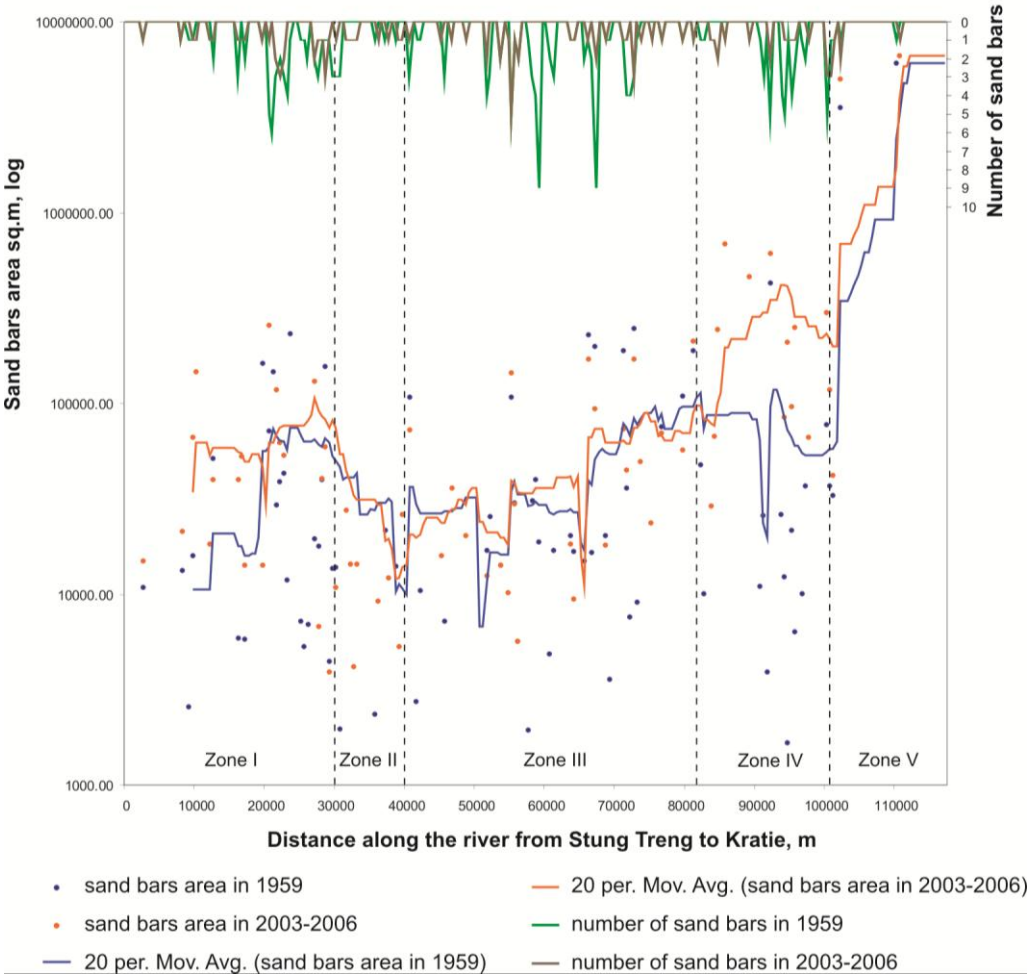

Figure 5.34. Sand bar numbers and area dynamics within the study area (years 1959/2003-2006). See text for more details.

A 20-point moving average function is used to provide the best visual impression of the overall trend of the sand bars area.

The areas and count of sandbars are shown on Figure 5.34. Moving-average trend lines, based on 20 values, are added to indicate overall trends throughout the area of interest. The largest number of sand bars (for instance, Zone III) is not correlated with

the greatest areas of sand deposition, which instead occurs in the south of the study area, Zone V. Deposition rates concluded from trend lines generally remain invariant for the given time lag apart from Zone IV (Sambor Rapids) where at present, the number of sand bars is less than 50 years ago but their total area seems to be larger. The Sambor Rapids area is established by stable bedrock outcrops forming a substrate for multiple sandbars where dense in-channel riverine vegetation (Zones 1-4 from scheme on Figure 5.21) facilitates sediment trapping. Such composition allows a suggestion of a possible switch between bare sands and vegetation cover under influence of floods and droughts. To clarify its dynamics more than two sets of time-series data would be required.

5.1.4.2 Riverbank erosion

The wide lateral extent of ancient Mekong terraces shown by observations of sections on the east river bank and the relatively narrow present day river corridor demonstrates that only minor lateral migration of the river has occurred since the river has incised into the terrain. Despite the indurating effect of the hot and humid tropical climate on previously deposited fluvial sediments, river bank erosion and accretion events nonetheless take place on the Mekong riverbanks, as within most fluvial systems. However, the character and scale of erosion differs with respect to the different geomorphological zones. For instance, according to field observations by the author, the length of eroded riverbanks within mixed bedrock-alluvial reaches (Zones II-IV) is of the order of a few to tens of metres. Limited mapping of erosion scars along these zones demonstrates that either inner and outer channel constructions or channel bends and bifurcations are the most important locations where bank erosion processes can be observed (Figure 5.35). Riparian vegetation destruction due to local livestock overgrazing may also provoke an increase in the number and severity of erosion events and locations. Additionally, observations had been made of the erosional ‘cuts’ in riverbanks produced by annual and/or extreme floods (Section 5.1.1.2, Figure 5.8 illustrating ‘cuts’ in riverbank).

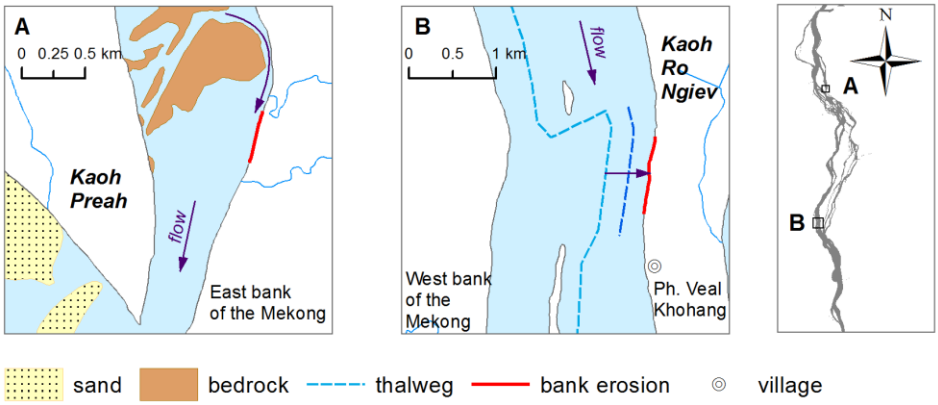

Figure 5.35. Examples of localized river bank erosion due to the channel constriction and in-channel flow adjustment. A) Bank erosion occurs due to the flow redirection by bedrock outcrops and B) Bank erosion due to the thalweg adjustment: blue dashed line show current thalweg, red dashed line – new thalweg position. Map on a right shows the location of maps A and B within the study area.

In order to determine the distribution of depositional and erosional events across the mixed bedrock-alluvial part of the river, comparison of high resolution remote sensing images of the study sub-area (Zone II) dating back to 1992 and 2005 was performed. The results reveal that sand deposition is attached to the island shores and there is very limited deposition of individual sand bars within the macrochannel. Bank erosion is noticed at the upstream ends of islands (Figure 5.36, A) although, the erosion pattern is not regular throughout the area, and due to the lack of intermediate data series, it is premature to draw definitive conclusions regarding the zonation of erosion within mixed bedrock-alluvial sections. In contrast to the focused character of erosion in mixed bedrock-alluvial channels, the length of eroded banks observed at alluvial reaches is greater. Around 22 km in total of the east riverbank downstream of Sambor Rapids (Figure 5.36, B) is identified as threatened by erratic riverbank erosion, where severe bank loss may happen in a given year but afterwards the bank remains stable over the next few years (MRC, 2009). Flooding, power boats and hydrological forces are named as the most frequent reasons for erosion in the Mekong in northern Cambodia (DelPHE, 2008; MRC 2009).

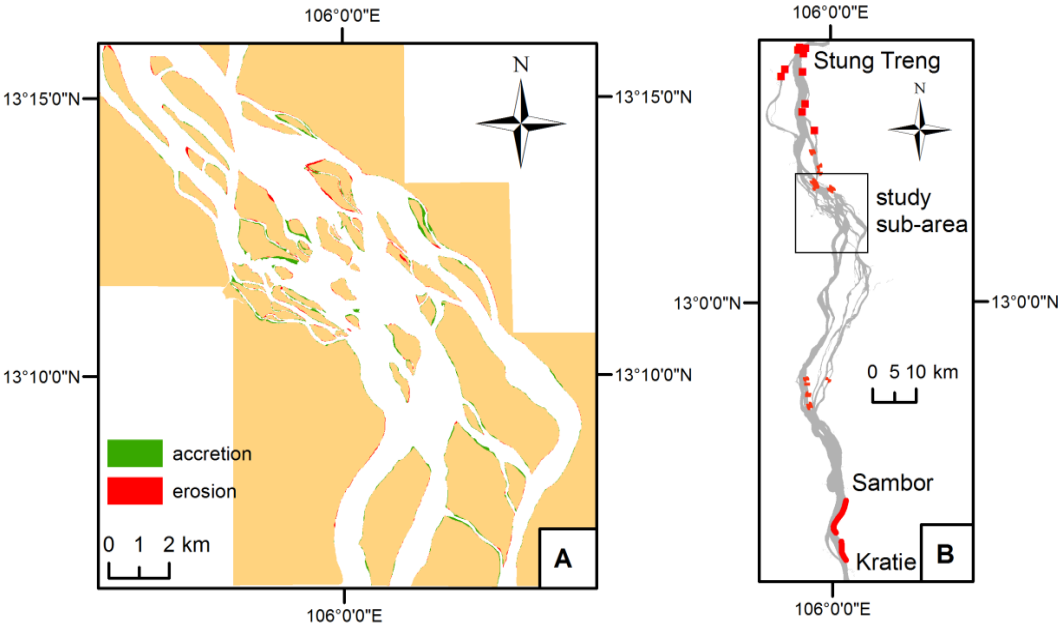

Figure 5.36. Distribution of erosion and deposition (accretion) within the study area: A) study sub-area erosion and accretion episodes over 1992-2005 period and B) erosion locations along the studied reach of the Mekong based on data collected by the author; DelPHE, 2008; MRC, 2009.

Areal and linear bank erosion/accretion rates calculated during the mapping exercise are established in Table 5.2.

Table 5.2. Accretion/erosion rates estimated from the comparison of the remote sensing data (1992 and 2005) covering the study sub-area.

Type of event	Number of episodes	Areal rate (m^2/y)			Linear rate (m/y)		
		Min	Max	Avg	Min	Max	Avg
Erosion	519	1.85	3495.25	116.81	0.03	4.87	0.39
Accretion	515	1.81	10699.04	275.31	0.04	14.1	0.54

The data indicate that within a period of 13 years accretion has exceeded the erosion by nearly twice in terms of linear distribution and more than twice in term of areal extent. That can be due to the occurrence of a single large sand bar which appeared within the investigated area and influenced the results of bank erosion calculations. Otherwise, linear erosion and accretion rates are not significant in changing the river pattern. This statement is supported by the outputs of the social survey conducted along the Mekong riverbanks upstream and downstream of Kratie (DelPHE, 2009) where the estimated average rate of erosion is 1.5m/year.

5.2 Channel metrics

5.2.1 Planimetric characteristics of multichannel river networks

There are no detailed studies of bank erosion and sand bar dynamics in other mixed alluvial-bedrock systems with which detailed comparisons might be made. However, the Mekong is a multichannel river and, importantly, given the structural controls noted above it is important to ascertain whether the network geometry differs significantly from other mixed bedrock-alluvial or alluvial multichannel systems. Thus, in order to make a comparison between planimetric parameters of different multichannel river networks, datasets representing topographic contours of three other rivers apart from the Mekong were gathered from manifold sources (see Section 4.1.1). The main characteristics are presented in Table 5.3 below.

Table 5.3. Main characteristics of rivers chosen for comparison of planview channel metrics.

River, ***location***	**Channel type**	**Climate**	**Annual mean discharge, cumecs**	**Sediment load, million tonnes per year**
Mekong, North-east *Cambodia*	Mixed bedrock-alluvial anastomosed (Carling, 2009)	Tropical monsoonal	13200	165
Orange, *North Cape Province, South Africa*	Anabranching mixed bedrock-alluvial (Tooth&McCarthy, 2004)	Arid	Variable from 2000 to 8000	41.5
Upper Columbia, *British Columbia, Canada*	Anastomosing (Makaske et al., 2009)	Humid continental	108	19 (based on 0.6 kg/s rate from Makaske et al., 2009)
Ganga, *India, West Bengal; Bangladesh*	Braided (Parua, 2009)	Monsoonal tropical	28000	729

Channel metrics describing the multichannel river patterns were extracted for all four rivers. Channel length, sinuosity and channel angles at bifurcations were derived directly from the topographic data using numerical values in attribute tables and/or consequent calculations based on their geometry (Section 4.1); other parameters, such as number of channels, mean slope of the riverbed and macrochannel width were referenced to the cross-sections spaced at equal intervals along each river (Section 4.1.3.2). The obtained numerical values were converted into tabular data and examined in different ways using statistical and graphical representations.

Comparison of 'braiding' intensity versus macrochannel width does not yield any significant result apart from showing that the number of channels increases together with macrochannel width (Figure 5.37). The data for the Orange River shows that this relationship is linear and so linear functions are fit to the other three systems although the regression is not significant in the case of the Upper Columbia River. However, the mixed bedrock-alluvial rivers have larger numbers of channels in a given cross-section of a given width, i.e. up to 25 versus up to eight for alluvial rivers. The average number of channels per cross-section at the observed rivers equals to three for the Upper Columbia and Ganga rivers whereas the Orange and the Mekong have six and four respectively.

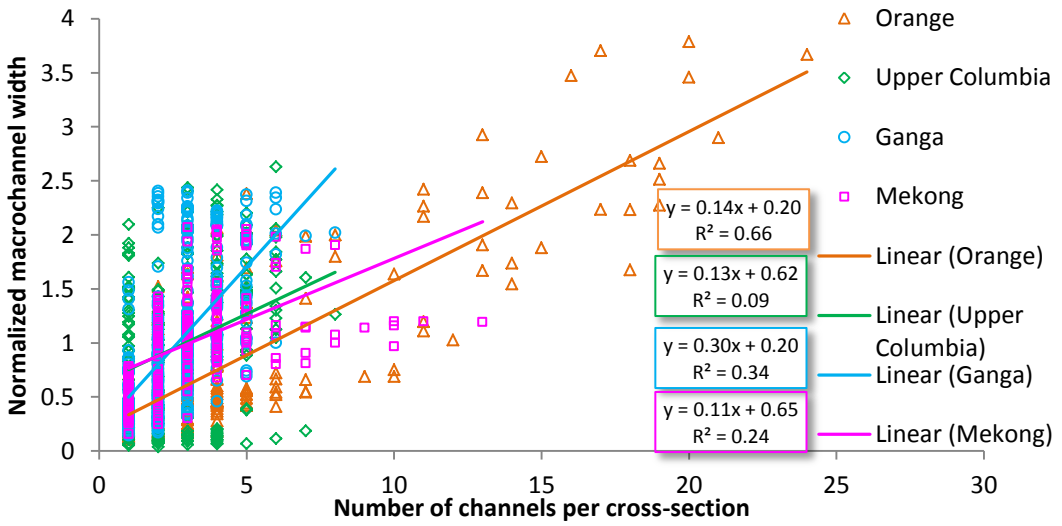

Figure 5.37. Comparing the number of channels per cross-section versus normalized macrochannel width (e.g. macrochannel width divided by the average macrochannel width).

Channel sinuosity in the case of mixed bedrock-alluvial rivers is better to be defined as "tortuosity" because channel configurations often have a zigzag shape controlled by fractured elements of terrain. A consideration of channel length and sinuosity does not allow any separation between the rivers (Figure 5.38) but shows that, in each river

system, longer channels tend to have higher sinuosity (alluvial) or tortuosity (mixed bedrock-alluvial).

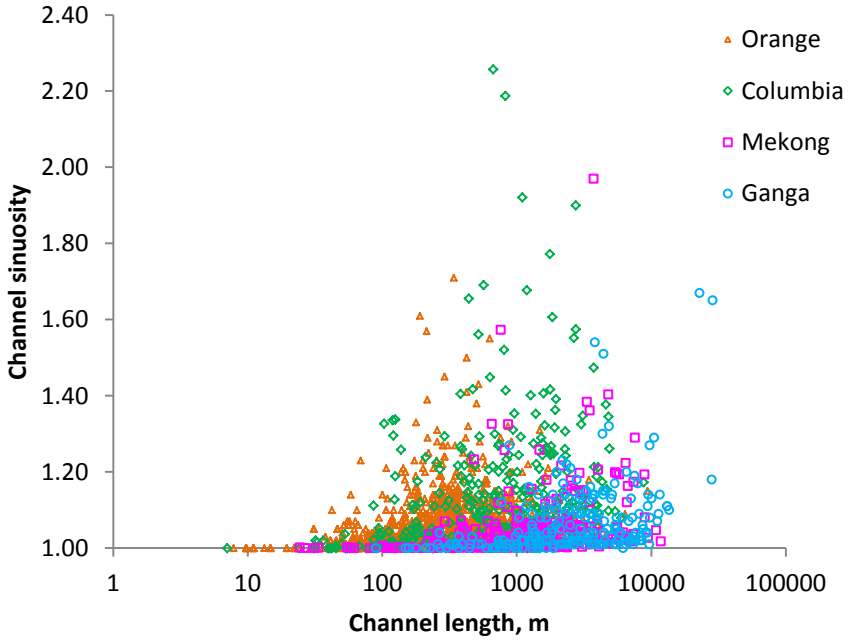

Figure 5.38. Channel length versus channel sinuosity/tortuosity.

Weathering processes in hot tropical or arid climates stimulates induration of older alluvial sediments composing riverbanks in the same way as was noted for anabranching rivers in the Australian monsoon tropics (Nanson et al., 2005). In the case of the Mekong laterites and pisolites have been recorded (see Chapter 5, Section 5.1.2) and the sediments in cut riverbank sections are generally indurated. There is no published information in this respect with regards to the Ganga and the Orange Rivers. However, mixed bedrock-alluvial rivers in such climatic conditions might become laterally constrained by indurated terrace sediments (or bedrock outcrops – see Chapter 6) which does not leave space for either lateral channel migration or development of smooth sinuous channel configurations. This quality can be demonstrated in principle by plotting channel sinuosity cumulative frequency on a normal probability plot (Figure 5.39). For the case of the humid continental Upper Columbia, sinuosity is generally higher than the tropical and dryland rivers in the dataset (Table 5.4) which is indicated on Figure 5.39 where the Upper Columbia plot separates from the other plots from the 10 per cent cumulative frequency.

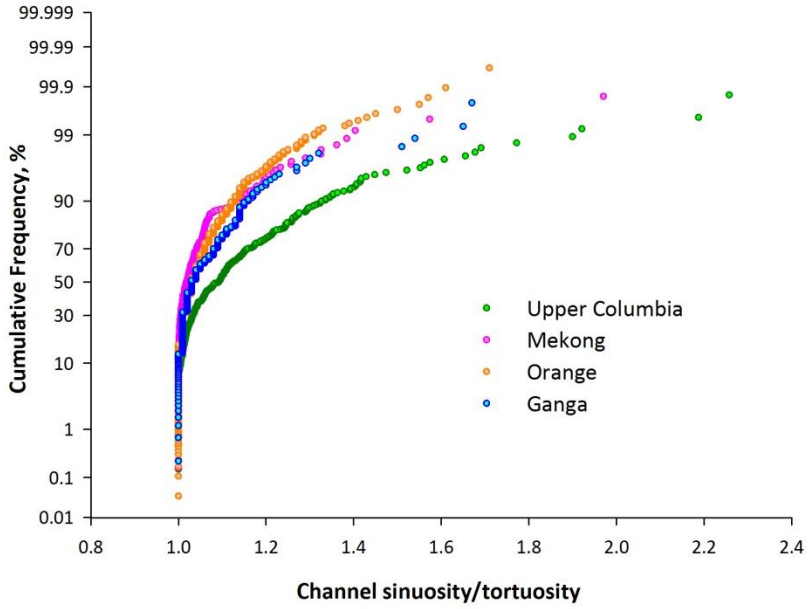

Figure 5.39. Normal probability plot for channels sinuosity/tortuosity.

Table 5.4. Sinuosity/tortuosity statistics.

River	Range		Mean	Std.Dev	P
	Min	Max			
Mekong	1.00	1.97	1.05	0.09	<0.001
Orange	1.00	1.71	1.05	0.07	<0.001
Ganga	1.00	1.67	1.07	0.09	<0.001
Upper Columbia	1.00	2.26	1.14	0.17	<0.001

The angles between channels at bifurcations extracted for each river channel network are given in Table 5.5.

Table 5.5. Bifurcation angles (degrees) statistics

River	Size	Mean	Std.Dev	Std.Error
Mekong	100	98.76	17.17	1.72
Orange	470	89.73	25.37	1.17
Ganga	69	100.79	18.60	2.24
Upper Columbia	104	89.69	26.35	2.59

Graphical representation of bifurcation angles clouds (Figure 5.40) shows that the Upper Columbia left or right angles at bifurcation often equal 50% of the angle sum at bifurcation (360°), e.g. 180°.

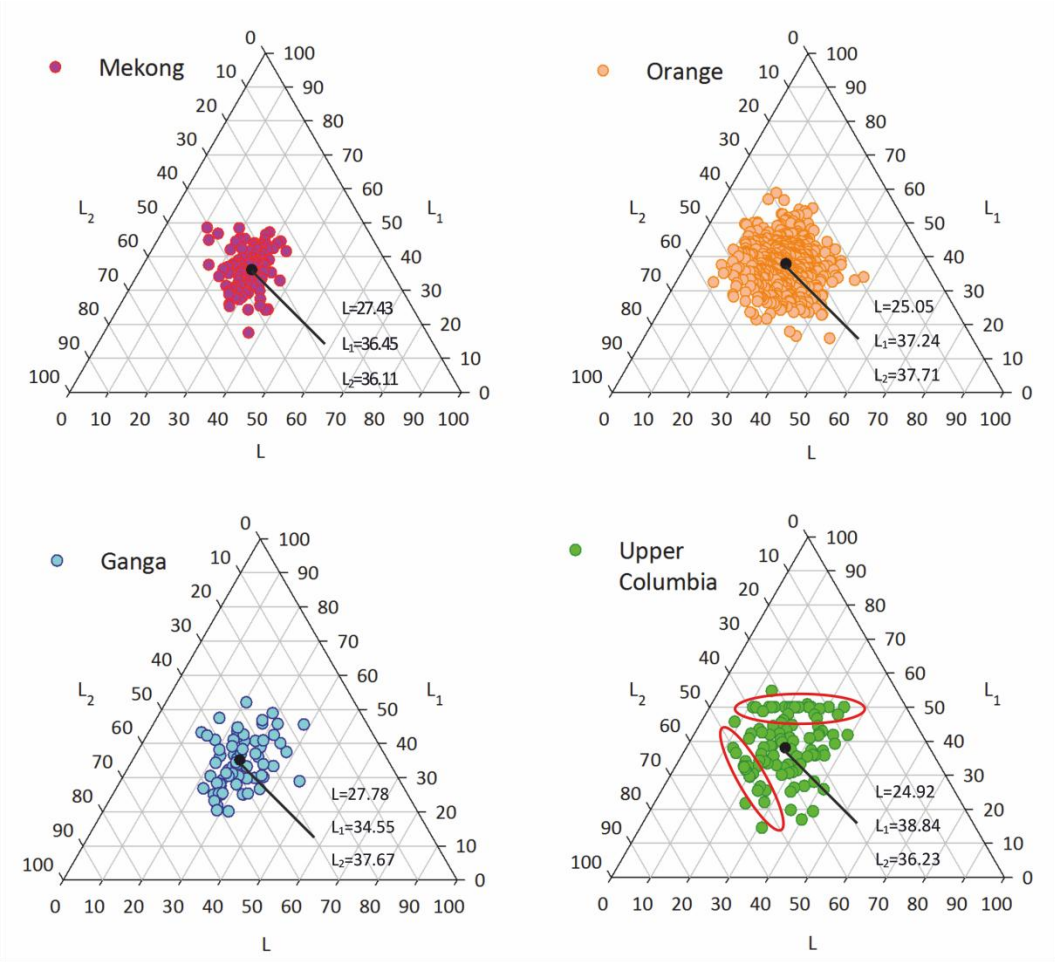

Figure 5.40. Distribution of angles at channel bifurcations; angle values originally in degrees were normalized so that $L+L_1+L_2=100$.

L is an angle between two bifurcating channels; L_1 is an angle between the upstream and right channel at bifurcation; L_2 is an angle between the upstream and left channel at bifurcation (see Section 4.1.3.2., Figure 4.11). Black dot in the middle of each data cloud corresponds to the dataset angles mean value given as numbers next to the point. Red ovals on the bottom right diagram (Upper Columbia River) highlight seemingly 'linear' limits to the trends of the left/right angles.

Plotting the bifurcation asymmetry ratios on a normal probability plot confirms this tendency as there are noticeable quantities of the Upper Columbia bifurcations with the asymmetry ratio equal to either 1 or -1 (Figure 5.41). These values result from bifurcations where the angle between the upstream and downstream channel links (main channel) is 180 degrees (i.e. no channel kinking) and where the third participating channel was formed by an avulsion through the Columbia levées and is incised into a portion of the floodplain. The most extreme values of bifurcation asymmetry at both the positive and negative end belong to the river Orange River;

these highly asymmetrical bifurcations in channel network are conditioned by bedrock structures.

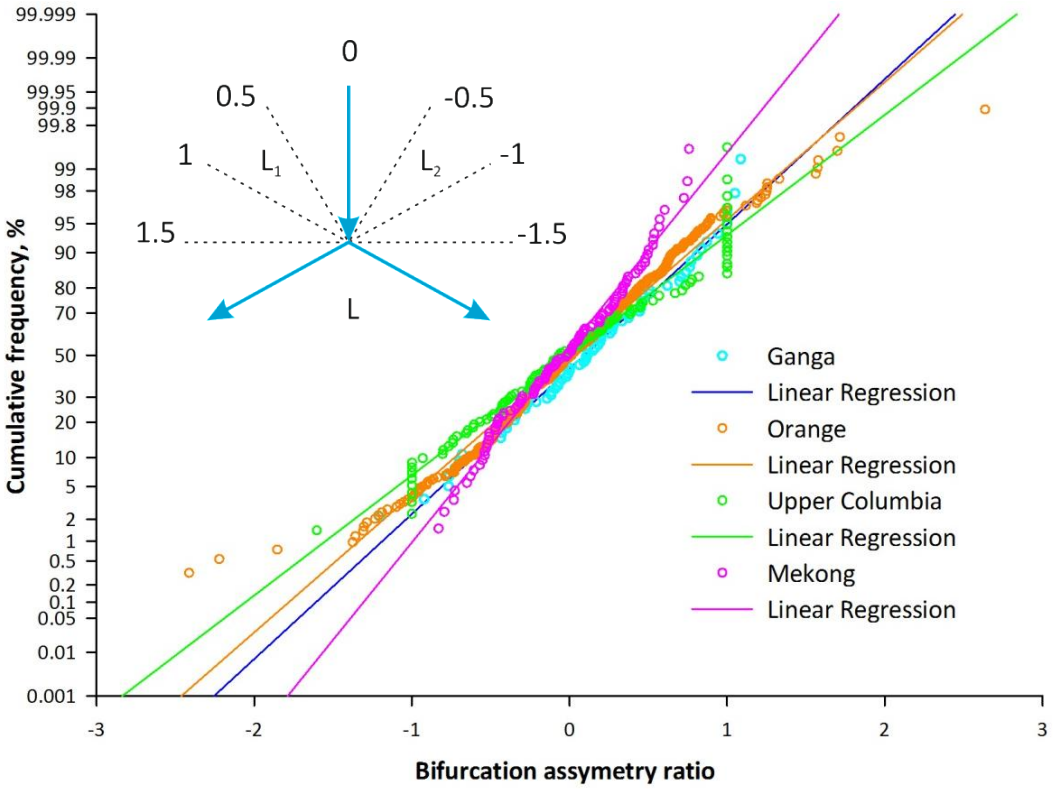

Figure 5.41. Normal probability plot of the bifurcation asymmetry ratio. The inset diagram shows asymmetry ratio values in accord to change of the upstream link position where L, L_1 and L_2 are downstream, right and left angles at the bifurcation respectfully.

Examination of channel slopes and macrochannel widths within each cross section allowed the covariations of these two parameters along the studied reaches to be established (Figure 5.42); the data processed using time series analyses (see Section 4.1.3.5).

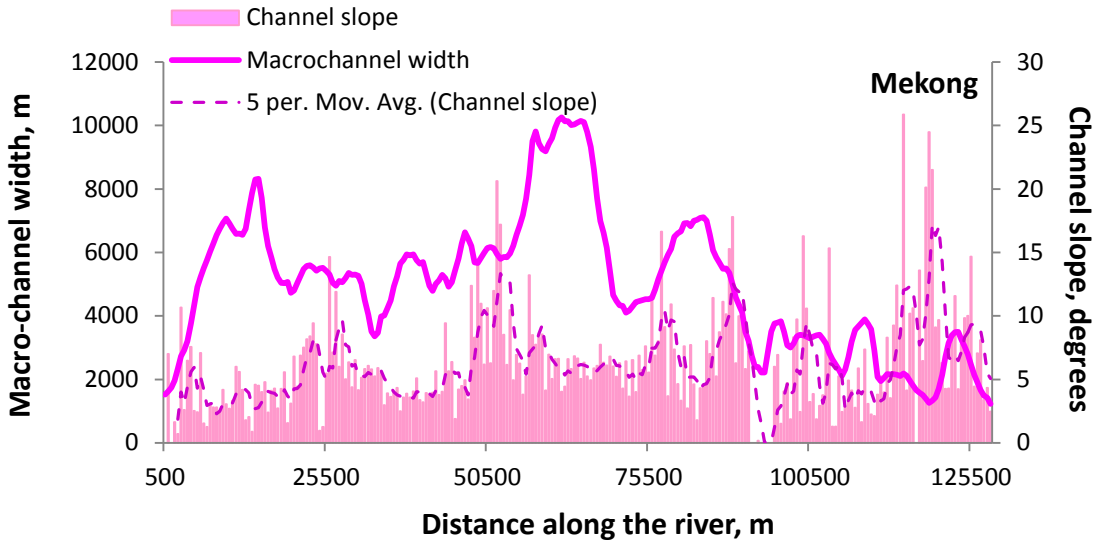
Channel slope
Macrochannel width
5 per. Mov. Avg. (Channel slope)
Mekong
Macro-channel width, m
Channel slope, degrees
Distance along the river, m
12000
10000
8000
6000
4000
2000
0
30
25
20
15
10
5
0
500
25500
50500
75500
100500
125500

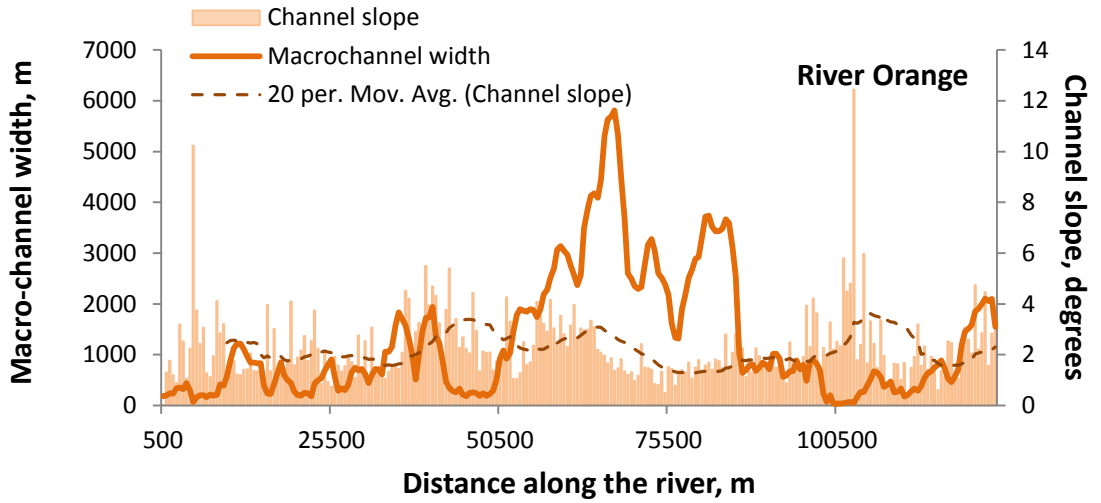
Channel slope
Macrochannel width
20 per. Mov. Avg. (Channel slope)
River Orange
Macro-channel width, m
Channel slope, degrees
Distance along the river, m
7000
6000
5000
4000
3000
2000
1000
0
14
12
10
8
6
4
2
0
500
25500
50500
75500
100500

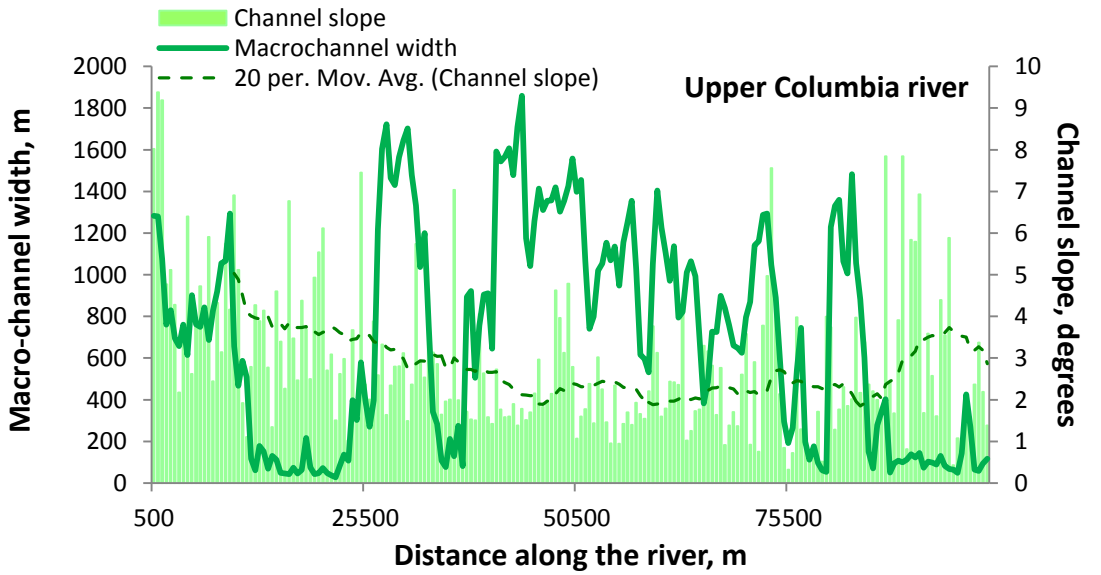
Channel slope
Macrochannel width
20 per. Mov. Avg. (Channel slope)
Upper Columbia river
Macro-channel width, m
Channel slope, degrees
Distance along the river, m
2000
1800
1600
1400
1200
1000
800
600
400
200
0
10
9
8
7
6
5
4
3
2
1
0
500
25500
50500
75500

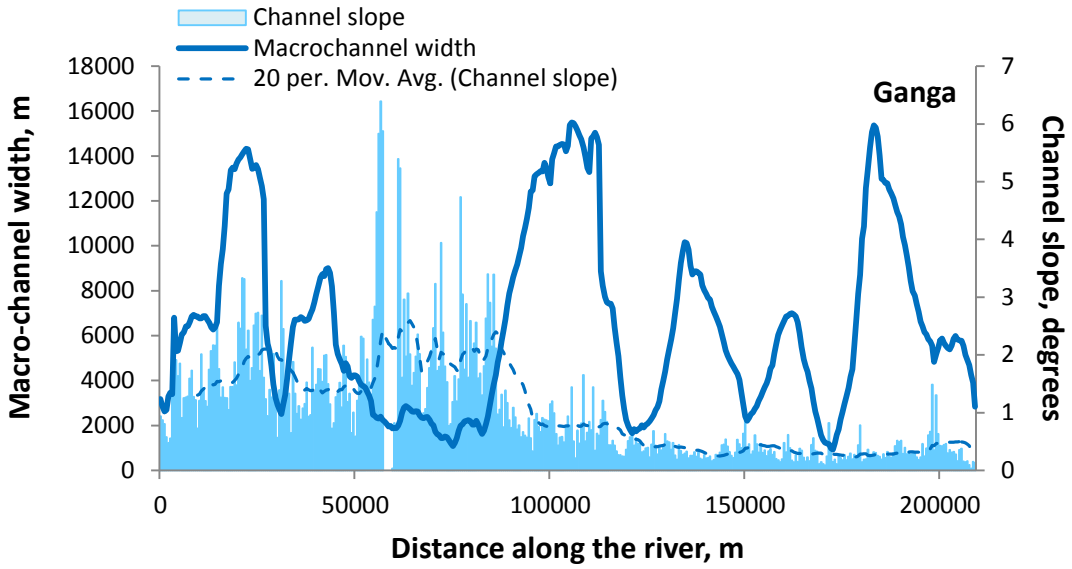

Figure 5.42. Macrochannel width and average channel slope within cross-section along the each of studied rivers.

A five-point moving average smoothing function is used for the Mekong in contrast to a 20-point moving average for the other rivers as these smoothings provide the best visual impression of the overall trend of the slope data.

Channel width and slope examined as spatial series indicated that all four systems exhibit autocorrelation in the data series with stronger autocorrelation being noted for the channel width series (Figure 5.43) in contrast to the weaker autocorrelation in the channel slope series (Figure 5.44). In all systems, the persistence is present in lag values of 1, 2 (occasionally 3) in the partial autocorrelation series which can be interpreted to indicate that there is no persistence (memory) beyond lag 2. It is not possible to identify significant differences in behaviour between the alluvial and the alluvial bedrock-constrained systems. However, both linear-detrended channel width series for the Ganga and the Orange Rivers exhibit cyclical behaviour in the spatial series that purposefully was not removed for the analysis reported above. This cyclicity sensibly is not evident in the bed slope series for these two rivers. In all four systems, there is a significant negative relationship between bed slope and channel width such that, as slope increases, channel width decreases and vice versa (Figure 5.45). The cyclic behaviour of the Ganga bed width data may represent the 'beaded' nature of the planform with reaches that are multichannel being interspersed with reaches that have a single or few channels. Such cyclic behaviour is also noted for the Orange River planform and for other rivers globally (Pelletier & DeLong, 2004; Tooth & McCarthy, 2004).

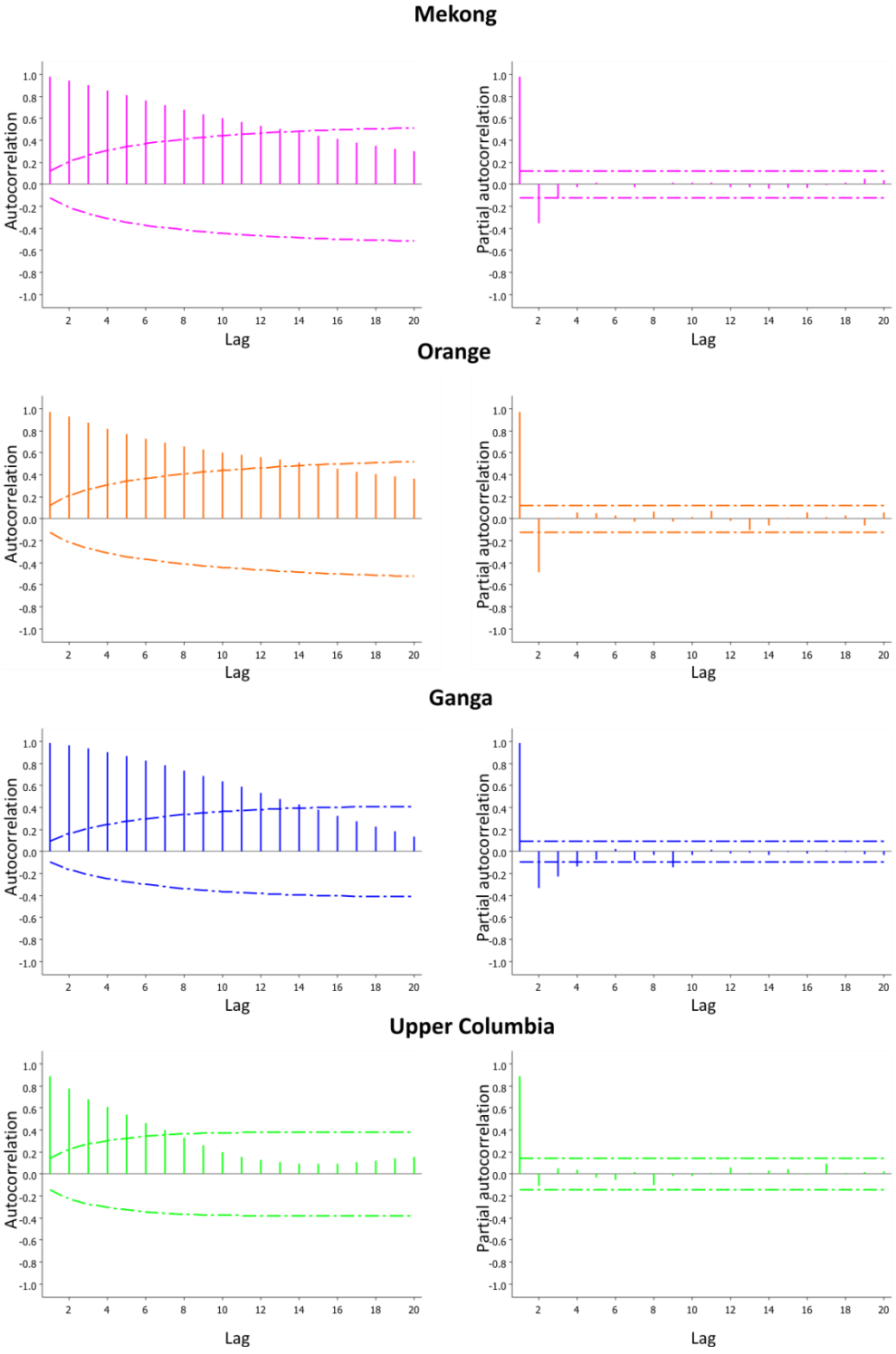

Figure 5.43. Autocorrelation (left) and Partial Autocorrelation functions (right) of macrochannel width at the given lag.

All rivers show strong autocorrelation functions with the data values declining exponentially but according to the partial autocorrelation functions suggesting low order (1 – Orange and 2- Mekong, Upper Columbia and Ganga) Auto Regression (AR) Models.

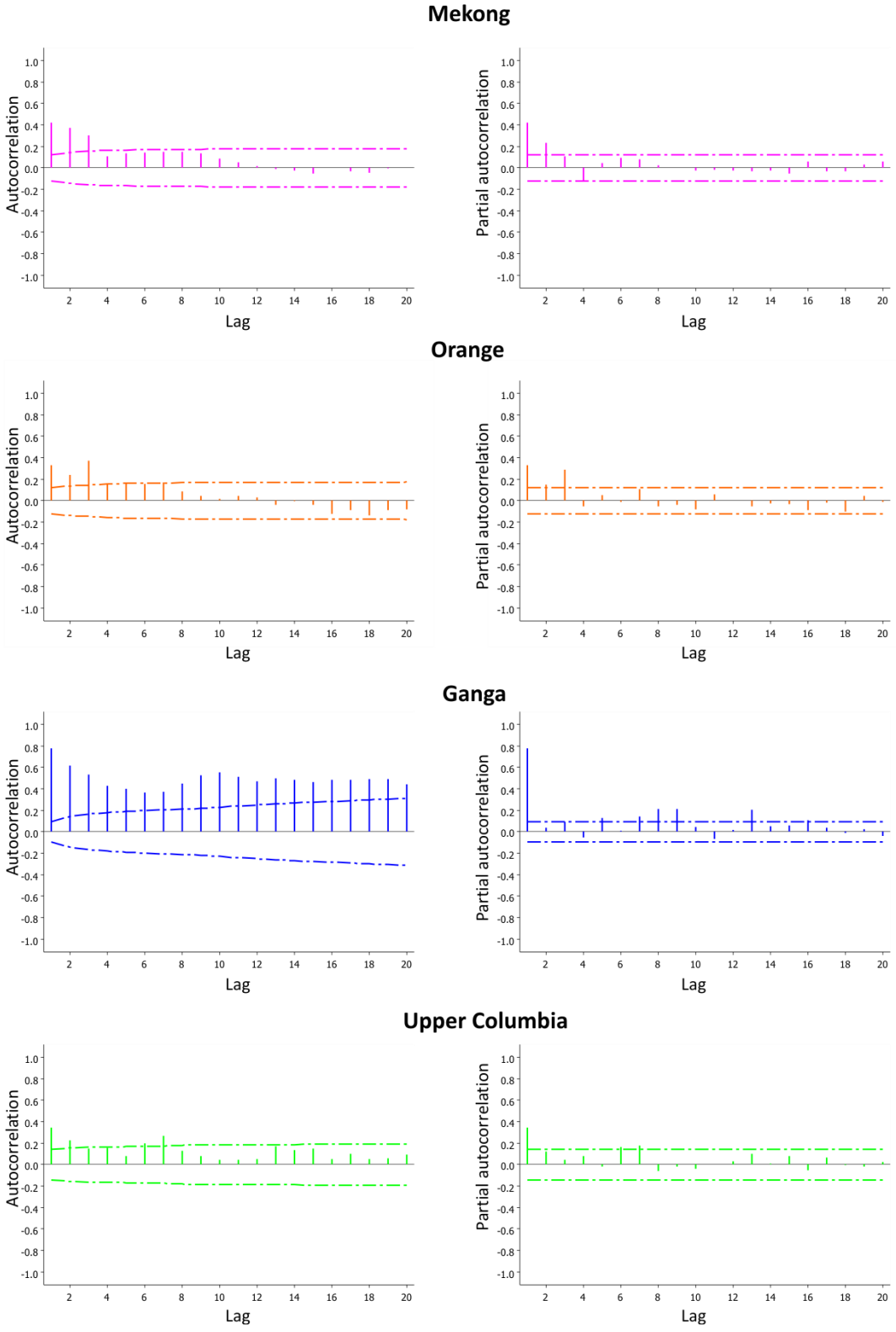

Figure 5.44. Autocorrelation (left) and Partial Autocorrelation (right) function of channel slope at the given lag.

The autocorrelation function of the Mekong, Orange and Upper Columbia is weak where data oscillate from positive to negative (Mekong and Orange). Strong autocorrelation function of the Ganga may indicate residual cyclicity in the data series. Partial autocorrelation functions suggest low order Auto Regression Models (1 – Ganga, 2 – Mekong and Upper Columbia and 3 – Orange)

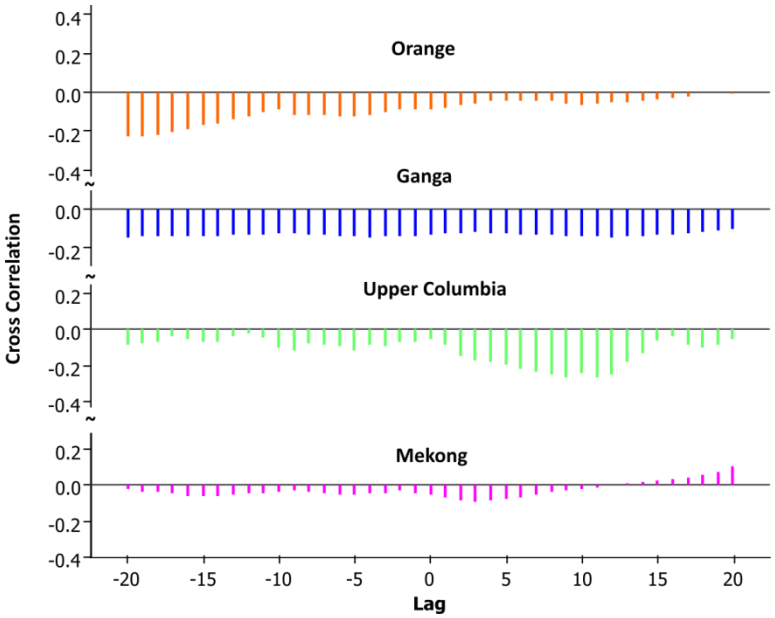

Figure 5.45. Cross Correlation function of channel width and average channel slope.

The cross correlation function for all rivers is weak and universally negative (apart from the Mekong which can be ignored due to the residual data cyclicity). It shows that when the slope increases the width declines at the variable lags: 3-4 (Mekong), 5 (Orange) or 9 – Upper Columbia river. Cross correlation function of the Ganga width and slope has a box distribution, e.g. no lag can be specified.

5.2.2 Planimetric characteristics of multichannel river islands

As described in Section 4.1.3.3., the Mekong island's width and length was derived using two methods (MBG and centrelines) in order to determine which method to apply when analysing multiple datasets. Figure 5.46 shows island length versus width (aspect ratio, R_A) plotted on logarithmic axes, and power functions for each dataset. Statistical comparison using Mann-Whitney Rank Sum test on two groups of length-width values confirms that the difference between the datasets is not statistically significant (P=0.086). Thus, due to the relative simplicity, the MBG method has been chosen for further use.

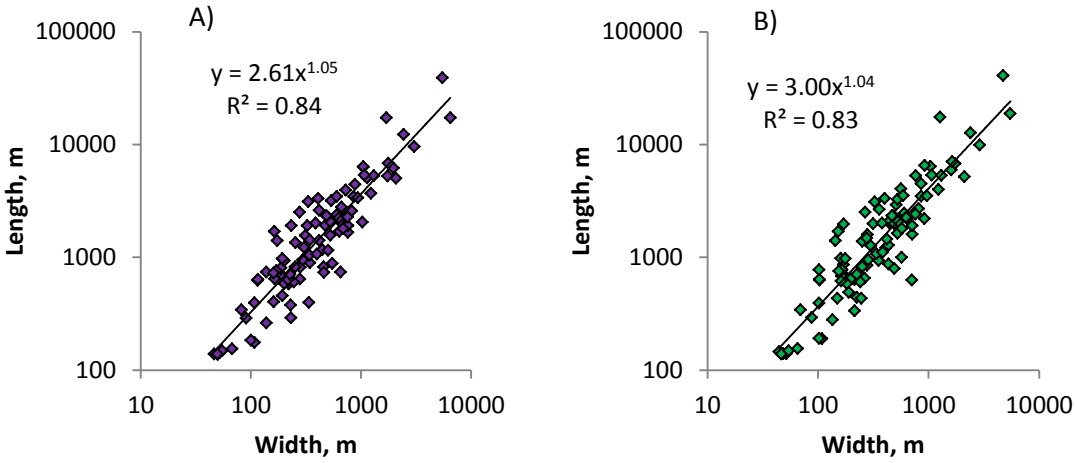

Figure 5.46. The Mekong primary islands width and length obtained using: A) MBG and B) islands centrelines methods. See text for more details.

Similar to the Mekong, the islands of the Upper Columbia, Orange and Ganga rivers were processed with the MBG method so that length and width values were extracted. In general, the data distributions show simple proportionalities between length and width. However, for comparison with the literature, power functions were fitted to each distribution, with R^2-values between 0.76 and 0.86 (Figure 5.47). Otherwise, despite dissimilarities observed on a physical level between the four rivers, Figure 5.47 shows that island aspect ratios alone do not indicate differences between river systems. This conclusion may be explained by the fact that primary island shapes are mainly adjusted by fluvial forces adapting their planview contours to the flow hydraulics through erosion or deposition in order to achieve an essential equilibrium within a system.

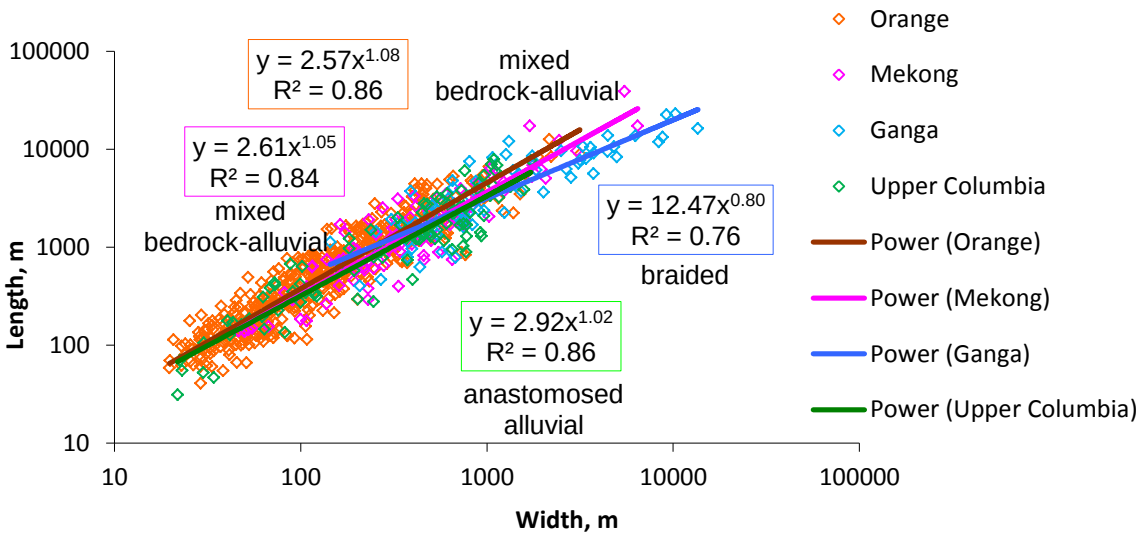

Figure 5.47. All islands aspect ratio comparison.

Nevertheless, shape assessment of each individual island on the basis of perimeter, area and convex hull polygon perimeter values enables an examination of the distinctive "look" of each channel pattern. Compactness compares island area with the circle of the same perimeter length as the island and roundness does the same but for the perimeter length of the convex hull polygon enclosing the island. The convexity measure indicates the presence of concaves between the contour of an actual island shape and the convex hull polygon outlining this shape (see Section 4.1.3.3. for more details and formulae for each parameter). Yet again, estimated compactness and roundness values and their cumulative frequency do not show clear contrasts between different multichannel rivers (Figure 5.48).

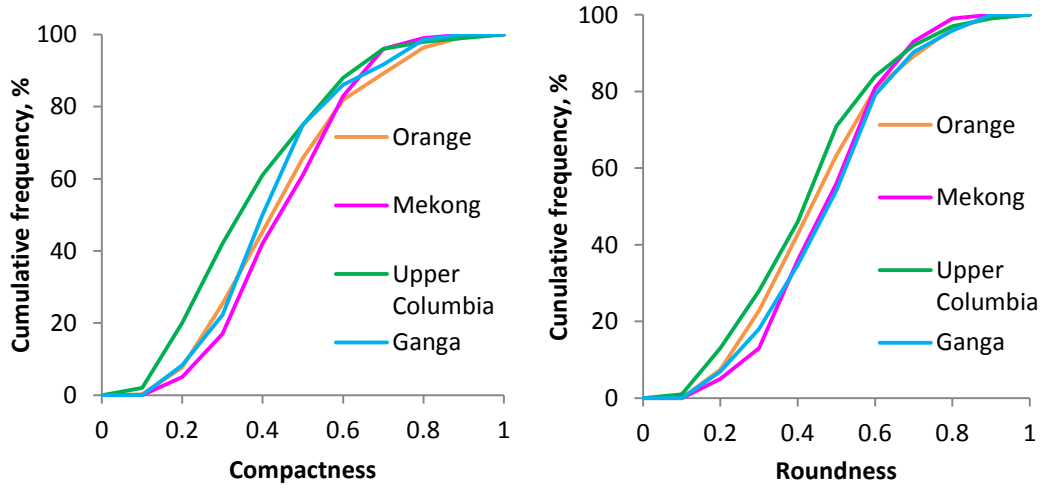

Figure 5.48. Cumulative frequency distribution of islands compactness (left) and roundness (right).

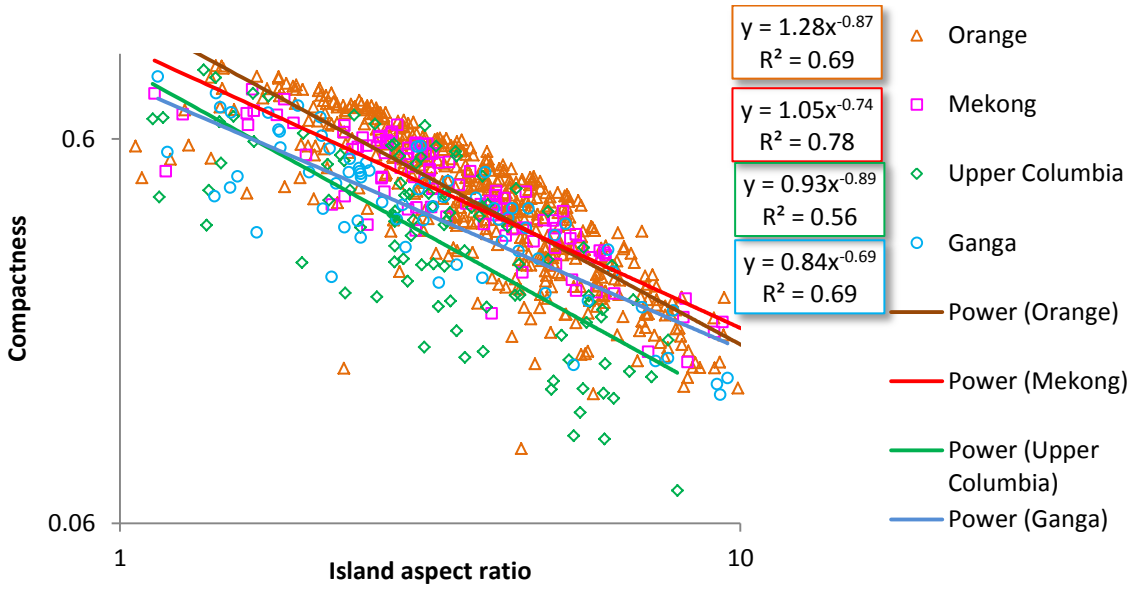

Figure 5.49. Relationship between island aspect ratio and island compactness on log axes.

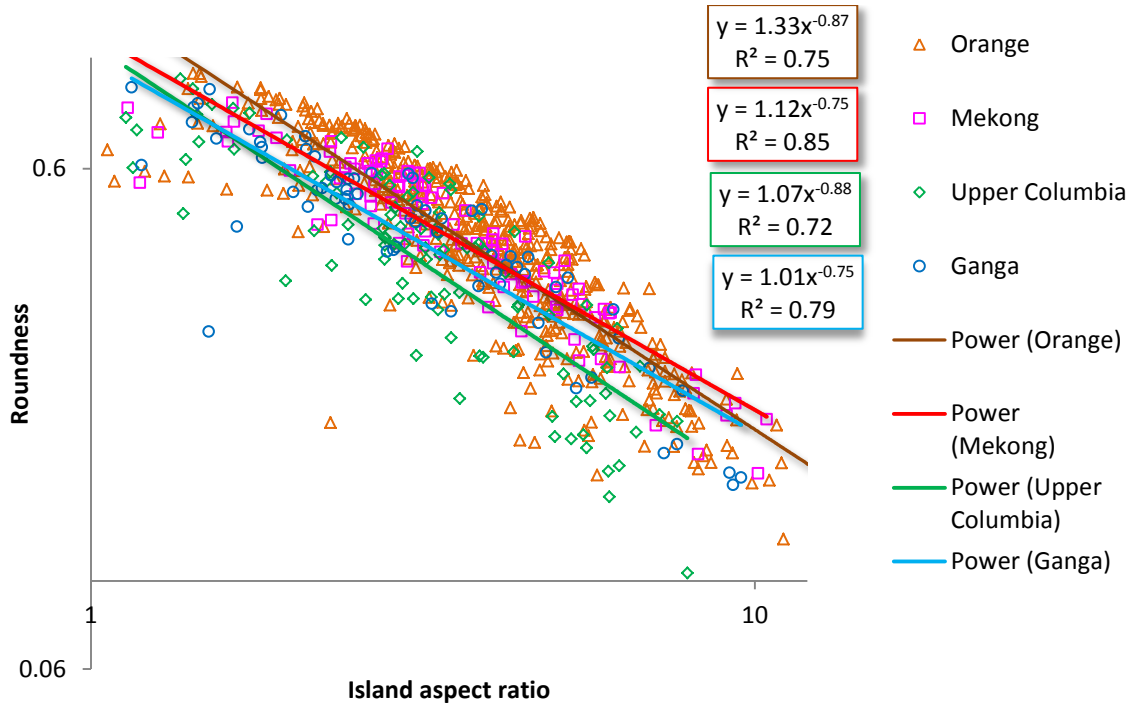

Figure 5.50. Relationship between island aspect ratio and island roundness on log axes.

Comparison of island aspect ratio with compactness (Figure 5.49) or roundness (Figure 5.50) reveals that the trend of decreasing compactness/roundness values with increasing aspect ratio is followed by all analysed island shapes with an apparent origin of unity, as expected, on both axes. However, for the same aspect ratio values, some islands of the Mekong and Orange Rivers seem to be more compact/rounded than those of the Ganga and the Upper Columbia Rivers. Although both diagrams look similar, the difference is conditioned by using islands shape (compactness) and island convex hull perimeter therefore the convexity parameter needs to be tested.

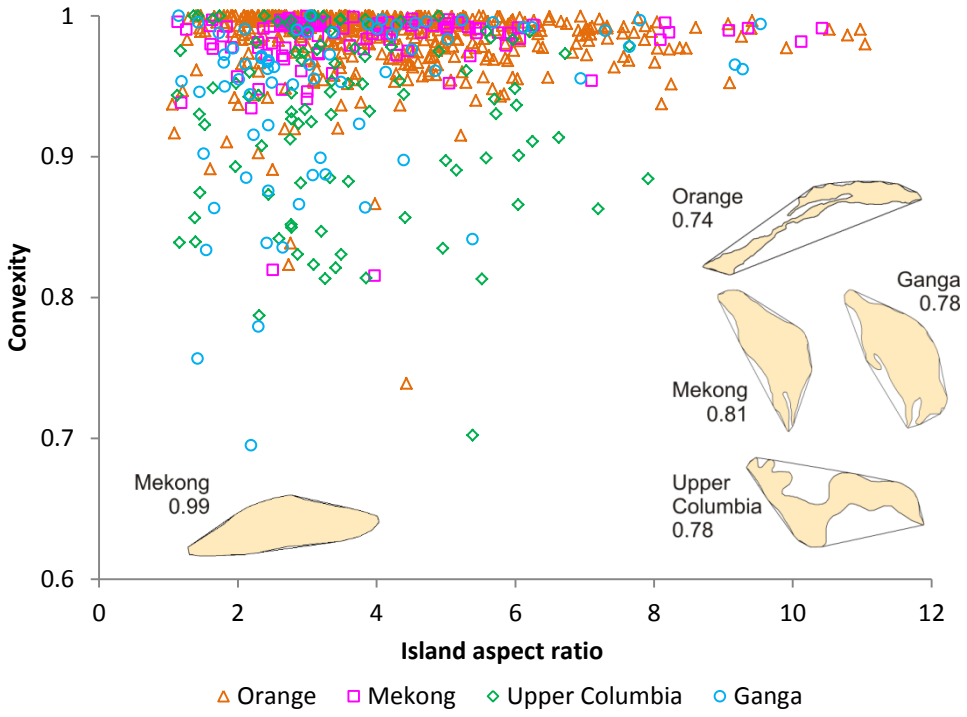

Figure 5.51. Islands convexity and aspect ratio with actual examples illustrated.

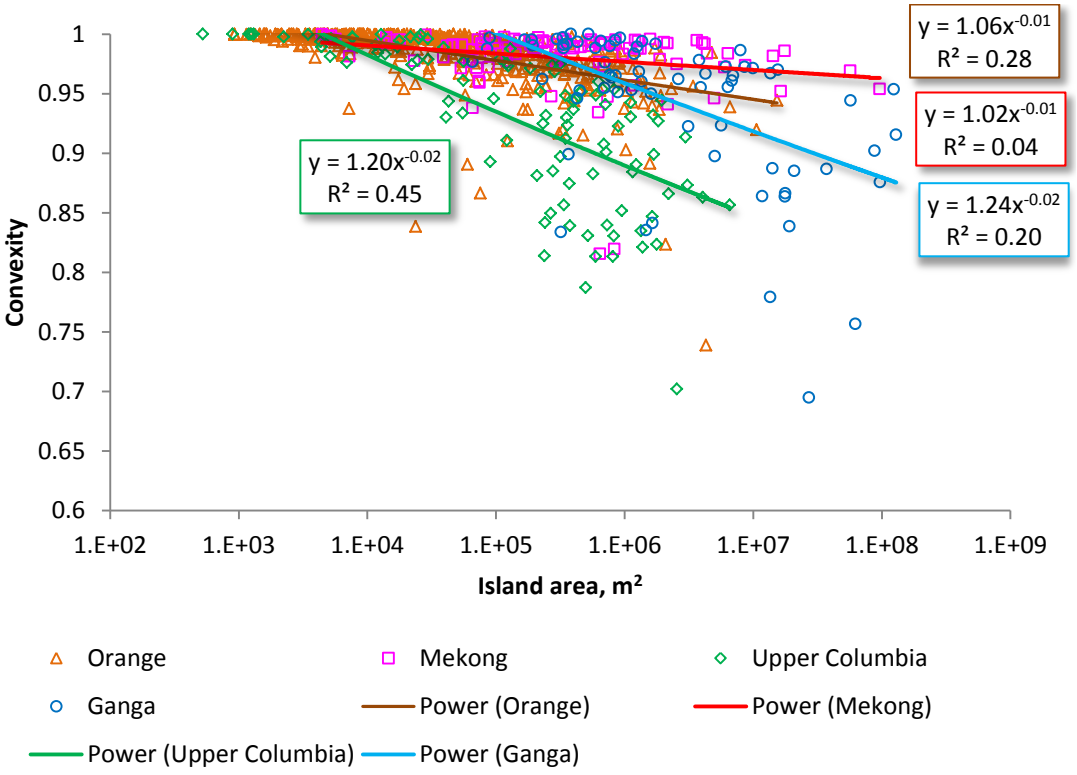

Figure 5.52. Island convexity and island area.

As seen from Figure 5.50 distribution of island convexity does not depend on the aspect ratio, hence islands of the Mekong and Orange with the highest aspect ratios are characterized by high (more than 0.9) convexity values whereas, for instance, the Upper Columbia has islands with high aspect ratio but smaller convexity. Additionally, the diagram indicates that both the Ganga and Columbia have plenty of islands with a relatively low convexity when compared with the Mekong and Orange rivers. On the other hand, larger islands are more prone to concave development, as is shown on Figure 5.52.

A cumulative frequency diagram (Figure 5.53) confirms and further clarifies this observation, showing that only a few percent of the Mekong and Orange islands have convexity less than 0.9, while the Ganga and the Upper Columbia Rivers reach this limit at ~20 and 30 percent, respectively. Thus, the island convexity parameter enables a separation of alluvial anastomosed and braided from mixed alluvial-bedrock anastomosed river systems. The process interpretation of this convexity result is considered in the Section 6.2.

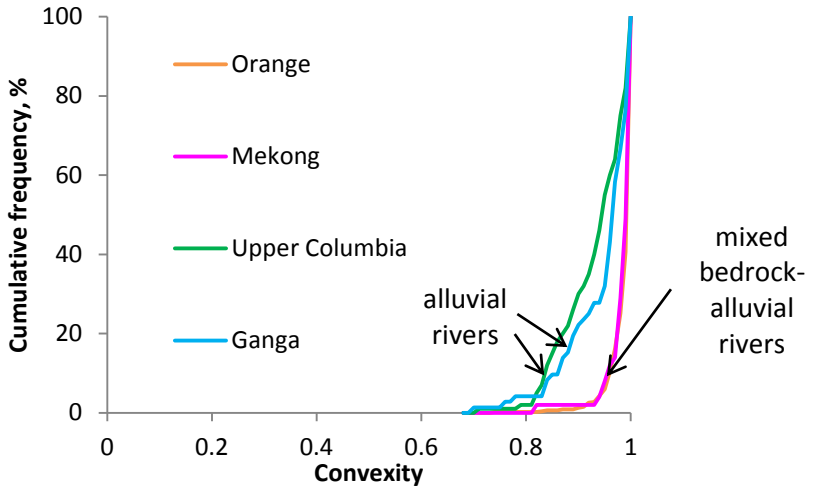

Figure 5.53. Cumulative frequency distribution of islands convexity.

5.2.3 Trend surface analyses

Processing the available DEMs for all four rivers using trend surface analyses (see Section 4.1.3.4 for details of the method) allows outlines to be produced of the topographic settings of mixed bedrock-alluvial and alluvial multichannel rivers (Figure 5.54 -5.57).

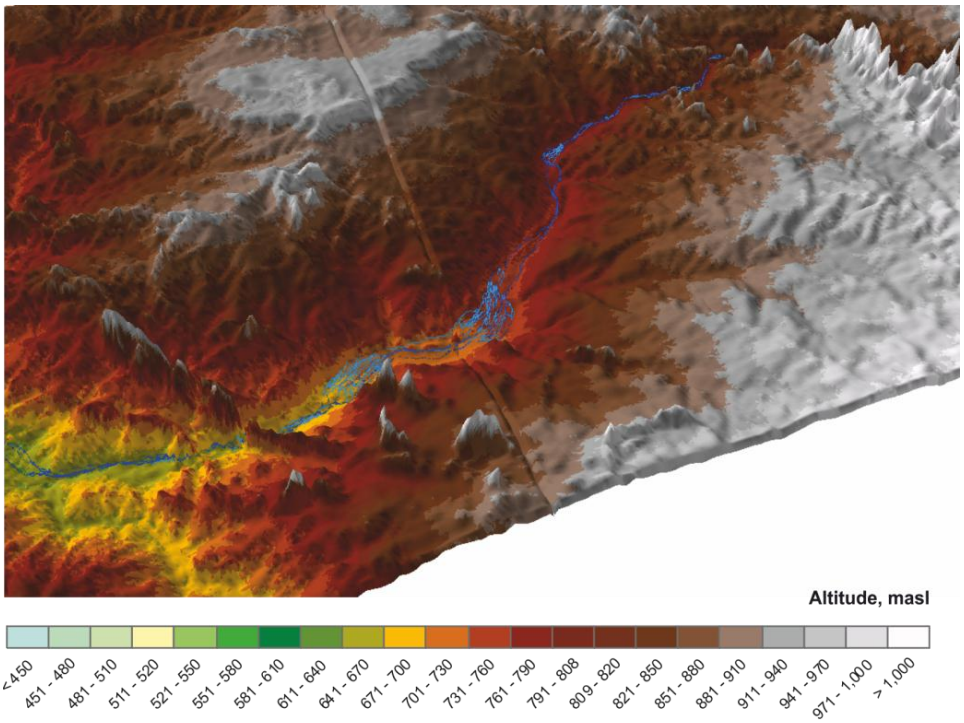

Figure 5.54. The Orange River DEM (see Chapter 1, Figure 1.4 for the location map).

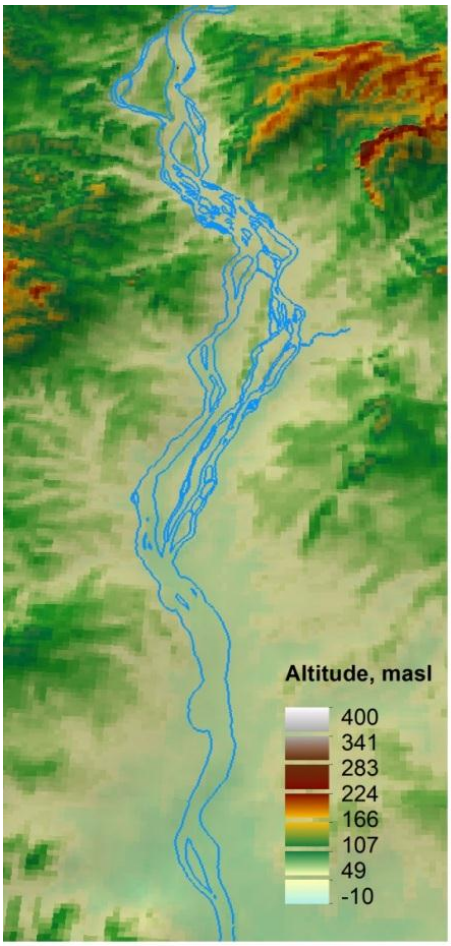

Figure 5.55. The Mekong River DEM (see Chapter 1, Figure 1.2. for the location map).

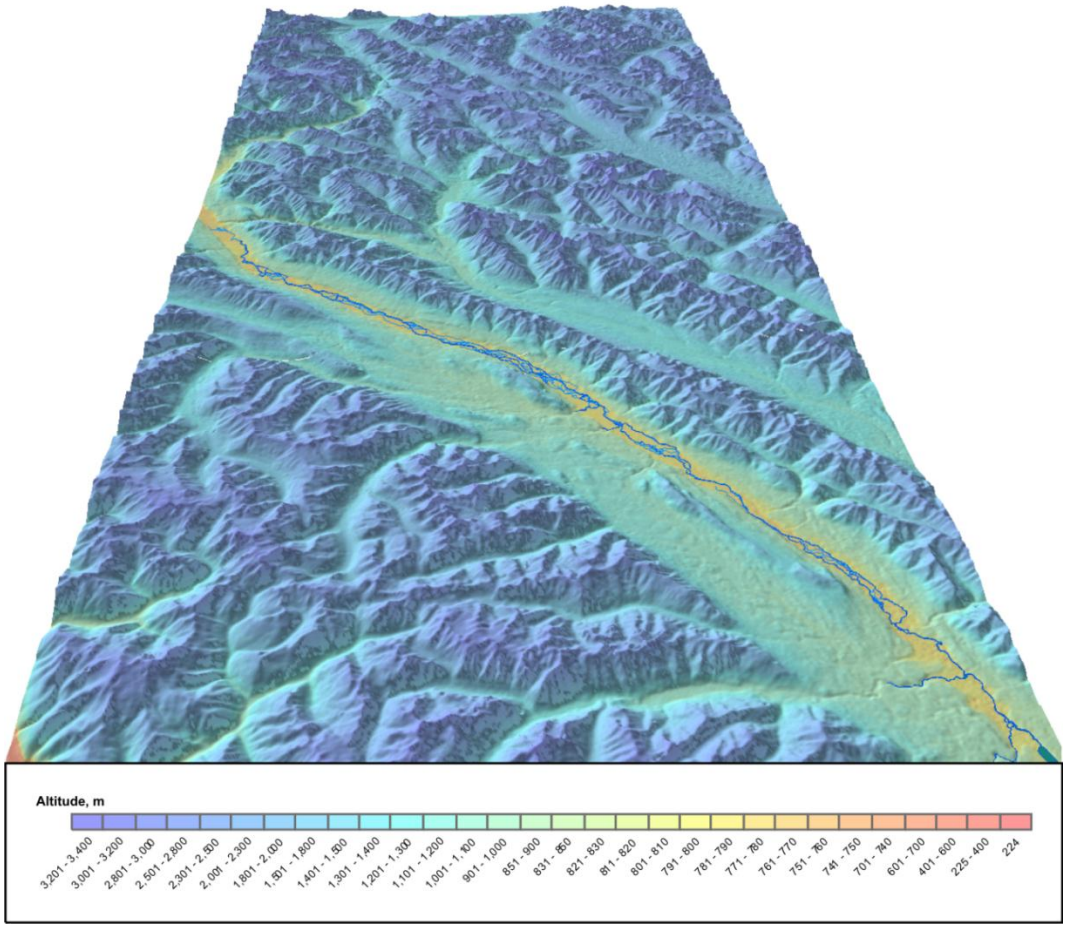

Figure 5.56. The Upper Columbia River DEM (see Chapter 1, Figure 1.5 for the location map).

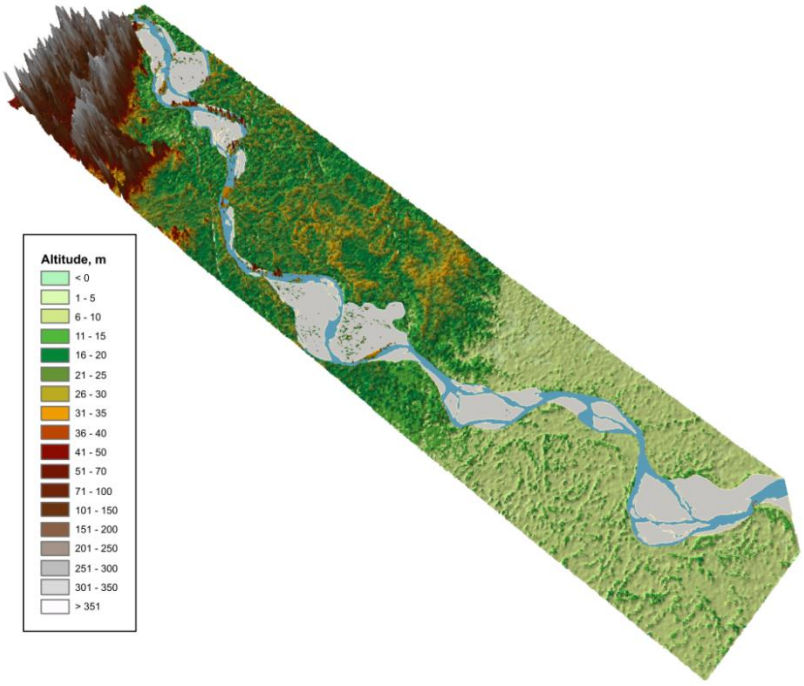

Figure 5.57. The Ganga River DEM (see Chapter 1, Figure 1.6 for the location map).

Mekong and Orange planforms are characterised by well-expressed regional trend surfaces declining from upstream to downstream along the studied reaches. Nevertheless, as seen from their long profiles (see Chapter 1, Figure 1.3 and Tooth & McCarthy, 2004, p.238), locally the rivers cross naturally formed geological steps (or barriers) which undoubtedly play significant roles in the overall channel pattern configurations via rapid gradient changes and (or) alteration in macrochannel widths.

When considering the primary channel pattern of the Mekong it was noticed that some locations (for instance the Rapids de Prek Patang, geomorphological Zone II on the Mekong) may also serve as points of transition from which the overall direction of a river course changes. These zones are recognized in planview by “bi-directional” system of channels, where some channels align with the flow direction immediately downstream, while others coincide with a new general alignment of the downstream river course. Thus, elevation data at such localities were obtained in order to create trend surfaces aiming to explain changes in the macrochannel directions and the controls on the bi-directional channel systems.

The results show (Figure 5.58 and Figure 5.59) that locally the topographic gradient contradicts the regional trend surface and influences the direction of the local channel pattern development quite specifically.

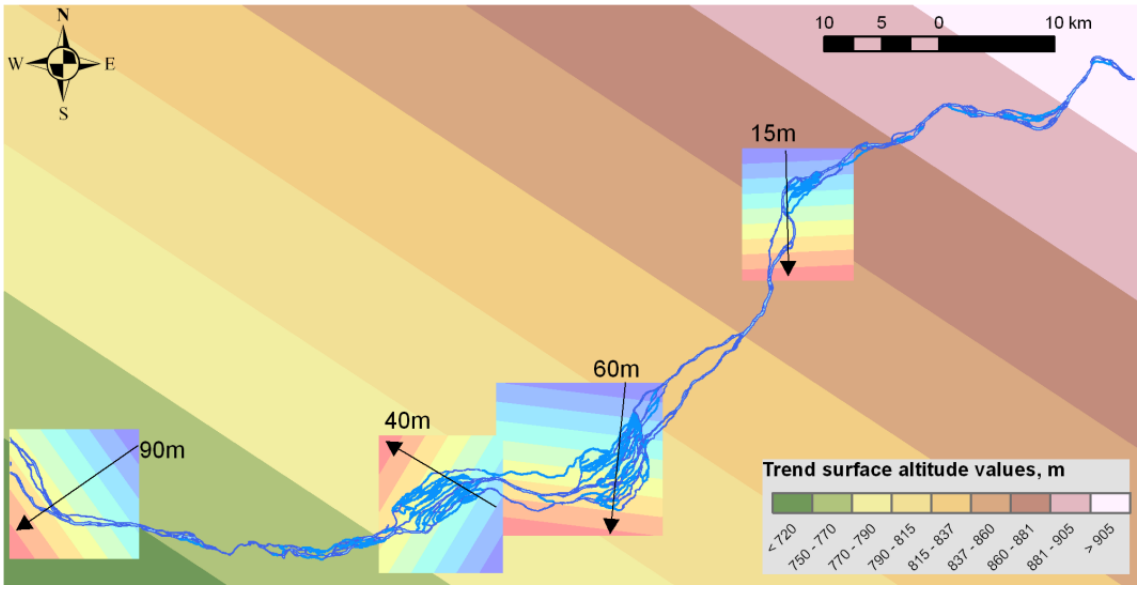

Figure 5.58. The Orange River regional and local first order topography trend surfaces (see Chapter 1, Figure 1.4 for the location map).

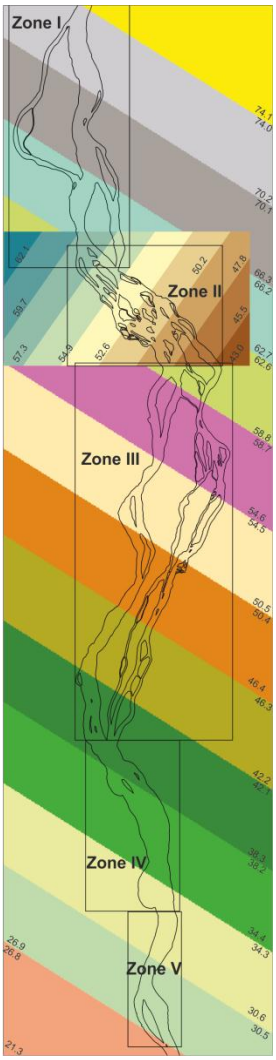

Figure 5.59. The Mekong River regional and local first order topography trend surfaces (see Chapter 1, Figure 1.2 for the location map).

The influence of the local topographic trend on the channel pattern configurations is a quality which neither of the two other rivers (the Upper Columbia and Ganga) exhibit. The trend surface of the Upper Columbia shows that it occupies a low gradient valley enclosed on either side by a hilly landscape and that there are no topographical opportunities which can stimulate significant changes in channel directions locally (Figure 5.60).

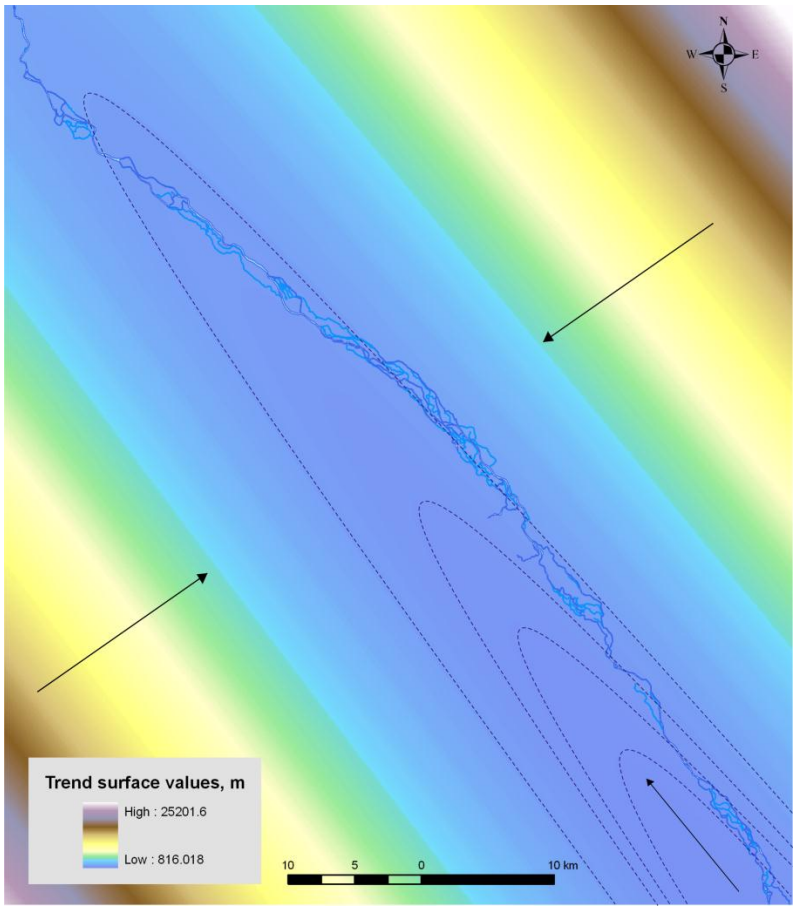

Figure 5.60. The Upper Columbia River regional second order topography trend surface (see Chapter 1, Figure 1.5 for the location map).

In comparison with the Upper Columbia, the terrain occupied by the Ganga is also flat but it is possible to extract some local topographic trend surfaces (Figure 5.61) which, however seem not to be related to changes in the number of channels. The 'beaded' pattern of the Ganga therefore has to be explained on a basis of other parameters not elucidated by the trend surfaces (e.g. lineaments and neotectonics) as the basement is not far beneath the alluvium and is locally exposed (Singh, 2007).

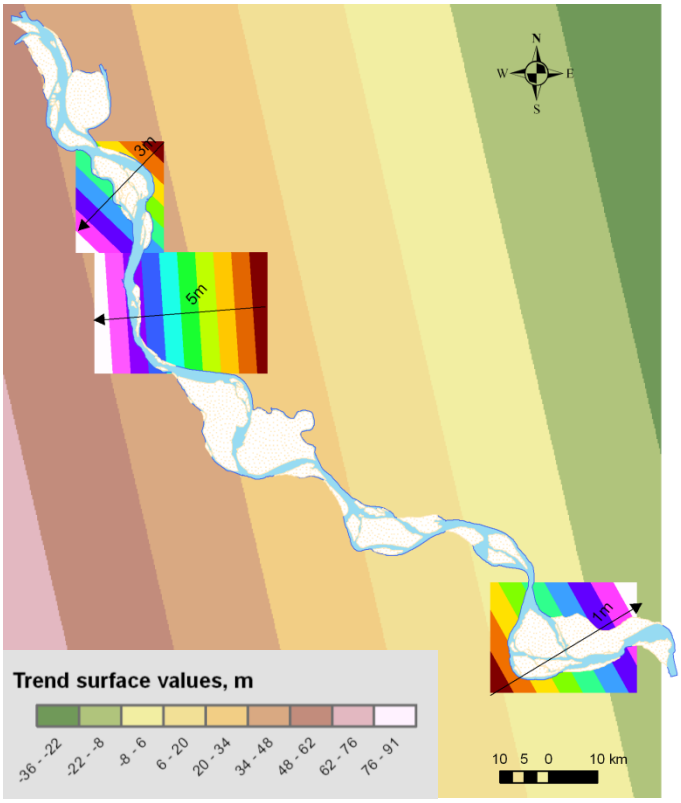

Figure 5.61. The Ganga River regional and local first order topography trend surfaces (see Chapter 1, Figure 1.6 for the location map).

6 Discussion

The discussion is structured into two sections. The first section (6.1) considers general issues of Mekong River evolution, and this section finished with some generic points, arising from this specific section. The second section (6.2) considers generic issues pertaining to the study of multichannel rivers more generally. In this discussion some additional data analysis is included to provide further explanation and interpretation of the results presented in Chapter 5.

6.1 The Mekong River

The river today is incised into a narrow corridor some ~5 km wide and shows no preference to align with either the east or west margins as might be expected if subsidence or uplift had occurred either to the east or to the west. The lack of abandoned primary channels within the modern floodway or on the terraces testifies to the plan-view stability of the river during the Quaternary. The single example of an abandoned channel (palaeochannel) at Sambor (see Sections 5.1.2 and 5.1.3) seems to be related to local faulting rather than regional tectonic adjustments. Instead and fundamentally, the multiple channel pattern of the Mekong is governed by: 1) a regional balance between the seaward gradient and the overall tectonic stability of the region, coupled with the distribution and alignment of the major fault lines and regional geological structures; 2) local geological structures (faults, strike, dip) which constrain the course of the individual channels at the local scale. Thus there are two plan-view scales of control evident in the channel network pattern.

The first type of control applies chiefly to the primary channels, whereas the second type applies chiefly to the secondary channels. In the case of normal faults transverse to the main flow if the down-throw block is in the seaward direction, the fault itself will not divert flow at the regional scale, although flow may later adopt the lineament of the fault plane locally. Rather, major diversions seem to be mediated by tectonic up-throws in the seaward direction (of limited vertical surface expression) forcing the flow to follow the alignment of the fault scarp. Thus the primary channels with the distinctive zig-zag regional pattern conform to regional controls, with the river being sequentially forced to the south-west by SW to NE trending structure before breaching

the major rockbed linear structures and flowing again down the regional topographic gradient to the south.

Whereas the origin and the control which dictates the loci of bifurcation nodes have been well-studied within alluvial branching systems (Kleinhans et al., 2008), the control on the secondary channel abrupt course changes and bifurcations is less evident within bedrock or mixed bedrock-alluvial systems. Although the spatial correlation of channels with linear structures may appear self-evident, the reason why some structures are preferentially eroded when neighbouring self-similar structural weaknesses do not become channelized requires additional consideration. In addition, some channels seemingly 'ignore' and cut across the underlying structure whereas neighbouring channels may closely be aligned with the structural trend (Carling, 2009). An issue is whether the river has cut down and the flow then has been superimposed onto the bedrock surfaces (as is clear for some cross-channels), or whether new bedrock channels are opened up by flooding-induced avulsion along lines of weakness. Without superimposition or flooding it is difficult to imagine an entrenched river opening linear weaknesses in the bedrock by lateral cutting alone, except through sandbar induced flow diversions (which are considered below). Rather the river seems to have begun to incise into an alluvial bed overlying bedrock during the Quaternary, sometime after 650 ka (Carbonnel, 1972; Demeter et al., 2010) leading to abandonment of the '100m terrace'. This period of incision was followed by a period of alluviation to form the '40m terrace' which was abandoned around 38 ka and a further period of incision followed to reach the modern river level. Consequently, the modern channel network, in part, must be the result of flow being superimposed on lines of bedrock weakness from some time after 38 ka until present. These issues are returned to below.

For more recent Holocene channel processes, the influence of the mobile sediment, the in-channel vegetation and the relative depth within the system may play a role. It is well known that downstream sedimentation in any alluviating river induces a variety of morphological feedback responses upstream (Cazanacli et al., 2002; Geleynse et al., 2010). In a mixed bedrock-alluvial system the interactions are not known so well and although faulting may influence channel alignment, as noted above, the role of sedimentation must also be accounted for (Humphrey & Konrad, 2000). Uplift at any point may reduce the energy slope of the upstream reach whilst the river downstream erodes and incises into the bedrock, beginning at the downstream end of the uplifted zone. However, alluviation will occur within the uplifted reach more rapidly than bedrock erosion downstream. In detail, the position of the bedrock-alluvial transition will vary depending on uplift rate and incision rate (Capart et al., 2007) and variation in

sediment supply through time (Tooth & McCarthy, 2004). These processes will create, or accentuate, local gradient changes but importantly alluviation may block some channels and will elevate the water surface, thus enhancing the propensity for flow to be redirected laterally (e.g. Jerolmack & Mohrig, 2007) and to occupy additional lineaments in the bedrock. The basic control of reach-scale bed elevation on the downstream distribution of sedimentation patterns is evident in the relationship between the dry season water surface level (Section 5.1.1.4, Figure 5.14) and the channel zones identified in Figure 5.13, Section 5.1.1.4. For example, where the water surface slope is steep, the channel bed is largely bedrock with sandy reaches occurring in less steep reaches. Such a pattern is consistent with similar reach-scale gradient controls observed within the Orange River (Tooth & McCarthy, 2004). However, the detailed within-reach variation in sedimentation patterns noted in Figure 5.13, Section 5.1.14 seemingly often reflects local flow controls imposed by local geological structure and these more complex issues require additional investigation.

During the annual flood stage the flow can be envisaged as occurring: (1) within relatively broad primary channels with the depths of the flow being only slightly greater than the channel depths; (2) within relatively narrow secondary channels with the depth of flow being considerably in excess of the channel depths; and (3) as unchannelised flow above bedrock platforms (i.e. between channels), that may be well-vegetated. The Mekong has a high annual sediment load (c. 160×10^6 t/yr; Milliman & Syvitski, 1992) consisting mainly of fine sand. This material is readily entrained during the flood season and then is deposited as bars during the recession. Such bars are then exposed as static bodies during the dry season. The analyzed pattern of the Mekong sand bars shows that the majority of the sand bodies accommodated within a studied reach do not relocate or accrete over time; instead, channel bars either split or merge while preserving their spatial reference and total areal extent. The observation is consistent with the negligible movement of gravel bars recorded for the mixed bedrock-alluvial Guadalupe River during an eight year timespan (Keen-Zebert & Curran, 2009). Insignificant changes in sand bars volume/area at the Mekong are conditioned by the steady sediment supply and low bank erosion rates reported in Section 5.1.4.2 as well as stable configuration of the annual hydrograph subject to the SE Asia monsoon governing the climate in the region. In addition, the Mekong in the LMB is one of the few large rivers which, so far, has experienced only minor human disturbance; the impact of new dams in the UMB (China) is not yet having a noticeable effect in northern Cambodia due to the distance of the UMB from the area of interest. The non-migrating nature of sand bars may additionally be developed due to spatial attachment to riverbed bedrock or to islands. At a much smaller scale, Siddiqui & Robert (2010) noted that individual clasts tend to be transported a short distance to be

trapped within depositional features on the bed of bedrock rivers. Thus in the Mekong, and possibly in other bedrock rivers, most bars are of the 'fixed' non-mobile class in contrast to mobile 'free bars' which move through river reaches (Seminara & Tubino, 1989). However, in certain localities the riverbed of the Mekong is predominantly alluvial within fixed banks and here too the bars are fixed which may represent the typical response of a straight channel with non-erodible banks and an alluvial riverbed, as is shown by Crosato & Mosselman (2009). It is worthwhile speculating what will happen if, in the near future, there are anthropogenic increases in sediment load without any concomitant change in the hydraulic regime. Will the number of 'free' bars increase and could this adjustment be an indicator of a disturbed bedrock channel regime?

The sand bars may close off secondary channels from time-to-time. Closure should induce other channels to open to maintain conveyance. Such a scenario could occur due to an exceptional annual flood modifying the hydraulic and sediment transport regimes such that the 'fixed' bars move their position locally but probably not permanently as the self-similar annual flood regime would reset the system. However, a noticeable fact is that despite the complexity of the secondary channel network and the density of in-channel vegetation, the majority of the network remains open water. A possible explanation is that as many secondary channels are transverse to the main flow direction and, deeply submerged, they act like slots in the bed of the Mekong macrochannel. Within such transverse slots, considerable vorticity will be generated (Toda, 1994; Pollard et al., 1996), enhanced by the macro-turbulence of the deep approach flow which is passing over and through dense woody vegetation (Buckley et al., 2010). Vorticity along transverse submerged slots is known to be very efficient at evacuating both fine sediment (Raudkivi, 1993) and coarse gravel from channels (Hayward & Sutherland; 1974; Klingeman & Milhous, 1970) and this might explain the open nature of so many tortuous secondary channel networks. During low flows, the primary and cross-channel network may provide a degree of increased hydraulic efficiency in a manner similar to that proposed by Nanson and Huang (1999), or at least a comparable efficiency to a single channel of comparable size (Jerolmack & Mohrig, 2007), for alluvial anastomosed rivers. However during low-flows, the tortuous secondary channel network in particular might be viewed as hydraulically and sediment-transport inefficient due to the imposed structural control (e.g. Tooth & McCarthy, 2004). Intriguingly, it remains an open question as to whether such a network is inefficient when deeply submerged by flood flows. During high flows, the Mekong is characterised by a network of primary and cross-channels flanked by flooded bedrock surfaces into which the secondary channel network is incised. The interaction of a relatively efficient network of larger channels with momentum exchange across the flooded surfaces may enhance sediment transport capacity but

may impede flood conveyance owing to enhanced energy dissipation. As in the case of the mixed bedrock-alluvial anabranching Orange River (Tooth & McCarthy, 2004), obtaining empirical flow and sediment transport data within the Mekong channel network to explore fluid and sediment transport efficiencies is a major logistical challenge. Progress in understanding the efficiencies of the Mekong network is presently limited to the constraints of available calibration data and hydraulic modelling (Van et al, 2012); these authors comment specifically on the difficulty in obtaining the necessary hydraulic data at scales appropriate to both modelling and interpreting the geomorphology of multichannel rivers.

Dating terrace and palaeochannel sediments has shed light on the history of the Mekong in the region. The combination of newly obtained information with that in the published literature enables reconstruction of generalized cross-sectional profiles of the river and its terraces with reference to their age in the geological time scale (Figure 6.1).

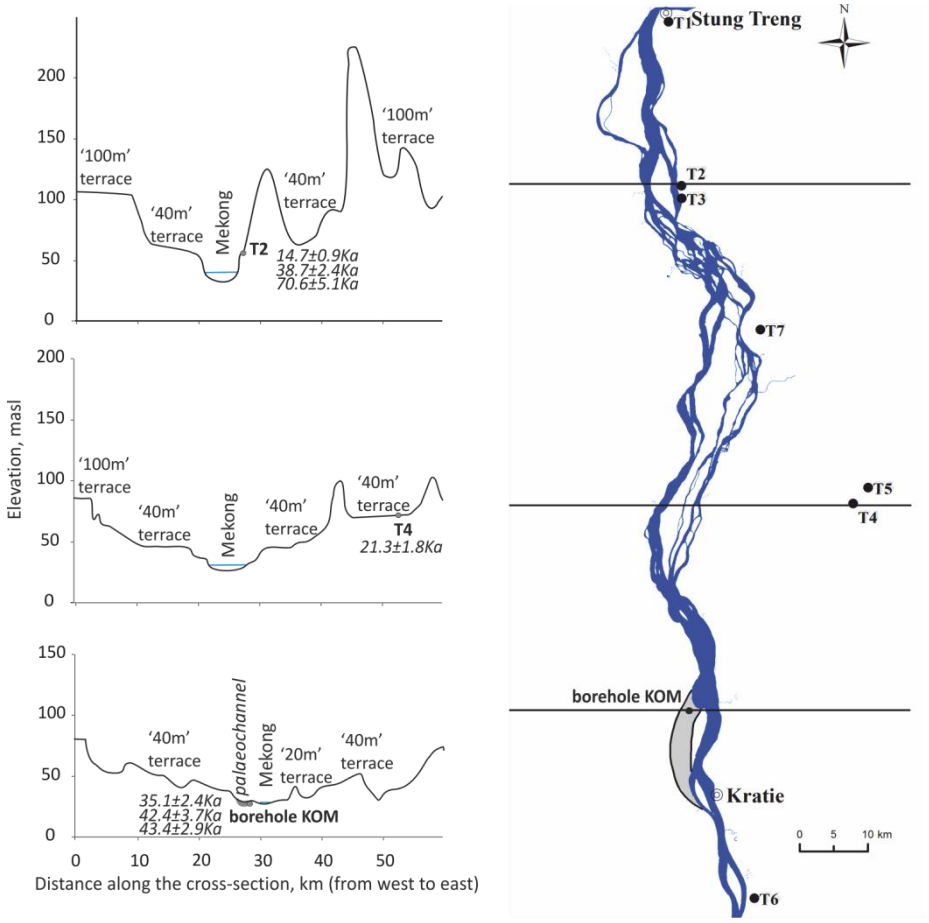

Figure 6.1. Generalized cross-sectional profiles of the Mekong River with respect to the terraces sampling sites (based on the 50m DEM, courtesy of MRC, 2006).

Dates given on the profiles correspond to the terrace sampling points. See Appendix I, Table A1 for more details on terraces location and Appendix II, Tables A6 and A7 for the terraces' luminescence dates.

As mentioned in previous chapters, the '100m terrace' established at the higher elevations within the study area is dated to 650 ka (Carbonnel, 1972) according to the Neogene-Quaternary basalts, on the terrace surfaces, that resulted from regional neotectonic activity (Ragin et al., 1995; Carter et al., 2000; Fyhn et al., 2009). The 100m terrace is represented by part strath (bedrock)/part alluvial planation surface which according to Carbonnel (1972) is heavily degraded and tectonically warped in places. The '40m terrace' embraces elevations, ranging from ~60 to ~20 masl, gradually decreasing downstream within the studied reach. As seen in Figure 6.1, both '100'm and '40'm terraces are observed on either side of the river whereas the '20m terrace' could be only identified at the lower cross-section (Figure 6.1) immediately downstream of the study area. Profiles at T2 and T4 site locations show a hilly landscape on the east riverbank where alluvial terraces are positioned in-between elevated peaks that are outcrops of Mesozoic bedrock. The established cross-sectional profiles illustrate up to 80 m of vertical incision along the studied reach. The obtained palaeo-sediments dates, ranging from ~70 to 21 ka, suggest that the latest incision from the highest elevations, e.g. '100m terrace', is most likely to have happened during the last ~100Ka climate cycle observed during the last ~700-0 ka (Fu et al., 2008; Maslin, 2009). Figure 6.2 shows that within the last ~120 ka, sea level gradually decreased from a value corresponding to the modern 0 masl (120 ka) to c. -50 masl (30 ka) and eventually dropped sharply and stayed at the -90 masl level during the Last Glacial Maximum (LGM) (Hanebuth et al., 2011).

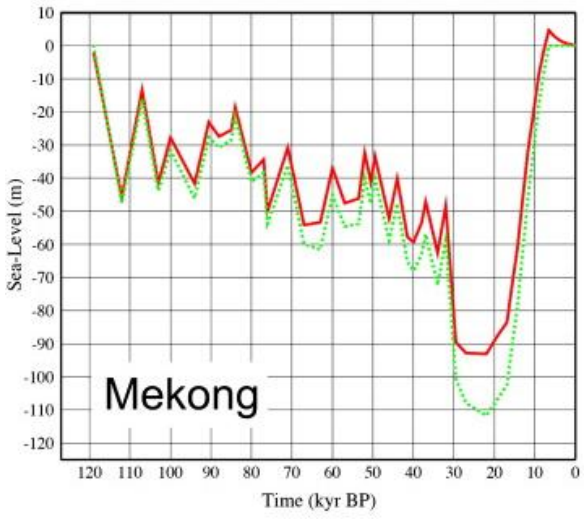

Figure 6.2. Sea-level reconstruction for the Mekong area of the Sunda Shelf according to the Hanebuth et al., 2011 (red line) and Nakada and Lambeck, 1989 (green line), (from Hanebuth et al., 2011).

The palaeochannel dates show continued aggradation until ~35 ka; sometime after which the channel switched its course to the east where it is currently located (Figure 6.1). The palaeochannel deposits above the 35 ka horizon were not likely to have been produced by deposition in an active channel as there is a high silt fraction content (see Appendix IV, Table A8, samples GSD 1, -2, -4 and -5), and organics are present that are similar to the sediments of modern dry channel slack water deposits (Appendix IV, Table A9, samples GSD 1,-2 and CS04) and the sediments are much finer than modern Mekong sand bar sediments (Appendix IV, Table A9). The effects of sealevel change are exclusively with respect to incision as the study area is too far inland for sea level rises to have affected the sedimentation patterns (Hanebuth et al., 2012). . First with respect to incision from the 100m terrace elevation and latterly with respect to incision within the 40m terrace it is reasonable to ascribe such major incision to falling sea levels during the Quaternary. A 38.7 ka date is also recorded close to the terrace surface at site T2 on the 40m terrace and so, in this context, it can be suggested that the palaeochannel was active and contemporaneous with the 40 m terrace and that the 30Ka drop in sea level caused the Mekong to incise rapidly, initiating abandonment of the '40m terrace' and further incision of the Mekong to the level which can be currently observed. However the effects of climatic control on incision, via changes in fluid and sediment quantities delivered to the lower Mekong River during the Quaternary has also to be factored into the interpretation of the incision and periods of alluviation. Changes in the Himalayan headwaters might be crucial in this respect but at present there are no robust interpretations of the effects of climate on the incision v. aggradation issue and this must be the subject of future investigations. In this context, the near-surface age of 14.7 ka at the T2 terrace sampling site seems to be too young for the upstream highly elevated part of a terrace. Similarly the near-surface date of 21.3 ka at the T4 sampling site more than 20km away to the east from the modern Mekong is 'young'. These young dates might reflect deposition from one of the many drainage channels often occurring across the broad Mekong 40m terrace or sample contamination due to vegetation roots (tree throw) disturbance. Further dating at additional carefully selected sites are necessary to confirm or modify these preliminary interpretations.

It might be noted that in the results the abandonment of the palaeochannel has been related to a possible local -fault movement (Section 5.1.3) and, at the same time of avulsion, incision was accelerating. Although at this time it is not possible to select one mechanism (fault v. incision) as the control on the avulsion, and it should be noted that channel realignment can be a complex process conditioned by fault and structural alignment as well as local topography, rock type and regional gradient, in addition to a propensity for incision with continuing falling sea levels after 30 ka.

Similar geomorphological evolution of fluvial terraces placed on underlying bedrock has been described for the Yellow River in China (Zhang et al., 2009). In this case, four terraces were formed during the last ~140 ka in association with up to 100m of vertical incision of the river channel. Zhang et al. (2009) believe that only the highest terrace formation, dated ~90 ka, resulted from tectonic uplift whereas the occurrence of the other three lower lying terraces (~30, 20-25, and 3.4-10 ka respectively) was driven by climatic factors. Altogether, the interpretations given for development of both the Mekong or the Yellow River terraces fit well with the hypothesis of the global staircase Quaternary terraces phenomena (Bridgland & Westaway, 2008), controlled by both relative surface uplift and climate triggering the incision. Bridgland & Westaway, 2008 argue that although river terrace development will have some basin-dependent characteristics there is commonality when comparing the Quaternary terrace sequences of many large rivers which relate to the balance between relative uplift and slimatic conditions. However, as noted above, no more can be said on this matter with respect to the study area until additional studies of incision and aggradation controls have been conducted.

Following the investigations of Mekong morphology, some observations related to its channel pattern can be made. Examples of mixed bedrock-alluvial multichannel river sections analogous to the Mekong are encountered across the world (Tooth & McCarthy, 2004), although the terminology used to describe such rivers is inconsistent. Mixed bedrock-alluvial multichannel patterns occur due to combination of several unique factors, for example joint-fracture rock outcrops, erosion resistant banks and islands, locally variable channel bed gradients and variable flow regimes (Tooth & McCarthy, 2004) but primarily they can be found in specifically designed areas composed by bedrock and alluvium as follows from the pattern name. These issues are considered below. For the Mekong, and for the few other rivers described in the literature, bedrock structures show non-conformal and highly resistant properties due to planform alternation of geological units (e.g. sedimentary and volcanic as in the Mekong) combined with elements of tectonic dissection and faulting. Altogether such a complexity offers diverse routes in which river channels can be developed and preserved. Variations in the position of bedding planes and degree of bedrock inclination peculiar to each rock type would guarantee gradient fluctuations and/or occurrence of natural channel barriers once the bedrock becomes part of a fluvial system. Incision into consolidated ancient alluvium formed by previously existing stream(s) is a second scenario suitable for occurrence of a mixed channel pattern, although for a ‘homogeneous’ alluvium the channel might be different from one conditioned by bedrock controls. Variations in surface topography trends, mainly

determined by bedrock structure, into which the river is incising, are found to represent a third component which distinctively describes the planform of these channels. On the Mekong, the topographic gradient is conditioned by the foothills of the Eastern Highlands situated just east of the study area (see Chapter 3.1, Figure 3.1); the junction of these highlands with the Cambodian Plain serve as a perfect location for the occurrence of a mixed-bedrock alluvial river as the juxtaposition of potential basement outcrops and a low-gradient plain conducive to deposition of sediment represents one of the specific environments where this river channel type can occur. As noted above, Tooth & McCarthy (2004) emphasied variable flow regime and Latrubesse (2008) argues that high discharge and low gradient conditions the anastomosed pattern of large alluvial rivers. In the case of the Mekong there is a considerable difference in both the low flow discharge and water level and the high flow discharge and water level, such that it can be argued that the Mekong discharge regime is highly variable. Although in part the discharge control may be significant, other factors must be considered in the case of some rivers, mixed bedrock alluvial rivers in particular. Note that the Mekong in the study area has a relatively high regional gradient (c. 0.0003 on average) which is higher than the gradient of the alluvial systems reported by Latrubesse (2008). Research on this topic may demonstrate that mixed bedrock alluvial rivers may be associated with specific similar geotectonic histories; for example, the Mekong, Orange, Sabie and the Upper Guadalupe Rivers (Heritage et al., 2004; Tooth & McCarthy, 2004; Keen-Zebert & Curran, 2009).

A major issue in understanding bedrock channel patterns is the role of cross-river tectonics in influencing the channel alignment. Commonly channels are drawn towards subsiding basins (Gawthorpe & Hurst, 1993) and to the lateral maximum in the subsidence rate (Kim et al., 2009) in particular. However, the known tectonic history of the region is evidently not a substantive control on the primary channel network geometry. The study area sits at the centre of the Sundaland coherent lithospheric block which is rotating about an axis such that, in the study area, lateral movement is less than 2mm a^{-1} with negligible internal deformation (< 7 nanostrain a^{-1}) with very low rates of shallow seismicity (Simons et al., 2007). However, geological structure, sutures and faultlines can influence channel alignment, as well. This general area is well reviewed by Gibling (2006).

Hickson et al. (2005) noted that the rate of alluvial channel adjustment is usually much slower than the rate of tectonic adjustment such that channels should be drawn towards subsiding basins. However, where the subsidence rate is insufficient to control channel migration the process of channel migration is effectively dominated by

sedimentation processes in alluvial systems. In bedrock systems, with little bed sediment, if subsidence is not sufficient to cause channel migration then evidently the river has the capacity to erode the lateral bedrock confining the channel margin or any in-channel obstructions so as to oppose any subsidence (i.e. the river will increase erosional capacity).

For channels to be steered by cross-channel tilting alone (i.e. no fault alignment) the condition is required:

$$\frac{S_x}{S_y} \leq \mathrm{O} \qquad \text{Equation 6.1}$$

where S_x is the channel slope in the downstream direction and S_y is the cross-channel slope. And 'O'denotes an order of magnitude.

Kim et al. (2011) refer to a time (T_t) necessary to satisfy Equation 6.1 as:

$$T_t = S_x\left(\frac{\partial S_y}{\partial t}\right)^{-1} = S_x\left(\frac{\Delta\sigma}{L_y}\right)^{-1} \qquad \text{Equation 6.2}$$

where Δσ is the differential subsidence rate over the lateral distance, L_y.

Similar to Kim et al.(2011), it is proposed here that tectonic dominance versus erosional capacity is constrained by the overall channel mobility compared with T_t. If channels are able to erode bedrock faster than tectonic tilting is able to develop a preferred flow path then the channel will be erosion capacity dominated and vice versa.

The definition of channel time scale (T_c) is a minimum when:

$$T_c = \frac{W_{cor} - W_c}{C} \qquad \text{Equation 6.3}$$

where W_{cor} is the width of river corridor and W_c is the total width of wetted channels (in the case of multichannel network) and C is the channel lateral rate of migration. C includes bedrock erosion and potentially avulsion but avulsion can only occur if sufficient marginal bedrock is eroded. The purpose of including this discussion point immediately above is as follows. Although the region is 'stable', small lateral movement has been measured. It is probable that this movement is associated with a

very small vertical motion. There have been no studies of this vertical motion and so it is not possible to quantify Equation 6.2. However, solving such equations for the Mekong, and other bedrock multichannel rivers, would provide some quantitative estimate of the nature of tectonic control on the channel network pattern against the degree of control exerted by local structure and sedimentation patterns on network pattern. If suitable sedimentation rates could be deduced, sedimentation control could be explored using the general approach of Jerolmack & Mohrig (2007), for example.

When considering channel pattern, the term 'mixed bedrock-alluvial river' generally refers to the composition of the channel boundary comprising of hard bedrock and a deposited (possibly consolidated) alluvium. Note here that the term 'alluvial' usually does not refer to the mobile sediment load, to which attention is given later in this Discussion. In planview the relative percentage of bedrock/alluvium exposures may vary across and along the river, although the overall channel classification as a mixed bedrock-alluvial river does not change. Seemingly arbitrary divisions between alluvial and bedrock rivers have been proposed. Kale (1990) proposed that when >40% of the planview of the bed is bedrock then the channel is bedrock controlled. In a similar manner, Tinkler & Wohl (1998) used >50%. These divisions, although seemingly quantitative, are not based on any understanding of the process-control exerted by the sediment cover in the channel versus the controlling influence of the bedrock. Such quantitative planview thresholds are ill-fitted to provide a complete definition of the mixed channels pattern, although such percentage descriptors can provide a useful initial characterization of subdivisions of different character reaches, e.g. geomorphological zones in this research. Therefore, instead of adopting a quantitative definition of the planview ratio of alluvium to bedrock, a more informative generalization can be provided by considering the cross-sectional profiles (Figure 6.3).

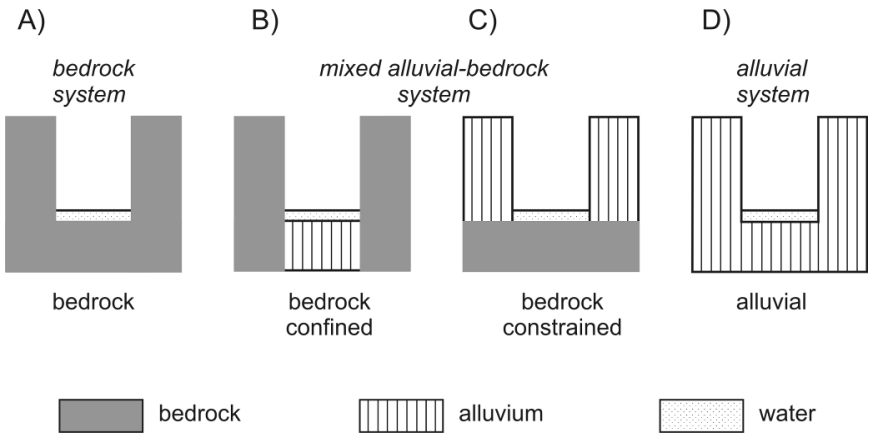

Figure 6.3. The end members in the continuum of channel types from bedrock to alluvial character (from Meshkova et al., 2012). See text for more details.

The cartoon in Figure 6.3 (A, B, C) is adapted from Turowski et al., (2008) and has been extended in order to establish the complete continuum of channel types by adding an alluvial system section (Figure 6.3, D). Channel type A (Figure 6.3) exists where there is negligible sediment accumulation on the bed and a negligible transported sediment load, and so this type of channel approaches an end-member classification of clear-water flow. Although such channels are unusual in nature, some bedrock step-pool systems approach this condition (Carling et al., 2005). Most natural bedrock channels studied to date would be classified as channel type B, as a deposited sediment fill covers at least a substantial part of the rock bed, although the side walls are bare bedrock. Note also that such systems also contain a mobile sediment load. As soon as there is a significant alluvial content, the channel cannot be considered to a bedrock channel; rather it is a 'mixed bedrock-alluvial system' because there is less opportunity for lateral erosion in contrast to a greater opportunity to either accrete or to erode the rock bed; the assumption being that loose sediment is more erodible than the confining bedrock walls and the rock bed is more subject to abrasion by bedload than the side walls. This class of channel can be referred as 'bedrock confined' and the channels are usually rather narrow with a sediment fill at the base (Figure 6.3 B). The third type of channel (Figure 6.3 C) has a rock bed but alluvial sidewalls. In this latter case, vertical incision is less readily accomplished in comparison with lateral erosion of the alluvium and to differentiate from class B, this channel type can be named as 'bedrock constrained' and is also subject to the effects of a mobile sediment load.

Mobile sediment load plays an important role in channel avulsion processes (Kleinhans, 2008). The presence of alluvium within the channel limits introduces additional control over the channel morphodynamics which is referred as a 'tool/cover' effect (Sklar & Deitrich, 2004; Turowski, 2009). When suspended load coupled with discharge facilitates erosion, it is considered as a tool, which impacts overall channel configurations. As soon as accumulation of sediments overruns erosional processes, deposited alluvium begins to act as a protective 'cover'. This research demonstrates that 'tool/cover' effects in a mixed bedrock-alluvial system are both present and interlinked. For example, in the context of the Mekong morphology, on a local scale the 'tool' effect is illustrated by frequently found bedrock erosion (sculpted) forms (Section 5.1.3, Appendix V) with polishing effects caused by abrasion. The same effect on a macroscale is partly responsible for the blind-channel and cross-channel development. Depending on a combination of annual load and discharge, blind-channels and cross-channels can be eroded and fully connected to the primary channel network. On the other hand, they may become partly of fully closed after being filled with sediments. Although, there been no immediate evidence of this processes dynamics from the results of historical channel comparisons within this study, such

processes may take much longer than just 50 years and thus it would be hard to detect them using currently available data.

The cover effect of a mobile load is well presented by the findings on the Mekong sand bars that are mostly fixed in their spatial distribution over time and space. As many of them have bedrock cores, in this case the mobile load protects channel bed features from continuous erosion. In the monsoonal tropical climate, the 'cover' effect is noticed to be emphasized by the riparian vegetation which often inhabits small mid-channel sand bars or traps sediments if it has colonized bedrock exposures.

6.2 Channel metrics

Prior to the discussion of the channel metrics results, a few observations concerning the framework developed to derive the planview network characteristics and island shape parameters shall be made. It is important to highlight methodological aspects because the current tendency to assemble large datasets needs to be supported with consistent proceedings if meaningful comparisons between results are to be made. Another restriction when dealing with large datasets is to choose semi-automated methods which can be successfully utilized independently of the generic qualities of source data.

Examination of channel network parameters is traditionally performed using sets of cross-sections along the river (e.g. Howard et al., 1970). It is simple to locate cross-sections when a river system has got a consistent width and more or less linear overall configuration. However, when it comes to the complex channel networks such as in mixed bedrock-alluvial rivers, the cross-sections may become less functionally effective for two reasons. Firstly, there is no unambiguous solution for drawing cross-sections at the bended sections of a macrochannel; tools adapted for single channel rivers, for instance circle-fitting the curvature of a stream in examining meandering river metrics (Lagasse et al., 2004), are not applicable to investigate multichannel networks due to a less pronounced curvature of its pattern. Assuming that each cross-section is spaced at equal intervals along the macrochannel centreline, cross-sections within curved sections of a macrochannel often have a 'fan-shaped' plan-view wherein the density of cross-sections in the immediate vicinity of one riverbank is much greater than that at the opposite site. As a consequence, some channels close to the riverbank with a sparser cross-sections distribution are to be missed from counting whereas at the other site channels may be double counted (e.g. high sinuosity channels). Second, as

was described in previous chapters (Section 5.1.1.2), mixed bedrock-alluvial primary channel networks in general, and secondary channels network in particular, have numerous cross-channels and blind channels. Cross-channels by definition lay perpendicular or oblique to the main flow course; blind channel bearings are often transverse to the overall flow direction too. Therefore, the same problem of miscounting channels arises as a result of these channels running in parallel to cross-sections employed to examine the network. The seemingly obvious solution to avoid channel miscounting is manual verification of the number of channels accounted by each cross-section (e.g., based on visual judgement of whether all channels are intersected by cross-sections) but it is less preferable when dealing with large datasets. Thus, as an alternative, the use of metrics characterizing the channel distribution per areal unit similar to a drainage density in drainage channel networks (see Altin & Altin, 2011) or density of bifurcation nodes (Bertoldi et al., 2009) along the river referenced to the distance along the river (e.g. macrochannel centerline) is recommended.

Within the scope of this study, several selected patterns on different rivers are visually and qualitatively distinctive, and yet an attempt to discriminate them with a set of traditional planimetric indexes (e.g. braiding intensity and channel sinuosity) generally failed. Nonetheless, measurements of network bifurcation angles, which have become more popular to include in quantitative fluvial system descriptions (Hardy et al., 2011), have brought moderate results. Collected data on bifurcation angles show that in natural rivers this parameter varies from as little as 30° (e.g., Orange River) up to 160° (e.g., Ganga) averaging for all rivers ~89-100°. Flume experiments with braided streams by Federici & Paola (2003) show that angles of the triangular-shape braided bar head vary between 60-90° and are 1.5 times larger than the angles at intersections of the corresponding channel centrelines. Transforming this range of bar head angles into channel network angles gives a value of 40-60°, confirmed by similar experimental values of 35-55° (Bertoldi & Turbino, 2005) and the average 47° reported for the (wandering) Renous River bifurcation angles measured using mid-channel lines (Burge, 2006). Original data for the highly dynamic braided Jamuna River under the CEGIS monitoring system are not directly available but the data range given in correlation with the progressive possibility of channel abandonment starts from 25° and goes up 80% for bifurcations with more than 85° between branches (Gupta, 2007). In deltas the reported angle range is 20-85° (Metz, 2010) whereas delta modelling shows that it depends on sediment cohesion, e.g. the less cohesive the sediments, the greater is the average angle (Edmond & Singerland, 2010). The fact that the investigated natural multichannel networks reveal higher average bifurcation angles is to be explained by either common or specific factors. For these systems, the generally larger number of examined bifurcations, the variety of either channels (inconsistent branches width) or

island shapes (e.g. rounded or elongated, convex or streamlined), and differences in measuring techniques are to be listed as general reasons to reject the direct comparison of this study's results with those in published literature. On the other hand, the average value of 90° for the Upper Columbia river is well illustrated by the asymmetry ratio (Figure 5.39) where one of the downstream branches follows the direction of the upstream channel whereas the other goes away at right angles, due to the relatively high frequency of 90° levee breaches (Figure 6.4). The Ganga average angle is close to 100° and, by analogy with the braided Jamuna River, may indicate a high degree of lateral instability.

Figure 6.4. Formation of 90° crevasse splays in the Columbia River, British Columbia, Canada (Picture by H.J.A. Berendsen).

Sourced http://www.geo.uu.nl/fg/palaeogeography/results/avulsions (accessed 06/10/2011)

The average value of the Mekong and Orange rivers is impacted by the diversity of channel types formed in different conditions which are to be illustrated in the next paragraph.

Consider the variability of bifurcation angles, channel length and sinuosity as the channel network is 'intensified' by using the example of a sample multichannel section from the Mekong River (Figure 6.5). The order of channel establishment is defined according to channel width/length and its connectivity to other channels (Williams & Rust, 1969) using the idea that initially the Mekong was present within the limits of the macrochannel boundaries by only one channel whose position is currently indicated by the river thalweg. Thus stage 1 is the navigable main channel of the modern Mekong.

Stage 3 channels cannot develop until links representing stage 2 channels have formed. The conceptual explanation as to how this is determined in a planform network is detailed by Williams & Rust, 1969 and is not developed further in this Discussion. This scenario is hypothetical and does not suggest that the Mekong in this area started to develop from a single channel configuration but is considered here in order to analyse the dynamics of multichannel river network metrics. The sequence of stages identified for an example of the network of the Mekong is shown in Figure 6.5. As the network becomes more complex the average channel link length and sinuosity linearly decrease and so decrease the standard deviation (Figure 6.6).

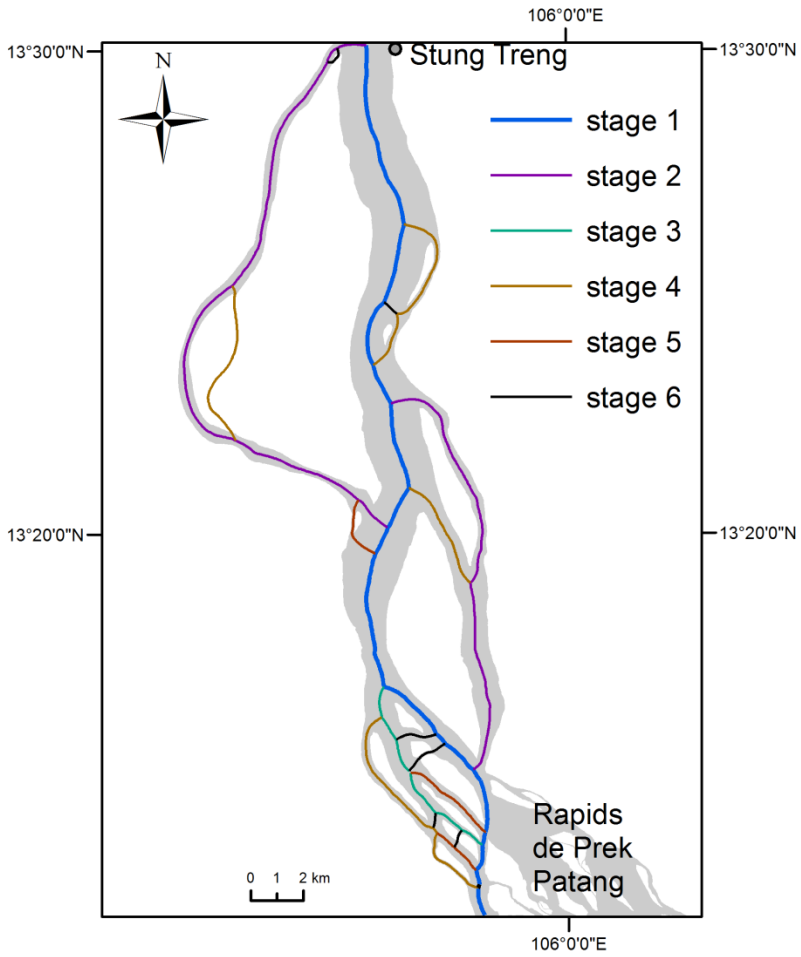

Figure 6.5. Suggested order of channels within the sample section of the Mekong downstream of Stung Treng. Stages from 1 to 6 indicate intensification of channel network.

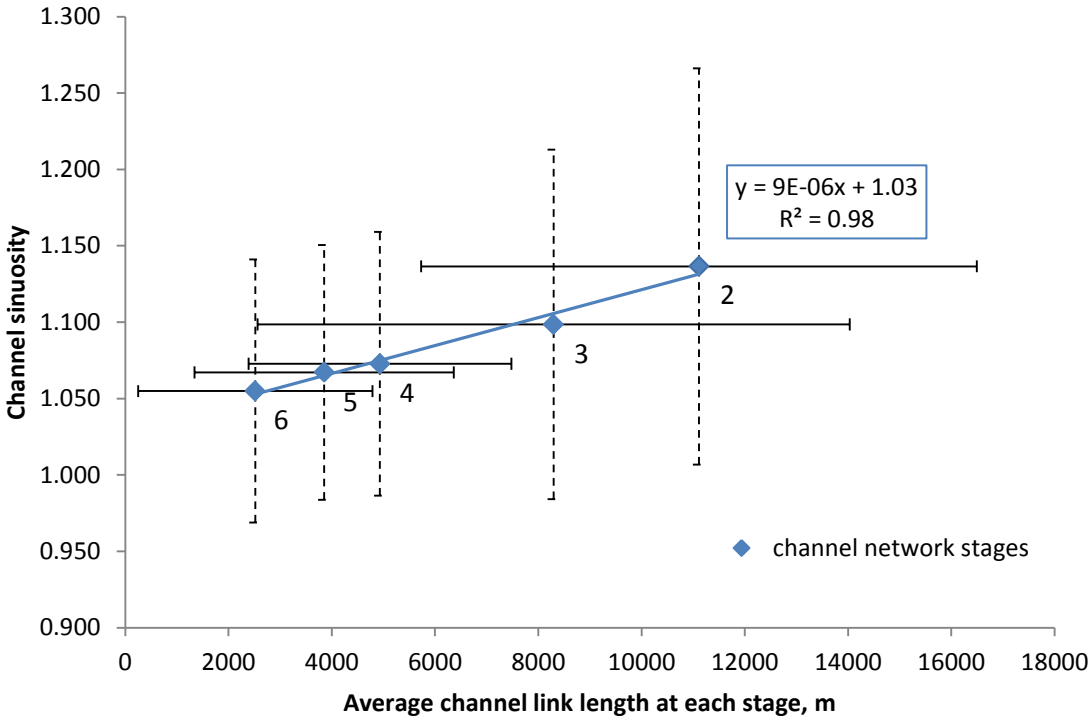

Figure 6.6. Changes in channel link length and sinuosity within each stage of an intensification of a sample section of the Mekong channel network (see text for details).

Vertical and horizontal standard error bars correspond to the channel sinuosity and link length respectfully.

Channel bifurcation order shows how many bifurcations occur relative to the initial primary bifurcation as the network stages intensifies. So as stage 1 is a single channel there are no bifurcations. For stage 2, two bifurcations occur on the primary channel which corresponds to the first channel bifurcation order values at values 1 on the abscissa of Figure 6.7. When these two channel bifurcate it is order 2 of channel bifurcation and similarly for order 3. If a cross-channel bifurcates from the primary channel network then this bifurcation is shown as a square symbol. The dotted lines show the sequential connection between channel bifurcations and two separate trend lines are shown for the primary channel network and for the cross-channel network which demonstrate a general tendency for bifurcation angle to reduce as more channels are present within the network.

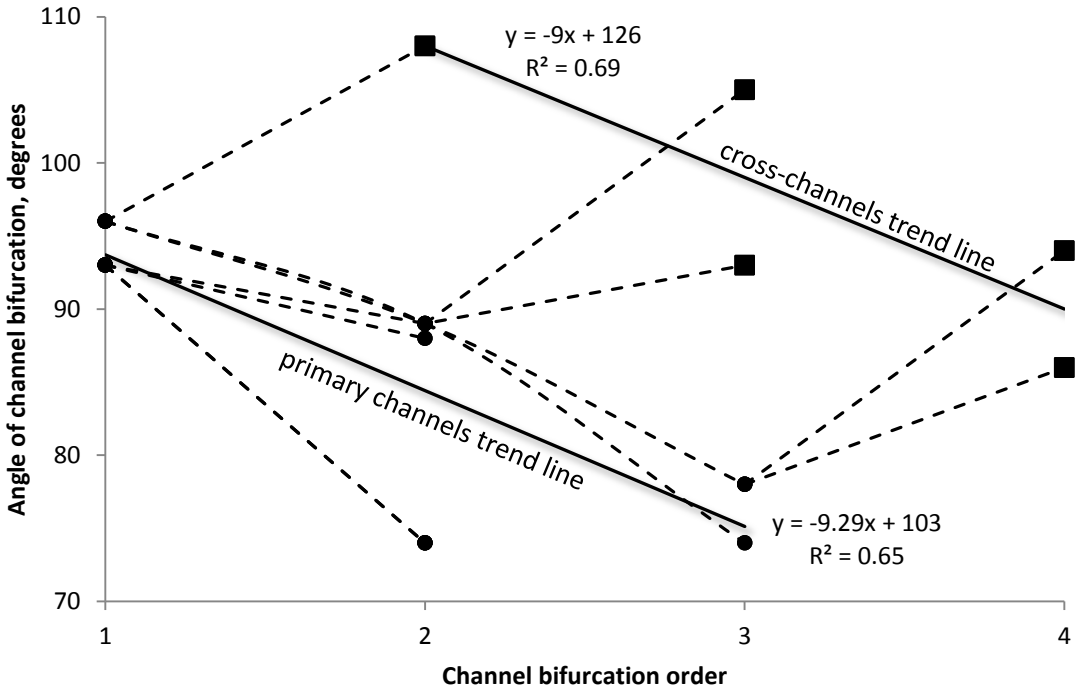

Figure 6.7. Progress in development of bifurcation angles of the primary and cross-channels with intensification of the sample channel network (see text for details).

Such a tendency can be explained by the fact that this part of the river floodway is limited by the macrochannel boundaries and new channels are formed due to incision and dissection of primary islands rather than flooding surface invasion. It suggests that every newly formed branch shall be positioned at the smaller angle unless it is a cross-channel running oblique to the mainflow; sinuosity development is also limited by either lateral space restrictions and/or cohesive banks and abundant bedrock outcrops/sand bars which are both fixed within the river planform.

Island shape analysis performed using the widely recognized aspect ratio parameter has not been sufficient in terms of separating different mixed bedrock-alluvial or alluvial anastomosed and braided rivers in the investigated dataset (Figure 5.46), while object based indices yield more prominent results (Figure 5.52). The values of convexity of mixed bedrock-alluvial multichannel river islands approach the maximum of 1 as well as the streamlined lemniscate shape which according to its properties minimizes total fluid drag (Komar, 1983). It is also decreasing for larger islands but is close to 1 for the smallest islands. Overall, the island convexity parameter shows the degree of sinuosity of channels better than the actual channel sinuosity index because the latter is estimated using channel centrelines (or channel network links), the positions of which are dependent on synchronized planview contours of riverbanks.

For instance, if in planview one riverbank is sinuous, but the opposite bank is straight, the difference in riverbank behaviour will be smoothed by selecting the channel centreline. Yet, in braided rivers (e.g. Ganga), island convexity reflects numerous blind channels rather than high channel sinuosity which implies that the geomorphological background is vital for interpretation of convexity parameter outputs. The other two shape based indexes - roundness and compactness – have shown more compact distribution of island area around its centre of mass for the mixed-bedrock alluvial rivers than alluvial anastomosed and braided river islands with the same aspect ratio. This is explained by the fact that islands from the latter two systems are more irregular relative to the optimum shape for a given aspect ratio.

As a final consideration, some comments can be made with respect to the spatial series analysis of channel corridor widths and slopes for bedrock rivers in relation to sediment cover. The inverse at-a-station relationship between channel width and slope is well known both for alluvial and bedrock rivers and the actual form of this relationship has recently been related to the incision rate (Yanites & Tucker, 2010). This latter study did not consider the downstream relationship between width and slope but the cyclicity in the behaviour noted for width on series both the Orange and the Ganga Rivers may demonstrate structural controls although this is not evident in the slope series for either river. The stronger downstream autocorrelation noted in the widths in contrast to the slope indicates the ready adjustment of width to imposed discharge and sediment loads as slope changes. Yanites & Tucker (2010) and Yanites et al. (2011) place particular emphasis on the spatial variability in the sediment cover in mediating incision rates. However, it is evident that for low incision rates (such as on the Mekong: c. 0.15m/ka – see section 5.1.2), the channel morphology will be dominated by the requirement to discharge both water and sediment for a given slope. Adjustment of the corridor width implies that the space in which networks of channels can form is variable and limited. The slope control mediates the thickness of any sediment which, in turn, can induce avulsion. Thus there will be subtle relationships between channel parameters, sediment cover and channel network geometries which are yet to be explored in mixed bedrock-alluvial rivers.

7 Conclusions

Cambodia and the Mekong River have been a subject of increased interest from the scientific society within recent years since the political situation became stable. This has enabled scientists to access this territory and collaborate with local authorities. Although the poverty level remains high, the population rapidly grows and uses natural resources more extensively than in the past. From this perspective the role of insightful investigation of the multichannel thread of the Mekong in north-east Cambodia cannot be underestimated because thousands of people's lives depend upon the riverine resources.

As only limited, outdated materials were available at the beginning of this study, field trips to the area of interest undertaken by the author allowed clarification of geomorphology, geology, ecosystem and palaeo development of the Mekong in accordance with up-to-date scientific knowledge. Combination of physical explorations of a territory with computer-based technologies enabled better understanding of the studied reach of the Mekong and comparison of its planview channel metrics with other fluvial systems. Thus, the conclusions drawn are both specific and generic.

Geomorphological features of the Mekong are found to be similar to these of the Orange (Tooth & McCarthy, 2004) and Sabie (van Niekerk et al., 1995) rivers neglecting the differences in their basin scale and macrochannel dimensions. In terms of the overall morphology of the Mekong, two interacting and stage dependant networks of primary and secondary channels have been identified. The primary channel network architecture is a result of alluvial channel superimposition onto structurally diverse older bedrock. The majority of the secondary channels network is formed along bedrock joints and foliation structures, but in places it is defined by sand bars. Depositional features of the macrochannel (i.e. sand bars) are reported to be spatially and temporally fixed. The stability of the sand bars is evidence of a balance achieved between the discharge and the spatial distribution of channels resulting in an overall lateral stability, however numerous deep pools and plentiful bedrock sculpted forms show continuing vertical erosion processes. The role of the vegetation and hydrological regime (flood/draught) in channel and sand bar distribution is yet to be explained. The development and mechanism of the cross- and blind channel establishment also needs further clarification.

The research on the pre-history of the Mekong River shows that incisional processes represent the response of a fluvial system to the climate and/or sea level change

during the LGM. Analyses of sediment samples of the older alluvium from the east bank of the Mekong provide a first insight into the recent development of the river within the study area. A greater number of spatially distributed sediment samples that are luminescence-dated are required to improve the understanding of when periods of incision and aggradation occurred throughout the Quaternary period. Without considerable additional investigation, the consideration in any detail of the balance between incision due to sea level fall and climate controlled incision and alluviation is speculative and premature. Nevertheless, a major period of incision occurred after c. 600 Ka, during which time sea level fell in the region and the Mekong River incised from the 100m terrace level. Subsequent alluviation to produce the 40m terrace level cannot be related to sea level rise, as the study reach is too far to landward, but almost certainly is related to climate change and associated changes in both fluid and sediment yield from the Himalayan headwaters and the delivery of same to the Cambodian Mekong. Similarly incision of the Mekong to its modern day level to form the 40m terrace cannot be related to sea level fluctuations. Alluvial facies observed in the 40 m river terraces were accumulated during fluctuating but gradually decreasing sea-level (from ~70 up to ~30 ka) which suggests that among the two major environmental conditions governing incision/aggradation behaviour (e.g., climate and tectonics) climate is the dominant one during this latter period of time. Stratigraphic sequences and composition of palaeo-deposits contrast with the modern Mekong alluvium which indicate a switch in sedimentation character from coarse (palaeo gravel on the 100 m terrace) to the medium grain fractions of the 40m terrace which are not dissimilar to the sediments found in the modern river. However, extensive clay deposits occurring towards the base of the sandy 40m terrace require further study and may represent laterally-distal deposition from the slow flow within primordial extensive forests, on braidplains that were inundated annually due to the monsoon high flows.In addition, the 3S Basin is recognized as a major palaeo-gravel supplier to the sandy 40 m terrace between Stung Treng and Kratie. The lens of gravel that thin downstream from the confluence of the Sekong and the Mekong appear to represent a singular event, or at least a short period of enhanced supply of coarse gravel to a Mekong river which is almost totally dominated by a sand load. Further research on both the Mekong and the 3S Basin sediments in context is required to determine whether these changes are also connected to climatic oscillations or subject to other specific factors. The broad lateral extent of the 40m terraces, the thin thickness of deposited alluvium and lack of palaeochannels at this level (apart from the Sambor palaeochannel), suggest that before post-30 ka incision the Mekong was a multichannel (braided?) system. However, more studies of exposures of the 40m terrace stratigraphy are required to determine if this preliminary interpretation of a prior braided system is correct. Understanding of the origins of the single

palaeochannel at Sambor might be viewed as a largely parochial problem. However, if a quantitative tectonic control can be adduced then further insight would be gained as to the necessary gradient changes in the Mekong River at this location to allow an avulsion to become permanent. Although little progress on understanding the geomorphological implications of this singular avulsion might not occur until better tectonic data are available, some understanding can be obtained using simple numerical avulsion models. This latter work is now in progress.

While the planview distribution of bedrock and mobile alluvial sediments in mixed-bedrock alluvial multichannel system is crucial for defining longitudinal geomorphological zonation, it is not a sufficient condition for the precise identification of a channel pattern type. Instead, the nature of channels is determined by variations in consolidated bedrock/alluvium units within the macrochannel cross-sectional profile. The research has shown that many traditional planview metrics are unable to draw a quantitative difference between selected multichannel mixed bedrock-alluvial and alluvial systems, therefore new parameters and methods will have to be introduced and explored. One metric that shows promise is an island convexity index which enables successful separation of mixed bedrock-alluvial multichannel islands from those islands in alluvial systems and indirectly emphasises the degree of local channel sinuosity. Another example is the angle asymmetry ratio at points of channel network bifurcation which enables one to highlight the character of avulsion in alluvial anastomosed rivers. Finally, the topographic trend surfaces extracted from DEMs help to explain the planview course of bedrock-alluvial rivers and thus contrast them with other multichannel alluvial rivers. Altogether the project has demonstrated the importance of a complex geoscientific approach for spatial data analyses. Therefore, is it believed that future research into channel pattern comparisons has to be considered as a multidisciplinary task supported by new development of standardized methodology and set of functions in GIS software, the lack of which currently obstructs research of this kind.

In term of the Mekong, future work should be focussed on key issues of terrace evolution in respect of climate-induced variation in water and sediment delivery to the lower Mekong throughout the Quaternary period. Terrace evolution can usefully be explored using field mapping and dating of the stratigraphy of the terrace sediments, together with an examination of the possibility to use fossil wood found in the terraces as a novel tracer to determine the relative contribution and timing of sediment delivery to the lower Mekong from the major tributary, the Sekong. Climate-induced variations in sediment delivery have been examined on other major river systems in respect of variation through time in the mineralogy of sediments deposited in the lower parts of

systems in comparison with their availability in the source areas. The use of mineralogy as a tracer has not been the focus of this thesis but there is great potential to apply such techniques to the Mekong. A more novel approach would be to examine the stratigraphy, including the mineralogy, of the landward parts of Mekong delta which are known to the largely freshwater alluvium rather than brackish or marine. Variations in the sedimentology of the delta strata could be used, with catchment sediment delivery models, to hindcast the variation through time in the relative quantities and qualities of sediment delivered to the delta. In such a manner the variations in sediment supply might be related to variations in climatic control in the hinterland.

Appendix I

Table A1. Samples location, character and method of analysis (see Section 4.2, Figure 4.15 for sample location in planview).

Number on Fig.4.15	Field Sample №	Location (latitude longitude/)	Sample character	Method applied
Rock samples				
1	CS01	13°28.240'N/ 105°56.398'E	Bedrock outcrop sample (Red sandstone)	Rock type identification
2	CS07	13°15.144'N/ 105°58.050'E	Bedrock outcrop sample (Ferruginous quartzite)	Rock type identification
3	CS08	13°15.144'N/ 105°58.050'E	Bedrock outcrop sample (Gneiss)	Rock type identification
4	CS11	13°14.769'N/ 105°57.119'E	Bedrock outcrop sample (Gneiss)	Rock type identification
5	CS12	13°13.209'N/ 106°58.016'E	Bedrock outcrop sample (Meta-sandstone)	Rock type identification
6	CS17	13°11.463'N/ 105°58.698'E	Bedrock outcrop sample (Quartz albitophyre)	Rock type identification
7	CS18	13°13.516'N/ 105°58.683'E	Bedrock outcrop sample (Quartzite)	Rock type identification
8	CS19	13°11.851'N/ 105°59.345'E	Bedrock outcrop sample (Quartzite)	Rock type identification
9	CS20	13°11.909'N/ 106°00.141'E	Bedrock outcrop sample (Andesite)	Rock type identification
10	CS23	13°10.926'N/ 106°01.756'E	Bedrock outcrop sample (Red Sandstone)	Rock type identification
11	CS26	13°10.143'N/ 106°03.051'E	Bedrock outcrop sample (Diorite/andesite)	Rock type identification

Number on Fig.4.15	Field Sample №	Location (latitude longitude/)	Sample character	Method applied
12	CS27	13°10.133'N/ 106°01.050E	Bedrock outcrop sample (Tuff or andesite)	Rock type identification
13	CK01	12°51.704'N/ 105°59.802'E	Bedrock outcrop sample (Diorite or andesite)	Rock type identification
14	CK03	12°52.824'N/ 105°59.628'E	Bedrock outcrop sample (Granite)	Rock type identification
15	CK04	12°54'42.8''N/ 106°00'27.3''E	Bedrock outcrop sample (Granite)	Rock type identification
16	CK05	12°50.559'N/ 105°59.471'E	Bedrock outcrop sample (Quartz-muscovite gneiss)	Rock type identification
17	CS61	12°47'15.4''N/ 105°56'56.2''E	Bedrock outcrop sample (Andesite)	Rock type identification
18	CS63	12°50'27.8''N/ 105°56'23.3''E	Bedrock outcrop sample (Andesite)	Rock type identification
19	CS64	12°58.442'N/ 105°59.233'E	Bedrock outcrop sample (Andesite)	Rock type identification
20	CS65	12°55.500'/ 105°58.934''	Bedrock outcrop sample (Quartzite)	Rock type identification
21	CS66	12°52.102'N/ 105°56.462'E	Bedrock outcrop sample (Granite)	Rock type identification
22	Leo1	13°08'02.0''N/ 106°03'33.5''E	Bedrock outcrop sample (Andesite)	Rock type identification
23	Leo3	13°09'27.0''N/ 106°03'51.6''E	Bedrock outcrop sample (Red Sandstone)	Rock type identification
24	Leo5	13°08'16.0''N/ 106°03'22.3''E	Bedrock outcrop sample (Red Sandstone)	Rock type identification

Number on Fig.4.15	Field Sample №	Location (latitude longitude/)	Sample character	Method applied
25	Leo6	13°07’36.1’’N/ 106°03’04.2’’E	Bedrock outcrop sample (Quartzite)	Rock type identification
26	Leo7	13°06’54.5’’N/ 106°02’43.4’’E	Bedrock outcrop sample (Red Sandstone)	Rock type identification
27	Leo8	13°09’05.2’’N/ 106°01’12.8’’E	Bedrock outcrop sample (Red Sandstone)	Rock type identification
28	Leo9	13°10’09.4’’N/ 106°04’51.8’’E	Bedrock outcrop sample (Quartzite)	Rock type identification
29	Leo10	13°09’55.1’’N/ 106°01’37.2’’E	Bedrock outcrop sample (Red Sandstone)	Rock type identification
30	Leo11	13°09’24.6’’N/ 106°00’48.1’’E	Bedrock outcrop sample (Quartzite)	Rock type identification
31	Leo12	13°07’40.0’’N/ 106°59’54.0’’E	Bedrock outcrop sample (Red Sandstone)	Rock type identification
32	Leo13	13°07’01.9’’N/ 106°01’13.6’’E	Bedrock outcrop sample (Red Sandstone)	Rock type identification
33	Leo14	13°07’27.9’’N/ 106°01’59.3’’E	Bedrock outcrop sample (Red Sandstone)	Rock type identification
34	Leo15	13°04’39.1’’N/ 106°03’23.2’’E	Bedrock outcrop sample (Andesite)	Rock type identification
35	Leo16	13°04’36.9’’N/ 106°04’09.7’’E	Bedrock outcrop sample (Andesite)	Rock type identification
36	Leo17	13°02’56.8’’N/ 106°04’21.2’’E	Bedrock outcrop sample (Andesite)	Rock type identification
37	Leo18	13°02’21.8’’N/ 106°04’17.7’’E	Bedrock outcrop sample (Andesite)	Rock type identification

Number on Fig.4.15	Field Sample №	Location (latitude longitude/)	Sample character	Method applied
Gravel, sand, silt, organics and soil samples				
38	CS10	13°14.769'N/ 105°57.119'E	Bedload gravel	Grain size (dry sieving)
39	CS09	13°14.769'N/ 105°57.119'E	Bedload sand	Grain size (dry sieving)
40	CS13	13°12.009'N/ 106°57.966'E	Bedload sand	Grain size (dry sieving)
41	CS15	13°11.463'N/ 105°58.698'E	Bedload sand	Grain size (dry sieving)
42	CS28	13°10.133'N/ 106°01.050E	Bedload sand	Grain size (dry sieving)
43	CK02	12°51.704'N/ 105°59.802'E	Bedload sand (cross-channel)	Grain size (dry sieving)
44	CS06	13°28.170'N/ 105°56.410'E	Sandbar sand	Grain size (dry sieving)
45	CS21	13°11.909'N/ 106°00.141'E	Sandbar sand	Grain size (dry sieving)
46	CS25	13°10.037'N/ 106°02.990'E	Sandbar sand	Grain size (dry sieving)
47	CS03	13°28.240'N/ 105°56.398'E	Sand-silt (riverbank)	Grain size (dry sieving) and organic assay
48	CS04	13°28.170'N/ 105°56.410'E	Silt slack water deposits from the tributary (dry) channel	Grain size (dry sieving) and organic assay
49	CS24	13°10.926'N/ 106°01.756'E	Silt (riverbank)	Organic assay

Number on Fig.4.15	Field Sample №	Location (latitude longitude/)	Sample character	Method applied
50	Leo4	13°09'03.6''N/ 106°03'44.6''E	Silt (riverbank)	Wet sieving and organic assay
51	CS05	13°28.170'N/ 105°56.410'E	Alluvial soil (riverbank)	Organic assay
52	CS14	13°12.009'N/ 106°57.966'E	Alluvial soil (seasonally flooded island)	Organic assay
53	CS22	13°11.909'N/ 106°00.141'E	Alluvial soil (primary island)	Organic assay
54	CS16	13°11.463'N/ 105°58.698'E	Organic reach (muddy, seasonally flooded island)	Organic assay
Palaeochannel borehole				
55	Borehole KOM	12°36'36.7''N/ 105°59'22.0''E	Sediments samples (see Table A2 below)	Wet sieving, organic assay and OSL
Terraces				
56	T1	13°31.026'N/ 105°56.950'E	terrace (60m)	Cross-section description
57	T2	13°17.597'N/ 105°58.429E	terrace (40masl) (see Table A3 below)	Cross-section description; OSL
58	T3	13°17.144'N/ 105°58.465'E	terrace deposits placed on bedrocks	Cross-section description
59	T4	12°52'44.0''N/ 106°11'46.2''E	terrace (64masl) (Terrace Sre Sbov) (see Table A4 below)	Cross-section description, OSL
60	T5	12°53.94'N/ 106°13.37'E	terrace (80masl) (see Table A4 below)	Cross-section description, OSL

Number on Fig.4.15	Field Sample №	Location (latitude longitude/)	Sample character	Method applied
61	T6	12°21'28.33''N/ 106°03'40.21''E	terrace (20masl) located within modern active floodplain	Cross-section description, wood samples for the radiocarbon dating analyses
62	T7	13°06'43.8''N/ 106°04'11.8''E	terrace (40masl)	Cross-section description

Table A2. Samples from the palaeochannel borehole KOM

Sample name	Borehole section	Depth below the ground, m	Depth, masl	Sample character	Method of processing
GSD1	Section II	1.40	23.60	Brown alluvial soil	Wet sieving and organic assay
GSD2	Section II	2.00	23.00	Silt	Wet sieving and organic assay
GSD4	Section IV	3.58	21.42	Silt	Wet sieving
GSD5	Section V	3.90-3.95	21.10-21.05	Silt	Wet sieving
Mekong2	Section V	4.10-4.30	20.90-20.70	Silt	OSL
GSD6	Section V	4.30	20.70	Fine sand with gravel	Wet sieving
GSD7	Section V	4.40-4.45	20.60-20.55	Gravel with sandy fill	Wet sieving
GSD8	Section V	4.55-4.60	20.45-20.40	Sand	Wet sieving
Mekong3	Section V	4.60-4.80	20.40-20.20	Sand	OSL
Mekong4	Section VI	5.10-5.20	19.90-19.80	Sand and clay	OSL

GSD10	Section VI	5.20-5.25	19.80-19.75	Sand and clay	Wet sieving
GSD11	Section VI	5.35-5.40	19.65-19.60	Clay	Wet sieving
Mekong5	Section VI	5.45-5.65	19.55-19.35	Sand and clay	OSL

Table A3. Samples from the 40 masl terrace

Sample name	Depth below the ground, m	Elevation, masl	Sample character	Method of processing
MEKT21	1.85m	39.15	Sand layer	OSL
MEKT22	0.80m	40.20	Gravel layer	OSL
MEKT23	0.55m	40.45	Base of the sand above the gravel	OSL

Table A 4. Samples from the 64 and 80 masl terraces (locations T4 and T5 in Table A1 and Figure 4.15 in Section 4.2)

Sample name	Depth below the ground, m	Depth, masl	Sample character	Method of processing
MEK6	1.10m	62.9	Clay below the gravel layer	OSL
MEKT25	1.95m	82.05	Sandy matrix	OSL

Table A5. Location of additional palaeochannel boreholes from inset map B in Figure 4.15, Section 4.2 (from Stapeldon et al., 1962)

Borehole number on Figure 4.15	Location (latitude/longitude)	Data used
Hole 4102	12°36’18’’N/105°59’27.59’’E	Borehole log
Hole 4103	12°36’28.80’’N/105°59’52.80’’E	Borehole log
Hole 4105	12°36’50.40’’N/105°58’58.80’’E	Borehole log

Appendix II

Abridged from the "OSL dating of the Mekong samples" Report produced by Dr. Ruth Robinson, University of St Andrews, Luminescence Laboratory, 24th of February 2010

Samples were processed by Ross Somerville and analyzed by Ruth Robinson.

Four samples collected from a vertically orientated core (palaeochannel borehole) were sent to the University of St Andrews for analysis in April 2009. The samples were opened carefully and material for dating was separated from tubes, weighed, dried, reweighed and sieved. Standard processing procedures to extract pure sand-sized quartz grains included HCl and H_2O_2 washes to remove carbonates and organics, lithium hetero- polytungstate (LST) heavy liquid separation (2.7g/cm^3) to settle out heavy minerals, and concentrated hydrofluoric acid (HF) treatment for 40 minutes to remove feldspars and the alpha layer (10μm) on the quartz grains. The residues were then treated to HCl washes followed by de-ionised water and acetone washes, were dried and then transferred into storage tubes for further analysis.

Laboratory measurements were performed using the Risø TL/OSL-DA-15 (SA-Riso I) and Risø TL/OSL-DA-20 (SA-Riso II) readers with stimulation by blue light (470 ± 30 nm) from a blue diode array, and light detection using Hoya U-340 filters and a 9635QA photomultiplier tube. The equivalent dose (D_e) for each quartz aliquot was measured at 125°C using the single aliquot regeneration-dose (SAR) protocol (Murray & Wintle 2000, 2003; Wintle & Murray, 2006) with preheat temperatures ranging from 200-240°C; the pre-heat temperatures for each sample were chosen after pre-heat feasibility tests on 6-8 aliquots per sample combined with a dose recovery test (Murray & Wintle, 2003). Internal assessment of the reliability of measured SAR data was therefore monitored using: 1) the ability to recover a known laboratory radiation dose (within 10% of given dose); 2) stability of D_e with preheat variation; 3) successful correction of sensitivity effects by replication of regenerated OSL at low and high doses; and 4) the absence of thermal transfer (<5%). Aliquots (40-80 grains) of quartz were measured using a standard SAR protocol for each sample after feasibility tests were completed. Rejected aliquots failed one or more of the above tests, D_e distributions of the accepted aliquots (see Table A6 for numbers) were analysed using radial plots and mixed age models (Galbraith et al., 1999; Rodnight et al., 2006; Spencer and Robinson, 2008).

OSL dating relies on a dosimetric measurement of environmental radiation that the sediment grains have been exposed to since deposition. No *in situ* dosimetry was conducted for the Mekong samples and the dosimetry is based on laboratory ICP-MS measurements of elemental concentration from a sub-sample of un-sieved sediment conducted at the University of St Andrews. For comparison, the top and the base of the vertical core sediment directly adjacent to the dated samples were measured and the difference between the U, Th and K values for the top and base makes no difference to the calculated ages. Dosimetry is fairly consistent for each sample in the core (about 2.1 - 2.5 Gy/ka for the older vertical core, and 3.6-3.8Gy/ka in the younger vertical core). Each ICP-MS measurement reported is the average of two measurements and three standards were measured at the beginning and end of the run. The final age is calculated from the equivalent dose, D_e, divided by the total dose rate. The water content used for the calculations of dose rate is the laboratory as-received moisture content and may underestimate the true annual-weighted moisture content as some of the sample locations were noted as flooded during the summer monsoon season. Although a negligible component at this altitude, cosmic flux contributions to the environmental dose rate are included.

The samples' D_e values are widely distributed (most likely due to partial bleaching typical in some fluvial deposits, or because the samples are mixtures of different aged layers) and finite age modeling (FAM) of the distributions for all the samples were conducted to determine the true burial age (e.g., Galbraith, 1999; Rodnight et al., 2006).

Mekong-2, -3, and -4 have FAM burial ages of 35.05 ± 2.42 ka, 42.42 ± 3.79 ka and 43.44 ± 2.91 ka and are in stratigraphic order; however Mekong-5 is only 31.57 ± 3.68 ka yet sits stratigraphically below Mekong.-4. The age would therefore appear to be too young.

Table below summarizes the results of the OSL and dosimetric measurements for the samples.

Table A6. OSL and dosimetric measurements of the Mekong palaeo-channel sediment samples.

Sample N/ OSL Parameter	Mekong 2	Mekong 3	Mekong 4	Mekong 5
Lab Code	4.12 - 4.16m STA-MK3	4.65 - 4.69m STA-MK4	5.12 - 5.18m STA-MK5	5.47 - 5.52m STA-MK6
U (ppm)	2.29	1.77	2.07	2.47
Uncertainty	0.07	0.05	0.06	0.07
Th (ppm)	11.86	4.22	4.99	7.84
Uncertainty	0.36	0.13	0.15	0.24
%K	1.51	1.09	1.18	1.26
Uncertainty	0.05	0.03	0.04	0.04
Rb (ppm)	100	100	100	100
Uncertainty	10	10	10	10
H_2O[1], %	11	10	13	16
Dose rate (Gy/ka)[2]	2.63	1.71	1.85	2.10
Uncertainty	0.16	0.10	0.11	0.12
N[3]	51	9	71	25
De (Gy)	92.11	54.60	78.51	37.05
Uncertainty (Gy)	3.15	7.20	2.32	1.48
Age (ka)[4]	35.05	42.42	43.44	31.57
Uncertainty (ka)	2.42	3.79	2.91	3.68

Table A6 notes:

1. Percent moisture compared to dry weight. Uncertainty taken as 5%.
2. Cosmic dose-rate calculated assuming constant burial depth using method described in Prescott and Hutton (1994).
3. Number of replicated De estimates.
Uncertainty taken as 10%.
4. De and ages calculated using mean value of first age cluster from finite age model and the relative error [FAM] (Galbraith et al., 1999).

Sediment samples from the terraces from the locations T2, T4 and T5 (Section 4.2., Figure 4.15) were proceeded with the same methodology as the palaeochannel borehole samples. The results are presented in a Table A7 below.

Table A7. OSL and dosimetric measurements of the Mekong 40, 64 and 80 m terraces (terraces T2, T4 and T5 in Table A1, Appendix I) sediment samples.

Sample N/ OSL Parameter	**MEKT21**	**MEKT22**	**MEKT23**	**MEK6**	**MEK25**
Lab Code	STA-MK21	STA-MK22	STA-MK23	STA-MK6	STA-MK25
U (ppm)	1.41	1.96	1.84	2.13	1.46
Uncertainty	0.04	0.06	0.06	0.06	0.04
Th (ppm)	6.58	6.75	4.93	10.74	7.63
Uncertainty	0.20	0.20	0.15	0.32	0.23
%K	0.89	1.05	0.34	1.20	1.28
Uncertainty	0.03	0.03	0.01	0.04	0.04
Rb (ppm)	100	100	100	68.66	64.87
Uncertainty	10	10	10	2.06	1.95
H2O[1]	13.00	8.00	7.50	1.00	2.50
Dose rate[2] **(Gy/ka)**	1.61	1.95	1.19	2.54	2.21
Uncertainty	0.09	0.12	0.07	0.21	0.18
N[3]	48	47	59	56	55
FAM De (Gy)	113.38	75.45	17.49	54.03	35.77
Uncertainty (Gy)	5.13	0.94	0.51	0.69	1.99
FAM Age[4] **(ka)**	70.65	38.66	14.72	21.30	16.20
Uncertainty (ka)	5.13	2.40	0.95	1.80	1.60

Table A7 notes:

1.Moisture content (%) based on laboratory measurement loss of moisture on "as received" samples.
2.Dose rate is based on in situ measurements of U, Th, and K, and includes an ionising cosmic radiation component following Prescott & Hutton (1994) assuming constant burial depth using present day overburden measurements, altitude and latitude.
3.Number of aliquots accepted from SAR analyses.
4.MEKT21, -22, -23: Finite age modeling (FAM) of equivalent doses (De) allows the statistical discrimination of multiple components or a single component in the populations measured, statistical analyses of individual components, and the proportion of aliquots each represents (e.g., Galbraith et al., 1999; Rodnight et al., 2006). MEKT6 age is based on the mean age (from a normal distribution). MEKT25 age is based on finite age modeling (FAM) of equivalent doses (De) of a broader distribution containing 3 components (Galbraith et al., 1999; Rodnight et al., 2006).

Appendix III

Abridged from the Report of Radiocarbon Dating Analyses produced by Beta Analytic Inc.

BETA ANALYTIC INC.
DR. M.A. TAMERS and MR. D.G. HOOD
4985 S.W. 74 COURT
MIAMI, FLORIDA, USA 33155
PH: 305-667-5167 FAX:305-663-0964
beta@radiocarbon.com

REPORT OF RADIOCARBON DATING ANALYSES

Report Date: 12/31/2010
Material Received: 12/1/2010

Sample Data	Measured Radiocarbon Age	13C/12C Ratio	Conventional Radiocarbon Age(*)
Beta - 289073	490 +/- 60 BP	-27.8 o/oo	450 +/- 50 BP

SAMPLE : Mekong wood sample
ANALYSIS : Radiometric-Standard delivery
MATERIAL/PRETREATMENT : (wood): acid/alkali/acid
2 SIGMA CALIBRATION : Cal AD 1410 to 1500 (Cal BP 540 to 440) AND Cal AD 1600 to 1610 (Cal BP 350 to 340)

Dates are reported as RCYBP (radiocarbon years before present, "present" = AD 1950). By international convention, the modern reference standard was 95% the 14C activity of the National Institute of Standards and Technology (NIST) Oxalic Acid (SRM 4990C) and calculated using the Libby 14C half-life (5568 years). Quoted errors represent 1 relative standard deviation statistics (68% probability) counting errors based on the combined measurements of the sample, background, and modern reference standards. Measured 13C/12C ratios (delta 13C) were calculated relative to the PDB-1 standard.

The Conventional Radiocarbon Age represents the Measured Radiocarbon Age corrected for isotopic fractionation, calculated using the delta 13C. On rare occasion where the Conventional Radiocarbon Age was calculated using an assumed delta 13C, the ratio and the Conventional Radiocarbon Age will be followed by "*". The Conventional Radiocarbon Age is not calendar calibrated. When available, the Calendar Calibrated result is calculated from the Conventional Radiocarbon Age and is listed as the "Two Sigma Calibrated Result" for each sample.

CALIBRATION OF RADIOCARBON AGE TO CALENDAR YEARS

(VARIABLES : C13/C12=-27.8 :LA B. MULT=1)

Laboratory number:	Beta-289073
Conventional radiocarbon age:	450±50 BP
2 Sigma calibrated results:	Cal AD 1410 to 1 500 (Cal BP 540 to 440)
	and
(95% probability):	Cal AD 1600 to 1 610 (Cal BP 350 to 340)

INTERCEPT DATA

Intercept of radiocarbon age	
with calibration curve:	Cal AD 1440 (Cal BP 510)
1 Sigma calibrated result:	
(68% probability)	Cal AD 1430 to 1460 (Cal BP 520 to 490)

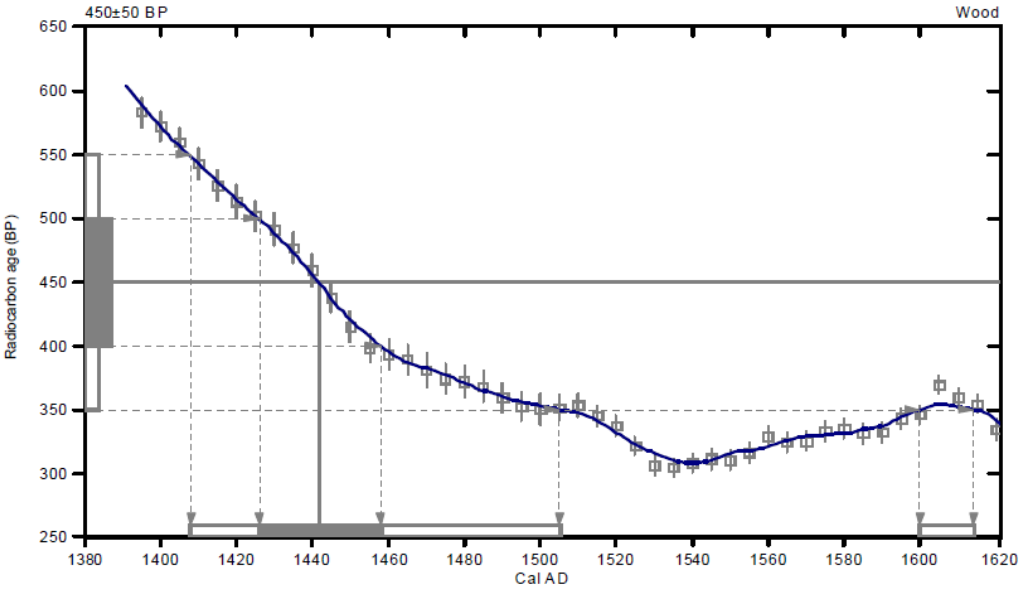

References:

Database used
INTCAL04
Calibration Database
INTCAL04 Radiocarbon Age Calibration
IntCal04: Calibration Issue of Radiocarbon (Volume 46, nr 3, 2004).
Mathematics
A Simplified Approach to Calibrating C14 Dates
Talma, A. S., Vogel, J. C., 1993, Radiocarbon 35(2), p317-322

Beta Analytic Radiocarbon Dating Laboratory
4985 S.W. 74th Court, Miami, Florida 33155 • Tel: (305)667-5167 • Fax: (305)663-0964 • E-Mail: beta@radiocarbon.com

Appendix IV

Table A8. Grain size data of the Mekong palaeo-channel samples from the borehole KOM (see Figure 4.15 in Section 4.2 for the location map).

Sample Identity as in Table A2, Appendix I	***GSD1***	***GSD2***	***GSD4***	***GSD5***	***GSD6***	***GSD7***	***GSD8***	***GSD10***	***GSD11***
Initial Sample Weight, g:	111.72	86.67	83.70	149.19	146.63	267.20	148.45	95.89	66.94
Aperture, microns	**Class weight retained in different samples, g**								
11200	0	0	0	0	0	17.04	1.12	0	0
8000	0	0	0	0	2.28	24.50	1.35	0	0
5600	0	0	1.60	0.57	1.61	30.70	2.50	0	0
4000	0	0	3.22	0.60	0.69	18.20	2.27	0	0
2800	0	0	2.22	0.21	0.70	11.20	0.93	0	0
2000	0	0.10	1.67	0.33	0.67	8.50	0.76	0.24	0
1400	0.07	0.20	1.55	0.40	0.45	8.17	1.04	0.77	0.05
1000	0.16	0.16	1.05	0.40	0.48	6.32	0.85	1.16	0.05
710	0.63	0.30	0.72	0.45	0.60	8.20	0.95	2.48	0.03
500	0.57	0.43	0.58	0.44	0.85	11.32	1.63	5.40	0.09
355	1.54	0.75	0.41	0.37	1.30	11.65	2.94	6.44	0.08
250	4.06	1.80	0.48	0.58	7.41	22.90	6.82	9.67	0.20
180	3.92	1.83	0.57	0.82	12.02	14.83	7.70	7.78	0.33
125	4.60	2.25	1.14	1.99	17.40	11.02	12.18	9.34	0.46
90	3.03	1.88	2.39	6.60	18.31	16.69	10.24	7.85	0.30
Less than 63	93.14	76.97	66.10	135.43	81.86	45.96	95.17	44.76	64.35
In % to a total sample weight: More than 63	16.63	11.19	21.03	9.22	43.28	82.80	35.89	53.32	2.38
In % to a total sample weight: Less than 63	83.37	88.81	78.97	90.78	54.72	17.20	64.11	46.68	96.13

Table A9. Organic assay data for the Mekong sand, silt, soil and borehole KOM samples (see Figure 4.15 in Section 4.2 for the location map).

Sample Identity as in Tables A1 and A2, Appendix I:	Sample weight, g			Portion taken for the organic assay, g		Organic content in portion taken for the organic assay	
	Fraction more than 63 microns	Fraction less than 63 microns	Total sample weight	Before burning	After burning	Weight, g	In % to initial portion weight
CS03	32.60	22.76	55.36	12.68	12.53	0.15	1.17
CS04	14.97	55.04	73.01	12.72	12.54	0.18	1.41
CS05	13.23	34.61	47.84	10.97	10.92	0.05	0.48
CS14	22.45	78.76	101.21	Not found			
CS16	50.19	60.82	111.01	8.47	8.25	0.22	2.57
CS22	56.1	17.84	73.94	13.88	13.34	0.54	3.87
GSD1	18.58	93.14	111.72	13.44	13.13	0.31	2.27
GSD2	9.7	76.97	86.67	15.21	14.93	0.28	1.82
Leo4	161.63	29.55	191.18	Not found			
CS24	96.46	16.60	113.06	Not found			

Table A10. Grain size data of the Mekong bedload samples (see Figure 4.15 in Section 4.2 for the location map)

Sample Identity as in Table A1, Appendix I:	***CS10***	***CS09***	***CS13***	***CS15***	***CS28***	***CK02***
Initial Sample weight, g:	404.10	119.61	159.42	126.70	185.55	239.01
Aperture, microns	**Class weight retained in different samples, g**					
31500	23.23					
22400	15.33					35.64
16000	17.98					20.82
11200	44.98					26.70
8000	224.60					32.81
5600	11.88					18.80
4000	9.50		0.53			7.89
2800	7.49		0.17			4.41
2000	4.70		0.45			3.08
1400	3.32	0.70	1.88			2.06
1000	2.18	0.02	9.00	0.02	0.02	2.48
710	2.52	0.43	30.73	0.25	0.02	3.85
500	6.79	2.66	62.29	0.32	0.15	8.69
355	11.66	5.57	28.48	0.38	0.67	9.45
250	7.60	25.55	9.01	6.20	7.82	20.68
180	4.27	53.99	7.25	36.34	40.14	13.77
125	3.53	24.79	5.86	56.04	79.94	15.46
90	0.08	4.52	2.23	24.75	51.83	7.02
Less than 63	0.19	0.22	0.26	2.40	4.96	0.83

Table A11. Grain size data of the Mekong sandbars samples (see Figure 4.15 in Section 4.2 for the location map)

Sample Identity as in Table A1, Appendix I:	***CS06***	***CS21***	***CS25***
Initial Sample weight, g:	144.16	84.31	87.49
Aperture, microns	**Class weight retained in different samples, g**		
1000	0.01		0.11
710	0.14	0.05	0.28
500	1.59	0.06	4.01
355	19.25	0.28	11.69
250	69.65	6.33	20.76
180	29.00	37.23	21.80
125	14.87	33.22	21.73
90	6.63	6.68	6.56
Less than 63	0.81	0.17	0.55

Appendix V

Table A12. Rock samples identity (see Figure 4.15 in Section 4.2. for the location map).

Rock type	Field sample N as in Table A1, Appendix I	Description
Red sandstone	CS01 CS23 Leo3 Leo5 Leo7 Leo8 Leo10 Leo12 Leo13 Leo14	Schistose, fine structure red arkose sandstone
Red meta-Sandstone	CS12	Fine-grained, dense structure with cavities filled by post-crystallized hematite minerals (limonite, goethite).
Andesite	CS20 CS27 CS61 CS63 CS64 Leo1 Leo15 Leo16 Leo17 Leo18	Big isometric quartz grains up to 2-3mm (20%), prismatic lathlike plagioclase (up to 3mm), isometric mafic minerals (5%), goethite (modified surface). Main mineral which compose ground mass is white matted cryptocrystalline quartz.
Andesite or Diorite	CK01, CS26	Fine-grained, fine crystalline. Quartz and feldspars are in equal parts, mafic 15%
Granite	CK03 CK04 CS66	Fine grained structure. Samples CK03 and CK04: quartz 50%, 40% of potassium feldspar, 5% - mafic and 5% of muscovite. CS66: quartz – 20%, feldspars 60%, mafic 5%, dark mica 15%.
Gneiss	CS08 CS11	Gneissose texture, structure is massive, dense, homogeneous, fine-grained, weathered along fissile planes. Mineral composition: 30% transparent (-brownish) (bi-)pyramidal quartz; bright green semi-transparent soft irregular shape mineral with grain size up to 0.1mm (amphibole); 30% white cryptocrystalline mineral (albite or calcite).
Quartz-muscovite gneiss	CK05	Massive, microgranular structure. Abundance of mica minerals both light colour (muscovite) and dark (phlogophite). Other minerals: albite, calcite, thin intercalations of yellow metaliferous mineral (dark platy mineral with up to 2mm particle size, perhaps, hornblende), <10% of quartz. Dyke rock.
Quartzite	CS18 CS19 CS65 Leo6 Leo9 Leo11	Translucent grey cryptocrystalline quartz. Massive, homogeneous structure with up to 30% inclusions of limonited hematite grains (up to 1mm).

Rock type	Field sample N as in Table A1, Appendix I	Description
Ferruginous quartzite	CS07	Modified (limonited) hematite on a surface. Greenish-grey cryptocrystalline quartz, numerous disseminations (10-15%) of hematite up to 2mm. Homogeneous massive dense structure.
Quartz albitophyre	CS17	Predominantly composed by grey cryptocrystalline quartz. Porphyritic disseminations are represented by cubic and domatic crystals of albite (15-20%); 3-5% are isometric grains of green amphibole (hornblende). Singular grains of ore mineral (supposedly, pyrites). Massive, homogeneous structure, texture is porphyritic. Hypabyssal rock (dyke).

Examples of the bedrock erosion observed within a study area.

Figure A.1. Potholes: the simple circular example on a right and smaller pothole with external entry furrow on a left.

The location is 13°13.516'N/105°58.683E, rock type: quartzite. Entry does not concur with main flow direction from right to left due to local flow pattern following the rock shape. Mobile phone 10 cm length is for scale.

Figure A.2. Transverse parallel sided furrows.

Location is 13°13.516'N/105°58.683E, rock type: quartzite. Mobile phone 10 cm length is for scale. Flow direction is from bottom right to top left.

Figure A.3. Near-vertical polished surface of boulder on the shore of an inundated island.

Location is 13°11.463'N/105°58.698'E, rock type: quartz albitophyre. Small-scale pitting (mixture of circular and elongated pits). High content of iron forms an iron crust. Flow direction is out of the image. Cigarette lighter (length 8 cm) is for scale.

Figure A.4. Outcrop on the shore of inundated island.

Location is 13°11.463'N/105°58.698'E, rock type: quartz albitophyre. Polished surface with structurally influenced pseudo-ripples. Flow direction is out of the image. 10 cm length GPS unit provides scale.

Figure A5. Volcanic rock outcrop on the shore of an inundated island.

Location is 13°11.463'N/105°58.698'E, rock type: quartz albitophyre. Polished surface with structurally controlled pseudo-ripples and polish provides visual effect of "wet rock" 10 cm GPS unit is for scale. Flow direction is out of the image.

Figure A.6. Divergent local flow pattern with flutes, spindle-shaped flutes and lineation developed at crack zones.

Location is 13°13.516'N/105°58.683E, rock type: quartzite. Flow direction is from bottom right to top left. Cigarette lighter 8 cm length provides scale.

Figure A.7. Divergent pattern of local flow vectors and small scale obstacle marks and flutes formed due to resistant (quartz) and soluble (calcite?) minerals presence.

Location is 13°13.425'N/106°00.387'E, rock type: gneiss. Flow originates from base of lighter and fans out above. Cigarette lighter (length 8 cm) is for scale.

Figure A.8. Pothole with a central boss.

Location is 12°36'35.877''N/106°0'6.193''E, rock type: sandstones. Flow directions complex. Cigarette lighter (length 8 cm) is for scale.

Figure A. 9. Bedrock erosion form filled during flooding season with coarse angular gravel of variable size, with sand.

Location 13°04'39.1''N/106°03'23.2''E, rock type: andesite. Flow directions complex. The key (4 cm) is for scale.

References

- Abbado, D., Slingerland, R. & Smith, N. D., (2009), 'Origin of anastomosis in the Upper Columbia River, British Columbia, Canada' IN, Blum, M. D., Marriott, S. B. and Leclair, S. F. (Eds), *Fluvial Sedimentology VII*, Oxford, Blackwell Publishing Ltd., UK, pp. 1-15.
- Adams, P.N., Slingerland, R.L., & Smith, N.D., (2004), 'Variations in natural levee morphology in anastomosed channel flood plain complexes', *Geomorphology*, vol. 61, pp. 127-142.
- Altin, T.B., & Altin, B.N., (2011), 'Drainage morphometry and its influence on landforms in volcanic terrain, Central Anatolia, Turkey', *Procedia-Social and Behavioral Sciences*, vol. 19, pp.732-740.
- Ashmore, P. & Church, M. (2001), 'The impact of climate change on rivers and river processes in Canada', *Geological Survey of Canada Bulletin,* 555, 60 pp.
- Ashwell, D., Miller, F., Dümmer, I., (2004), 'Ecology, forest cover and quality', IN, Working Group on Natural Resource Management (WGNRM) and Royal Government of Cambodia (RGC), *Cambodia Independent Forest Sector Review*, http://www.cambodia-forest-sector.net/ [Accessed on 20.10.2008].
- Ashworth, P.J., Best, J.L. and Jones, M.A., (2007), 'The relationship between channel avulsion, flow occupancy and aggradation in braided rivers: insights from an experimental model', *Sedimentology*, vol.54, no. 3, pp 497-513.
- Aslan, A., & Blum, M.D., (1999), 'Contrasting styles of Holocene avulsion, Texas coastal plain', IN, Smith, N.D. & Rogers, J.J. (Eds), *Current Research in Fluvial Sedimentology. Proceedings of the 6th International Conference on Fluvial Sedimentology*, International Association of Sedimentologists, Special Publication, 28, pp. 193-209.
- Aslan, A., Autin, W.J., Blum, M.D., (2005), 'Causes of river avulsion: insights from the late Holocene avulsion history of the Mississippi River, USA', *Journal of Sedimentary Research*, vol. 75, pp. 650-664.
- Baird, I. G., & Phylavanh, B., (1999), 'Fishes and Forests: Fish Foods and the Importance of Seasonally Flooded Riverine Habitats for Mekong River Fish Species', Unpublished Technical Report Prepared for the Environmental Protection and Community Development in Siphandone Wetlands Project, CESVI, Pakse, Lao PDR, 46pp.
- Baker, V.R., & Kochel, R.C., (1979), 'Martian channel morphology: Maja and Kasei Valles', *Journal of Geophysical Research*, vol. 84, pp. 7961-7983.

- Baker, V.R., (1979), 'Erosional processes in channelized water flows on Mars', *Journal of Geophysical Research*, vol. 84, pp. 7985-7993.
- Beasley, I., Somany, P., Gilbert, M., Phothitay, C., Saksang, San, L. K. & Sokha, K., (2007), 'Review of the status and conservation of Irrawasy dolphins *Orcaella brevirostris* in the Mekong River of Cambodia, LAO PDR and Vietnam', IN, Smith, B.D., Shore, R.G. & Lopez A. (Eds.), *Status and conservation of freshwater populations of Irrawaddy dolphins*, *WCS Working Paper Series 31*, Wild Conservation Society, Bronx, NY, pp. 67-82.
- Bellin, J.N., (1751), 'Carte Des Royaumes De Siam, De Tunquin, Pegu, Ava, Arcana &co. (Indonesia). Scale 1:8 870 000', Paris: Chez Didot from A.F. Prevost's *Histoire Generale Des Voyages*, Tome IX, No.8
- Bertoldi, W., & Tubino, M., (2005). 'Bed and bank evolution of bifurcating channels,' *Water Resources Research*, vol. 41, W07001, doi:10.1029/2004WR003333.
- Bertoldi, W., & Turbino, M., (2007), 'River bifurcations: experimental observations on equilibrium configurations', *Water Resources Research*, vol. 43, W10437, doi:10.1029/2007WR005907.
- Bertoldi, W., Zanoni, L., & Tubino, M., (2009), 'Planform dynamics of braided streams', *Earth Surface Processes and Landforms*, vol.34, pp. 547-557.
- Bezuijen, M.R., Timmins, R., & Seng, T., (Eds), (2008), *Biological surveys of the Mekong River between Kratie and Stung Treng town, northeast Cambodia, 2006-2007*, WWF greater Mekong – Cambodia Country Programme, Cambodia Fishers Administration and Cambodia Forestry Administration, Phnom Penh, 220pp.
- Brice, J.C., (1960), 'Index for description of channel braiding', *Geological Society of America Bulletin*, 71, pp.1833.
- Brice, J.C., (1964), 'Channel patterns and terraces of the Loup Rivers in Nebraska', *Geological Survey Professional Paper*, 422-D, pp.1-41.
- Brice, J.C., (1975), 'Air photo interpretation of the form and behaviour of alluvial rivers', *Final report to the U.S.Army Research Office*, Durham, North Carolina, 65pp.
- Brice, J.C., (1982), 'Stream channel stability assessment', *Federal Highway Administration Report,* no. FHWA/RD – 82/021, Washington DC, 42pp.
- Bridge, J.S., & Demicco, R.V., (2008), *Earth Surface Processes, Landforms and Sediment Deposits*, Cambridge University Press, 815pp.
- Bridge, J.S., (2003), *Rivers and Floodplains: Forms, Processes and Sedimentary Record*, Blackwell Publishing, 494pp.

- Bridgeland, D.R., & Westway, R., (2008), 'Climatically controlled river terrace staircases: a worldwide Quaternary phenomenon', *Geomorphology*, vol.98, no.3-4, pp. 285-315.
- Bristow, C.S., & Best, J.L., (1993), 'Braided rivers: perspectives and problems'. IN, Best, J.L., & Bristow, C.S., (Eds), *Braided Rivers*, Geological Society, London, Special Publications, vol. 75, pp. 1-11.
- Broadhurst, L.J., & Heritage, G.L., (1998), 'Modelling stage-discharge relationships in anastomosed bedrock-influenced sections of the Sabie River system', *Earth Surface Processes and Landforms*, vol.23, no. 5, pp. 455-465.
- Bruun, P., (1988), 'The Bruun rule of erosion by sea-level rise: a discussion on large scale two- and three dimensional usages', *Journal of Coastal Research*, vol. 4, no. 4, pp.627-648.
- Buckingham, S.E., & Whitney, J.W., (2007), 'GIS methodology for quantifying channel change in Las Vegas, Nevada', *American Water Resources Association*, vol. 43, no. 4, pp.888-898.
- Buckley, B.M., Anchukaitis, K.J., Penny, D., Fletcher, R., Cook, E.R., Sano, M., Nam, L.C., Wichienkeeo, A., Minh, T.T., and Hong, T.M., (2010), 'Climate as a contributing factor in the demise of Angkor, Cambodia', *Proceedings of the National Academy of Science of the United States of America*, vol.107, no.15, pp.6748-6752.
- Burge, L.M., (2006), 'Stability, morphology and surface grain size patterns of channel bifurcation in gravel-cobble bedded anabranching rivers', *Earth Surface Processes and Landforms*, 32, pp.1211-1226.
- Buschmann, J., Berg, M., Stengel, C., Winkel, L., Sampson, M.L., Trang, P.T.K., & Viet, P.H., (2008), 'Contamination of drinking water resources in the Mekong delta floodplains: Arsenic and other trace metals pose serious health risks to population', *Environment International*, vol.34, no.6, pp.756-764.
- Campbell, I., (Ed.), (2009), *The Mekong. Biophysical Environment of an International River Basin,* Oxford, GB, Academic Press, 464pp.
- Capart, H., Bellal, M., & Young, D-L., (2007), 'Self-similar evolution of semi-infinite alluvial channels with moving boundaries', *Journal of Sedimentary Research*, vol. 717, no.1, pp.13-22.
- Carbonnel, J-P., (1972), 'Le Quaternaire Cambodgien. Structure et stratigraphie. (Thése présentée á l'Université de Paris- VI)', Mémories O.R.S.T.O.M., N°60, 248pp., 4pl. (in French).
- Carling, P.A., (2009), 'The Geology of the Lower Mekong River', IN, Campbell, I., (Ed.), *The Mekong. Biophysical Environment of an International River Basin,* Oxford, GB, Academic Press, pp.13-28.

- Carling, P.A., Tych, W., & Richardson, K., (2005), 'The hydraulic scaling of step-pool systems', IN, Parker, G., & Garcia, M.H., (Eds.), *River, Coastal and Estuarine Morphodynamics*, vol. 1, Balkema, Taylor and Francis, NY, pp. 55-63.
- Carter, A., Roques, D., Bristow, C.S., (2000), 'Denudation history of onshore central Vietnam: constraints on the Cenozoic evolution of the western margin of the South China Sea', *Tectonophysics*, vol.322, pp.265-277.
- Cazanacli, D., Paola, C., & Parker, G., (2002), 'Experimental steep, braided flow: application to flooding risk on fans', *Journal of Hydraulic Engineering*, vol.322, pp.232-330.
- CEGIS (Centre for Environment and Geographic Information Services), (2010), www.cegisbd.com [Accessed on 11.10.2010].
- Chalov, R.S., & Chalov, S.R., (2009), 'The morphology of the rocky channel of the Angara River in its stretches within the Bofuchanskoe and Motyginskoe reservoirs', *Geography and Natural Resources*, vol. 30, pp.47-53.
- Chan, S., Putrea, S., & Hortle, H.G., (2003), 'Using local knowledge to inventory deep pools, important fish habitats in Cambodia', IN, *Proceedings of the 6th Technical symposium on Mekong Fisheries*, Lao PDR, 65pp.
- Chandler, D.P., (2000), *A history of Cambodia,* Westview Press, 296pp.
- Charlton, R., (2007), *Fundamentals of Fluvial Geomorphology,* Routledge, 234pp.
- Chatfield, C., (1996), *The Analysis of Time Series*, 5th Edition, Chapman & Hall, London, 279pp.
- Cheng, S., Deng, Q., Zhou, S & Yang, G., (2002), 'Strath terraces of Jinshaan Canyon, Yellow River, and Quaternary tectonic movements of the Ordos Plateau, North China', *Terra Nova,* vol. 14, pp.215-224.
- Chengkun, L., (1985), 'Cause of formation and classification of river pattern', *International Journal of Sediment Research*, vol. 2, pp.1-11.
- Chew, L.C., & Ashmore, P.E., (2001), 'Channel adjustment and test of rational regime theory in a proglacial braided stream', *Geomorphology*, vol. 37, pp.43-63.
- Church, M., & Jones, D., (1982), 'Channel bars in gravel-bed rivers', IN, Hey, R.D., Bathurst, J.C. & Thorne, C.R., (Eds), *Gravel-Bed Rivers*, Wiley, Chichester, UK, pp.291-324.
- Church, M., (1992), 'Channel morphology and typology', IN, Calow, P., & Petts, G.E. (Eds), *The Rivers Handbook*, ed.1, , Oxford, Blackwell Science, pp.126-143.
- Church, M., (2006), 'Bed material transport and the morphology of alluvial river channels', *The Annual Review of Earth and Planetary Science*, vol. 34, pp.325-354.

- Clark, A., Robinson, M., Jackson, C., McCabe, C. & Crass, D., (2008) 'Threatened archaeological, historical and cultural resources of the Georgia coast: identification, prioritization and management using GIS technology', *Final report prepared for Georgia Coastal Zone Management Program*, 23pp.
- CNMC (Cambodia National Mekong Committee), (2006), 'Cambodia Country Report: Flood information in Cambodia', IN, *Improving Flood Forecasting and Warning Systems for Flood Management and Mitigation in the Lower Mekong Basin*, Proceedings of the 4th Annual Mekong Flood Forum, Siem Reap, Cambodia, pp.23-36.
- Colombo, R., Vogt, J.V., Soille, P., Paracchini, M.L., D'Jager, A., (2007), 'Deriving river networks and catchments at the European scale from medium resolution digital elevation data', *Catena*, vol. 70, pp.296-305.
- Committee for Coordination of Investigations of the Lower Mekong Basin, (1959), Aerial photography of the Mekong main stem at the scale 1:40 000, Sheet 10, Mekong River Project, Canada.
- Conlan, I., Rutherfurd, I., Finlayson, B. & Western, A., (2008), '*The geomorphology of deep pools on the lower-Mekong River: Controls on pool spacing and dimensions, processes of pool maintenance and potential future changes to pool morphology*', Final report submitted to the Mekong River Commission Secretariat, The University of Melbourne, Australia, 100pp.
- Costa-Cabral, M.C., Richey, J.E., Goteti, G., Lettenmaier, D.P., Feldkotter, C. & Shidvongs, A., (2008), 'Landscape structure and use, climate, and water movement in the Mekong River basin', *Hydrological Processes*, vol. 22, pp.1731-1746.
- Crocker C.D., (1962), '*The general soil map of the Kingdom of Cambodia and the exploratory survey of the soils of Cambodia. Joint publication'*, Phnom Penh (Cambodia): Royal Cambodian Government Soil Commission/USAID.
- Crosato, A., & Mosselman, E., (2009), 'Simple physics-based predictor for the number of river bars and the transition between meandering and braiding', *Water Resources Research*, vol. 45, pp.1-14.
- CTSP/Danida, (2000), 'Cambodia Tree Seed Project/ Danida', National Priority Tree Species Workshop, Forest Administration, Phnom Penh, Cambodia, 69pp.
- Dankworth, F., (1832), 'Birman Empire with Anam, Siam & Cochin China', Map in scale of 1:27 800 000, Philadelphia: Carey & Lea, from Carey & Lea's *Family Cabinet Atlas*, First American Edition.
- De Rose, R.C., Barret, D., Marks, A., Caitcheon, G., Chen, Y., Simon, D., Lymburner, L., Douglas, G. & Palmer, M., (2005), '*Regional Patterns of Riparian Vegetation, Erosion and Sediment Transport in the Ovens River Basin*', CSIRO Land and Water Client Report, Canberra, Australia, 26pp.

- DelPHE (Development Partnerships in Higher Education), (2008), '*Socio-economic survey in Stung Treng province, Cambodia',* Project (2.68): Sustainable management of river bank erosion along the Mekong River in Bangladesh, Cambodia and Vietnam, Phnom Penh, Cambodia, 13pp.
- Demeter, F., Patole-Edoumba, E., Duringer, P., Bacon, A-M., Sytha, P., Bano, M., Laychour, V., Cheangleng, M. & Sari, V., (2010), 'Reinterpretation of an Archaeological Pebble Culture from the Middle Mekong River Valley, Cambodia', *Geoarchaeology: An International Journal*, vol. 25, no. 1, pp.75-95.
- DGM (Department of Geology and Mines), Lao PDR, (2000), 'Part 1. General geology', IN, Tran van Ban, (Ed), *Mineral investigation and geological mapping at 1:200 000 scale of Mid Central Laos region,* Intergeo, Viet Nam, 300pp.
- DHRW (Department of Hydrology and River Works), (2008), 'Cambodia', http://www.hydrologycambodia.50megs.com/hydrograph.htm [Accessed on 10.09.2008]
- Dickins, J. M., Zunyi, Y., Hongfu, Y., Lucas, S.G., & Acharyya, S.K., (1997), *Late Palaeozoic and Early Mesozoic Circum-Pacific events and Their Global Correlation,* Cambridge, Cambridge University Press, UK, 300pp.
- Dudgeon, D., (1999), *Tropical Asian streams: Zoobenthos, Ecology and Conservation,* Hong Kong, Hong Kong University Press, 830pp.
- Edmonds, D.A., & Singerland, R.L., (2010), 'Significant effect of sediment cohesion on delta morphology', *Nature Geoscience*, vol. 3, pp.105-109.
- Egozi, R., & Ashmore, P., (2008), 'Defining and measuring braiding intensity', *Earth Surface Processes and Landforms*, vol. 33, pp.2121-2138.
- Egozi, R., & Ashmore, P., (2009), 'Experimental analysis of braided channel pattern response to increased discharge', *Journal of Geophysical. Research,* vol. 114, pp. 1-15.
- ESRI (Environmental Systems Research Institute), (1994), *ARC/INFO data management: concepts, data models, database design, and storage,* Redlands, CA, Environmental Systems Research Institute,302pp.
- ESRI (Environmental Systems Research Institute), (2007), *ArcGIS Desktop Help,* http://webhelp.esri.com/arcgisdesktop/9.2/index.cfm?TopicName=welcome [Accessed on 10/09/2009].
- ESRI (Environmental Systems Research Institute), (2008), 'New geoprocessing features in ArcGIS 9.3', *ArcUser*, Summer 2008, pp.44-45.
- FA/Danida/DED, T.S.P., (2003), '*Gene-Ecological Zonation of Cambodia*', Forestry Administration, Phnom Penh, Cambodia, 65pp.
- FAO/UNESCO, (1988), '*Soil Map of the World; Revised legend*', Rome, FAO, 119pp.

- Federici, B., & Paola, C., (2003), 'Dynamics of bifurcations in noncohensive sediments', *Water Resources Research*, vol. 38, no. 6, pp.3-15.
- Fontaine, H., & Workman, D.R., (1997), 'Cambodia', IN, Moores, E.M., and Fairbridge, R.W., (Eds), *Encyclopedia of European and Asian Regional Geology*, Chapman & Hall, London, UK, pp.122-127.
- Frohn, R.C., Hinkel, K.M., Eisner, W.R., (2005), 'Satellite remote sensing classification of thaw lakes and drained thaw lake basins on the North Slope of Alaska', *Remote Sensing of Environment*, vol. 97, no.1, pp.116-126.
- Fu, C., Guan, Z., He, J. (Eds.), (2008), *Regional Climate Studies of China,* Springer, 476pp.
- Fuller, I.C., (2007), 'Geomorphic impacts of a 100-year flood: Kiwitea Stream, Manawatu catchment, New Zealand', *Geomorphology*, vol.98, no. 1-2, pp.84-95.
- Fyhn, M.B.W., Boldreel, L.O. & Nielsen, L.H., (2009), 'Geological development of the central and south Vietnamese margin: implications for the establishment of the South China Sea, Indochinese escape tectonics and Cenozoic volcanism', *Tectonophysics,* vol.478, pp.184–204.
- Galbraith, R.F., R. G. Roberts, G. M. Laslett, H. Yoshida, & J. M. Olley, (1999), 'Optical dating of single and multiple grains of quartz from Jinmium rock shelter, northern Australia: Part I, Experimental design and statistical models', *Archaeometry,* vol. 41, pp.339–364.
- Garner, H.F., (1966), 'Derangement of the Rio Caroni, Venezuela', *Revue de Géomorphologie Dynamique*, vol. 16, pp.54–83.
- Gawthorpe, R.L., & Hurst, J.M., (1993), 'Transfer zones in extensional basins: their structural style and influence on drainage development and stratigraphy', *Journal of the Geological Society of London*, vol.150, pp.1137-1152.
- Geleynse, N., Storms, J.E.A., Stive, M.J.F., Jagers, H.R.A., and Walstra, D.J.R., (2010), 'Modeling of a mixed-load fluvio-deltaic system', *Geophysical Research Letters*,vol. 37, L05402, doi: 10.1029/2009GL042000.
- Germanoski, D., & Schumm, S.A., (1993), 'Changes in braided river morphology resulting from aggradation and degradation', *Journal of Geology*, vol.101, pp. 451-466.
- Gibling, M.R., (2006), 'Width and thickness of fluvial channel bodies and valley fills in the geological record: a literature compilation and classification', *Journal of Sedimentary Research*, vol.76, pp.731-770.
- Glasbey, C.A., & Horgan, G.W.,(Eds.), (1995), *Image Analysis for the Biological Sciences*, John Wiley & Sons Ltd., Chichester, UK, 230pp.
- Gomarasca, M.A., (2009), *Basics of Geomatics,* Spriger, 697pp.
- Gottman, J.M. (1981), *Time-series Analysis: A Comprehensive Introduction for Social Scientists,* Cambridge University Press, Cambridge, 400pp.

- Government of Canada, Natural Resources Canada, Centre for Topographic Information, (2005), Vector digital data of the National Topographic Data Base (NTDB), 3rd Edition, Sherbrooke, Quebec, Canada.
- Gradziński, R, Baryła, J., Doktor, M., Gmur, D., Gradziński, M., Kędzior, A., Paszkowski, M., Soja, R., Zieliński, T., Żurek, S., (2003), 'Vegetation-controlled modern anastomosing system of the upper Narew River (NE Poland) and its sediments', *Sedimentary Geology*, vol. 157, pp.253-276.
- Gregorio, A.D, (2005), 'Land Cover Classification System (LCCS), version 2: Classification Concepts and User Manual', *FAO Environmental and Natural Resources Service Series*, no. 8 , FAO, Rome, 208pp.
- Gupta, A., & Liew, S.C., (2007), 'The Mekong from satellite imagery: A quick look at a large river', *Geomorphology*, vol.85, no.3-4, pp.259-274.
- Gupta, A., (2007), *Large Rivers: Geomorphology and Management*, John Wiley Chichester, England, 728pp.
- Gupta, A., Kale, V.S., Rajaguru, S.N., (1999), 'The Narmada River, India, through space and time', IN, Miller, A.J., Gupta, A., (Eds), *Varieties of Fluvial Form*, Wiley, Chichester, pp.113-143.
- Gurnell, A., (1997), 'Channel change on the River Dee meanders, 1946-1992, from the analysis of air photographs', *Regulated Rivers: Research and Management*, vol.13, no.1, pp.13-26.
- Hall, R., (2002), 'Cenozoic geological and plate tectonic evolution of SE Asia and the SW Pacific: computer-based reconstructions, model and animations', *Journal of Asian Earth Sciences, vol.* 20, pp.353-431.
- Halls, A.S., & Kshatriya, M., (2009*), Modelling the cumulative barrier and passage effects of mainstream hydropower dams on migratory fish populations in the Lower Mekong Basin*, MRC Technical Paper No. 25, Mekong River Commission, Vientiane, 104pp.
- Hamilton, J.D., (1994), *Time Series Analysis*, Princeton University Press, Princeton, 820pp.
- Hanebuth, T.J.J., Proske, U., Saito, Y., Nguyen, V.L., Ta, T.K.O., (2012), Early growth stage of a large delta – transformation from estuarine-platform to deltaic-progradational conditions (the northeastern Mekong River Delta, Vietnam), *Sedimentary Geology (2012)*, doi: 10.1016/j.sedgeo.2012.03.014.
- Hanebuth, T.J.J., Voris, H.K., Yokoyama, Y., Saito, Y., Okuno, J., (2011), 'Formation and fate of sedimentary depocentres on Southeast Asia's Sunda Shelf over the past sea-level cycle and biogeographic implications', *Earth-Science Reviews*, vol.104, pp.92-110.

- Hården, P-O., Sunborg, Å., (1992), '*The Lower Mekong Basin Suspended Sediment Transport and Sedimentation Problems*' Report to Mekong River Secretariat by Hydroconsult, Uppsala, Sweden, p.71.
- Hardy, R.J., Lane, S.N., Yu, D., (2011), 'Flow structures at an idealized bifurcation: a numerical experiment', *Earth Surface Processes and Landforms*, vol. 36, no. 15, pp. 2083-2096.
- Harwood, K., & Brown, A.G., (1993), 'Fluvial processes in a forested anastomosing river: Flood partitioning and changing flow patterns', *Earth Surface Processes and Landforms*, vol.18, no.8, pp. 741-748.
- Hasthorpe, J., & Mount, N.J., (2007), 'The generation of river channel skeletons from binary images using raster thinning algorithms', IN, Winstanley, A.,(Ed), *Proceedings of the 15th Geographical Information Science Research UK Conference*, NUIM, Ireland, pp.477-483.
- Hayward, J.A., & Sutherland, A.J., (1974), 'The Torlesse stream vortex-tube sediment trap', *Journal of Hydrology* (New Zealand), vol.13, pp.41-53.
- Heller, D.J., Paola, C., (1996), 'Downstream changes in alluvial architecture: an exploration of controls on channel-stacking patterns', *Journal of Sedimentary Research*, vol. 66, no. 2, pp.297-306.
- Heritage, G.L., Charlton, M.E., and O'Regan, S., (2001), 'Morphological classification of fluvial environments: an investigation of the continuum of channel types', *The Journal of Geology*, vol. 109, pp.21-33.
- Heritage, G.L., Moon, B.P., Broadhurst, L.J., and James, C.S., (2004), 'The frictional resistance characteristics of a bedrock-influenced river channel', *Earth Surface Processes and Landforms*, vol.29, pp.611-627.
- Heritage, G.L., van Niekerk, A.W., Moon, B.P., (1999). Geomorphology of the Sabie River, South Africa: an incised bedrock-influenced channel. In: Miller, A.J., Gupta, A. (Eds.), *Varieties of Fluvial Form*, Wiley, Chichester, pp. 53– 79.
- Hess, L.L., Melack, J.M., Filoso, S., & Wang, Y., (1995), 'Delineation of inundated area and vegetation along the Amazon floodplain with the SIR-C synthetic aperture radar', *IEEE Transactions on Geoscience and Remote Sensing*, vol. 33, pp.896-904.
- Hess, L.L., Melack, J.M., Novo, E.M.L.M., Barbosa, C.C.F., Gastil, M., (2003), 'Dual-season mapping of wetlands inundation and vegetation for the central Amazon basin', *Remote Sensing and Environment,* vol.87, pp.404-428.
- Hickson, T.A., Sheets, B.A., Paola, C., & Kelberer, M., (2005), 'Experimental test of tectonic controls on three-dimensional alluvial facies architecture, *Journal of Sedimentary Research*, vol. 75, no.4, pp.710-722.
- Hong, L.B., & Davies, T.R.H., (1979), 'A study of stream braiding', *Geological Society of America Bulletin*, vol.90, Part II, pp.1839-1859.

- Hori, H., (2000), *The Mekong: Environment and Development,* The United Nations University Press, 398pp.
- Howard, A.D., Dietrich, W.E., & Seidl, M.A., (1994), 'Modelling fluvial erosion on regional to continental scales', *Journal of Geophysical Research*, vol. 99, no. B7, pp.13971-13986.
- Howard, A.D., Keeth, M.E., Vincent, C.L., (1970), 'Topological and geometrical properties of braided streams', *Water Resources Research,* vol. 6, pp.1674-1688.
- Huang, H.Q. & Nanson, G.C., (2007), 'Why some alluvial rivers develop an anabranching pattern', *Water Resources Research*, vol. 43, W07441, doi:10.1029/2006WR005223.
- Humphrey, N.F., & Konrad, S.K., (2000), 'River incision or diversion in response to bedrock uplift', *Geology*, vol.28, pp.43-46.
- Hundey, E.J., & Ashmore, P.E., (2009), 'Length scale of braided river morphology', *Water Resources Research*, vol.45, W08409, doi:10.1029/2008WR007521.
- Hutchinson, C.S., (1989), *Geological Evolution of South-East Asia*, Oxford Scientific Publications, Oxford, UK, 368pp.
- ICEM (International Centre for Environmental Management), (2003), *Cambodia National Report on Protected Areas and Development. Review of Protected Areas and Development in the Lower Mekong River Region*, Indooroopilly, Queensland, Australia, 148pp.
- ICEM (International Centre for Environmental Management), (2010), *MRC Strategic Environmental Assessment (SEA) of hydropower on the Mekong mainstream*, Hanoi, Viet Nam, 198pp.
- ITTO (International Tropical Timber Organization), (2006), *Status of tropical forest management 2005,* ITTO Technical Series No. 24, International Tropical Timber Organization, Yokohama, Japan, 302pp.
- Jansen, J. D., Codilean, A.T., Bishop, P., & Hoey, T.B., (2010), 'Scale dependence of lithological control on topography: bedrock channel geometry and catchment morphometry in western Scotland', *The Journal of Geology*, vol. 118, pp.223-246.
- Jansen, J.D., and Brierley, G.J., (2004), 'Pool-fills: a window to palaeoflood history and response in bedrock-confined rivers', *Sedimentology*, vol.52, pp. 901-925.
- Jerolmack, D.J., & Mohrig, D., (2007), 'Conditions for branching in depositional rivers', *Geology*, vol.35, pp.463-466

- JICA (Japan International Cooperation Agency), (2003), *Cambodia Reconnaissance Survey Digital Data,* Ministry of Public Works and Transportation (MPWT), Kingdom of Cambodia, [digital dataset].
- Jones, L.S., & Schumm, S.A., (1999), 'Causes of avulsion: an overview', IN, Smith, N.D., & Rogers, J.J., (Eds), *Fluvial Sedimentology VI*, International Association of Sedimentologists Special Publication, vol.28, pp.171-178.
- Jumsai, M.L., (1996), *History of Thailand & Cambodia: From the Days of Angkor to the Present*, Chalermnit Press, 226pp.
- Kale, V.S., (1990), 'Morphological and hidrological characteristics of some allochthonous river channels, Western Deccan Trap Upland region, India', *Geomorphology*, vol.3, pp.31-43.
- Kale, V.S., Baker, V.R., & Mishra, C., (1996), 'Multi-channel patterns of bedrock rivers: an example from the central Narmada basin, India', *Catena*, vol.26, pp.85-98.
- Keen-Zebert, A., & Curran, J.C., (2009), 'Regional and local controls on the spatial distribution of bedrock reaches in the Upper Guadalupe River, Texas', *Geomorphology*, vol.112, pp.295-305.
- Keen-Zebert, A., & Tooth, S., (2009), 'Bedrock channel incision controls Quaternary wetland development cycles on the South African Highveld', Poster at the 7th International Conference on Geomorphology, Melbourne, 6-11 of July 2009.
- Kehew, A.E., and Lord, M.L., (1986), 'Origin and large scale erosional features of glacial-lake spillways in the northern Great Plains', *Geological Society of America Bulletin*, vol. 97, pp.162-177.
- Kellerhals, R., & Church, M., (1989), 'The morphology of large rivers: characterization and management', IN, Douglas, P., & Dodge, P., (Eds.), *Proceedings of the International Large River Symposium*, Honey Harbour, Ontario, Canada, pp.31-48.
- Kelly, S., (2006), 'Scaling and hierarchy in braided rivers and their deposits: examples and implications for reservoir modelling', IN, Sambrook Smith, G.H., Best, J.L., Bristow, C.S., Petts, G.E., (Eds), *Braided Rivers: Process, Deposits, Ecology and Management*, Blackwell Publishing Ltd, pp. 75-106.
- Kiernan, B., (2002), *The Pol Pot Regime: Race, Power and Genocide in Cambodia under the Khmer Rouge*, *1975-79*, Yale University Press, 477pp.
- Kim, W., Connell, S.D., Steel, E., Smith, G.A., & Paola, C., (2011), 'Mass-balance control on the interaction of axial and transverse channel systems', *Geology*, vol. 39, no. 7, pp. 611-614,
- Kim, W., Sheets, B., Paola, C., (2009), 'Steering of experimental channels by lateral basin tilting', *Basin Research,* vol.22, no.3, pp.286–301.

- King, P., Basiuk, R., Chan, B.S., and Yem, D., (2009), '*Strengthening Sustainable Tourism. Strategic Environmental Assessment of the Tourism Sector in Cambodia*', Report for the Asian Development Bank, Bangkok, 120pp.
- Kleinhans, M. G., & van den Berg, J. H., (2011), 'River channel and bar patterns explained and predicted by an empirical and a physics-based method', *Earth Surface Processes and Landforms*, vol.36, pp.721–738.
- Kleinhans, M.G., (2010), 'Sorting out channel patterns', *Progress in Physical Geography*, vol.34, no.3, pp.287-326.
- Kleinhans, M.G., Jagers, H.R.A., Mosselman, E., & Sloff, C.J., (2008), 'Bifurcation dynamics and avulsion duration in meandering rivers by one-dimensional and three-dimensional models', *Water Resources Research*, 44, W08545, doi:10.1029/2007WR005912.
- Klingeman, P. C., & Milhous, R. T., (1970), '*Oak Creek vortex bedload sampler*', Paper presented to 17th Annual Pacific Northwest Regional Meeting, American Geophysical Union, Tacoma, Washington, Oct. 14-16 1970, 17pp.
- Knighton, D.A., & Nanson, G.C., (1993), 'Anastomosis and the continuum of channel pattern', *Earth Surface Processes and Landforms*, vol.18, pp.613-625.
- Knighton, D.A., & Nanson, G.C., (2000), 'Waterhole form and process in the anastomosing channel system of Cooper Creek, Australia', *Geomorphology*, vol.35, pp.101-117.
- Komar, P.D., (1983), 'Shapes of streamlined islands on Earth and Mars: Experiments and analyses of the minimum drag-form', *Geology*, vol. 11, pp.651-654.
- Kubo, S., (2008), 'Geomorphological features and subsurface geology of the Lower Mekong Plain around Phnom Penh city, Cambodia (Southeast Asia)', *Revista Geográfica Académica*, vol 2, n.1, pp.20-32.
- Kummu, M., & Varis, A., (2007), 'Sediment-related impacts due to upstream reservoir trapping, the Lower Mekong River', *Geomorphology*, vol. 85, iss.3-4, pp.275-293.
- Kummu, M., Lu, X.X., Rasphone, A., Sarkkula, J., & Koponen, J., (2008), 'Riverbank changes along the Mekong River: Remote sensing detection in the Vientiane-Nong Khai area', *Quaternary International*, vol.186, pp.100-112.
- Lagasse, P.F., Spitz W.J., Zevenbergen, L.W., & Zachmann, D.W., (2004), '*Handbook for predicting stream meander migration using aerial photographs and maps'*, NCHRP Report 533, TRB, National Research Council, Washington, D.C., 107pp.
- Latrubesse, E.M., (2008), 'Patterns of anabranching channels: The ultimate end-member adjustment of mega rivers', *Geomorphology*, vol. 101, no. 1-2, pp.130-145.

- Latrubesse, E.M., Amsler, M.L., de Morais, R.P., Aquino, S., (2009), 'The geomorphologic response of a large pristine alluvial river to tremendous deforestation in the South American tropics: The case of Araguaia River', *Geomorphology*, vol.113, pp.239-252.
- Lawler, D.M., (1993), 'The measurement of river bank erosion and lateral channel change: a review', *Earth Surface Processes and Landforms*, vol. 18, pp.777-821.
- Lehotský, M., Novotný, J., Szmańda, J.B., & Grešková, A., (2009), 'A suburban inter-dike river reach of a large river: modern morphological and sedimentary changes (the Bratislava reach of the Danube River, Slovakia)', *Geomorphology*, vol. 117, pp. 298-308.
- Leopold, L.B., & Woolman, M.G., (1957). '*River channel patterns; braided, meandering, and straight*', United States Geological Survey Professional Paper 282-B, pp.1-85.
- Lepvrier, C., Maluski, H., Vu Van Tich, Leyreloup, A., Phan Truong Thi, Nguyen Van Vuong, (2004), 'The Early Triassic Indosinian orogeny in Vietnam (Truong Son Belt and Kontum Massif); implications for the geodynamic evolution of Indochina', *Tectonophysics*, vol. 393, no.1-4, pp.87-118.
- Leys, K.F., & Werritty, A., (1999), 'River channel planform change: software for historical analysis', *Geomorphology*, vol. 29, pp.107-120.
- Li, L., Lu, X.X., & Chen, Z., (2007), 'River channel change during the last 50 years in the middle Yangtze River, the Jianli reach', *Geomorphology*, vol.85, pp.185-196.
- Liu, H., & Sherman, D., (2008), '*Quantitative Analysis of Short-term Shoreline Change Using High-resolution Satellite Imagery and GIS Techniques',* Final Project Report, Department of Geography, Texas A&M University, College Station, 161pp.
- Lo, C.P., & Yeung, A.K.W., (2007), *Concepts and Techniques in Geographic Information Systems*, Second Edition, Pearson Prentice Hall, Upper Saddle River, NJ, 532pp.
- Lovatt Smith, P.F., Stokes, R.B., Bristow, C.C., Carter, A., (1996), 'Mid-Cretaceous inversion in the Northern Khorat Plateau of Lao PDR and Thailand', IN, Hall, R., Blundell, D.J., (Eds.), *Tectonic Evolution of Southeast Asia,* Geological Society, London, Special Publications, vol. 106, pp.233-247.
- Luu, T.T.G., Sthiannopkao, S., Kim, K-W., (2009), 'Arsenic and other trace elements contamination in groundwater and a risk assessment study for the residents in the Kandal Province of Cambodia', *Environment International*, vol.5, no.3, pp.455-460.

- MacAlister, C., & Mahaxay, M., (2009), 'Mapping wetlands in the Lower Mekong Basin for wetland resource and conservation management using Landsat ETM images and field survey data', *Journal of Environmental Management*, vol.90, pp.2130-2137.
- Makaske, B., (2001), 'Anastomosing rivers: a review of their classification, origin and sedimentary products', *Earth-Science Reviews*, vol.53, pp.149-196.
- Makaske, B., Smith, D.G., and Berendsen, H.J.A., (2002), 'Avulsion, channel evolution and floodplain sedimentation rates of the anastomosed upper Columbia River, British Columbia, Canada', *Sedimentology*, vol.49, pp.1049-1071.
- Makaske, B., Smith, D.G., Berendsen, H.J.A., de Boer, A.G., Nielen Kiezebrink, M.F., Locking, T., (2009), 'Hydraulic and sedimentary processes causing anastomosing morphology of the upper Columbia River, British Columbia, Canada', *Geomorphology*, vol.111, pp.194-205.
- Marston, R.A., Girel, J., Pautou, G., Piegay, H., Bravard, J-P., Arneson, C., (1995), 'Channel metamorphosis, floodplain disturbance, and vegetation development: Ain River, France', *Geomorphology*, vol.13, pp121-131.
- Martinez, J-M., Toan, T.L., (2007), 'Mapping of flood dynamics and spatial distribution of vegetation in the Amazon floodplain using multitemporal SAR data', *Remote Sensing of Environment*, vol.108, pp.209-223.
- Maslin, M., (2008), 'Quaternary climate transitions and cycles', IN, Gornitz, V. (Ed.), *Encyclopedia of Earth Sciences Series: Encyclopedia of Paleoclimatology and Ancient Environments*. Springer, pp.841-855.
- Maxwell, A.L., & Liu, K., (2002), 'Late Quaternary terrestrial pollen records from the monsoonal areas of continental south and southeast Asia', IN, Kershaw, A.P., David, B., Tapper, N., Penny, D., Brown, J. (Eds.), *Bridging Wallace's Line: The Environmental and Cultural History and Dynamics of the SE-Asian-Australasian Region,* Catena Verlag, Reiskirchen, Germany, pp.189–228.
- Maxwell, A.L., (2001a), 'Holocene monsoon changes inferred from lake sediment pollen and carbonate records, northeastern Cambodia', *Quaternary Research*, vol.56, pp.390-400.
- Maxwell, J. F., (2001b), 'Vegetation in the Siphandone wetlands' IN, Daconto, G., (Ed.), *Siphandone Wetlands*, Bergamo, Italy: CESVI, pp.49-54.
- Mayorga, E., Logsdon, M.G., Ballester, M.V.R., Richey, J.E., (2005), 'Estimating cell-to-cell land surface drainage paths from digital channel networks, with an application to the Amazon basin', *Journal of Hydrology*, vol.315, pp.167-182.
- Meshkova, L.V., Carling, P.A., Buffin-Banger, T., (2012), 'Nomenclature, complexity, semi-alluvial channels and sediment-flux-driven bedrock erosion',

IN, Church, M., Biron, P., Roy, A., (Eds.), *Gravel Bed Rivers: Processes, Tools, Environments*, John Wiley & Sons, Ltd., Chichester, UK, pp.424-431.

- Metz, J.M., (2010). '*A study of the record of ancient sedimentary rocks on Mars using MER, HiRISA and CRISM images*', Dissertation (PhD), California Institute of Technology, available on-line http://resolver.caltech.edu/CaltechTHESIS:04102010-113856474
- Miall, A.D., (1977), 'A review of the braided river depositional environment', *Earth Science Reviews*, vol.13, pp.1-62.
- Miall, A.D., (1981), 'Alluvial sedimentary basins: tectonic setting and basin architecture', IN, Miall, A.D., (Ed.), *Sedimentation and Tectonics in Alluvial Basins*, Geological Association of Canada, Special Paper, vol.23, pp.1-33.
- Miall, A.D., (1996), *The Geology of Fluvial Deposits: Sedimentary Facies, Basin Analysis, and Petroleum Geology*, Springer, 582pp.
- Micheli, E.R., & Kirchner, J.W., (2002), 'Effects of wet meadow riparian vegetation on streambank erosion. 1. Remote sensing measurements of streambank migration and erodibility', *Earth Surface Processes and Landforms*, vol.27, pp.627-639.
- Migeon, J., (1880), *La France - Cochinchine, Cambodge, Annam and Tonkin*, Map scale of 1:7 400 000. Paris from *Geographie Universelle.*
- Milliman, J.D., & Syvitski, J.P.M., (1992), 'Geomorphic/tectonic control of sediment discharge to the ocean: the importance of small mountainous rivers', *The Journal of Geology*, vol.100, no. 5, pp.525-544.
- Miori, S., Repetto, R., & Tubino, M., (2006), 'A one-dimensional model of bifurcations in gravel bed channels with erodible banks', *Water Resources Research*, vol. 42, W11413, doi:10.1029/2006WR004863.
- Mittelman A., (2001), 'Secondary forests in the Lower Mekong Subregion: an overview of their extent, roles and importance', *Journal of Tropical Forest Science*, vol. 13, no. 4, pp.671-690.
- Mollard, J.D., (1973), 'Air photo interpretation of fluvial features', IN, *Fluvial Processes and Sedimentation*, Research Council of Canada, pp. 341-380.
- Moon, B.P., van Niekerk, A.W., Heritage, G.L., Rogers, K.H. and James, C.S., (1997), 'A geomorphological approach to the ecological management of rivers in the Kruger National Park: the case of the Sabie River', *Transactions of the Institute of British Geographers, New Series*, vol. 22, no.1, pp.31-48.
- Moran, C.A.A., (2003), 'Spatio-temporal analysis of Texas shoreline changes using GIS technique', *Geography Master of Science Thesis*, Texas A&M University, 117pp.
- Morley, C.K., (2002), 'A tectonic model for the Tertiary evolution of strike-slip faults and rift basins in SE Asia', *Tectonophysics, vol.* 347, pp.189-215.

- Morozova, G.S., & Smith, N.D., (2000), 'Holocene avulsion styles and sedimentation patterns of the Saskatchewan River, Cumberland Marshes, Canada', *Sedimentary Geology*, vol.130, pp.81-105.
- Mosley, P.M., (1981), 'Semi-determinate hydraulic geometry of river channels, South Island, New Zealand', *Earth Surface Processes and Landforms*, vol.6, pp.127-137.
- MRC (Mekong River Commission), (2002), '*Digital Soil Map of the Lower Mekong Basin'*, Mekong River Commission, Phnom Penh, Cambodia.
- MRC (Mekong River Commission), (2003), '*Digital Hydrographic Atlas of the Mekong River at the scale 1:20 000'*.
- MRC (Mekong River Commission), (2005), *Overview of the Hydrology of the Mekong Basin*, Vientiane, 73pp.
- MRC (Mekong River Commission), (2007a), *Annual Mekong Flood Report 2006*, Mekong River Commission, Vientiane. 76pp.
- MRC (Mekong River Commission), (2007b), *Diagnostic study of water quality in the Lower Mekong Basin,* MRC Technical Paper No. 15, Vientiane, 57pp.
- MRC (Mekong River Commission), (2008), *Annual Mekong Flood Report 2007*, Mekong River Commission, Vientiane, 86pp.
- MRC (Mekong River Commission), (2009), '*Strategic directions for integrated flood risk management in focal areas*', The Flood Management and Mitigation Programme, Component 2: Structural Measures & Flood Proofing in the Lower Mekong Basin, Draft Final Report, volume 2D, 150pp.
- MRC-RFMMC (MRC Regional Flood Management and Mitigation Centre) & MRC (Mekong River Comission), (2007), '*The hydrological situation in the Lower Mekong Basin in 2006*', Paper on 3rd South East Asia Water Forum, Malasia, 9pp.
- Mund, J-P., (2003), '*Land Dynamics in rural Cambodia – From accessibility via suitability to social land concessions*', Processing of XXIII FIG Congress: Shaping the Change, Munich, Germany, 10pp.
- Murray, A. S., & Wintle, A. G., (2000), 'Luminescence dating of quartz using an improved single-aliquot regenerative-dose protocol', *Radiation Measurements,* vol. 32, no. 1, pp.57-73.
- Murray, A. S., & Wintle, A. G., (2003), 'The single aliquot regenerative dose protocol: potential for improvements in reliability', *Radiation Measurements,* vol. 37, no. 4-5, pp.377-381.
- MWBCSUP (Mekong Wetlands Biodiversity Conservation and Sustainable Use Programme), (2005), *Vulnerability Assessment of Climate Risks in Stung Treng Province, Cambodia*, 30pp.
- MWBP, (2004), '*Mekong Wetland Biodiversity Programme Home Page'* [On-line] http://www.mekongwetlands.org/ [Accessed on 10.10.2008].

- Nanson, G.C., & Croke, J.C., (1992), 'A genetic classification of floodplains' *Geomorphology*, vol.4, pp.459-486.
- Nanson, G.C., & Huang, H.Q., (1999), 'Anabranching rivers: divided efficiency leading to fluvial diversity', IN, Miller, A.J., Gupta, A. (Eds.), *Varieties of Fluvial Form*, Wiley, Chichester, pp. 477-494.
- Nanson, G.C., & Knighton, A.D., (1996), 'Anabranching rivers: their cause, character and classification', *Earth Surface Processes and Landforms*, vol. 21, pp. 217-239.
- Nanson, G.C., Jones, B.G., Price, D.M., & Pietsch, T.J., (2005), 'Rivers turned to rock: Late Quaternary alluvial induration influencing the behaviour and morphology of an anabranching river in the Australian monsoon tropics', *Geomorphology*, vol.70, no. 3-4, pp.398-420.
- National Geographic, Esri, DeLorme, NAVTEQ, UNEP-WCMC, USGS, NASA, ESA, METI, NRCAN, GEBCO, NOAA, iPC, (2011). National Geographic World Map, digital topographic basemap of the world [on-line] http://www.arcgis.com/home/item.html...5250b3241691b6 [Accessed on 20.01.2012].
- Ohnuki, Y., Shimizu, A., Chann, S., Toriyama, J., Kimhean, C. & Araki, M., (2008), 'Seasonal change in thick regolith hardness and water content in a dry evergreen forest in Kampong Thom Province, Cambodia', *Geoderma*, vol. 146, no. 1-2, pp.94-101.
- Olivera, F., Koka, S., Nelson, J., (2006), 'WaterNet: A GIS application for the analysis of hydrologic networks using vector spatial data', *Transactions in GIS*, vol.10, no.3, pp. 335-375.
- Ooi, K.G., (2004), *Southeast Asia: a Historical Encyclopedia, from Angkor Wat to East Timor*, ABC-CLIO, 1791pp.
- Osborne, M., (1996), *River Road to China: the Mekong River Expedition 1866-1873,* Second Edition, Archipelago Press, 247pp.
- Parsons, D.R., Best, J.L., Lane, S.N., Orfeo, O., Hardy, R.J. & Kostaschuk, R., (2007), 'Form roughness and the absence of secondary flow in a large confluence-diffluence, Rio Paraná, Argentina', *Earth Surface Processes and Landforms*, vol. 32, pp. 155-162.
- Parua, P.K., (2009), *The Ganga*, 1st. Edition, Water Science and Technology Library, vol. 64, p.391.
- Pavelsky, T., & Smith, L.C., (2008), 'RivWidth: a software tool for the calculation of river width from remotely sensed imagery', *IEEE Geoscience and remote sensing letters*, vol. 5, no. 1, pp. 70-73.

- Peakall, J., Leeder, M., Best, J. & Ashworth, P., (2000), 'River response to lateral ground tilting: a synthesis and some implications for the modelling of alluvial architecture in extensional basins', *Basin Research*, vol. 12, pp. 413-424.
- Peixoto, J.M.A., Nelson, B.W., Wittmann, F., (2009), 'Spatial and temporal dynamics of river channel migration and vegetation in central Amazonian white-water floodplains by remote-sensing techniques', *Remote Sensing of Environment*, vol. 113, pp.2258-2266.
- Pelletier, J.D. & DeLong, S., (2004), @Oscillations in arid alluvial-channel geometry', *Geology*, 32, pp.713-716, doi:10.1130/G20512.1
- Peng, P. & Pin, N., (2003), '*Groundwater contamination in Cambodia'*, Proceedings of the ESCAP (Economic and Social Commission for Asia & the Pacific) – IWMI (International Water Management Institute) seminar on environmental and public health risks due to contamination of soils, crops, surface and groundwater from urban, industrial and natural sources in South East Asia, Hanoi, Vietnam, December 2002, pp. 77-82.
- Philippe, M., Suteethorn, V., Lutat, P., Buffetaut, E., Cavin, L., Cuny, G., & Barale, G., (2004), 'Stratigraphical and palaeobiogeographical significance of fossil wood from the Mesozoic Khorat Group of Thailand', *Geological Magazine*, vol. 143, no. 3, pp.319-328.
- Phillips, J.D., (2009), 'Avulsion regimes in southeast Texas rivers', *Earth Surface Processes and Landforms*, vol.34, iss.1, pp.75-87.
- Poduzeće za primijenjenu Geofizika, (1968), '*Final report on seismic investigation of Stung Treng damsite, Lower Mekong Basin, Cambodia,* 1967-68. Zagreb, Yugoslavia, Geofizika.
- Pollard, A., Wakarani, N., & Shaw, J., (1996), 'Genesis and morphology of erosional shapes associated with turbulent flow over a forward-facing step', IN, Ashworth, P.J., Bennett, P.J., Best, J.L., & McLelland, S.J., (Eds.), *Coherent Flow Structures in Open Channels*, Wiley, Chichester, pp. 249-265.
- Pourghahramani, P., & Forssberg, E., (2005), 'Review of applied particle shape descriptors and produced particle shapes in grinding environments. Part 1: Particle shape descriptions', *Mineral Processing Extractive Metallurgy Review*, vol.26, no. 2, pp.145-166.
- Prescott, J.R., & Hutton, J.T., (1994), 'Cosmic ray contributions to dose rates for luminescence and ESR dating: large depths and long-term time variations', *Radiation Measurements*, 23, pp. 497–500.
- Rangin., C., Huchon, P., Le Pichon, X., Bellon, H., Lepvrier., C., Roques, D., Hoe, N.D., Quynh, P.V., (1995), 'Cenozoic deformation of central and south Vietnam', *Tectonophysics*, vol. 251, pp. 179-196.

- Raudkivi, A.J., (1993), '*Sedimentation: Exclusion and Removal of Sediment From Diverted Water*', IAHR Hydraulic Structures Design Manual, vol.6, Balkema, Rotterdam, 167pp.
- Rhoades, E.L., O'Neal, M.A. & Pizzuto, J.E., (2009), 'Quantifying bank erosion on the South River from 1937 to 2005, and its importance in assessing Hg contamination', *Applied Geography*, vol. 29, no. 1, pp.125-134.
- Rhoads, B.L., Ridley, J.D., Mayer, D.R., (2009), 'Response of bed morphology and bed material texture to hydrological conditions at an asymmetrical stream confluence', *Geomorphology*, vol.109, pp. 169-173.
- Richardson, K., & Carling, P. A., (2005), *A Typology of Sculpted Forms in Open Bedrock Channels*, Boulder, Colorado, USA, Geological Society of America, Special Publication, 108pp.
- Rodnight, H., Duller, G.A.T., Wintle, A.G., and Tooth, S., (2006), 'Assessing the reproducibility and accuracy of optical dating of fluvial deposits', *Quaternary Geochronology*, vol.1, pp.109-120.
- Rosenbloom, N.A., & Anderson, R.S., (1994), 'Evolution of the marine terraced landscape, Santa Cruz, California', *Journal of Geophysical Research*, vol.99, pp.14013-14030.
- Rosgen, D.L., (1994). 'A classification of natural rivers', *Catena*, vol.22, pp.169-199.
- Roussilon, T., Piégay, H., Sivignon, I., Tougne, L, Lavigne, F., (2009), 'Automatic computation of pebble roundness using digital imagery and discrete geometry', *Computers and Geosciences*, vol. 35, pp. 1992-2000.
- Royal Geographical Society, (1893), '*French Indo-China and Siam*', Map scale 1:4 000 000. London.
- Rust, B.R., (1978), 'Depositional models for braided alluvium', IN, Miall, A.D. (ed.), *Fluvial Sedimentology*, Memoir 5, Canadian Society of Petroleum Geologists, Calgary, pp. 605–625.
- Sapozhnikov, V.B., Murray, A.B., Paola, C., Foufoula-Georgiou, E., (1998) 'Validation of braided-stream models: Spatial state-space plots, self-affine scaling, and islands shapes', *Water Resources Research*, vol.34, no. 9, pp. 2353-2364.
- Saravuth, L., (2008), '*Meteorological Disasters and Early Warning System*', Presentation at the First International Workshop on Prevention and Mitigation of Meteorological Disasters in Southeast Asia, Kyoto.
- Sarma, J.N., & Phukan, M.K., (2004), 'Origin and some geomorphological changes of Majuli island of the Brahmaputra River in Assam, India', *Geomorphology*, vol.60, no. 1-2, pp.1-19.

- Schumm, S.A., (1968), 'Speculations concerning paleohydrologic controls on terrestrial sedimentation', *Geological Society of America Bulletin*, vol. 79, pp.1573–1588.
- Schumm, S.A., (1977), *The Fluvial System*, John Wiley and Sons, New York, 338pp.
- Schumm, S.A., (1981), 'Evolution and response of the fluvial system, sedimentologic implications', IN, Ethridge, F.G., Flores, R.M. (Eds.), '*Recent and Ancient Nonmarine Depositional Environments: Models For Exploration',* Society of Economic Paleontologists and Mineralogists Special Publication, vol. 31, Blackwell, Oxford, pp. 19–29.
- Schumm, S.A., (1985), 'Patterns of alluvial rivers', *Annual Review of Earth and Planetary Sciences*, vol.13, pp. 5–27.
- SCW (Save Cambodia's Wildlife), (2006), *The Atlas of Cambodia: National Poverty and Environment Maps*, Phnom Penh, Cambodia, 139pp.
- Seminara, G., & Turbino, M., (1989), 'Alternate bars and meandering: free, forced and mixed interactions', IN, Ikeda, S., & Parker, G., (Eds.), *River Meandering*, Water Resources Monograph, vol.12, pp.267-320.
- Sen, D.J., & Garg, N.K., (2002), 'Efficient algorithm for gradually varied flows in channel networks', *Journal of Irrigation and Drainage Engineering*, vol.131, no.5, pp.457-465.
- Siddiqui, A., & Robert, A., (2010), 'Thresholds of erosion and sediment movement in bedrock channels', *Geomorphology*, vol.118, no.3-4, pp.301-313.
- Silva, T.A.M., & Bigg, G.R., (2004), 'Computer-based identification and tracking of Antarctic icebergs in SAR images', *Remote sensing of Environment*, vol.94, no.3, pp.287-297.
- Simons, W.J.F., Socquet, A., Vigny, C., Amrosius, B.A.C., Haji Abu, S., Chaiwat, P., Subarya, C., Sarito, D.A., Matheussen, S., Morgan, P., & Spakman, W., (2007), 'A decade of GPS in Southeast Asia: Resolving Sundaland motion and boundaries', *Journal of Geophysical Research*, vol.112, B06420, doi: 10.1029/2005JB003868.
- Singh,I.B., (2007), 'The Ganga River', IN, Gupta, A., (Ed.), *Large Rivers: Geomorphology and Management*, John Wiley & Sons Ltd, pp. 347-371.
- Sklar, L., & Deitrich, W.E., (2004), 'A mechanistic model for river incision into bedrock by saltating bed load', *Water Resources Research*, vol. 40, W06301, doi:10.1029.2003WR002496.
- Slingerland, R., & Smith, N.D., (2004), 'River avulsions and their deposits', *Annual Review of Earth and Planetary Sciences*, vol.32, pp. 257-285.

- Smith, D.G., & Smith, N.D., (1980), 'Sedimentation in anastomosed river systems: examples from alluvial valleys near Banff, Alberta', *Journal of Sedimentary Research*, vol.50, no.1, pp.157-164.
- Smith, N.D., McCarthy, T.S., Ellery, W.N., Merry, C.L., Rüther, H., (1997), 'Avulsion and anastomosis in the panhandle region of the Okavango Fan, Botswana', *Geomorphology*, vol.20, pp. 49-65.
- SNMGP (Service National Des Mines, de la Géologique et du Pétrole), (1973), *Carte Geologique de Reconnaissance. République Khmére. Scale 1:200 000*, Paris.
- Spencer, J.Q.G, & Robinson, R.A.J., (2008), 'Dating intramontane alluvial deposits from NW Argentina using luminescence techniques: problems and potential', *Geomorphology*, vol.93, pp.144-155.
- Stapledon, D.H., Wood, C.C., & Harrison, J., (1961), '*Progress report on geological investigations Sambor Dam sites, Cambodia'*, Colombo Plan, Snowy Mountains Hydroelectric Authority, Cooma, 34pp. Plus drill logs and drawings.
- Stapledon, D.H., Wood, C.C.., McCahon, B.K., Harrison, J., (1962), '*Geological investigations of Sambor Dam site, Cambodia*', Geological Report, Colombo Plan, Snowy Mountains, Hydroelectric Authority, Cooma, Australia, vol.1, 61pp. Plus drill logs and drawings.
- Steinshouer, D.W., Qiang, J., McCabe, P.J.M. and Ryder, R.T., (1997), '*Maps Showing Geology, Oil and Gas Fields, and Geological Provinces of the Asia Pacific Region',* U.S. Geological Survey Open-File Report 97-470F.
- Stibig, H-J., & Beuchle, R., (2003), '*Forest cover map of continental Southeast Asia at 1:4 000 000 derived from SPOT4-VEGETATION satellite images*', TREES Publication Series D: Thematic outputs N 4, EUR 20856 EN, Germany, 22pp.
- Stouthamer, E. & Berendsen, H.J.A., (2007), 'Avulsion: the relative roles of autogenic and allogenic processes', *Sedimentary Geology*, vol.198, pp. 309-325.
- Suárez, T., (1999), *Early Mapping of Southeast Asia*, Tuttle Publishing, 280pp.
- Takagi, T., Oguchi, T., Matsumoto, J., Grossman, M.J. Sarker, M.H. & Martin, M.A. (2007), 'Channel braiding and stability of the Brahmaputra river, Bangladesh, since 1967: GIS and remote sensing analyses', *Geomorphology*, vol. 85, no. 3-4, pp. 294-305.
- Takaya, Y., (1967), 'Observations on some Pleistocene outcrops in Cambodia', *The Southeast Asian Studies*, Kyoto University, vol. V, no. 3, pp. 122-137.
- Thieler, E. R., Martin, D., & Ergul, A., (2003), '*The Digital Shoreline Analysis System, version 2.0: Shoreline change measurement software extension for ArcView'*, USGS Open-File Report 03-076.

- Timmins, R., (2006), '*Biodiversity Conservation Significance and Priorities for Action in the Mekong Ramsar Site, Stung Treng, Cambodia',* Report prepared for the Mekong Wetlands Conservation and Sustainable Use Programme (MWBP), Stung Treng, Cambodia, 124pp.
- Tinkler, K. & Wohl, E., (1998), 'A Primer on Bedrock Channels', IN: Tinkler, K., Wohl, E., (Eds), *Rivers Over Rock: Fluvial Processes in Bedrock Channels*, AGU, Washington, Geophysical Monograph, vol.107, pp.1-18.
- Toda, M., (1994), 'Bedrock channel erosion on the Upper Obitsu, Boso Peninsula: A field experiment on the influence of a fissure on erosion', *Geographical Review of Japan*, 67A, pp.14-25.
- Tooth, S., & McCarthy, T.S., (2004), 'Anabranching in mixed bedrock-alluvial rivers: the example of the Orange River above Augrabies Falls, Northern Cape Province, South Africa', *Geomorphology*, vol.57, pp. 235-262.
- Tooth, S., & Nanson, G.C., (1999), 'Anabranching rivers on the Northern Plains of arid central Australia', *Geomorphology*, vol.29, no.3-4, pp.211-33.
- Tooth, S., & Nanson, G.C., (2000), 'The role of vegetation in the formation of anabranching channels in an ephemeral river, Northern plains, arid central Australia', *Hydrological Processes*, vol.14, pp. 3099-3117.
- Tooth, S., & Nanson, G.C., (2004), 'Forms and processes of two highly contrasting rivers in arid central Australia, and the implications for channel-pattern discrimination and prediction', *Geological Society of America Bulletin*, vol.166, no. 7-8, pp.802-816.
- Tooth, S., Rodnight, H., Duller, G.A.T., McCarthy, T.S., Marren, P.M., and Brandt, D., (2007), 'Chronology and controls of avulsion along a mixed bedrock-alluvial river', *Geological Society of America Bulletin*, vol.119, pp. 452-461.
- Törnqvist, T.E., (1993), 'Holocene alternation of meandering and anastomosing fluvial systems in the Rhine-Meuse Delta (Central Netherlands) controlled by sea-level rise and subsoil erodobility', *Journal of Sedimentary Petrology*, vol. 63, no. 4, pp. 683-693.
- Try, T., & Chambers, M., (2006), '*Situation Analysis: Stung Treng Province, Cambodia*', Mekong Wetland Biodiversity Conservation and Sustainable Use Programme, Vientiane, Lao PDR, 93pp.
- Turcotte, R., Fortin, J-P, Rousseau, A.N., Massicotte, S., Villeneuve, J.-P., (2001), 'Determination of the drainage structure of a watershed using a digital elevation model and a digital river and lake network', *Journal of Hydrology,* vol. 240, pp.225-242.
- Turowski, J.M., (2009), 'Stochastic modelling of the cover and bedrock erosion', *Water Resources Research*, vol. 45, W03422, doi:10.1029/2008WR007262.

- Turowski, J.M., Hovius, N., Wilson, A., Horng, M-J., (2008), 'Hydraulic geometry, river sediment and the definition of bedrock channels', *Geomorphology*, vol.99, pp.26-38.
- TWG-F&E (Technical Working Group on Forestry and Environment), (2008), Mining Concession Zones in Cambodia, http://www.twgfe.org/Docs/Presentations/ [Accessed on 10.06.2008].
- UN, (United Nations), (1968), *Atlas of Physical, Economic and Social resources of the Lower Mekong Basin*, New York, United Nations, 257pp.
- UN, (United Nations), (1993), *Atlas of Mineral Resources of the ESCAP Region*, Explanatory Brochure, vol. 10, Cambodia, New York, 87pp.
- UNESCO, (1972), *Geological Map of Asia and the Far East*, Second edition, Scale 1:5 000 000,Explanatory notes, Paris, 100pp.
- Unwin, D.J., (1995), 'Geographic Information Systems and problems of 'error and uncertainty', *Progress in Human Geography*, vol.19, pp.549-558.
- Urban, M.A., & Rhoads, B.L., (2004), 'Catastrophic human-induced change in stream-channel planform and geometry in an agricultural watershed, Illinois, USA', *Annals of the Association of American Geographers*, vol.93, no.4, pp.783-796.
- Uribelarrea, D., Pérez-González, A. ,& Benito, G., (2003), 'Channel changes in the Jarama and Tagus rivers (central Spain) over the past 500 years', *Quaternary Science Reviews*, vol. 22, pp.2209-2221.
- Van Coller, A.L., Rogers, K.H., & Heritage, G.L., (1997), 'Linking riparian vegetation types and fluvial geomorphology along the Sabie River within the Kruger National Park, South Africa', *African Journal of Ecology*, vol. 35, pp. 194-212.
- van den Berg, J.H., (1995), 'Prediction of alluvial channel pattern of perennial rivers', *Geomorphology*, vol.12, pp. 259-279.
- van der Werff, H.M.A., & van der Meer, F.D., (2008), 'Shape-based classification of spectrally identical objects', *ISPRS Journal of Photogrammetry and Remote Sensing*, vol. 63, pp. 251-258.
- van Niekerk, A. W., Heritage, G. L., & Moon, B. P., (1995), 'River classification for management: the geomorphology of the Sabie River in the eastern Transvaal', *South African Geographical Journal*, vol.77, pp.68-76.
- Van, T.P.D., Carling, P.A., & Atkinson, P.M., (2012), 'Modelling the bulk flow of a bedrock-constrained, multi-channel reach of the Mekong River, Siphandone, southern Laos', *Earth Surface Processes and Landforms*, doi:10.1002/esp.2270.

- Vila, D., & Machado, L.A.T., (2004), 'Shape and radiative properties of convective systems observed from infrared satellite images', *International Journal of Remote Sensing,* vol. 25, no.21, pp.4441-4456.
- Vozenin-Serra, C., et Privé-Gill, C., (1991a), 'Les terrasses lluviales pléistocènes du Mékong (Cambodge). I – Bois silicifiés homoxylés récoltés entre Stung-Treng et Snoul', *Review of Palaeobotany and Palynology*, vol.67, pp. 115-132 (in French).
- Vozenin-Serra, C., et Privé-Gill, C., (1991b), 'Les terrasses lluviales pléistocènes du Mékong (Cambodge). II - Bois silicifiés hétéroxylés récoltés entre Stung-Treng et Snoul', *Review of Palaeobotany and Palynology*, vol.68, pp.87-117 (in French).
- Wang, P., Clemens, S., Beaufort, L., Braconnot, P., Ganssen, G., Jian, Z., Kershaw, P., Sarnthein, M., (2005a), 'Evolution and variability of the Asian monsoon system: state of the art and outstanding issues', *Quaternary Science Reviews,* vol.24, pp. 595-629.
- Wang, S., Chen, Z., Smith, D.G., (2005b), 'Anastomosing river system along the subsiding middle Yangtze River basin, southern China', *Catena*, vol.60, pp. 147-163.
- Wang, Z.B., Fokkink, R.J., & De Vries, M., (1995), 'Stability of river bifurcations in 1D morphodynamics models', *Journal of Hydraulic Research*, vol. 33, no. 6, pp. 739-750.
- Wende, R., & Nanson, G.C., (1998), 'Anabranching rivers: ridge-form alluvial channels in tropical northern Australia', *Geomorphology*, vol.22, pp. 205-224.
- Wentworth, C.K., (1922), 'A scale of grade and class terms for clastic sediments', *Journal of Geology*, vol. 30, pp.377–392.
- White, P.F., Oberthur, T., Pheav, S., (1997), '*The Soils Used for Rice Production in Cambodia. A Manual for their Recognition and Management'*, International Rice Research Institute, Manila, Philippines, 71pp.
- Williams, P.F., & Rust, B.R., (1968), 'The sedimentology of braided rivers;, *Journal of Sedimentary Petrology*, vol. 39, pp. 649-679.
- Wintle, A. G., & Murray, A. S., (2006), 'A review of quartz optically stimulated luminescence characteristics and their relevance in single-aliquot regeneration dating protocols', *Radiation Measurements*, vol. 41, pp.369-391.
- Wittman, F., & Parolin, P., (2005), 'Aboveground roots in Amazonian floodplain trees', *Biotropica*, vol.4, no.37, pp.609-619.
- Wittman, F., Junk, W.J., Piedade, M.T.F., (2004), 'The várzea forests in Amazonia flooding and the highly dynamic geomorphology interact with natural forest succession', *Forest Ecology and Management*, vol. 196, pp.199-212.

- Wohl, E.E., (1999), 'Incised bedrock channels', IN, Darby, S.E., Simon, A., (Eds.), *Incised river channels*, Chichester, UK, Wiley and Sons, pp. 187-218.
- Wongsomsak, S., (1992), 'Preliminary investigation on Mekong terraces in Nakhon Phanom Province: distribution, characteristic, age and imbrication', Proceedings of a National Conference on Geologic Resources of Thailand: Potential for future Development, Department of Mineral Resources, Bangkok, pp. 326-331.
- Wu, W., (2007), *Computational river dynamics,* Routledge, 494pp.
- Wyrick, J.R., & Klingeman, P.C., (2010), 'Proposed fluvial island classification scheme and its use for river restoration', *River Research and Applications*, vol. 27, no. 7, pp. 814-825.
- Wyrick, J.R., (2005), *Formation of Fluvial Islands,* Dissertation for the degree of Doctor of Philosophy in Civil Engineering, Oregon State University, 285pp.
- Yanites, B.J., & Tucker, G.E., (2010), 'Controls and limits on bedrock channel geometry', *Journal of Geophysical Research*, vol. 115, F04019, doi:10.1029/2009JF001601.
- Yanites, B.J., Tucker, G.E., Hsu, H.-L., Chen, C.-C., Chen, Y.-G. & Mueller, K.J., (2011), 'The influence of sediment cover variability on long-term river incision rates: an example from the Peikang River, central Taiwan', *Journal of Geophysical Research,* vol. 116, F03016, doi:1029/2010JF001933.
- Zanoni, L., Gurnell, A., Drake, N., and Surian, N., (2008), 'Island dynamics in a braided river from analysis of historical maps and air photographs', *River Research and Applications*, vol.24, pp. 1141-1159.
- Zhang, H., & Huang, G., (2009), 'Building channel networks for flat regions in digital elevation models', *Hydrological Processes*, vol.23, pp. 2879-2887.
- Zhang, J-F., Qiu, W-L., Li, R-Q., Zhou, L-P., (2009), 'The evolution of a terrace sequence along the Yellow River (HuangHe) in Hequ, Shanxi, China, as inferred from optical dating', *Geomorphology*, vol.109, no.1-2, pp. 54-65.

Geomorphology 147-148 (2012) 2–17

Contents lists available at SciVerse ScienceDirect

Geomorphology

journal homepage: www.elsevier.com/locate/geomorph

The geomorphological characteristics of the Mekong River in northern Cambodia: A mixed bedrock–alluvial multi-channel network

Liubov V. Meshkova *, Paul A. Carling [1]

Geography and Environment, University of Southampton, Southampton, UK

ARTICLE INFO

Article history:
Received 11 May 2010
Received in revised form 9 June 2011
Accepted 14 June 2011
Available online 27 August 2011

Keywords:
Mekong
Multi-channel network
Bedrock channels
River islands
Riparian vegetation
Tectonic control

ABSTRACT

The controls on the development of channel morphology of bedrock-constrained rivers are poorly known. The relative importance of lithological and structural control on channel alignment and character in comparison with the role of hydraulic erosion of the substratum is unclear. In addition, bedrock rivers often have a variable sediment fill and can be described as mixed bedrock–alluvial systems. The Mekong River in northern Cambodia is an anastomosed mixed bedrock–alluvial channel, but little and poorly researched. In this paper information has been gathered from diverse literature sources; digital data sets showing topography, hydrology, geology and land cover; past aerial photographs; and maps. Such data, together with field survey, provide a clear picture of the Mekong River in this region.

The channels may be classified into three types: primary, secondary, cross channels. The varying characteristics of these three help towards understanding the evolution of the modern Mekong. Similarly the two-fold classification of the islands reveals the relationship between island inundation characteristics and the annual monsoon flood cycle. The associated riparian vegetation ecotones include a rare and unusual seasonally-inundated forest. Spatial variations in lithology and structure, when combined with maps of river networks, reveals that the channel alignments locally reflect the geological factors that cause the regional topographical gradient. Fault-line constraints on the local slopes of the channel may induce backwater effects and consequent sedimentation patterns (alluvial overprints) or alternatively, steepening of the channels with concomitant reduction in sedimentation. These structural constraints, taken together, lead to the identification of a mixed bedrock–alluvial five-fold geomorphological zonation within the study area. The general absence of paleochannels, and terraces close to the modern river, indicates that the Mekong is laterally stable with a dominating channel that downcuts. Consequently, a flood surface of limited lateral extent constrains entire floods.

1. Introduction

Although there are important exceptions, for example, the Mississippi, Colorado, Nile and Danube, the dynamics and morphology of the majority of the world's largest rivers are relatively little known except at the coarsest scales of resolution (Gupta, 2007; Latrubesse, 2008; Campbell, 2009; Latrubesse et al., 2009). Remote sensing data covering extensive territories are used to provide general descriptions for particular areas rather than ground-based data. For many of these rivers, the collection of field survey data remains difficult not only due to the scale of the system but also its remoteness and inaccessibility. In particular, detailed geomorphological descriptions of large mixed bedrock–alluvial rivers are limited (van Niekerk et al., 1995; Heritage et al., 2004; Tooth and McCarthy, 2004) and there is no detailed description of channels of this type for a large river within South East Asia. The Mekong River, in the north-east of Cambodia is one such example. Access is complicated due to remoteness, and the complex bedrock–alluvial network character of the channel (Gupta and Liew, 2007) hinders navigation by vessels. The purpose of this paper is to describe the multi-channel network of the Mekong River in north east Cambodia as a precursor to reporting more detailed studies of the river geomorphology. The use of 'multi-channel' as a descriptor of the channel planform is in accordance with the usage proposed by Schumm (1968), Church (2002) and Gurnell et al. (2009) and avoids the unresolved issues of classification associated with such terms as 'anabranched' or 'anastomosed'.

The study area lies between the towns of Stung Treng and Kratie (Fig. 1). Existing regional studies are too generalised to provide detail on the river in this area and explicit local, detailed investigations of river geomorphology and hydraulics have never been instigated. Previous systematic works on the geology, tectonics, vegetation and soils of Cambodia (e.g., Crocker, 1962; Carbonnel, 1972; Legris et al., 1972; Rollét, 1972; UN, 1993; Fontaine and Workman, 1997) were carried out during the first half of the twentieth century but often not published until recently. The imposition of the Khmer Rouge (Pol Pot) regime in 1975–1979 and the following two decades of civil war

* Corresponding author. Tel.: +44 23 8059 8906.
E-mail addresses: lvm@soton.ac.uk (L.V. Meshkova), P.A.Carling@soton.ac.uk (P.A. Carling).
[1] Tel.: +44 23 8059 2214.

0169-555X/$ – see front matter © 2011 Elsevier B.V. All rights reserved.
doi:10.1016/j.geomorph.2011.06.041

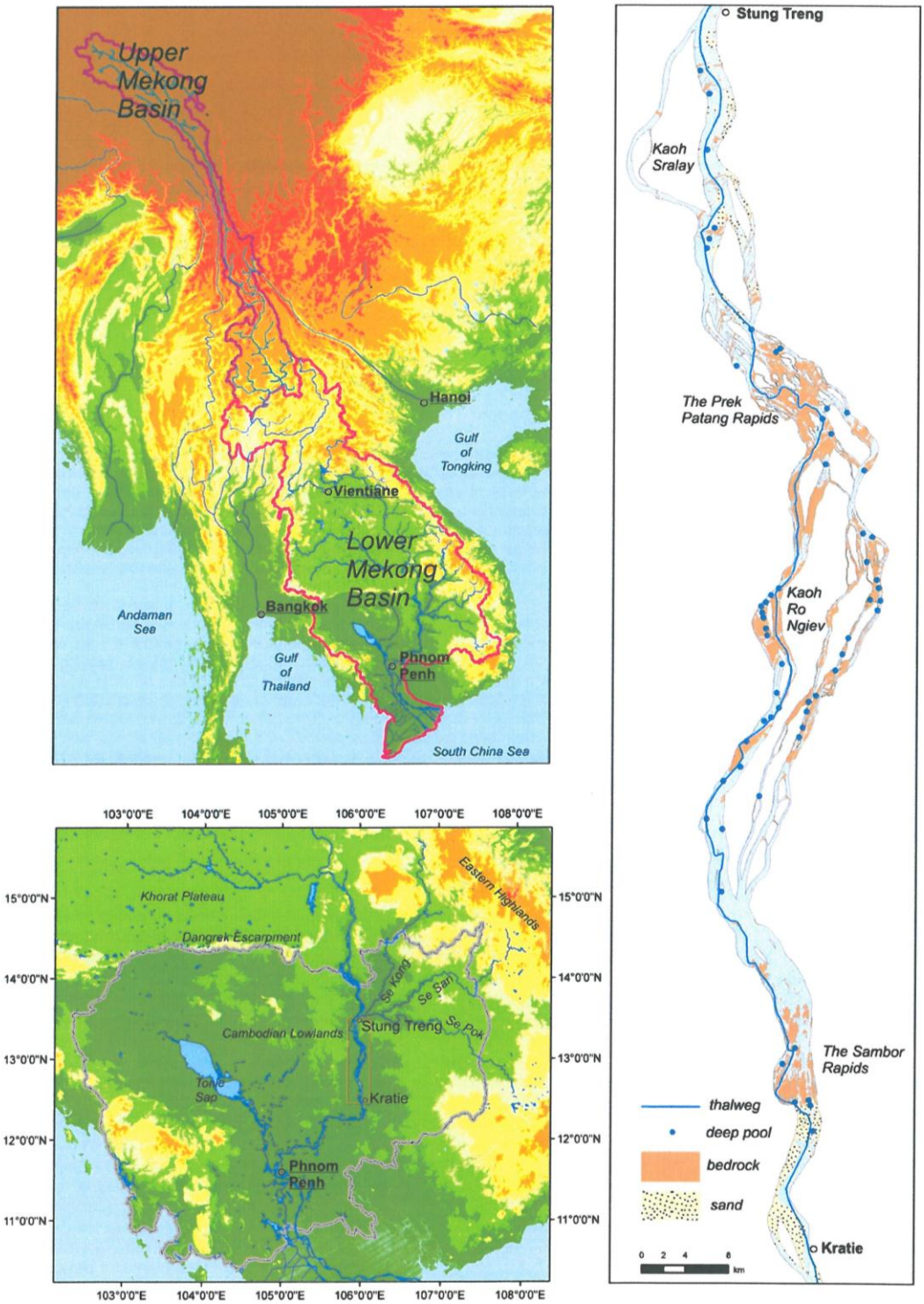

Fig. 1. Location map: the Upper and Lower Mekong Basins (left top), Cambodia (left bottom with study area boxed) and study area (right).

stopped all types of scientific exploration in the country (Kiernan, 2002). Scientific activity has resumed in the last decade and publications related to the Mekong are available from manifold sources. The majority of them either consider the area of interest at a regional scale, focusing on parts other than Cambodia, or are devoted to different geo-disciplines with only tangential relevance to river geomorphology (Hori, 2000; FA/Danida/DED, 2003; ICEM, 2003; MWBP, 2005; Try and Chambers, 2006; Gupta, 2007; Gupta and Liew, 2007; Kummu and Varis, 2007; Bezuijen et al., 2008; Conlan et al., 2008; Costa-Cabral et al., 2008; Kummu et al., 2008; Campbell, 2009).

Yet, a channel belt of up to 4.5 km width and river islands of a length from 100 m to 40 km together with complex topography, geology, tectonics, specific riverine vegetation and fauna comprise a unique environmental setting for the river and its floodway and thus deserve special attention. The importance of documenting this system is even more urgent as there are proposals to impose a series of dams on the river which would result in an impoundment from the Lao PDR border to Kratie (Fig. 1).

Thus the specific aims of this paper are to characterize the Mekong within the chosen study area in order to: 1) describe the geomorphological features of a large mixed bedrock–alluvial river of the monsoonal climatic zone; 2) specify (clarify) the geological composition of the channel belt; 3) determine the tectonic structures and their relevance to this channel type; 4) consider the factors controlling the river pattern; and 5) outline the Cenozoic history of river incision to provide context for the modern river pattern. The completed description should serve as a basis for later investigations of the Mekong.

2. Regional setting

The regional settings of the Mekong River are highly diverse because the river traverses a large portion of South East Asia. Its headwaters are located in the Himalaya at ~4970 m above the sea level and it flows for 4800 km through China, Myanmar, Lao PDR, Thailand, Cambodia, to debouche in the South China Sea via a large complex delta system in Vietnam. The total watershed area (the Greater Mekong Basin — GMB) is estimated around 795,000 km^2, the annual flow volume is ~475 km^3. The Greater Mekong Basin (GMB) is traditionally subdivided into the Upper and the Lower Mekong Basins

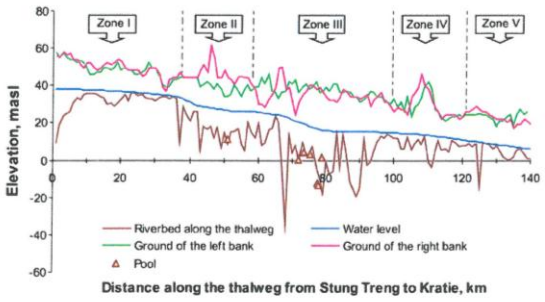

Fig. 2. The elevation of the riverbed, dry season water level, main-channel deep pools and the ground elevation of both riverbanks. Reproduced with permission from Meshkova et al. (in press). Notes: here and in Fig. 12 elevation data were obtained using cross-sections at every kilometre along the thalweg; for more information about the extent of each 'Zone', please see section 4.4. Only the deep pools along the thalweg are shown in the illustration. (Note: Bathymetric data for the riverbed profile are based on soundings performed in October 2003 by MRC for the Hydrographic Atlas of the Mekong River; Water level profile is based on the Mekong River Project data (Hunting Survey Corporation Limited) obtained in April, 1960 with horizontal scale 1:1,000,000 and vertical 1:1000; Ground elevation of the river banks is obtained using the GIS database digital layers of the Hydrographic Atlas of the Mekong River, MRC, 2003; Deep pool locations from Chan et al., 2003).

(UMB and LMB respectively) (MRC, 2005). The Mekong in the UMI is usually called the Lancang, a single bedrock channel, deeply incisec into mountainous valleys which produce more than 50% of the tota sediment supply to the LMB (Kummu and Varis, 2007). Seasona snow melt in the headwaters generates a significant portion of the annual discharge noticeable as far downstream as Kratie (Cambodia) This so-called 'Yunnan component' is important as it sustains abou 30% of the LMB dry season flow. The Chinese part of the basin is obstructed by several dams affecting the mainstream by prolongatior of the dry season immediately downstream in the LMB (Toda et al. 2004), increasing downstream seasonal water level fluctuations anc trapping sediments (Kummu and Varis, 2007).

Within the LMB, the river remains incised into bedrock as far south as Vientiane in Lao PDR. Further south the river wanders within Quaternary alluvium until it switches to a bedrock-constrained multi-channel pattern close to the border between Lao PDR and Cambodia. This pattern persists for nearly 300 km as far as Kratie in Cambodia. After passing Kratie, the river is alluvial; either single channel, braided or multichannel until it reaches the delta (Gupta and Liew, 2007; Carling, 2009).

The study area is situated within the limits of the Cambodian northern plain (Cambodian Lowlands) framed by the Dangrek Escarpment to the north that is aligned with 14°30′ latitude. The escarpment forms a natural border between the Khorat Plateau in Lao PDR, the Cambodian Lowlands and the Eastern Highlands; the latter extending north to south in eastern Indochina (Fig. 1). Hence, within the study area, low ridges that are terminations of ranges of the Eastern Highlands are the only features that provide the highest elevation marks (up to 130 m asl).

The drainage network within the LMB contributes 40 and 45% of the Mekong annual discharge for the wet and dry seasons respectively (Toda et al., 2004). At the upstream limit of the study area, the Se Kong, Se San and Sre Pok Rivers are major left bank tributaries which join the Mekong just north of Stung Treng at one conjoined confluence. These rivers make the largest single inflow to the Mekong; equal to 25% of the mean annual flow volume at Kratie (~416 km^3: MRC, 2008). There are no significant tributaries southwards within the study area, and tributaries play no part in determining the reach characteristics described below.

The climate in the South-East Asia region, including Cambodia, is controlled by the monsoon, with two main seasons alternating each other with short transition periods in April–May and October (ADB, 2007). Around 80% of the annual precipitation arrives during the monsoon season from May to October with the heaviest rainfalls between August and September. The study area annual precipitation, amounting to ~2000 mm, is distributed with a south-east/north-west gradient due to orographic effects as Cambodia is framed by mountains towards the south-west and north-east borders. The monsoon climate pattern determines, as for all South East Asian rivers, a one-peak hydrograph (Dudgeon, 1999) occasionally moderated by cyclone incursions which may produce secondary peaks in some years.

There are two hydrological stations within the study area which provide discharge measurements. The gauge at Stung Treng records river level and discharge for the Mekong since 1910 until present. It is located within a bedrock section of the river and is characterised by a stable rating. The gauge at Kratie dates from 1924 and measures stage and discharge from a 646,000 km^2 watershed area but unlike the data from the upstream Stung Treng station, the records are not continuous. More importantly the gauged section at Kratie is alluvial and unstable. Consequently there are significant shifts in the rating curve from year to year and the data must be treated with caution. Daily water level information is available (www.mrcmekong.org) whilst archive records are stored by the Mekong River Commission (MRC) and statistical summaries for these stations are published in MRC annual reports.

Until recently, suspended sediment data for the Cambodian part of the Mekong remained largely unavailable. Walling (2008) performed

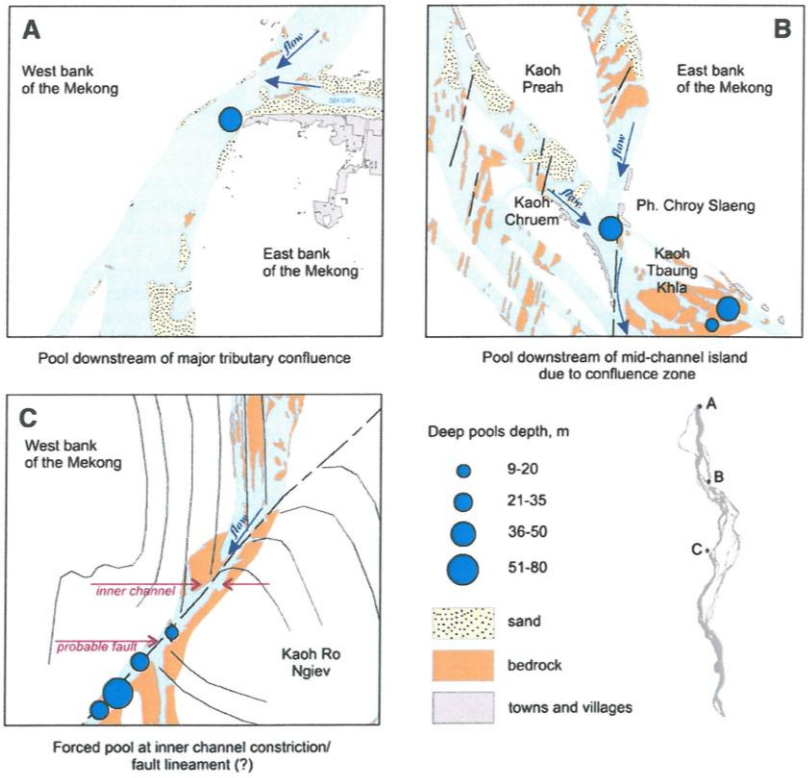

Fig. 3. Explanatory diagram indicating key concepts with respect to location of deep pools, bedrock outcrops and sand bars (Deep pool locations from Chan et al., 2003).

an evaluation of those relevant parameters for the Lower Mekong Basin based on data for the Mekong from the Chinese border to Pakse (Lao PDR). Using limited data for Stung Treng and Kratie from the 1960's, Hården and Sundborg (1992) found a positive relationship between suspended sediment concentrations (minimum = 2 mg l^{-1}; maximum = 1097 mg l^{-1}) and discharge within the study area and argued for an annual load of 146 10^6 tonnes (s.d. = 44 10^6; s.e. 14 10^6 for a 10-year period). In 1992, total suspended sediment concentration (TSS) data collection was restarted at Kratie (Try and Chambers, 2006) but these data have yet to be evaluated.

The monsoon tropical climate and the consequent annual flooding regime of the Mekong River support substantial natural vegetation cover and biodiversity, to be discussed later.

3. Materials and methods

The overall interpretation of the geomorphological and geological setting of the study area has been obtained, in part, by review of the published literature; much of which is dated. As a result, two visits to the study area (2008 and 2009, dry season) were made to: 1) check the literature against field evidence; 2) observe and classify geomorphological units comprising river landforms; 3) collect rock samples from geological sub-divisions within the riverbanks, islands and bedrock outcrops and thus to update and to extend the boundaries of the geological knowledge; and 4) document key vegetation types associated with the river and its floodway for subsequent understanding of its role in a riverine ecosystem.

The descriptive synthesis obtained from the literature and the new field data were combined with interpretation of historical (1959) aerial photographs (Committee for Coordination of Investigations of the Lower Mekong Basin, 1959) at a scale of 1:40,000, in order to delineate clearly visible structural elements in certain localities which dissect or otherwise influence the river plan-view pattern. Geological maps of scale 1:200,000 (SNMGP, 1973) based on field survey and the geology layer from 1:500,000 JICA dataset resulting from remote sensing data interpretation (JICA, 2003) were used to summarise the regional geology, moderated by the fieldwork noted above. In addition to these, a digital data set at a scale of 1:500,000 (JICA, 2003), hard and digital copies of hydrological atlas of the Mekong (MRC, 2003) and some additional general information also was obtained from the various spatial digital datasets covering the LMB at different scales and resolutions (MRC, 2006).

4. Results

4.1. Topography and morphology of the channels and floodway

The study area frames a 140 km stretch of the Mekong River between the towns of Stung Treng and Kratie in the north-east of Cambodia. Only one former paleochannel occurs within the study area, at the west bank of the Mekong 15 km upstream of Kratie (see Section 4.2).

In general, elevation reduces from the north to the south through the study area from 60 m above the mean sea level at Stung Treng to 20 m at Kratie showing the gradient to be ~3.5 m per kilometre on average. Cross-sectional vertical profiles (Fig. 2) show that the plain either side of the river is slightly undulating, which mostly likely is due to Cenozoic epeirogenic folding (UN, 1993), with swells and lows orientated approximately west to east. Often elevations correlate on

either side of the river (Fig. 2) which indicates that the river has incised predominately vertically into an ancient terrain with only local lateral movements of the river channel. The river 'macro-channel' consists of a usually planar, flooding surface, mainly comprised of bedrock, which throughout is incised within the older plain. The flooding surface locally gently elevates away from the river, the margins of the Cenozoic plain close to the river typically lie between 80 and160 m asl. The Cenozoic plain is not flooded by contemporary flows whereas the full width of the macro-channel (*sensu* van Niekerk et al., 1995) is usually flooded each year. Between the western and eastern bluffs of the ancient terrain and the macro-channel, a narrow zone may occur locally (but usually is absent) that consists of areas that do not flood annually due to elevation. The complete zone between bluffs is referred to herein as the 'river corridor'.

Relatively small alluvial floodplains occur east, west and south of Kratie Town and extend one to three km from the river. In the dry season these are extensively cultivated but in the wet season are flooded to 3 m + depth.

4.1.1. Natural levées and river terraces

Natural levées appear on both riverbanks only in the south of the area of interest immediately downstream of the Sambor Rapids (JICA, 2003) and these are well-developed further downstream on the Mekong south from Kratie. Their width varies from 200 to 600 metres; the height of levées may be up to 10–15 m above the floodplain (UN, 1968). It remains unclear whether the levées are ancient or recently active flood features but the current extent of annual flooding includes the area of their development.

The presence of river terraces within the LMB to the north of Stung Treng is ill-defined as there is only one published study north of Cambodia (Wongsomsak, 1992). Within Cambodia, Takaya (1967) and Carbonnel (1972) provide general descriptions of terraces. South of Stung Treng, Carbonnel (1972) reports several surfaces he refers to as terraces; the significant altitudes being a 100, 40 and a 20 m asl level. Carbonnel reported the 100 m terrace to be severely degraded and tectonically warped and in places covered by basalt flows. This 100 m level was dated in the 1960s as c. 650,000 years BP using fission track dating of the basalts with a similar age ascribed to tektites found on the terrace gravels (Carbonnel, 1972). In this study the relationship of the 100 m level to the modern river has not been determined with any assurance but the 40 m terrace of Carbonnel corresponds to the Cenozoic plain noted in this study and a 20 m level has been noted locally north of Kratie and southwards to Phnom Penh. Carbonnel (1972) also reported possible terrace fragments between 15 m and 2 m above the low flow level of the river. In part, these lower levels may correspond with the planar bedrock surfaces of the flooding surface of the modern river. However, locally small benches are noted in the banklines which, in terms of elevation range, correspond to cutting of the Cenozoic plain by extreme floods and the mean annual flood of the modern river (see Section 4.1.3).

4.1.2. Deep pools

Reporting and interpretation of the average depth of the river in this area would have no physical meaning because the Mekong has multiple channels, plentiful rapids, local shallows and minor pools as well as so-called 'deep pools' within all channels. The deep pools are defined as elongated bathymetric lows in accordance with the direction of the main stream flow which are significantly deeper than the surrounding riverbed (Chan et al., 2003). Among 65 pools identified in the study area, the majority are 25–30 m deep during the dry season whereas the deepest ones reach up to 80 m; areas may vary from 10 ha to 200 ha as a maximum. Deep pools provide an important habitat for fish, dolphins and other aquatic biota.

A classification of deep pools, according to Conlan et al. (2008), and their spatial allocation show their association with channel constrictions (Fig. 3) and often an alignment with the trend of known and probable faults. The number and type of observed pools contribute towards the idea that locally vertical erosion predominates rather than lateral channel movements. Narrow channels, frequently obstructed by rock outcrops, are often occupied by a constellation of closely-spaced, short, pools in contrast to alluvial reaches where pools are fewer, more extensive and relatively shallow.

4.1.3. River channels

The set of multiple channels taken together defines the Mekong river system as a complex network. However, plan views of the complete channel network allow distinction of three main channel types that collectively compose the 'Mekong river system' in the study area: (i) *primary channels* (*sensu* Knighton and Nanson, 1993) are the major waterways which are permanently wet and define the major element of the plan view of the macro-channel. These channels are influenced by regional tectonics and macro-scale geological structure (ii) *secondary channels* (*sensu* Knighton and Nanson, 1993), are smaller than primary channels, their courses influenced strongly by local sand bars and bedrock outcrops, may be dry or isolated at times of low water, (iii) *cross-channels*, as specifically defined here, are usually of similar scale to primary channels and may be seasonally

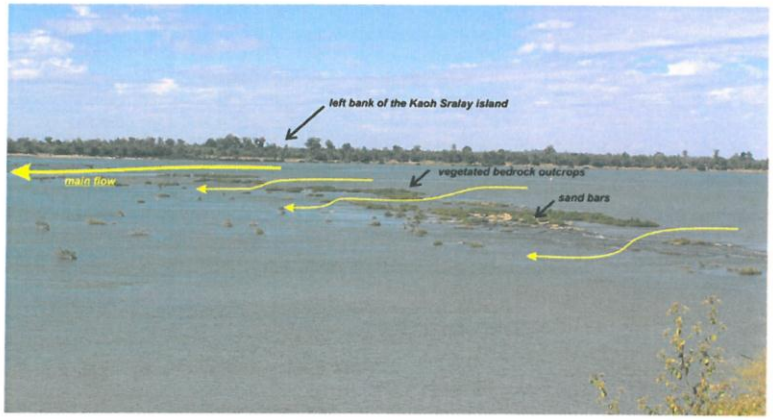

Fig. 4. The channel between the Kaoh Sralay island and the left riverbank during dry season low flow, near Kangdeisar village (few kilometres downstream of Stung Treng). Flow can over-top the barrier as well as pass it through narrow gaps, but the majority of flow is forced towards the right bank where a major gap allows flow to pass.

Fig. 5. Typical rock exposures at the Prek Patang Rapids during a dry season (13°13.425′N/106°00.387′E). Primary flow direction is away from the camera: figure for scale 1.7 m. The secondary channel at the top of the image is flowing transverse to the direction of the neighbouring primary flow (not visible).

dry but importantly they dissect large islands, the surface of the latter rising well above maximum flood levels. The primary and cross-channels network remains visible in planview during high flows, operating as a single integrated network. In contrast, the majority of the secondary channel network is only visible when the water level is low. Thus, the complexity of the channel network is strongly stage dependant.

4.1.3.1. Primary channels. The width of permanently wet '*primary channels*' (macro-channels of van Niekerk et al., 1995) starts from around thirty metres and can reach up to 4.5 km. Depth varies from branch to branch and during the low flow period is typically 5 m on average (CNMC, 2006). The *primary channels* are separated by large well-vegetated islands that rise about 7–10 m above the average low water level. The basic character of the *primary channels* is determined by the relative contribution of sand to bedrock within the channel boundaries but the intimate spatial association of sand-filled reaches and bedrock reaches allows the definition of the system as a mixed bedrock–alluvial river.

Sand bars are classified accordingly to Church and Jones (1982) in the terms of size and location as: longitudinal, lateral, diagonal and medial. Longitudinal bars of considerable dimensions (100 m to 1 km in length) are situated at the upstream end of main islands; where the *primary channels* broaden significantly, lateral (point- and counter-point) sand bars can be observed adjoined and elongated (up to 2 km) against the river/island banks. Diagonal bars are found at the locations where the water slows down after passing over bedrock outcrops; the length of these bars can be estimated at up to 800 m. The smallest, (length scale 10s of metres) but, perhaps, the most numerous medial bars are located all around submerged rocky exposures and are well exposed only during the dry season. The form and volume of the first three types are persistent year to year and in some instances form a significant 'alluvial overprint' within the bedrock channel. Meanwhile small medial bars maintain their spatial locations year to year but change shape and volume and are thus seasonal in character unless 'fixed' by vegetation.

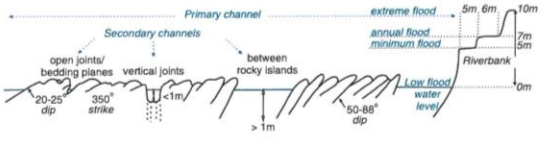

Fig. 6. Looking along strike of beds at the Prek Patang Rapids (modified from sketches by Stapledon et al., 1962). Main flow out of image.

Variations in the lithology of the bedrock in combination with local tectonic structure determine the appearance of rock outcrops within the river system. Within the study area, the rock types include a range of sedimentary, volcanic and metamorphic formations which vary from north to south (see Section 4.2). Outcrops of metamorphic rocks within the channels from Stung Treng to the Prek Patang Rapids (~20 km river section) form narrow extensive parallel ridges oblique to the flow direction (Fig. 4). These lineated structures form natural barriers, acting like low artificial weirs, and during the low water season are visualised as shallow waterfalls and rapids. Some of them appear to coincide with probable fault lines dissecting the area.

Elsewhere, for example at the Prek Patang Rapids, the appearance of the rock outcrops differs from those within the metamorphic formations, as metamorphic rocks are replaced by broad fields of intrusive volcanic and pyroclastic rocks (Fig. 5) which are manifest as extensive bedrock platforms. As the majority of all these various rock types are submerged during the high water period, frequently the visible rock surfaces are water-smoothed and characterized by fluvial abrasion marks.

The composition of the basement rocks becomes more diverse downstream of the Prek Patang Rapids. Prevailing sedimentary units are interstratified with volcanic and metamorphic formations in the form of ridges parallel to the main flow direction. Overall, the proportion of outcrops within the primary channels is decreasing north to south until it becomes completely absent, whilst at the same time the channel alignments are increasingly adjusted to the bedrock strike and to a series of faults (see Section 4.4). The most southerly outcrops are a mix of sedimentary and volcanic rocks, that densely pack the main single channel as the Sambor Rapids. South of the Sambor Rapids the river is alluvial.

4.1.3.2. Secondary channels. Given the geological and structural control, the local planview pattern of outcrops defines the appearance of a network of *secondary channels* that may be dry during low flows. However, often these channel networks remain intimately connected with the primary channels during low flows and so cannot be considered to be 'flood channels' active only during high flows. These channels are usually less than 30 m wide and may be deep, narrow channels between rocky islands or slots formed along zones of near parallel vertical joints and bedding planes. Importantly, because of

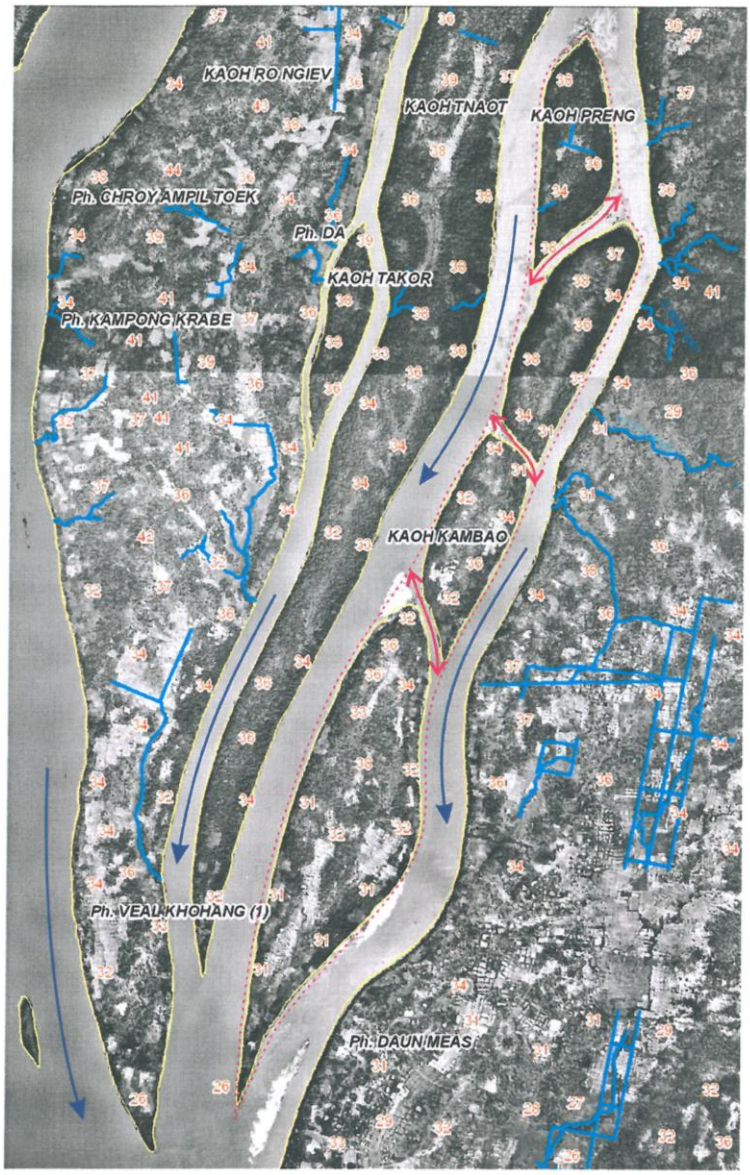

Fig. 7. River cross-channels upstream of Sambor Rapids. Primary channels shown by arrows and three persistent cross-channels shown by bi-directional arrows. Dashed line depicts contour of the initial island before division by cross-channels. Aerial photograph (Committee for Coordination of Investigations of the Lower Mekong Basin, 1959), courtesy of MRC. Island contours obtained from MRC Hydrographic Atlas (MRC, 2003) and demonstrate island stability between 1959 and 2003.

the local structural control the alignment of the *secondary channels* may be acute to that of the *primary channels*, including obtuse alignments at 90° or more.

Although these channels convey water during high monsoon stage, at that time they are completely inundated and their effect on the bulk flow structure is unknown. Despite being often obtusely angled, and within dense stands of low woody shrubs, the majority remain open without substantial sedimentary fill, which is a point returned to within the 'Discussion'. Locally, joints are filled by sand, pebbles and vegetation roots. This *channel type* can also be observed at the Sambor Rapids. A cartoon of the nature of primary and secondary channels at Prek Patang Rapids is shown in Fig. 6.

4.1.3.3. Cross-channels. This kind of channel is defined as a comparatively narrow alluvial river channel (in contrast to primary channels) connecting two primary channels by flowing across a large island at an angle that is acute to the flow direction within the primary channels. As is demonstrated in the next section, these islands are not alluvial bars and so the cross-channels cannot be classified as 'bar-top channels'. In each case the *cross-channels* 'appear' simply to 'cut' a

Fig. 8. Example of seasonally-inundated forest at the northern end of Kaoh Toan Han island(13°12.009′N/105°57.966′E). Flow left to right. Note buttress roots of the tree centre foreground. Aerial roots and lower branches generally are flow-aligned in the downstream direction.

previously undivided island onto two or more separate parts (Fig. 7). By correlating the elevations on the islands and the Cenozoic plain on either side of the river, the surfaces of the higher islands can be shown to largely be extensions of the surfaces of the Cenozoic plain. Often the cross-channels occupy slight topographic lows across the islands that can be also seen on the adjacent plains. The inference is that the cross-channels occupied the topographic hollows as the main channels have incised. As a result it may be concluded that the cross-channels .are more ancient than the secondary channels; the latter only developing once incision reached the basement. During the dry season, cross-channels may remain wet, but usually they are partly dry due to their elevation and due to bars that accumulate at the entrance or exit of each channel. These bars may become persistent such that some cross-channels become alluviated with mature tree growth, or the bars may be ephemeral such that the channels can be open one year and closed another. The channel beds are predominately sand with a small admixture of fine gravel and may be characterised by fluvial dunes and ripples with seasonal development of aeolian dunes and ripples and growth of annual plants. However, a number of *cross-channels* have considerable depth and contain running water all through the year. Fig. 7 presents an example of persistent cross-channels which have been stable in planview and partially dry during low water periods for a long time (i.e. from at least 44 years ago).

4.1.4. River Islands

River islands can be classified according to their elevation and consequent differences in morphology. The first category is comprised of *major islands* in term of overall large plan area that have their highest elevations well above mean annual flood level. There are about 100 such islands within the study area boundaries. In a context of length, the biggest one, Kaoh Ro Ngiev is nearly 40 km long (Fig. 1); the few others that are significantly elongated are from 10 to 17 km in length. Maximum width of the islands can be up to 5.6 km but mainly this parameter is 2–3 km. As noted within section 4.1.3, the sub-aerial vegetated surface of the islands is similar to that of mainland, often mimicking the swells and lows of the high plain surface (Fig. 2) and sometimes can be slightly higher. As such the surface of these islands must be of similar age to the Cenozoic plain either side of the river. Usually, the main island surfaces lie between 7 and 10 meters above the average low water level, they have steep bank lines and the majority of the island margins might get flooded very occasionally whereas the 'core' is never flooded. These major islands often seem to have a significant alluvial component to their mass formed around bedrock cores, with well-developed soils over large parts of the higher surfaces and raw alluvium in those areas that flood occasionally.

However, if the elevation of the island is less than 7 metres above low flow water level, it falls into a category of *seasonally inundated islands* which can be observed commonly throughout the multi-channel sections of the Mekong. These islands usually are of smaller plan area than the major islands. The banks of seasonally flooded islands are often low angle, smoothly sloping towards the water surface in contrast to the high, steep and abrupt cut-banks of the major islands. Seasonally flooded islands are abundantly vegetated by specific trees and bushes which comprise an important ecotone of the fluvial environment. The riparian vegetation often occupies sandy dunes formed by the river during the flooding period and during the dry season some water still remains in shallow ephemeral scour pools and channels crossing the islands in parallel to the mainstream flow (Fig. 8). As a rule, these seasonally inundated islands have a small alluvial component to their mass and little or no soil development except on the highest prominences and may be predominately bedrock complexes. This class of island is of low altitude and has none of the characteristic swells and lows of the high plain surface. Thus the island surfaces are younger than the major islands. There are two possibilities to explain the occurrence of seasonally inundated islands. One is that the rocky shoals on which they are developed trapped sufficient sediment to allow the growth of specialised tree species which further retard flow velocities and promote additional alluviation. The alternative is that they are dissected and eroded plinths – remnants of large islands. Currently it is not possible to choose between these possibilities.

Fig. 9. Weathered granite outcrops at an island (12°54′42.8″N/106°00′27.3″E) typically inundated by wet season flows. The bent tree indicates flow direction from right to left and the flood level (note the woody debris in the tree top) at approximately 5 m above the ground.

4.2. Geology and tectonics

In order to properly understand the influence of the geology on the river channel patterns it is necessary to describe the geology and tectonic setting in some detail as this information is not available elsewhere as a coherent statement. The territory of Cambodia is situated within the Indochina tectonic terrain, which also includes a southwestern part of China, eastern part of Thailand, Lao PDR and Vietnam (Lepvrier et al., 2004). During the Palaeozoic, two independent Precambrian continental terrains of Sibumasu and Indochina were separated from one another by branches of the Palaeotethys Ocean. The collision between them has resulted in consolidation of two geoblocks throughout the full (Indosinian) orogenic cycle. The two major strata of the Terraine Rouge and the Grés Supérieures of the latitudinal strike are widespread in the north-east of the country, including the study area. These strata were formed and faulted during the orogeny dated to the Triassic and Jurassic but possibly late Permian (Dickins et al., 1997). Lines of regional faults as well as synclinal/anticlinal axes observed within the study area are characterised by north-west/south-east directions across Cambodia (UN, 1993). Post-Indosinian tectonic adjustments to the Cambodian territory are characterised by uplifting and erosion events during the Cretaceous and Palaeogene Periods. The most recent Neogenic and Quaternary surfaces were formed in continental conditions under the influence of weathering and fluvial processes and were effected by minor tectonic movements and volcanism during the Quaternary in the Khorat Plateau area (Carling, 2009).

Terrain Rouge (red terrain) sedimentary deposits extend in a west-east direction and can be observed as far as 30 km downstream of Stung Treng. The name of this unit is due to the dominating continental red beds comprised of sandstones, conglomerates and siltstones. Together with "Gres Superieures" (see below) these deposits comprise the Lower and Upper "Indosinias" respectively (Hutchinson, 1989). The thickness of the Terrain Rouge deposits may be up to 2000 m; they generally grade upwards from marine through lagoonal to continental sedimentary units. Associated with this formation, volcanic products such as rhyolites, dacites, andesites, diorites and equivalent tuffs, (ferruginous) quartzites and quartz albitophires appear in the form of lava flows, dykes and sills (UNESCO, 1972). Abundant intercalations of these rocks are observed within the in-channel bedrock outcrops of the Prek Patang Rapids.

The appearance of sedimentary units of the Terraine Rouge varies from massive to thin, fine to coarse graded, hard to weakly cemented (UN, 1968). In the vicinity to Stung Treng, layers of red sandstones are described as slightly folded, but mainly sub-horizontal continental and lagoonal facies with well recognizable joints and bedding planes (Poduzeće za primijenjenu Geofizika, 1968). Also, outcrops of sandstones frequently occur within the riverbed (SNMGP, 1973) from Stung Treng up to the Prek Patang Rapids and occur at the surface as exposures of folded beds, transverse to the river course, immediately downstream of the rapids. The exposures coincide with delineation of possible fault lines. Rock samples collected at these locations are meta-sandstones which together with a tuffaceous component is evidence for regional metamorphism and active volcanism during the Indosinian orogeny.

The Grés Supérieures (upper sandstones) is the Upper/Middle Jurassic sub-division of Indosinias comprising the South-East (Dalat) Fold Belt (UN, 1993). It occurs on a base of Terraine Rouge sediments and can be distinguished from the latter by lithological constitution or superimposition. Generally, Grés Supérieures sandstones, conglomerates, marls and shales are similar to Triassic bottomset beds (Hutchinson, 1989). Light colour, coarse-grained quartz sandstones may be cemented by argillaceous material, but frequently they are not. Intercalations or nodules of chert are likely to be found.

Volcanic rocks are represented by andesites/diorites and their tuffs, similar to those associated with the Terrain Rouge. However, there are granitic and granodiotic intrusions belonging to the Jurassic–Early Cretaceous Diorite–Granodiorite Suite (Dinhquan Complex) (UN, 1993) which can be seen at the vicinity of the Sambor Rapids. Rocks of this intrusive complex form stocks, plugs and batholiths sparsely through the region, being mainly exposed in the Dalat region of Vietnam (UNESCO, 1972). Radiometric dates of the granites

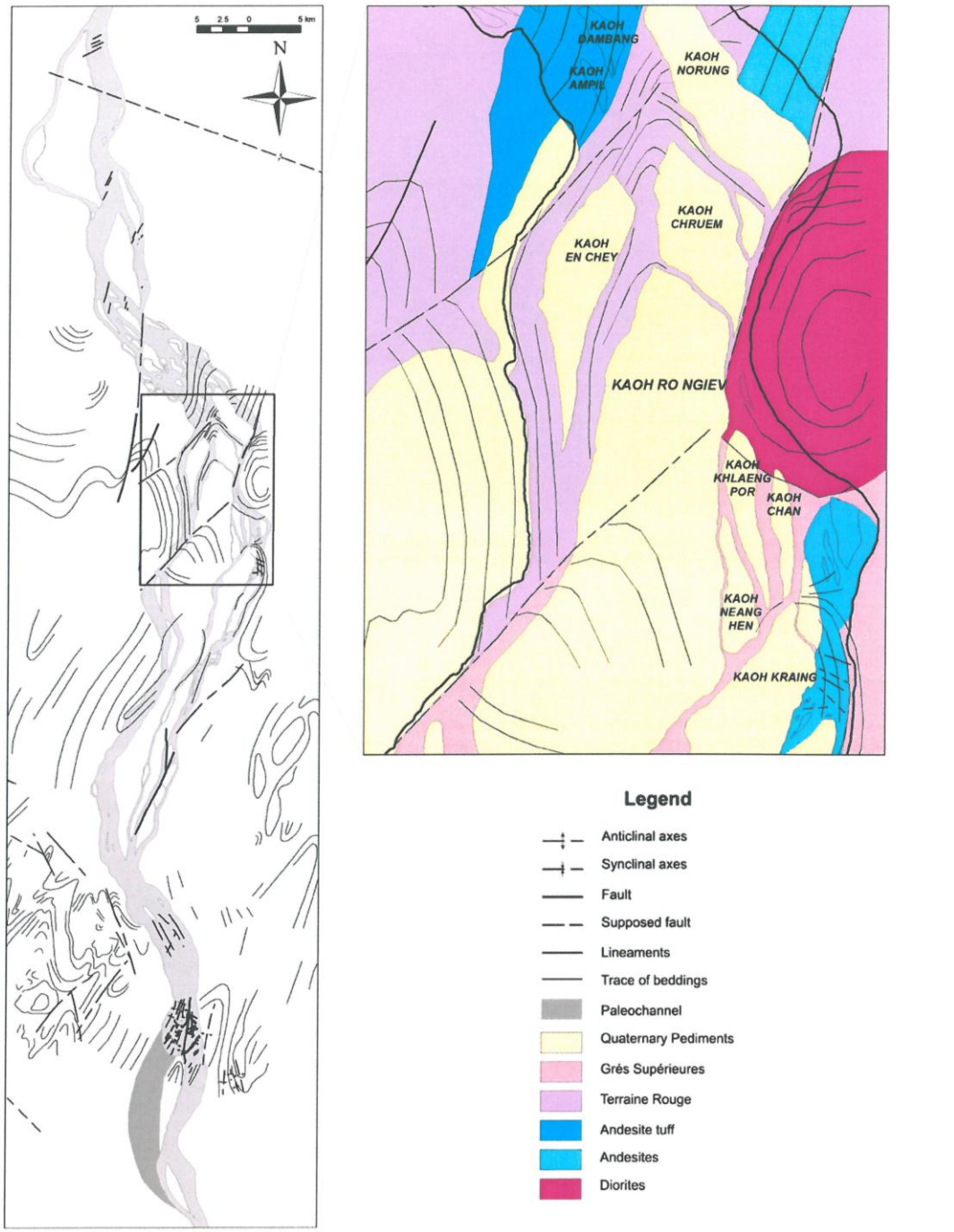

Fig. 10. Tectonic and structural elements of the study area (left) and updated geological units of the sample sub-area (right). Based on Stapledon et al. (1961, 1962); SNMGP (1973); JICA (2003); MRC (2003); interpretation of aerial photography (Committee for Coordination of Investigations of the Lower Mekong Basin, 1959) and rock samples collected by the authors.

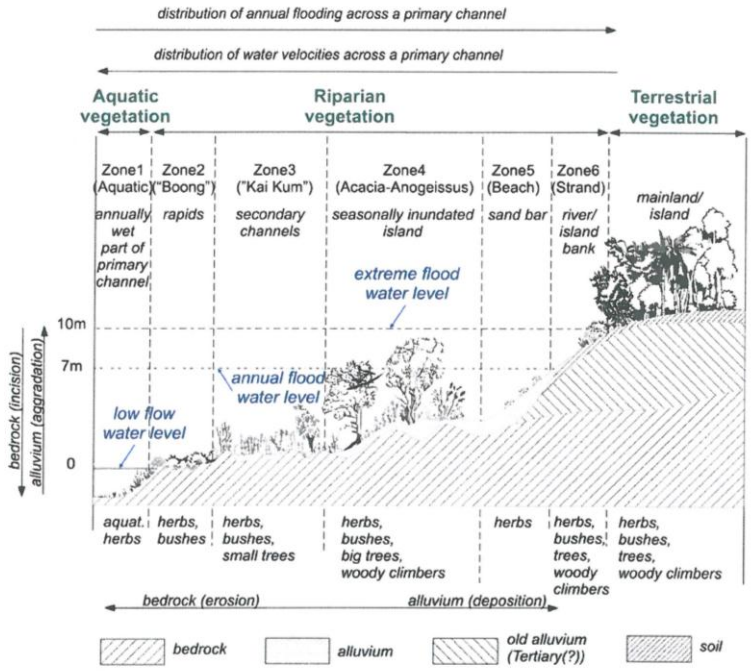

Fig. 11. Stylised cross-section profile of vegetation types and related fluvial processes observed at the mixed-bedrock alluvial sections of the Mekong in Cambodia (modified from Bezuijen et al., 2008). The core of the mainland/island may be also represented by bedrock.

range from 64 to 172 My (UN, 1993). The thickness of effusives associated with Grés Supérieures at some locations may vary from 300–400 m up to 1000 m (Dickins et al., 1997).

A Neogene–Quaternary plain surface consisting of "old alluvium" dates to 650,000 years BP (UN, 1993) and consist of sands, silts, gravels and claystones. These gravel-rich sediments extensively cover areas of older bedrocks on the west and east banks of the river and comprise the majority of the larger islands within the study area. The thickness of the old alluvium can be up to 7 to 10 m, although the origins of the old alluvium remain unclear. Exposures of volcanic rocks found within primary channels are considerably weathered by sub-aerial processes and sometimes characterised by the development of hydraulically controlled erosion features such as potholes, furrows, polished surfaces, scallops and obstacle marks, reflecting divergent patterns of flow direction. The larger examples may form chains of linked depressions which can contain stagnant or flowing water through the dry season and so collectively comprise examples of smaller *'secondary channels'*. The sculpted forms noted above can only be observed and studied during periods of low water. The lack of evidence of signs of chemical weathering and biological growth at these lower elevations supports a supposition of dominance of active hydraulic erosion (Wohl, 1999) at lower elevations within both primary and secondary channels within the study area. Weathering acting at the macro-scale is evident most visually in the case of volcanic rocks separating into distinct blocks along joints and other fissures which edges are then subject to a degree of fluvial rounding. As shown in Fig. 9, the conformability of the alignment and dip of the 'fitted' boulders testifies to the original presence of a massive but jointed rock body the joints of which have been subject to weathering.

Interpretation of the aerial photography shows several certain and probable NE–SW faults and well-defined contorted beds (Fig. 10). Triassic-Jurassic structures can be observed crossing both channels and island surfaces and continuing as surface features on the mainland either side of the river. The strike of bedrock outcrops within the Prek Patang Rapids is not as clear as everywhere else due to the ongoing vertical bedrock incision indicated by the numerous sculpted forms. Nevertheless, the relatively narrow river corridor demonstrates that only minor lateral migration of the river has occurred as it has incised into the ancient terrain. More-over there is only one major paleochannel in the study area (at Sambor; Stapledon et al., 1961, 1962) which indicates the relative lateral stability of the course of the Mekong. The shift of the river course at the Sambor rapids from west to east into its modern configuration may be related to movement of a large fault

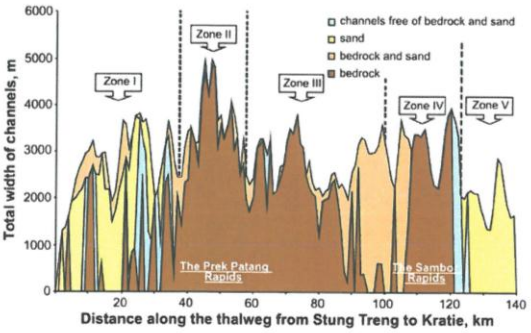

Fig. 12. Character of each channel within a cross-channel and total width of the macro-channel of the Mekong within the study area from Stung Treng to Kratie. Based on the digital data set (MRC, 2003). Reproduced with permission from Meshkova et al. (in press). Please, note that sand features of zones II and III are not indicated due to their insignificant extent.

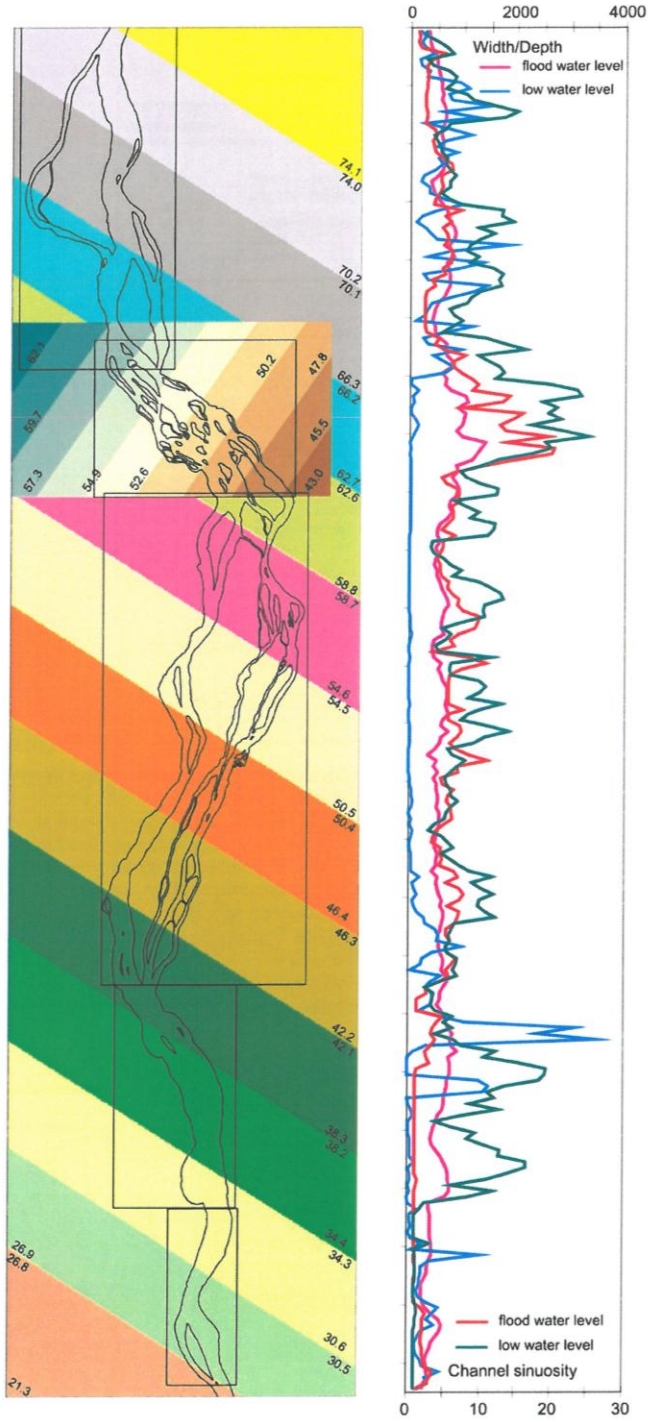

Zone I includes bedrock-alluvial reach of the Mekong between Stung Treng and the Prek Patang Rapids. Main channels are wide, rocky river bottom exposed over the dry season oblique to the main stream direction, sand bars are well developed. Character of observed outcrops changes within latitude from the closely spaced parallel ridges of the Terrain Rouge sandstones extended 40° to NE to gneisses, meta-sandstones and andesites towards the Prek Patang Rapids. Outcropping rocky ridges form rapids and shallow waterfalls. In the south of this zone, lineation of bedrocks is coincident with probable parallel fault lines of the same direction. Main islands are flooded occasionally; three of them have settlements. Bank erosion areas, mainly due to confluence flow convergence are rare.

Extent of **Zone II** is comprised by the Prek Patang Rapids. Within the study area the width of the Mekong at this zone reaches maximum value of 4600m. However, the broad area is nearly entirely occupied by vegetated outcrops of diverse volcanic, sedimentary and sedimentary volcanic bedrocks. Bedrock fluvial erosion comprises variety of sculpted forms. River depths are generally low, apart from those for the inner channel suitable for navigation. Rapids and shallow waterfalls appear frequently. Among 30 islands in this area there are those from the seasonally inundated category which provide a unique habitat for a number of species. Deep pools are rare as are areas of bank erosion.

Kaoh Ro Ngiev island is the biggest within the study area and is the key feature which is determining the extent of the **Zone III**. Streamlined main islands are elongated and frequently, apart from primary channels, are divided by so-called cross-channels. Narrow main channels are characterised by abundant deep pools. Bedrock outcrops are volcanic and sedimentary rocks confined by structural tectonic elements. The proportion of outcrops within the channels is decreasing north to south until complete absence.

At the upstream of **Zone IV** river is represented by a single channel mainly free of sandbars and bedrock outcrops, however multi-channel character can be observed further downstream. It is expressed by the secondary channels network at the surface of bedrock exposures of the Sambor Rapids.

The Mekong at the **Zone V** is a single meandering alluvial channel with large sandbars and mid-channel island. Natural levées appear on both riverbanks, modern floodplain is extending several kilometres inland.

Fig. 13. Geomorphological zones of the study area. Left: study area with frames suggesting an extent of each zone; background surfaces indicate regional and local (Zone II) topography trends based on 50 m DEM (MRC, 2006).

dissecting the channel in the north-south direction at this location (Fig. 10). This conjecture is the subject of on-going investigation by the authors. Thus, although it is clear that many channels are fault-aligned, only at Sambor does there appear to be evidence for fault movement influencing the locus of the main river course.

4.3. Vegetation and soils

The monsoon tropical climate and the consequent annual flooding regime of the Mekong River support substantial natural vegetation cover and biodiversity. In alluvial systems, vegetation is identified as one of the key factors controlling multi-channel river patterns by increasing channel roughness leading to flow reduction, channel narrowing and decrease of a channel gradient, protecting river banks against erosion, trapping sediments resulting in island forming processes and by providing the woody debris that forms wood jams consequently blocking minor channels over the flood periods (Nanson and Knighton, 1996; Tal et al., 2004; Gurnell et al., 2009; Osterkamp and Hupp, 2010). Similarly, the distribution of plants within multi-channel, mixed bedrock–alluvial systems may intimately effect the regime of sedimentation and the succession stages may indicate channel evolution processes such as channel age, sediment and flood fluxes as has been shown for other rivers (Moon et al., 1997). In this study an overview of the vegetation supports the interpretation of geomorphological structures and river processes across the channel belt.

There are three major vegetation associations observed within the Mekong and its riparian zone in north-eastern Cambodia (Bezuijen et al., 2008). A terrestrial group includes (a) evergreen broad-leaved moist, (b) dry deciduous, and (c) mixed and bamboo (secondary) forests. The first three forest types represent the natural vegetation of the mainland and only locations subject to expansive agriculture, logging or fires are occupied by the bamboo (secondary) forest patches (Mittelman, 2001). The vegetation cover of the major islands mimics that of the mainland unless disturbed by humans. The terrestrial vegetation rarely gets flooded, e.g. during extreme flood discharges when the period of inundation does not exceed one month.

The riverine vegetation of the Mekong primary channels and its islands is classified into six zones (Fig. 11) accordingly to the floristic components and specific environmental conditions (substrate, flow regime, sediments) comprising its habitat (Bezuijen et al., 2008). The zones are laterally distributed away from the primary channels and for a given elevation correspondence to a range of river stages, and hence annual duration of submergence, associated with the annual discharge regime. The longitudinal distribution of these zones varies accordingly to the bedrock/alluvium content comprising the river.

Water is essential for the life-cycle of aquatic plants (zone 1) therefore they occur only within permanently wet parts of primary channels. Riverine vegetation of zones 2, 3 and 4 requires a bedrock substrate which provides root-hold in fissures, nutrients from the water and sediments. Larger trees often have buttress roots to enable them to withstand strong currents occurring during floods as well as aerial roots. The three zones 2 through 4 are recognised locally and named from the dominant plant species as: "Boong", "Kai Kum" and trees (Acacia-Anogeissus) species. Together the zones represent components of the Mekong 'seasonally-flooded forest' ecosystem framed by primary channels edges. The uniqueness of this forest is that it is composed of highly specialized rheophytic and amphibious flora adapted to partial or full submergence during most of the year, apart from the dry season. As seen on Fig. 11, the variety of the 'flooded forest' species increases from zone 2 to zone 4 in accord with the increase in the quantity of sediment covering the bedrock and the reduction in the depth and duration of inundation: from herbs and bushes (zones 2, 3) to trees up to 15 m tall (zone 4) (Maxwell, 2009). Small riverine trees (zone 3) and bushes (zone 2 and 3) are characterized by a 'water-swept' appearance due to annual submergence within strong currents (Try and Chambers, 2006). Taller trees of the Acacia–Anogeissus group have aerial roots growing up to 4 m from the ground (Fig. 8) and often the tree crowns accumulate debris brought by previous floods (Fig. 9). It was noticed that a shoreline band of the species *Anogeissus rivularis* found in the riverbed community indicates a short time exposure of rocky or pebbly substrate and strong currents during flooding. Meanwhile the *Acacia* plants grow at higher elevations subject to short inundation during the flood season where gentler currents are expressed through an abundance of sandy deposits (Timmins, 2006). In planview, seasonally-flooded trees often form ridges that parallel the direction of the main river channels with sand bars developed between the trees as vague, incomplete ridges. An ecosystem analogous to the Mekong flooded forest called "várzea"or "igapo˜" exists in the Amazon River in Brazil (Franzinelli and Igreja, 2002; Wittman and Parolin, 2005).

Sandy beaches along riverbanks (zone 5) and islands are sparsely vegetated by seasonal opportunistic herbs but vegetation is predominantly absent. 'Strand' vegetation (zone 6) consists of terrestrial plants found on the mainland that are tolerant of disturbance.

The zones of riverine vegetation are sensitive to the presence of bare rock and the accumulation of sand-splays and large sand-bars that constitute the fluctuating annual storage of sediment moving through the system. Consequently, it can be assumed that the sensitive balance between the two processes of sediment deposition and entrainment within the river across the channel belt is essential to maintain the ecotones.

There are six soil types identified within the study area accordingly to Crocker (1962). Those are brown alluvial and alluvial soils, red-yellow and plinthite podzols, grey hydromorphics, and acid lithosols. Taken together the distributions of the brown earth alluvial soils and the alluvial soils help map the extent of flooding of the modern Mekong; the later soil type indicating areas where flooding events are frequent. In any case, the soils maps in NE Cambodia are in need of revision.

4.4. Geomorphological zones

A regional zonation of the area has been performed considering only the terrestrial ecology (FA/Danida/DED, 2003) and more recently the floristic composition of the in-channel vegetation has been assayed (Bezuijen et al., 2008). However, reviewing the known geomorphologic characteristics of the Mekong within the study area, several different and easily recognizable streamwise *longitudinal* geomorphological zones can be distinguished. Initially, the extent of each zone can be defined with respect to planview variations of sand/bedrock composition throughout the channel belt (Fig. 12). The attributes of the river in each zone are given in Fig. 13.

5. Discussion

It is well known that in the presence of cross-stream tectonic tilting, rivers are attracted to the maxima in the subsidence rate (Kim et al., 2009). However, the known tectonic history of the region evidently is not a substantive control on the primary channel network geometry. The study area sits at the centre of the Sundaland coherent lithospheric block which is rotating about an axis such that, in the study area, lateral movement is less than 2 mm a^{-1} with negligible internal deformation (<7 nanostrain a^{-1}) with very low rates of shallow seismicity (Simons et al., 2007). The river today is incised into a narrow corridor some 5 km wide and shows no preference to align with either the east or west margins as might be expected if subsidence or uplift occurred either to the east or to the west. The lack of abandoned primary channels within the corridor testifies to the plan-view stability of the river during the Quaternary. The single example of an abandoned channel (paleochannel) at Sambor seems to be related to local faulting rather than regional tectonic adjustments.

Instead and fundamentally, the pattern of the bedrock channel network within the Mekong is governed by: 1) regional balance between the seaward gradient and the tectonic stability of the region coupled with the distribution and alignment of the major fault lines and geological structures; 2) a local control induced by the local structure which constrains the course of the individual channels at the local scale. Thus there are two plan-view scales of control evident in the channel network patterns.

Category 1 applies chiefly to the primary channels (Fig. 6) and category 2 applies chiefly to the secondary channels. In the case of normal faults transverse to the main flow if the down-throw block is in the seaward direction, the fault itself will not divert flow at the regional scale although flow may later adopt the lineament of the fault plane but only locally. Rather major diversions seem to be mediated by tectonic up-throws in the seaward direction (of limited vertical surface expression) forcing the flow to follow the alignment of the fault scarp. Thus the primary channels (Fig. 13) with the distinctive zig-zag regional pattern conform to control (1), with the river being sequentially forced to the south-west by SW to NE trending structure before breaching the major rockbed linear structures and flowing again down the regional topographic gradient to the south.

Whereas the origin and the control which dictates the locus of bifurcation nodes have been well-studied within alluvial branching systems (Kleinhans et al., 2008) the control on the secondary channel abrupt course changes and bifurcations is less evident within bedrock systems. Although the spatial correlation of channels with linear structures may appear self-evident, the reason why some structures are preferentially eroded when neighbouring, similar structural weaknesses do not become channelized requires additional consideration. In addition, some channels seemingly 'ignore' and cut across the underlying structure whereas neighbouring channels may closely be aligned with the structural trend (Carling, 2009). An issue is whether the river has cut down and the flow then has been superimposed on the bedrock surfaces (as is a fact for some cross-channels) or whether new bedrock channels are opened up by flooding-induced avulsion along lines of weakness. Without superimposition or flooding it is difficult to imagine an entrenched river opening linear weaknesses in the bedrock by lateral cutting alone. Rather the river seems to have begun to incise into an alluvial bed during the Quaternary, some 600,000 years BP (Carbonnel, 1972; Demeter et al., 2010). Consequently, the channel network, in part, must be the result of flow being superimposed on lines of bedrock weakness from that time until present. Luminescence dating of sediment from the flooding surface, islands and ancient terrain is in progress and will provide a better understanding of the incision process and timing.

In addition, for more recent Holocene channel processes, the influence of the mobile sediment, the in-channel vegetation and the relative depth within the system may play a role. It is well known that the downstream sedimentation in any alluviating river induces a variety of morphological feedback responses upstream (Cazanacli et al., 2002; Geleynse et al., 2010). In an alluvial-bedrock system the interactions are not known so well and although faulting may influence channel alignment, as noted above, the role of sedimentation must also be accounted (Humphrey and Konrad, 2000). Uplift at any point may reduce the energy slope of the upstream reach whilst the river downstream erodes and incises into the bedrock, beginning at the downstream end of the uplifted zone. However, alluviation will occur within the uplifted reach more rapidly than bedrock erosion downstream. In detail, the position of the bedrock-alluvium transition will vary depending on uplift rate and incision rate (Capart et al., 2007) and variation in sediment supply through time (Tooth and McCarthy, 2004). These processes will create or accentuate local gradient changes but importantly alluviation may block some channels and will elevate the water surface, thus enhancing the propensity for flow to be redirect laterally and to occupy additional lineaments in the bedrock. The basic control of reach-scale bed elevation on downstream distribution of sedimentation patterns is evident in the relationship between the dry season water surface level (Fig. 2) and the channel zones identified in Fig. 12. For example, where the water surface slope is steep, the channel bed is largely bedrock with sandy reaches occurring in less steep reaches. Such a pattern is consistent with similar reach-scale gradient controls observed within the Orange River (Tooth and McCarthy, 2004). However, the detailed within reach variation in sedimentation patterns noted in Fig. 12 seemingly often reflects local flow controls imposed by local geological structure and these more complex issues are subject to on-going investigation.

During the annual flood stage the flow can be envisaged as occurring (1) within relatively broad primary channels; the depths of the flow being only slightly greater than the channel depths; (2) within relatively narrow secondary channels; the depth of flow being considerably in excess of the channel depths, and; (3) as unchannelised flow above bedrock platforms, between channels, that may be well-vegetated. The Mekong has a high annual sediment load (c. 160 M tonnes a^{-1}; Milliman and Syvitski, 1992) consisting mainly of fine sand. The material is readily entrained during the flood season and then deposited as bars during the recession. Such bars are exposed as static bodies during the dry season. The bars may close off-secondary channels; closure should induce other channels to open to maintain conveyance. However, despite the complexity of the secondary channel network and the density of in-channel vegetation the majority of the network remains open water. A possible explanation is that as many secondary channels are transverse to the main flow direction and, deeply submerged, they act like slots in the bed of the Mekong 'macro-channel'. Within such transverse slots, considerable vorticity will be generated (Toda, 1994; Pollard et al., 1996), enhanced by the macro-turbulence of the deep approach flow which is passing over and through dense woody vegetation (Buckley et al., 2010). Vorticity along transverse submerged slots is known to be very efficient at evacuating both fine sediment (Raudkivi, 1993) and coarse gravel from channels (Klingeman and Milhous, 1970; Hayward and Sutherland, 1974) and this might explain the open nature of so many tortuous secondary channel networks. During low flows, the primary and cross-channel network may provide a degree of hydraulic efficiency in a manner similar to that proposed by Nanson and Huang (1999) for alluvial river networks. However during low-flows, the tortuous secondary channel network in particular might be viewed as hydraulically and sediment-transport inefficient due to the imposed structural control (e.g. Tooth and McCarthy, 2004). Intriguingly, it remains an open question as to whether such a network is inefficient when deeply submerged by flood flows. During high flows, the Mekong is characterised by a network of primary and cross-channels flanked by flooded bedrock surfaces into which the secondary channel network is incised. The interaction of a relatively efficient network of larger channels with the momentum exchange across the flooded surfaces will enhance energy dissipation and possibly sediment transport capacity but may impede flood conveyance. As in the case of the mixed bedrock–alluvial Orange River (Tooth and McCarthy, 2004), obtaining empirical flow and sediment transport data within the Mekong channel network to explore fluid and sediment transport efficiencies is a major logistical challenge. Progress in understanding the efficiencies of the Mekong network is presently limited to the constrains of available calibrated data and hydraulic modelling (Van, 2010). In addition, current work by the authors is comparing the network metrics of the Mekong channels within the study area with other bedrock and alluvial river networks to ascertain whether there are fundamental differences in the configuration of these fluvial systems.

6. Conclusions

Information gathered from diverse sources has enabled a précised portrait of the bedrock-constrained Mekong River in Northern Cambodia to be developed. Classification of the channel network

reveals three types of channel: primary, secondary and cross-channels; the characteristics of which help elucidate the evolution of the modern river. Similarly, classification of the islands into two types helps understand the relationship between island inundation characteristics and the annual monsoonal flood cycle. Riparian vegetation zonation also reflects the spatial variation in the depth and flow speed of the annual flood cycle. Vegetation in all probability both responds to and influences sedimentation processes producing unique ecotones.

Lithological and structural maps when combined with the maps of the river network in relationship to the regional topographic gradient reveal the factors controlling the river pattern. Faults and bedrock structural alignments provide a constraint on local channel alignments, causing the river channels to deviate systematically from a regional trend in channel alignment and configuration due to the regional topographical gradient. Fault-line constraints on the local slope of the channels can induce backwater effects and consequent sedimentation patterns (alluvial overprint) or, alternatively, steepening of the channels with concomitant reduced sedimentation. These structural constraints, when taken together, have led to the identification of a mixed bedrock–alluvial five-fold geomorphological zonation within the study area. The general absence of paleochannels combined with the evidence of terraces occurring only a limited distance from the modern river leads to the conclusion that the river is laterally stable with incision dominating, as expressed throughout by a number of deep pools and the evident sculpted forms on bedrock outcrops. Consequently a flooding surface of limited lateral extent constrains the annual flood.

Acknowledgements

Thanks are due to Penroong Bamrungrach, Manithaphone Mahaxay, Jorma Koponen, and Matti Kummu of the Mekong River Commission for preparing the bathymetry data. Local people in riparian villages provided information on flood history and river transport by canoe. The comments of three anonymous referees and the editors helped shape the arguments more clearly.

References

Asian Development Bank (ADB), 2007. Tourism development scenarios. Strategic environmental assessment of the Tourism Sector, Cambodia. Technical report.

Biological surveys of the Mekong River between Kratie and Stung Treng town, northeast Cambodia, 2006–2007. In: Bezuijen, M.R., Timmins, R., Seng, T. (Eds.), WWF greater Mekong – Cambodia Country Programme, Cambodia Fisheries Administration and Cambodia Forestry Administration, Phnom Penh. 220 pp.

Buckley, B.M., Anchukaitis, K.J., Penny, D., Fletcher, R., Cook, E.R., Sano, M., Nam, L.C., Wichienkeeo, A., Minh, T.T., Hong, T.M., 2010. Climate as a Contributing Factor in the Demise of Angkor, Cambodia. Proceedings of the National Academy of Science of the United States of America 107 (15), 6748–6752.

Cambodia National Mekong Committee (CNMC), 2006. Cambodia Country Report: Flood information in Cambodia. Improving Flood Forecasting and Warning Systems for Flood Management and Mitigation in the Lower Mekong Basin. Proceedings of the 4th Annual Mekong Flood Forum, Siem Reap, Cambodia, pp. 23–36.

Campbell, I. (Ed.), 2009. The Mekong: Biophysical Environment of an International River Basin. Academic Press, p. 464.

Capart, H., Bellal, M., Young, D.-L., 2007. Self-similar evolution of semi-infinite alluvial channels with moving boundaries. Journal of Sedimentary Research 77 (1), 13–22.

Carbonnel, J-P., 1972. Le Quaternaire Cambodgien. Structure et stratigraphie. (Thése présentée á l'Université de Paris- VI), 297 pp. ronéot., et 1972, Mémories O.R.S.T.O.M., N°60, 248pp., 4pl. (in French).

Carling, P.A., 2009. The geology of the Lower Mekong River. In: Campbell, I. (Ed.), The Mekong: biophysical environment of an international river basin. Academic Press, pp. 17–38.

Cazanacli, D., Paola, C., Parker, G., 2002. Experimental steep, braided flow: application to flooding risk on fans. Journal of Hydraulic Engineering 322, 232–330.

Chan, S., Putrea, S., Hortle, H.G., 2003. Using local knowledge to inventory deep pools, important fish habitats in Cambodia. Proceedings of the 6th Technical symposium on Mekong Fisheries, Lao PDR, pp. 57–78.

Church, M., 2002. Geomorphic thresholds in riverine landscapes. Freshwater Biology 47, 541–557.

Church, M., Jones, D., 1982. Channel bars in gravel-bed rivers. In: Hey, R.D., Bathurst, J.C., Thorne, C.R. (Eds.), Gravel-bed rivers. Wiley, Chichester, pp. 291–324.

Committee for Coordination of Investigations of the Lower Mekong Basin, 1959. Aerial photography of the Mekong main stem at the scale 1:40 000. Sheet 10, Mekong River Project, Canada.

Conlan, I., Rutherfurd, I., Finlayson, B., Western, A., 2008. The geomorphology of deep pools on the lower-Mekong River: Controls on pool spacing and dimensions, processes of pool maintenance and potential future changes to pool morphology. Final report submitted to the Mekong River Commission Secretariat. The University of Melbourne, Australia, p. 100.

Costa-Cabral, M.C., Richey, J.E., Goteti, G., Lettenmaier, D.P., Feldkotter, C., Shidvongs, A., 2008. Landscape structure and use, climate, and water movement in the Mekong River basin. Hydrological Processes 22, 1731–1746.

Crocker, C.D., 1962. The general soil map of the Kingdom of Cambodia and the exploratory survey of the soils of Cambodia. Joint publication. Royal Cambodian Government Soil Commission/USAID, Phnom Penh (Cambodia).

Demeter, F., Patole-Edoumba, E., Duringer, P., Bacon, A.-M., Sytha, P., Bano, M., Laychour, V., Cheangleng, M., Sari, V., 2010. Reinterpretation of an archaeological pebble culture from the middle Mekong river valley, Cambodia. Geoarcheology: An international Journal 25 (1), 75–95.

Dickins, J.M., Zuni, Y., Hongfu, Y., Lucas, S.G., Acharyya, S.K. (Eds.), 1997. Late Palaeozoic and early Mesozoic circum-Pacific events and their global correlation. Cambridge University Press, Cambridge, p. 300.

Dudgeon, D., 1999. Tropical Asian streams: Zoobenthos, ecology and conservation. Hong Kong University Press, Hong Kong. 830 pp.

FA/Danida/DED, T.S.P., 2003. Gene-Ecological Zonation of Cambodia, vol. 65.

Fontaine, H., Workman, D.R., 1997. Cambodia. In: Moores, E.M., Fairbridge, R.W. (Eds.), Encyclopedia of European and Asian Regional Geology. Chapman & Hall, London, pp. 122–127.

Franzinelli, E., Igreja, H., 2002. Modern sedimentation in the Lower Negro River, Amazonas State, Brazil. Geomorphology 44 (3–4), 259–271.

Geleynse, N., Storms, J.E.A., Stive, M.J.F., Jagers, H.R.A., Walstra, D.J.R., 2010. Modeling of a mixed-load fluvio-deltaic system. Geophysical Research Letters 37, L05402. doi:10.1029/2009GL042000.

Gupta, A. (Ed.), 2007. Large rivers: geomorphology and management. John Wiley & Sons, p. 689.

Gupta, A., Liew, S.C., 2007. The Mekong from satellite imagery: a quick look at a large river. Geomorphology 85 (3–4), 259–274.

Gurnell, A., Surian, N., Zanoni, L., 2009. Multi-thread river channels: a perspective on changing European alpine river systems. Aquatic Sciences 71, 253–265.

Hården, P.-O., Sundborg, Å., 1992. The Lower Mekong Basin Suspended Sediment Transport and Sedimentation Problems. Report to Mekong River Secretariat by Hydroconsult, Uppsala, Sweden. 71 pp.

Hayward, J.A., Sutherland, A.J., 1974. The Torlesse stream vortex-tube sediment trap. Journal of Hydrology (New Zealand) 13, 41–53.

Heritage, G.L., Moon, B.P., Broadhurst, L.J., James, C.S., 2004. The frictional resistance characteristics of a bedrock-influenced river channel. Earth Surface Processes and Landforms 29, 611–627.

Hori, H., 2000. The Mekong: environment and development. The United Nations University Press. 398 pp.

Humphrey, N.F., Konrad, S.K., 2000. River incision or diversion in response to bedrock uplift. Geology 28, 43–46.

Hutchinson, C.S., 1989. Geological Evolution of South-East Asia. Oxford Scientific Publications, Oxford. 368 pp.

ICEM, 2003. Cambodia National Report on Protected Areas and Development. Review of Protected Areas and Development in the Lower Mekong River Region. ICEM, Indooroopilly, Queensland, Australia, 148 pp.

Japan International Cooperation Agency (JICA), 2003. Cambodia Reconnaissance Survey Digital Data. Ministry of Public Works and Transportation (MPWT), Kingdom of Cambodia.

Kiernan, B., 2002. The Pol Pot regime: race, power and genocide in Cambodia under the Khmer Rouge, 1975–79. Yale University Press. 477 pp.

Kim, W., Sheets, B., Paola, C., 2009. Steering of experimental channels by lateral basin tilting. Basin Research 22 (3), 286–301.

Kleinhans, M.G., Jagers, H.R.A., Mosselman, E., Sloff, C.J., 2008. Bifurcation dynamics and avulsion duration in meandering rivers by one-dimensional and three-dimensional models. Water Resources Research 44, W08454. doi:10.1029/2007WR005912.

Klingeman, P.C., Milhous, R.T., 1970. Oak Creek vortex bedload sampler. Paper presented to 17th Annual Pacific Northwest Regional Meeting. American Geophysical Union, Tacoma, Washington, p. 17. Oct. 14–16.

Knighton, A.D., Nanson, G.C., 1993. Anastomosis and the continuum of channel patterns. Earth Surface Processes and Landforms 18, 613–625.

Kummu, M., Varis, A., 2007. Sediment-related impacts due to upstream reservoir trapping, the Lower Mekong River. Geomorphology 85 (3–4), 275–293.

Kummu, M., Lu, X.X., Rasphone, A., Sarkkula, J., Koponen, J., 2008. Riverbank changes along the Mekong River: Remote sensing detection in the Vientiane-Nong Khai area. Quaternary International 186, 100–112.

Latrubesse, E.M., 2008. Patterns of anabranching channels: the ultimate end-member adjustment of mega rivers. Geomorphology 101 (1–2), 130–145.

Latrubesse, E.M., Chen, Z., Stevaux, J.C., 2009. Preface to the special volume short and long term processes, landforms and responses in large rivers. Geomorphology 113 (3–4), 127–128.

Legris, P., Blasco, F., Dottin, O., Fontanel, J., Migozzi, J., Tichit, L., 1972. Carte Internationale du tapis vegetal et des conditions écologiques á 1/1 000 000. Notice de la carte. Cambodge. Extrait des Travaux de la Section Scientifique et Technique de L'Institut Francais de Pondichéry, Hors Série 11, pp. 1–278 (In French).

Lepvrier, C., Maluski, H., Tich, V.V., Leyreloup, A., Thi, P.T., Vuong, N.V., 2004. The Early Triassic Indosinian orogeny in Vietnam (Truong Son Belt and Kontum Massif); implications for the geodynamic evolution of Indochina. Tectonophysics 393, 87–118.

Maxwell, J.F., 2009. Vegetation and vascular flora of the Mekong River, Kratie and Steung Treng Provinces, Cambodia. Maejo International Journal of Science and Technology 3 (1), 143–211.
Mekong River Commission (MRC), 2003. Digital Hydrographic Atlas of the Mekong River at the scale 1:20 000.
Mekong River Commission (MRC), 2005. Overview of the Hydrology of the Mekong Basin. MRC, Vientiane, 73 pp.
Mekong River Commission (MRC), 2006. Spatial datasets of Mekong River Commission. Mekong River Commission, Vientiane, Lao PDR.
Mekong River Commission (MRC), 2008. Annual Mekong Flood Report 2007. Mekong River Commission, Vientiane. 86 pp.
Mekong Wetlands Biodiversity Conservation and Sustainable Use Programme (MWBP), 2005. Vulnerability assessment of climate risks in Stung Treng Province, Cambodia. MWBP, Vientiane, Lao PDR, 30 pp.
Meshkova, L.V., Carling, P.A., Buffin-Bélanger, T., in press. Nomenclature, complexity, semi-alluvial channels and sediment-flux-driven bedrock erosion. In: Church, M., Biron, P., Roy, A. (Eds.), Gravel Bed Rivers: Processes, Tools, Environments. John Wiley & Sons, Ltd., Chichester, UK.
Milliman, J.D., Syvitski, J.P.M., 1992. Geomorphic/tectonic control of sediment discharge to the ocean: the importance of small mountainous rivers. Journal of Geology 100, 525–544.
Mittelman, A., 2001. Secondary forests in the Lower Mekong Subregion: an overview of their extent, roles and importance. Journal of Tropical Forest Science 13 (4), 671–690.
Moon, B.P., van Niekerk, A.W., Heritage, G.L., Rogers, K.H., James, C.S., 1997. A geomorphological approach to the ecological management of rivers in the Kruger National Park: the case of the Sabie River. Transactions of the Institute of British Geographers, New Series 22 (1), 31–48.
Nanson, G.C., Huang, H.Q., 1999. Anabranching rivers: divided efficiency leading to fluvial diversity. In: Miller, A.J., Gupta, A. (Eds.), Varieties of Fluvial Form. Wiley, Chichester, pp. 477–494.
Nanson, G.C., Knighton, A.D., 1996. Anabranching rivers: their cause, character and classification. Earth Surface Processes and Landforms 21, 217–239.
Osterkamp, W.R., Hupp, C.R., 2010. Fluvial processes and vegetation – Glimpses of the past, the present, and perhaps the future. Geomorphology 116, 274–285.
Poduzeće za primijenjenu Geofizika, 1968. Final report on seismic investigation of Stung Treng damsite, Lower Mekong Basin, Cambodia, 1967–68. Zagreb, Yugoslavia, Geofizika.
Pollard, A., Wakarani, N., Shaw, J., 1996. Genesis and morphology of erosional shapes associated with turbulent flow over a forward-facing step. In: Ashworth, P.J., Bennett, P.J., Best, J.L., McLelland, S.J. (Eds.), Coherent Flow Structures in Open Channels. Wiley, Chichester, pp. 249–265.
Raudkivi, A.J., 1993. Sedimentation: exclusion and removal of sediment from diverted water. IAHR Hydraulic Structures Design Manual, vol. 6, p. 167. A.A. Balkema, Rotterdam.
Rollét, B., 1972. La Végétation du Cambodge. Rev. Bois et For. des Trop. 144, 3–16; 145, 23–38; 146, 3–20. (in French).
Schumm, S.A., 1968. Speculations concerning paleohydrologic controls of terrestrial sedimentation. Geological Society of America Bulletin 79, 1573–1588.
Service National Des Mines, de la Géologique et du Pétrole (SNMGP), 1973. Carte Geologique de Reconnaissance. République Khmére. Scale 1:200 000. Paris.
Simons, W.J.F., Socquet, A., Vigny, C., Amrosius, B.A.C., Haji Abu, S., Chaiwat, P., Subarya, C., Sarito, D.A., Matheussen, S., Morgan, P., Spakman, W., 2007. A decade of GPS in Southeast Asia: resolving Sundaland motion and boundaries. Journal of Geophysical Research 112, B06420. doi:10.1029/2005JB003868.
Stapledon, D.H., Wood, C.C., Harrison, J., 1961. Progress report on geological investigations Sambor Dam sites, Cambodia. Colombo Plan, Snowy Mountains Hydro-electric Authority, Cooma, p. 34. Plus drill logs and drawings.
Stapledon, D.H., Wood, C.C., McCahon, B.K., Harrison, J., 1962. Geological Investigations Sambor Dam site, Cambodia. Geological Report, Colombo Plan, Snowy Mountains Hydro-electric Authority, Cooma, Australia, Vol. 1, p. 61. Plus drill logs and drawings.
Takaya, Y., 1967. Observations on some Pleistocene outcrops in Cambodia. The South-east Asian Studies 'Kyoto University' V, pp. 122–137.
Tal, M., Gran, K., Murray, A.B., Paola, C., Hicks, D.M., 2004. Riparian vegetation as a primary control on channel characteristics in multi-thread rivers. In: Bennett, S.J., Simon, A. (Eds.), Riparian Vegetation and Fluvial Geomorphology. : Water Sci. Appl., vol. 8. AGU, pp. 43–58.
Timmins, R., 2006. Biodiversity Conservation Significance and Priorities for Action in the Mekong Ramsar Site, Stung Treng, Cambodia. Report prepared for the Mekong Wetlands Conservation and Sustainable Use Programme (MWBP), Stung Treng, Cambodia. 124 pp.
Toda, M., 1994. Bedrock channel erosion on the Upper Obitsu, Boso Peninsula: A field experiment on the influence of a fissure on erosion. Geographical Review of Japan 67A, 14–25.
Toda, O., Tanji, H., Somura, H., Higuchi, K., Yoshida, K., 2004. Evaluation of tributaries contribution in the Mekong River Basin during rainy and dry season. Proc. of the Second Conference of the Asia Pacific Association of Hydrology and Water Resources, Singapore, vol. 1, pp. 239–248.
Tooth, S., McCarthy, T.S., 2004. Anabranching in mixed bedrock–alluvial rivers: the example of the Orange River above Augrabies Falls, Northern Cape Province, South Africa. Geomorphology 57, 235–262.
Try, T., Chambers, M., 2006. Situation Analysis: Stung Treng Province, Cambodia. Mekong Wetland Biodiversity Conservation and Sustainable Use Programme, Vientiane, Lao PDR. 93 pp.
UNESCO, 1972. Geological map of Asia and the Far East, Scale 1:5 000 000.Explanatory notes, Paris, Second edition. 100 pp.
United Nations (UN), 1968. Atlas of Physical, Economic and Social resources of the Lower Mekong Basin. United Nations, New York, 257 pp.
United Nations (UN), 1993. Atlas of mineral resources of the ESCAP region. Explanatory Brochure, Vol. 10, p. 87. Cambodia. United Nations, New York.
Van, P.D.T., 2010. Hydraulic modelling and flood inundation mapping in a bedrock-confined anabranching network: the Mekong River in the Siphandone Wetlands, Lao PDR. Unpublished PhD thesis, University of Southampton, UK, 305 pp.
Van Niekerk, A.W., Heritage, G.L., Moon, B.P., 1995. River classification management: the geomorphology of the Sabie River. South African Geographical Journal 77, 68–76.
Walling, D.E., 2008. The changing sediment load of the Mekong. Ambio 37, 150–157.
Wittman, F., Parolin, P., 2005. Aboveground roots in Amazonian floodplain trees. Biotropica 37 (4), 609–619.
Wohl, E.E., 1999. Incised bedrock channels. In: Darby, S.E., Simon, A. (Eds.), Incised river channels. Wiley, Chichester, pp. 187–218.
Wongsomsak, S., 1992. Preliminary investigation on Mekhong terraces in Nakhon Phanom Province: Distribution.Characteristic, age and imbrication. Proceedings of a National Conference on "Geologic Resources of Thailand: Potential for future Development". Department of Mineral Resources, Bangkok, pp. 326–331.

31

Nomenclature, Complexity, Semi-alluvial Channels and Sediment-flux-driven Bedrock Erosion

Lyubov V. Meshkova, Paul A. Carling, and Thomas Buffin-Bélanger

31.1 INTRODUCTION

The purpose of this discussion is not to provide a critique of the chapter by Turowksi, but to amplify issues that we think are important and to which Turowski's written contribution draws attention.

31.2 DEFINITION OF CHANNEL TYPES

For consistency of nomenclature it is worth noting that the term "rock-bed" river should be preferred as this is consistent with the accepted terms: "gravel-bed" river and "sand-bed" river. Turowski *et al.* (2008) commented on nomenclature but used both "rock-bed" and "bedrock" in their terminology; applying the former adjective to channel-shaping processes and the latter to a description of a channel at a given location in time. Both adjectives are used commonly in the literature and it is likely that attempts to introduce such a finessed differentiation and standardization will be resisted. In addition, often "bedrock" grammatically is a more convenient adjective than "rock-bed" and so both terms are used herein interchangeably.

Turowski *et al.* (2008, p.28) provided the following definition of a bedrock channel: "A bedrock channel cannot substantially widen, lower or shift its bed without eroding bedrock". Given that a lateral shift in a bedrock channel cannot be accomplished without erosion of the lateral margin we can simplify the definition of Turowski *et al.* (2008) to include only two, rather than three, adjustments in geometry through the statement: "A bedrock channel cannot adjust laterally, nor incise without eroding bedrock".

Turowski *et al.* (2008) also introduced a useful definition cartoon (Figure 31.1, parts a, b and c) that prompts additional comment. Channel type A exists where there is negligible sediment accumulation on the bed and a negligible transported sediment load and as such this type of channel approaches an end-member classification of clear-water flow. Such channels are unusual in nature although some bedrock step-pool systems approach this condition (Carling *et al.*, 2005). Physical wear due to sparse sediment tool effects allows limited opportunity to adjust width or depth. Rather, at the extreme, corrosion and chemical weathering will be the primary mechanisms for inducing changes in channel geometry where the rock-type permits, and subaerial weathering will pertain in the case of all rock types. In principle, adding a substantial suspended load (but no bedload) would induce channel adjustments (Turowski *et al.*, 2008), for case A, through abrasion of both the side walls and the bed. However, it is difficult to envisage a natural system wherein suspended load was not associated with a bedload. This end-member channel type we refer to as a "rock-bed" or "bedrock" channel. We also include in Figure 31.1 the alluvial end-member for completeness.

Most natural bedrock channels studied to date would be classified as channel type B, as these systems contain a mobile bedload and usually a deposited sediment filament that covers at least a substantial part of the rock bed, although the side walls are bare bedrock. As soon as there is a significant alluvial content, the channel cannot be considered a bedrock channel; rather it is a "mixed bedrock-alluvial system". General reference to bedrock "constrained" and "confined" channels has been made previously (e.g., Montgomery and Buffington, 1997; Schumm, 2005), but below we provide more precise definitions.

Where the channel is laterally confined by competent bedrock, but there is a live bedload layer or an alluvial bed, there is less opportunity for lateral erosion, in

Gravel-bed Rivers: Processes, Tools, Environments, First Edition. Edited by Michael Church, Pascale M. Biron and André G. Roy.

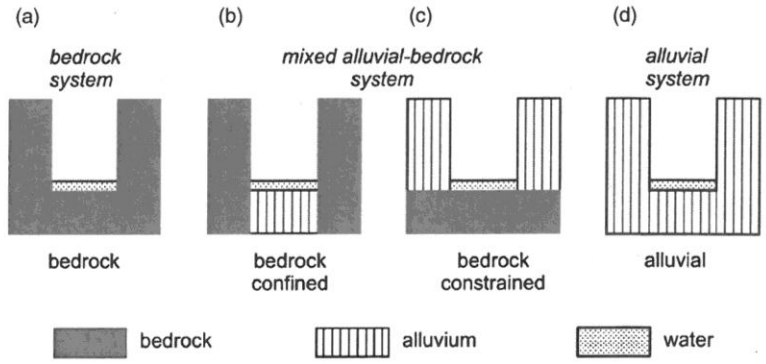

Figure 31.1 The end members in the continuum of channel types from bedrock to alluvial character.

contrast to a greater opportunity either to accrete the sediment fill or to erode the rock bed; the assumptions being that loose sediment is more erodible than the confining bedrock walls and the rock bed is more subject to abrasion by bedload than the side walls. This class of channel we refer to as "bedrock confined" and the channels are usually rather narrow with a sediment fillet at the base (Figure 31.1b). The third type of channel has a rock bed, but alluvial sidewalls. In this latter case, vertical incision is less readily accomplished in comparison with lateral erosion of the alluvium (Figure 31.1c) and to differentiate from class B, we term this channel type "bedrock constrained". We return to this class later, but it is class B which has been subject to the majority of research to date.

31.3 STEADY-STATE, DYNAMIC EQUILIBRIUM AND THE ROLE OF SEDIMENT

Turowski (Chapter 29, this volume) considers channels in steady state where bedrock erosion equals uplift. Here we do not challenge the conceptual model advanced by Turowski, but seek to clarify some issues which highlight the significance of any sediment fill to the equilibrium of a rock-bed channel. Steady state might be defined as "a stable condition that does not change over time or in which change in one direction is continually balanced by change in another". The alternative to steady state is defined by Turowski as "transient conditions". Transience implies impermanence to any adjustment and consequently this latter system state is a form of dynamic equilibrium. Dynamic equilibrium might be defined as "a lack of change in a system as inputs and outputs remain in balance because if changes do occur, then feedbacks will allow for correction". More usually the state of such a system is such that the output continually changes, but remains within fairly narrow bounds. The output is characterized by a mean value and a bounded range around that mean value.

It is important to consider the implications of these two system states for the evolution of the geometry of a bedrock channel. Where uplift equals incision, the channel slot will deepen over time such that the side walls of the slot become higher. It is important to note that reference is made here to the depth of the slot and not the wetted depth. This is a simple example of a steady-state system, but note that an increasing slot depth has implications for the distribution of erosional forces on the channel boundary if discharge were to increase above a discharge reference value associated with a given wetted depth. Thus, although uplift supplies additional bedrock for erosion, the width–depth ratio of the slot changes through time with channel width changing less as the slot deepens. Although discharge variability through time may be important for adjustments in bedrock channel geometry, it is important to note that given a sufficiently low base level, a competent steady discharge can still lead to changes in the slot geometry through abrasion and solution, including width adjustments (Turowski *et al.*, 2008) if incision is halted. Even if channel geometry refers to a constant value of, say, width–depth ratio, the actual channel dimensions in principle could change; i.e., both width and depth increase whilst W/d remains static.

If we define the physical boundary of the channel as consisting of bedrock (i.e., width and depth, for example, are defined by the bedrock surfaces rather than any sediment fillet sitting on the bedrock), then a bedrock channel can only be in dynamic equilibrium (as defined above) if the overall size of the channel increases through time, as bedrock erosion is a one-way process. As noted above, W/d might remain constant, but overall slot size

cannot remain constant. Either W/d has to change, in which case there is no dynamic equilibrium, or the channel size has to change. If W/d changes, as is likely, then a bedrock channel can only maintain dynamic equilibrium if there is sediment deposition on the bed to counter any bedrock erosion. Therefore the spatial disposition of sediment within mixed bedrock-alluvial streams is an important systems response to maintain dynamic equilibrium. Thus, in this context, the balance between a tools-dominated domain and a cover-dominated domain becomes of greater significance than determining the local vertical erosion rate alone; rather, the variation in the loci of sediment covers in space and time will influence the shape of the bedrock long profile, as well as any propensity for the river to move laterally.

Class C, the bedrock constrained system, is the least well-investigated type of river. The best published examples of such a system are reaches within the Orange River, South Africa (Tooth and McCarthy, 2004). The Orange River has a tendency to be anastomosed with locally two or more bedrock-floored channels with alluvial banks. Although the Orange River is a large system (individual channels up to $\sim 3000\,m^3\,s^{-1}$), there are numerous examples of small, single-channel bedrock constrained channels in nature which seem to have been over-looked. The Mekong River in northern Cambodia near Kratie is a further example of a large, constrained system (Meshkova and Carling, in press) incised some 20 m into ancient alluvium (Figure 31.2) with a bedrock floor and with evidence of lateral stability since the mid-Quaternary. The Mekong is of particular interest because it is anastomosed, with a low Quaternary rate of vertical incision (possibly 40 to 100 m in 600 000 years; Carbonnel, 1972). Low incision rates in this case are not conditioned by an extensive sediment cover, but rather by a relatively low channel gradient (0.00027) close to the base level and by tectonic stability. The mean peak annual discharge for the last 90 years at Kratie is in excess of $50\,000\,m^3\,s^{-1}$ (MRC, 2009) and is contained within the channel boundary. However, although total peak power is high, around 132 300 W, this is distributed across an anastomosed channel network in places up to 5 km wide, giving an average unit stream power as low as $26\,W\,m^{-1}$, such that incision is slight and highly localized across the sections. Nevertheless, the annual power is sufficient to transport an annual suspended fine sand load of 160 megatonnes with an unknown sandy bedload component, there being negligible gravel. Despite the competence to transport sand, the river exhibits persistent zones of sedimentation and zones of bare bedrock (Figure 31.3). Quantitative study of air photographs has shown that the loci and size of sand bars have remained constant over the last 50 years or so. At the regional scale, and as might be expected, it is evident that bare rock reaches correspond to the steepest reaches of the river, with the intervening lower slope bedrock reaches having variable degrees of alluviation. However, it is the local controls on sedimentation in this complex anastomosed network that provide the reach-scale complexity in the sedimentation pattern and these controls are more difficult to ascertain.

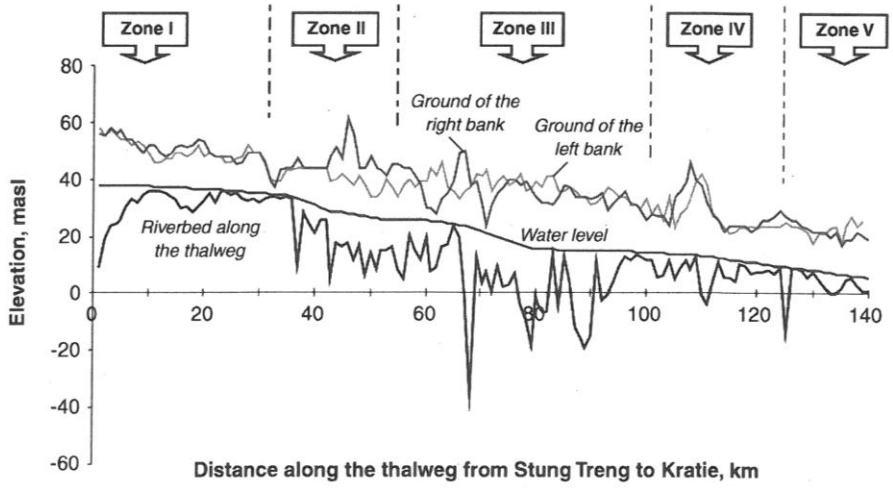

Figure 31.2 The elevation of the riverbed, dry season water level and the ground elevation of the western and eastern banks of the Mekong in northern Cambodia. Modified after Meshkova and Carling, in press. Zones correspond to those explained in Figure 31.3.

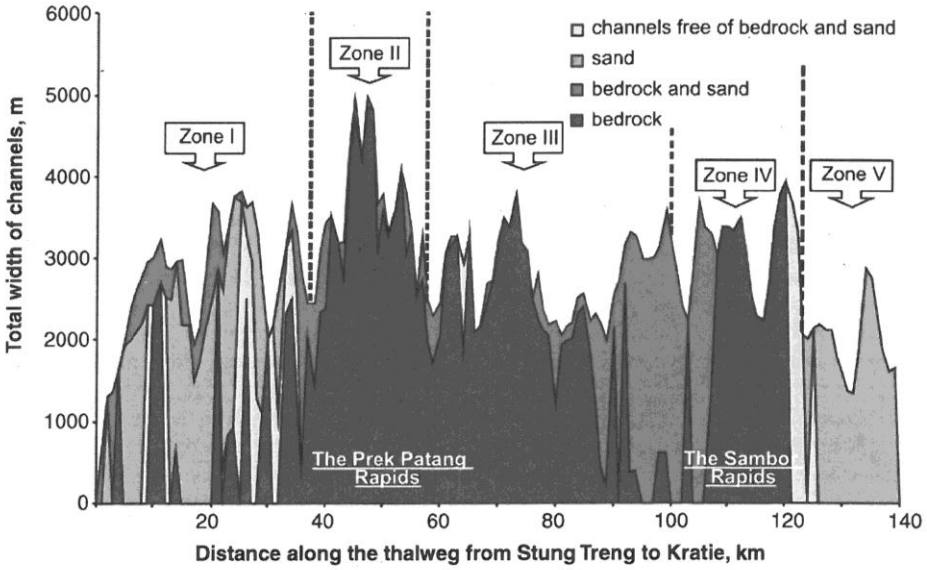

Figure 31.3 Zonation of the channel of the Mekong shown in Figure 31.2 is based in part on the proportion of the channel width occupied by sand fillet over bedrock as shown here. The detail of sand distribution in Zones II and III in particular is complex and is highly simplified here. Modified after Meshkova and Carling, in press. Lightest sections are deep-water with indeterminate bed type. (See the color version of this figure in color plate section)

Yet these local controls may be important, inducing avulsion of individual Mekong subchannels (Meshkova and Carling, in press). These effects of alluviation in bedrock systems on backwater effects and channel shifting are only recently being explored (Humphrey and Konrad, 2000; Capart *et al.*, 2007). The Mekong in northern Cambodia remains a topic of investigation by the authors, with several luminescence dates imminent to define the incision history more precisely.

31.4 NEW CONCEPTS

31.4.1 "Alluvial Overprint"

To the north of Cambodia in southern Laos, the Mekong is also a bedrock constrained anastomosed system that is incised into ancient alluvium, flowing across bedrock. However, there has been considerable lateral movement during the Quaternary such that it is often bounded laterally by its own alluvium. Satellite images show that a regional-scale meandering pattern is super-imposed onto local bedrock control (Figure 31.4). The meandering pattern has not been investigated, but seemingly "sweeps" across the bedrock surface such that the meander planforms have the characteristics of an alluvial system. This style of alluviation we here term an "alluvial overprint" and the interaction of alluvial channel processes, including bank cutting and bank accretion with a bedrock constraining floor, introduces further intriguing complexity to the future understanding of rock-bedded rivers and re-inforces the need to document these specific river styles (Heritage *et al.*, 2001).

31.4.2 "Bedrock Footprint"

The presence of moving sediments plays a key role in the evolution and nature of the bedrock sections in semi-alluvial channels. Similarly, several authors have highlighted that the presence of rock outcrops plays a crucial role in the morphodynamics of semi-alluvial channels. This issue is addressed here briefly using three recent examples from the literature.

Nicol and Hickin (2010) studied the planform geometry and the migration behaviour of confined meandering rivers. These are rivers in valleys that are laterally constrained and in which planform geometry of free meanders cannot develop fully. Figure 31.5 presents a LiDAR image from the Matane River, Eastern Québec, illustrating the planform geometry of such a confined meandering river. Although relations between planform geometry variables extracted from 23 locations along confined meandering rivers are generally not inconsistent with those for freely meandering rivers, Nicol and Hickin (2010) observed significant differences in the ratio of channel length/channel width and the bend curvature. For the migrating behaviour, they observed

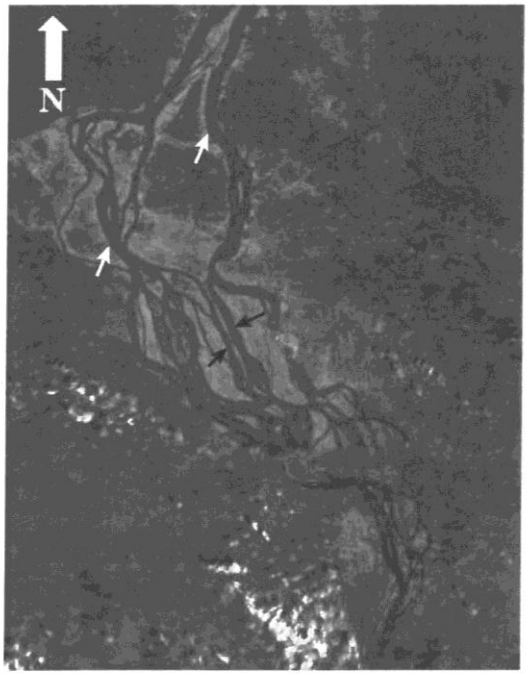

Figure 31.4 Anastomosed bedrock-constrained fluvial network of the Mekong River, Siphandone, southern Laos. Landsat-7, horizontal field of view approximately 40 km. Virgin and degraded forest (dark shades) on ancient alluvium flank the river system, whereas the recent river corridor is now largely denuded of natural vegetation (light shades). Although "linear" reaches of the river reflect structural control (e.g. black arrows), it is also evident that curvilinear alluvial-controlled reaches occur (e.g., white arrows) (see text for detail). Reproduced, with permission, from Carling, P.A. 2009. Geomorphology and Sedimentology of the Lower Mekong River. In Campbell, I.C., editor. *The Mekong: Biophysical Environment of an International River Basin*. New York, Academic Press: 77–111.

that these confined meandering rivers rarely develop cutoffs and that the dominating migrating pattern is the downstream translation of meander bends as a coherent waveform. These observations suggest specific morphodynamics and planform geometries that pertain for confined meanders.

Lamarre *et al.* (2010) compared a large number of alluvial and semi-alluvial river sections in order to identify the dominant control variables of the morphological features found in these two types of channels in several rivers of the Gaspé peninsula, Québec. Semi-alluvial river sections essentially were dominated by the presence of a large bedrock outcrop constricting the flow and generating large bedforms. Lamarre *et al.* (2010) performed a discriminant analysis on 68 river sections from which eight variables were measured (slope, pool depth, bar D_{50}, bar size, deflection angle, floodplain width, channel width, and floodplain asymmetry), which indicated that the main variables explaining the differences between the alluvial, atypical and typical semi-alluvial sections are the deflection angle and the pool depth. Hence, there are specific channel morphologies associated with the presence of bedrock outcrops.

Finally, Ebisa-Fola and Rennie (2010) presented the first downstream hydraulic geometry relations for non-alluvial consolidated clay-dominated cohesive-bed river channels. They reported higher values for the depth exponent for those channels than for typical alluvial gravel-bed and sand-bed rivers. Although not from rock-bed channels, their findings highlight some specific hydraulic geometry relations for channels that are laterally constrained.

These studies highlight the role of bedrock outcrop (or cohesive material) on the planform geometry and the migrating pattern of meanders, the morphology of river section, and the downstream hydraulic geometry relations. They thus suggest that there is a "bedrock footprint" that influences river morphodynamics and morphologies in semi-alluvial channels. The presence of moving sediments is crucial in the evolution of rock-bed channels but, similarly, the bedrock outcrop may play a distinctive role in the dynamics of the river system and its morphological evolution.

31.4.3 Extension of the Channel Types Definition

As alluded to in the previous section, the concepts of constrained and confined rivers might be applied also to channels that exhibit cohesive boundaries. The term semi-alluvial is being used in the literature loosely, but largely to define river sections that have a solid boundary other than natural hard bedrock. As such, it can be suggested that the proposed channel type definitions (Section 31.1) can be extended to define types of semi-alluvial channels. Figure 31.6 presents the two main elements of the definition for semi-alluvial channels. Other than the example of cohesive boundaries depicted in Figure 31.6, confined semi-alluvial configurations can occur in several other settings. The presence of bank protection (Figure 31.7a), roots and woody debris can be seen as confining the river laterally and hence contribute to channel morphodynamics in a similar way to bedrock outcrops. For the constrained semi-alluvial configuration, the presence of marine or lacustrine clay deposits is probably the most frequent configuration observed (Figure 31.7b).

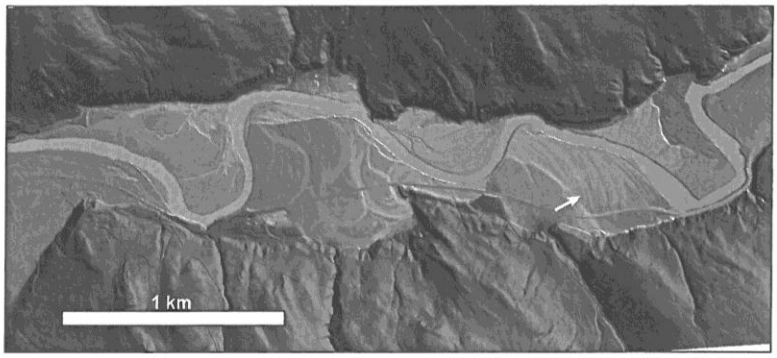

Figure 31.5 Confined meanders of the Matane River, Eastern Québec. The LiDAR image reveals the translating migration pattern of meander bends typical of confined meanders (white arrow). (See the color version of this figure in color plate section.)

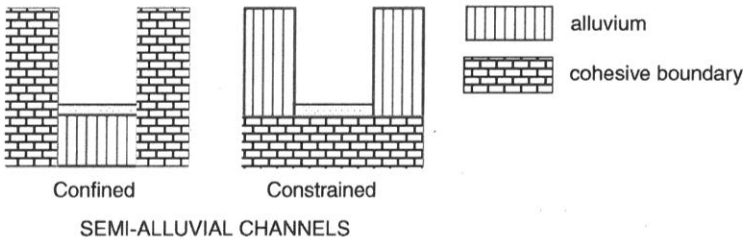

Figure 31.6 General semi-alluvial channel types.

Figure 31.8 can be used to discuss the usefulness of such a general semi-alluvial river classification. Figure 31.8 represents the rate of migration for 100 m long river segments along 50 km of the Matane River over the last decade. The Matane River is a highly dynamic gravel-bed river that led to several human interventions to decrease the lateral migration of the river. Locations of bank protection constructed in the last half century are indicated for both sides of the river corridor. The density of bank protections is higher in the downstream (18% of river bank) than in the upstream section where less bank protection is found (4% of river bank). As a consequence, the proportion of eroding banks has decreased in the downstream section (20%) as compared to the upstream section (40%), with the mean migration rate being also smaller in the downstream ($0.8\,m\,a^{-1}$) than in the upstream section ($1.1\,m\,a^{-1}$) of the river. This figure shows that the confinement of the Matane River has increased due to human interventions and that the river is now more likely to behave as a confined

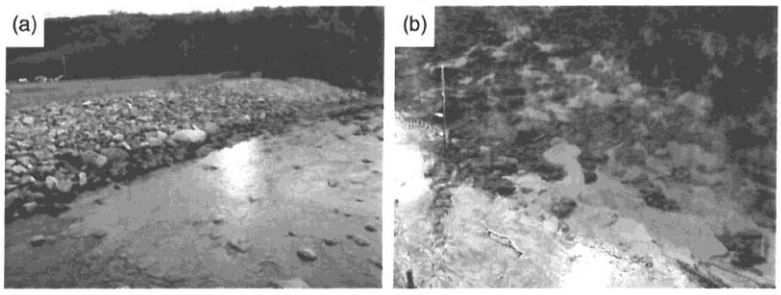

Figure 31.7 (a) Bank protection on the Matane River, Québec, that contributes to confining the river; (b) a section of the Ste-Marguerite River, Québec, revealing the Goldthwait marine clay deposit constraining the river.

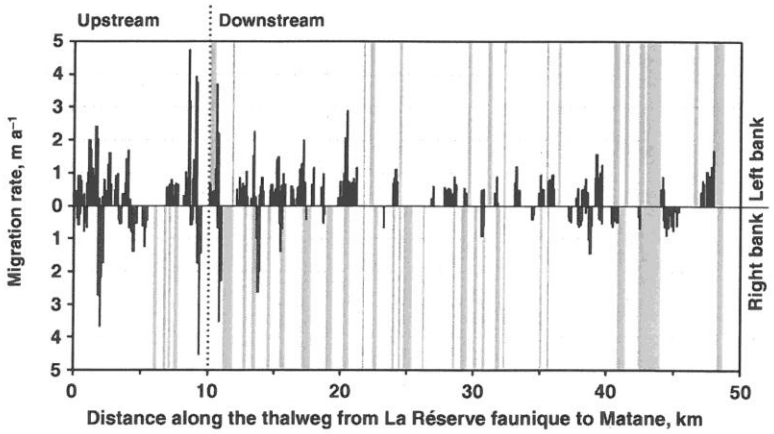

Figure 31.8 Migration rate measured on the Matane River for 100 m long river segments. Grey areas indicate locations of bank protection along the distance downstream for both river banks. Left and right banks are separated by the line of zero migration.

semi-alluvial river. Hence, when managing the Matane River system, one has to understand the river in the light of the knowledge that has been gained by work on confined semi-alluvial rivers, whether that constraint is due to a bedrock outcrop or other cohesive boundary. In the same vein, given the plethora of engineering studies into the behaviour of artificially controlled rivers, much can be learnt about natural semi-alluvial rivers by considering the effects of artificial constraints on alluvial rivers.

This extension of definitions is pragmatic and is useful in applied situations, as is shown in the final example (Figure 31.8). However, it is clear that there is a continuum of channel types considered herein from those channels exhibiting boundaries consisting of solid unweathered rock, through to consolidated clays and artificial constraints. Given that some definitions of rock can include soft clays, it remains to be seen whether a morphological distinction needs be drawn between hard rock and clay-bounded river channels. Nevertheless, although Figure 31.1 describes channels at a given time and location rather than specify the controlling processes, we believe that distinctive process domains will dominate in each end-member type such that distinctive dynamics might be elucidated for each member.

31.5 ACKNOWLEDGEMENTS

The authors would like to thank Hélène Lamarre, Mathieu Roy, Taylor Olsen and Sylvio Demers for providing unpublished data from posters presented at GBR7 (Lamarre *et al.*, 2010; Olsen *et al.*, 2010) to generate clear illustratations of ideas presented herein.

31.6 REFERENCES

Capart, H., Bellal, M., and Young, D-L. 2007. Self-similar evolution of semi-infinite alluvial channels with moving boundaries. *Journal of Sedimentary Research* **7**: 13–22.

Carbonnel, J-P. 1972. *Le Quaternaire Cambodgien. Structure et stratigraphie.* Thesis, University of Paris. Also published (1972) as *Mémoires O.R.S.T.O.M.,* No. 60. [in French].

Carling, P.A. 2009. Geomorphology and Sedimentology of the Lower Mekong River. In Campbell, I.C., editor. *The Mekong: Biophysical Environment of an International River Basin.* New York, Academic Press, pp. 77–111.

Carling, P.A., Tych, W., and Richardson, K. 2005. The hydraulic scaling of step-pool systems. In Parker, G. and Garcia, M.H., editors. *River, Coastal and Estuarine Morphodynamics*, vol. 1. New York, Balkema, Taylor and Francis, pp. 55–63.

Ebisa-Fola, M. and Rennie, C. 2010. Downstream hydraulic geometry of clay-dominated cohesive bed rivers. *Journal of Hydraulic Engineering* **136**: 524–527.

Heritage, G.L., Charlton, M.E., and O'Regan, S. 2001. Morphological classification of fluvial environments: an investigation of the continuum of channel types. *Journal of Geology* **109**: 21–33.

Humphrey, N.F. and Konrad, S.K. 2000. River incision or diversion in response to bedrock uplift. *Geology* **28**: 43–46.

Meshkova, L. V. and Carling, P.A. in press. The geomorphological characteristics of the Mekong River in northern Cambodia: a mixed bedrock-alluvial multi-channel network. *Geomorphology.* doi: 10.1016/j.geomorph.20101.06.041. Published online 27 August, 2011.

Montgomery, D.R. and Buffington, J.M. 1997. Channel-reach morphology in mountain drainage basins. *Bulletin, Geological Society of America* **109**: 596–611.

MRC (Mekong River Commission). 2009. *The Flow of the Mekong.* MRC Management Information Booklet No. 2.

Nicoll, T.J. and Hickin, E.J. 2010. Planform geometry and channel migration of confined meandering rivers on the Canadian Prairies. *Geomorphology* **116**: 37–47.

Schumm, S.A. 2005. *River Variability and Complexity*. Cambridge, Cambridge University Press.

Tooth, S. and McCarthy, T.S. 2004. Anabranching in mixed bedrock-alluvial rivers: the example of the Orange River above Augrabies Falls, Northern Cape Province, South Africa. *Geomorphology* **57**: 235–262.

Turowski, J.M., Hovius, N., Wilson, A., and Horng, M.J. 2008. Hydraulic geometry, river sediment and the definition of bedrock channels. *Geomorphology* **99**: 26–38.